Investigation of Hydrologic and Sediment Transport Processes on Riparian Hillslopes

by

Shreeram P. Inamdar

Dissertation Submitted to the Faculty of the

Virginia Polytechnic Institute and State University

in partial fulfillment of the requirements for the degree of
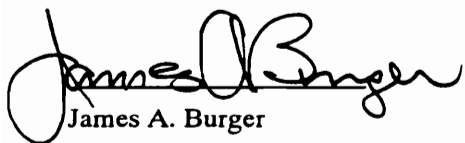
DOCTOR OF PHILOSOPHY

in

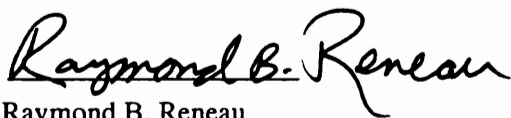BIOLOGICAL SYSTEMS ENGINEERING

APPROVED

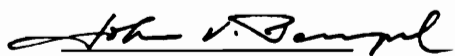Theo A. Dillaha III, Chairman

James A. Burger

Saied Mostaghimi

Raymond B. Reneau

Mary Leigh Wolfe

John V. Perumpral

May, 1996
Blacksburg, Virginia

Keywords: Riparian Zones, Hillslope Catchments, Representative Scale, Interflow, Hillslope Model

INVESTIGATION OF HYDROLOGIC AND SEDIMENT TRANSPORT PROCESSES ON RIPARIAN HILLSLOPES

by

Shreeram P. Inamdar

Theo A. Dillaha, Chairman

Biological Systems Engineering

(ABSTRACT)

Riparian zones are increasingly being adopted as best management practices (BMPs) to control nonpoint source pollution. The effectiveness of these zones in mitigating pollution is a function of the distribution, nature, and rate of water and sediment movement through these zones. The intent of this research was to investigate the influence of site conditions on the hydrologic and sediment transport response of riparian zones/hillslopes.

Research investigations were focused in two major areas: field investigations of riparian hillslopes and development of a riparian hillslope model. The objective of the field investigations was to characterize and quantify geomorphic features of riparian slopes that can be used to quantify flow concentration on hillslopes. The riparian hillslope model was used to investigate the dynamics of hydrologic and sediment transport processes.

Field investigations revealed that riparian hillslopes were dissected into distinct convergent, divergent, or straight slope segments. In profile, these segments were either concave, straight, or convex. It was hypothesized that the size of such segments reflects the "representative hillslope scale". Probability distributions of catchment area showed that catchment area decreases with slope gradient. Distributions of catchment shape revealed that catchment shape elongates with increasing gradient. Distributions of drainage channel cross-sectional shape data showed a decreasing trend in width to depth ratio with increasing slope gradient. These results indicate that geomorphic features characterizing flow concentration vary with slope gradient and should not be neglected when simulating riparian hillslopes.

Model simulations revealed that site conditions such as slope gradient, slope shape, flow concentration, and soil horizon thickness and characteristics play a significant role in shaping the hydrologic and sediment phenomena on these hillslopes. These results underscore the need for evaluation of riparian zones considering specific site conditions. Interflow was the dominant

hillslope runoff mechanism. A large fraction of the interflow occurred via macropores. Macropore flow was orders of magnitude quicker than soil matrix flow. Overland flow was found to occur primarily due to saturation excess or return flow. Simulations showed that thinning of soil layers and/or concave-convergent slope shapes provide favorable conditions for generation of saturation excess or return flow.   Sediment delivery down the slope increased with increasing flow concentration.

Dedicated in loving memory of my dearest mother.

My accomplishments are due to her love and sacrifices.

ACKNOWLEDGEMENTS

TABLE OF CONTENTS

LIST OF FIGURES

LIST OF TABLES

1 INTRODUCTION

Riparian zones can be defined as zones of vegetation adjacent to drainage channels, streams or rivers. This vegetation can be either grasses, shrubs or trees. Previous research has indicated that riparian zones are effective in filtering and sequestering pollutants from upland runoff and thus act as natural buffers for streams and drainage channels (Peterjohn and Correll, 1984; Lowrance et al., 1983, 84; Fail et al., 1986; Dillaha et al., 1987, 88, 89). Pollutants trapped include sediment, nitrogen, and phosphorous. This "buffering ability"of riparian zones has been primarily attributed to their topographic location, the unique nature of site and soil conditions, and the vegetation. This effectiveness has led to their adoption as a Best Management Practice (BMP) to reduce and mitigate nonpoint source pollution.

Welsch (1991) proposed a three-zone approach to management and establishment of riparian buffer zones (see Figure 1.1). This management approach has now been adopted as an "Interim Standard and Specification" for the eastern region of the US by the South and Northeast National Technical Centers of the Natural Resources Conservation Service (NRCS) (Sweeney, 1992). Though the three-zone approach provides an excellent description of management guidelines for various component zones, a number of key issues remain unresolved. Some of these issues include:

- What length of riparian buffer should be used to achieve a desired level of pollutant reduction?
- How does pollutant trapping within riparian zones vary with site conditions or how do site conditions such as slope angle, slope shape, flow concentration, soil type and condition and vegetation influence water and pollutant movement?
- How is water/pollutant movement influenced by antecedent storm conditions and storm event loadings?

To utilize riparian zones as BMPs to their full potential, these issues must be resolved. To determine the size of riparian buffers, an estimate of the pollutant trapping within the zone is required. Prior to estimating pollutant trapping, an accurate understanding of the pathways and dynamics of water and sediment movement is essential. This research attempts to take the initial

---

steps toward answering some of these key issues by investigating in detail the hydrologic and sediment transport phenomena occurring in riparian zones. It is expected that the detailed information on hydrology and sediment transport generated through this research will provide a sound basis for a future "design model" required to estimate pollutant trapping within riparian buffers.

First order streams/drainage channels are believed to occupy a major portion of the stream miles within a watershed. It is thus expected that the riparian zones located adjacent to such first order streams/drainage channels will have the greatest impact on mitigating nonpoint source pollution. Considering these facts, this research was targeted towards investigating the hydrologic and sediment phenomena in riparian zones located adjacent to first order streams/drainage channels. This investigation into hydrologic and sediment transport processes included:

- Field investigation into riparian slopes to determine the appropriate scale and geomorphologic attributes required to represent flow on riparian hillslopes.
- Development of a detailed hydrologic and sediment transport model to test specific process hypotheses and provide insight into the dynamics of water and sediment movement on these slopes.

Specific objectives and hypotheses under these two major research areas are described in the following chapter.

Cropland	Grass filter zone	Managed forest zone	Undisturbed forest zone	Stream
Source of sediment & nutrients	Reduction in runoff - increased roughness enhanced infiltration Sediment deposition	Reduction in nutrients N & P - plant uptake , denitrification	Stream temperature control Wood debris Habitat	-
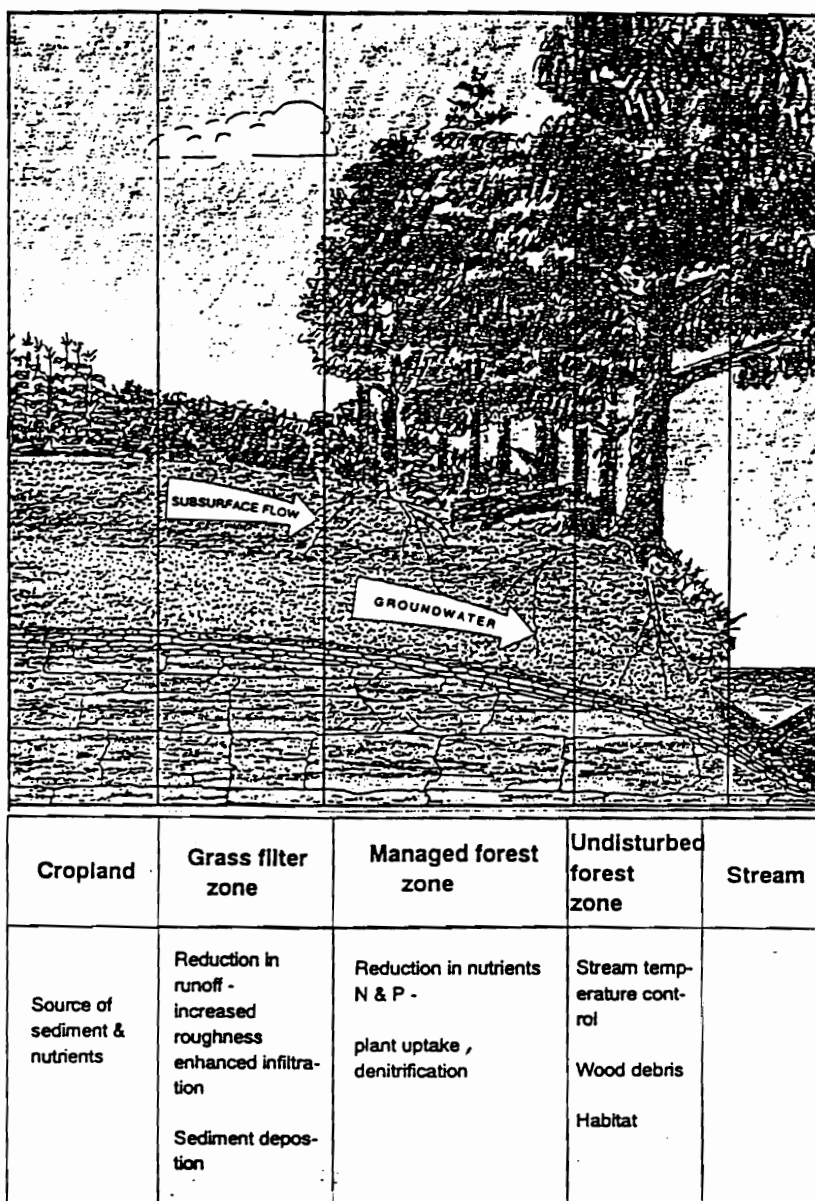
Figure 1.1: Managed riparian buffer with three distinct vegetation zones (Welsch, 1991).

2 RESEARCH OBJECTIVES

Research was focussed in two major areas - (I) field investigations of riparian hillslopes, and, (II) development of a hydrologic and sediment transport model. Specific objectives under each focus area are listed below.

I) Field investigations

- Identify the "representative hillslope scale" for simulating riparian hillslopes.
- Characterize and quantify geomorphologic features of riparian slopes that can provide an estimate of flow concentration on these hillslopes. Specifically this involved:
    - Determining probability distributions for contributing area size for "representative hillslope units" across a range of slope gradients.
    - Determining distributions for contributing area shapes (expressed as length to area ratio of the catchment) across a range of slope gradients.
    - Determining distributions for drainage channel shapes for different slope categories.

The null and alternate hypotheses behind these specific objectives were:

H_o: Catchment area size does not decrease with increasing slope gradient.

H_a: Catchment area size decreases with increasing slope gradient.

H_o: Catchment area length to area ratio does not increase with increasing slope gradient.

H_a: Catchment area length to area ratio increases with increasing slope gradient.

H_o: Drainage channel width to depth ratio does not decrease with increase in slope gradient.

H_a: Drainage channel width to depth ratio decreases with increase in slope gradient.

The assumption behind the objectives and hypotheses is that slope gradient is the primary and overriding determinant of flow concentration on riparian hillslopes.

II)   Model development

- Develop a detailed hillslope scale, continuous simulation model for predicting water and sediment movement on riparian hillslopes.
- Test the model using measured riparian hillslope data and express model predictions with associated "confidence bounds".
- Perform sensitivity analysis on model components.
- Evaluate model predictions by determining if the model simulates process phenomena unique to riparian hillslopes. The process phenomena that were considered were:
    - For riparian hillslopes with a subsurface restricting soil layer, subsurface lateral flow is the major runoff contributor.
    - Time to initiation of lateral subsurface flow is controlled by the depth of the unsaturated zone.
    - Under saturated conditions, macropore flow is orders of magnitude greater than soil matrix flow.
    - Concave-convergent slopes provide more favorable conditions for build up of the saturation wedge compared to straight or convex slopes.
    - Sediment delivery increases with increasing runoff concentration.

3 LITERATURE REVIEW

The literature review presented below is divided into five major sections. The first part discusses the role of riparian buffers in trapping and sequestering pollutants and the mechanisms that are responsible for their effectiveness. Knowledge of these mechanisms will help better target simulation efforts. The second part provides a brief background on scale issues and hillslope forms pertinent to riparian hillslopes. The third and fourth sections review the present state of knowledge of hydrologic and sediment transport processes. The final section provides a review of the approaches used to evaluate models. Though the primary emphasis is to describe the basic dynamics of each of the hydrologic and sediment transport process, an effort is made to illustrate the nature of each of the processes under forested and grassland conditions.

3.1 Riparian buffer zones: Mechanisms responsible for their effectiveness

As defined in Chapter I, managed riparian zones may be composed of grass and/or forested vegetation. Each of the vegetation types have unique functional attributes that lead to pollutants being trapped in the riparian zone. The following section discusses mechanisms that are responsible for trapping of sediment and nutrients in grass and forested zones.

3.1.1 Trapping in riparian grass filters

Most of the previous research in grass filters has concentrated on determining the effectiveness of grass filters in removing sediment from upland runoff. Detailed studies of trapping mechanisms in grass filter strips were conducted at the University of Kentucky (Barfield et al., 1977; Kao and Barfield, 1978; Tollner et al., 1976, 1978, 1982; Hayes et al., 1979, 1984). Observations from this research were:

- As runoff enters grass filters its velocity is reduced which leads to reduction in its sediment transport capacity and thus deposition of excess sediment in the upslope edge of the filter. This also leads to the removal of chemicals adsorbed on the active phase of the

sediment.

- Infiltration in grass filters is enhanced due to the presence of macropores created as a result of grass root activity. This infiltration leads to the trapping of fine sediment and dissolved chemicals in the soil matrix.
- Chemicals trapped in the soil surface are lost with time as a result of biological and chemical transformations and plant uptake.
- Vegetal media retards the surface flow and provides an opportunity for chemicals to be adsorbed to vegetation, litter, or the surface layer of the soil.
- Coarser sediment fractions are trapped near the upslope edge of the filter, whereas finer particles are trapped within the filter.

Following these studies, research by Tollner et al. (1976) led to the formulation of design equations for determining sediment trapping in grass filters, which, were then used to develop an event based model (GRASFIL, Barfield et al., 1979). Sediment trapped in the grass filters was found to be a function of the mean flow velocity, flow depth, particle fall velocity, filter length, and spacing hydraulic radius of the grass media.

Long-term effectiveness of grass filters or vegetated filter strips (VFS) was investigated by Hayes and Hairston (1983) and Dillaha et al. (1986,1989). Dillaha et al. observed that as sediment was trapped at the filter edge, berms formed that forced inflows from subsequent storms to flow parallel to the filters until channels were encountered that allowed flow to cross the VFS as concentrated flow. This channelization of flow led to reduction in effectiveness of the grass filter. Recent studies have attempted to model this phenomenon (Inamdar, 1993).

Though grass filters have been proven effective in controlling sediment and sediment bound pollutants (particulate phosphorous, ammonium) over the short term, they have not been as successful in controlling dissolved nutrients such as nitrate. Magette et al. (1989) and Dillaha et al. (1989) investigated the effectiveness of 4.6 and 9.2 m long grass filters in removing nutrients and sediment from agricultural runoff. Nutrient removal efficiency of the filters decreased as the number of runoff events increased. Lee et al. (1989) developed an event based model, GRAPH (GRAss-PHosphorous), to simulate surface P transport in vegetative filter strips by incorporating chemical transport submodels into the grass filter model (GRASFIL). A similar approach is being

developed for nitrogen transport in surface runoff (Delgado et al., 1992). Table 3.1 provides a summary of results from selected studies of grass filters.

Table 3.1: Summary of results of selected grass filter studies

Reference	Filter description	Trapping Efficiency or % reduction*		
		Sediment	Nitrogen	Phosphorous
Dillaha et al., 1989	Orchardgrass (5-16% slope)	70 - 91	61	75 87
Magette et al., 1989	Fescue (varying slope)	52 - 75	(-15) - 35	6 - 20
Hayes & Hairston 1983	Fescue (3% slope)	> 90	--	--
Parsons et al., 1991	Bermuda & Crab grass	70	--	--
Young et al., 1980	Corn-Oats orchardgrass (4%), Sorghum Sudangrass (4%)	--	84 - 87	81 - 88
Thompson et al., 1978	Orchardgrass (4%)	--	45 - 69	55 - 61
Neibling and Alberts, 1979	Bluegrass Sod (7%)	> 90	--	--
Hayes et al., 1984	Fescue (3 - 20%) slope	87 - 99	--	--
Dillaha et al., 1988	Orchardgrass (5-16%)	--	43 - 52	39 - 52

* indicates range of trapping observed

3.1.2 Role of riparian forest buffers

Similar to research on sediment removal in grass filters, research in riparian forests has been primarily targeted towards determining their nutrient removal (specifically nitrogen and phosphorous) ability. Past studies have indicated that riparian forest buffers are effective nutrient

sinks, removing and sequestering nitrogen and phosphorous from upland runoff (Lowrance et al.,
1983, 1985; Yates and Sheridan, 1983; Brinson et al., 1984; Jacobs and Gilliam, 1985; Peterjohn
and Correll, 1984; Fail et al., 1986). A detailed investigation of a 50 m wide riparian forest in the
Maryland Coastal Plain (Peterjohn and Correll, 1984) reported that plant uptake and possibly
denitrification were the two major pathways of nitrate loss. Their study indicated that subsurface
flow was responsible for most of the N movement in forest buffer zones and that 89% of the
incoming N was retained in the riparian forest. Phosphorous trapping, however, was primarily
due to trapping of sediment-bound P carried by surface runoff. Uptake and consequent long-term
storage of N and P in riparian vegetation were estimated to be 15 and 2.1 kg/ha, respectively.

Studies in the North Carolina Coastal Plain (Cooper and Gilliam, 1987) indicated that P
retention in riparian forests was the result of two mechanisms, adsorption, and deposition of
enriched sediment. They observed that P concentrations in the sediment near streams and
floodplains were higher than that in the parent upland soils. They found a direct correlation
between P and the clay content of riparian buffer soils. They concluded that riparian buffers had a
finite capacity to trap and store P that depended on the deposition of fresh sediment and continual
nutrient uptake by vegetation.

Other recent studies have indicated that mechanisms of N loss such as plant uptake and
denitrification are site specific and seasonal. Jacobs and Gilliam (1985), investigating forested
buffers with poorly drained soils in the North Carolina Coastal Plain, attributed most nitrate loss
in forested buffers to denitrification (9.9 to 54.9 kg/ha). A high water table and high soil organic
content seem to provide optimum denitrifying conditions. Similar observations have also been
reported by Hendrickson (1981) and Herrick (1981). In contrast, studies on well drained
agricultural upland soils (Fail et al., 1986) have indicated that plant uptake is the dominant N sink.
Fail et al. (1986) compared plant production rates, tissue nutrient concentrations and nutrient
accretion rates of woody plants adjacent to a hog production facility and cropland. They observed
higher uptake rates with higher nutrient loadings. The N uptake rate of the riparian forests
adjacent to the hog production facility and cropland were 97.6 and 36 kg/ha, respectively. Other
studies have confirmed the importance of riparian zones as sinks for nutrients (Pinay and
Decamps, 1988; Jordan et al., 1993; Lowrance, 1992; Simmons et al., 1992; Groffman et al.,
1992). These studies provided results similar to those above, but emphasized the variability of

nutrient retention mechanisms with changing site, vegetative and soil conditions. Table 3.2
provides a summary of results from selected riparian forest studies.

Table 3.2: Summary of results of selected forest buffer studies

Reference	Forest width (m)	% Reduction *			
		Surface		Subsurface	
		N	P	N	P
Peterjohn & Corell, 1984	19	--	74	93	33
Peterjohn & Corell, 1984	50	79	85	99	- 114
Jacobs & Gilliam, 1985	16	--	--	93	--
Lowrance et al., 1984	25	--	--	68	--
Pinay & Decamps, 1988	30	--	--	100	--
Doyle et al., 1977	30	98	--	--	--
Cooper & Gilliam, 1987	16	--	50	--	--

* indicates % reduction in surface and subsurface flows

Some important observations and conclusions that can be derived (or that need to be
repeated) from the multitude of studies described above are:

- Riparian forest buffers act as effective nutrient sinks only when - [a] surface runoff (if
  present) is not excessively channelized; [b] there exists an impeding layer at a shallow
  depth that forces most of the subsurface flow to pass through the root zone; [c] the riparian
  forest vegetation is in a state of continuous growth; or [d] riparian soils are sufficiently
  moist and anaerobic to ensure denitrification loss.
- Surface runoff in riparian buffers is rarely observed. The predominant mechanism of
  water flux is subsurface flow - either in form of matrix flow or pipeflow.
- Total P is predominantly trapped as a result of sediment deposition in the forest zone and

grass filter.

- Nitrate (and total N) from upland runoff is primarily removed via plant uptake or denitrification.
- Riparian forests have typically been observed to have higher growth/uptake rates than neighboring upland forests.
- Presence of moisture, a carbon source (from the forest litter) and anaerobic microsites in riparian soils provide an optimum environment for denitrification to occur.
- Over a long period, riparian buffers can be expected to become nutrient saturated.

3.1.3 Conclusions from literature

As can be seen from the information presented above, grass filters and forest buffers have been found effective in trapping and sequestering sediment and nutrients. However, one needs to note that these zones may not be equally effective at all sites. The effectiveness of these buffers is highly dependent on site conditions such as site slope, soil type, soil layers and their depths, vegetation, surface characteristics, and moisture status. Sites conditions directly influence important pollutant sequestration processes such as sediment deposition, nutrient uptake, and denitrification. Thus, any model that attempts to simulate riparian buffer performance should have the ability to consider this site to site variability and thereafter adjust the buffer zone processes accordingly.

For simulation purposes the above studies indicate that:

- Grass filters can be expected to be effective in controlling sediment bound pollutants traveling with surface runoff. Their effects on subsurface flow are unknown. Hence while simulating riparian buffer zone behavior, effects of grass filters on surface runoff and sediment transport need to be considered.
- Major phenomena by which grass filters influence surface runoff include reduction in surface flow velocity due to increased surface roughness provided by dense grass vegetation; and enhanced infiltration due to porous nature of the grassland soils. While simulating grass filter performance these two characteristics namely, increased surface roughness and enhanced infiltration, need to be represented.

- Channelization of flow can significantly reduce filter effectiveness (this is also true for forest buffers). The riparian zone model should be able to represent the dynamic nature of these channel networks and their influence on surface runoff and sediment trapping.

- Enhanced infiltration and shallow subsurface flows (if an impeding layer exists) are the predominant hydrologic phenomena that occur in the forest zone. If a restricting soil layer is not present most of the subsurface flows might be lost to deeper groundwater flows. A riparian forest zone model should be able to simulate these two contrasting scenarios (i.e, presence or absence of shallow subsurface flow depending on the presence/absence of an impeding layer). Subsurface flows might occur via matrix flow or pipeflow. These two distinct flow types should be represented.

- Fine sediment and other suspended particulate matter can be expected to be trapped in the forest zone, primarily due to loss of surface runoff to infiltration and by resistance offered by the thick litter layer. Simulation approaches need to be developed to represent these phenomena.

3.2 Scale and hillslope forms

3.2.1 Concept of "representative scale"

The increasing use of models to simulate field, hillslope, catchment hydrology has resulted in greater attention and scrutiny of the concept of scale in hydrology. Recent reviews have identified the "scale problem" as a major unresolved problem in hydrology (e.g., NRC, 1991). The most relevant publications on this issue include Dooge (1982; 1986), Klemes (1983), Wood et al. (1988, 1990), Beven (1991) and a host of recent publications presented at the recent Robertson Workshop on "Scale Problems in Hydrology" (Sivapalan and Kalma, 1995).

The scale issue is especially critical for models that simulate hydrologic processes whose response is influenced by spatial variability. Almost all runoff production models fall in this category. Wood et al. (1988) described the representative scale as "representative elementary area" (REA). They defined REA as the critical area that is large enough to sample a sufficient population of the parameter values such that the variability in parameter values can be expressed in

terms of a probability distribution. The salient observations made by Wood et al. (1988) include: (a) the representative elementary area (REA) does exist in the context of the runoff generation response of catchments, and (b) REA is strongly influenced by the topography, through the sizes and shapes of subcatchments and its role in hydrologic response.

Though there is an increasing interest in investigating scale issues with respect to modeling, research is still in the initial stages. Information is lacking regarding the representative scales for hillslope and catchment investigations.

3.2.2 Hillslope drainage attributes

Past research has indicated that, in general, drainage areas tend to decrease with increasing slope gradients (Leopold and Miller, 1956; Hack, 1957). Recently, research has been directed towards determining the relation between slope gradients and source areas up slope of channel heads (Dietrich et al., 1986; Kirkby, 1987; Montgomery and Dietrich, 1988, 92). There are two quantitative and contrasting theories that exist with respect to the drainage/source area and slope gradient relationship. Research by Dietrich et al. (1986) indicated that for steep hillslopes where subsurface flow predominates, and where the terrain is subjected to landsliding or subsurface forces of erosion, drainage areas decrease with increasing slope gradient. In contrast, the other theory (Kirkby, 1987) predicted that for low gradient areas where overland flow predominates (saturation excess or infiltration excess), drainage areas are positively correlated to the slope gradient. Recent research by Montgomery and Dietrich (1988) on hillslopes in grass covered humid catchments revealed a distinct inverse trend between slope gradient and source areas up slope of channel heads. Despite all this information, conclusive results are still lacking. This is complicated by the fact that most hillslopes have moderate slopes where runoff generation is typically a combination of subsurface and overland flow mechanisms.

3.2.3 Hillslope forms

Research has revealed that hillslope hydrologic responses are strongly influenced by hillslope topography and shape (Freeze, 1972; Anderson and Burt, 1978, O'Loughlin, 1986;

Beven et al., 1988). Zaslavsky and Sinai (1981) in particular found slope curvature to be the most important parameter. Nieber (1979) indicated that hillslopes are dissected into valley basins and interbasins. Valley basins were defined as segments with concave slopes and concave contours whereas interbasins had convex slopes and convex contours. Tsukamato and Ohta (1988) described nine possible forms that hillslope segments can possess (Figure 3.1). They emphasized that results obtained on a single hillslope segment cannot represent runoff processes for the entire hillslope because an actual hillslope is composed of several hillslope segments with different topographic attributes. Kirkby (1986) suggests that a majority of hillslopes in humid temperate landscapes tend to have the convex profile. This is attributed to the stability convex forms possess over concave shapes in landscapes subjected to fluvial erosion (Kirkby 1986).
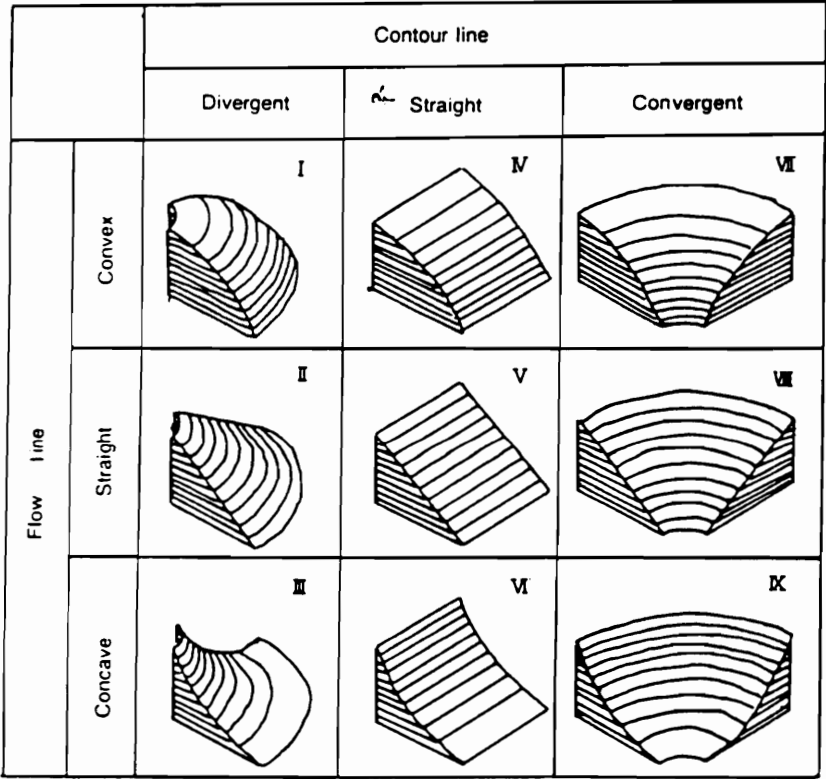
Figure 3.1: Hillslope topographic forms (Tsukamoto and Ohta, 1988)

3.3 Hydrologic processes

The following sections provide a review of hydrologic processes and approaches that can be used to simulate these processes. A majority of the information regarding these processes is available from studies performed on agricultural lands, grass filters, and hillslope forests rather than riparian forests per se, but most of the principles developed in these studies are also applicable and can be extended to describe and simulate riparian grass and forested situations.

3.3.1 Interception, stemflow and throughfall

3.3.1.1 Process description

Interception is considered a combination of processes which determine the amount of water storage on tree foliage, branches and stems. The change in water storage on foliage, branches, and stems is the sum of [a] intercepted precipitation, minus [b] drainage from canopy and stem drip, [c] stemflow to the ground, and [d] evaporation from vegetation surfaces. On an annual basis interception losses have been shown to account for 10 to 35% of the precipitation (Kittredge, 1948; Zinke, 1967). The actual amount of water intercepted may be a function of surface tension forces of water molecules and surfaces, surface area of the intercepting surfaces, configuration and texture of these surfaces, amount and intensity of precipitation, velocity of wind, humidity, evaporation rate, and antecedent moisture condition of the intercepting surfaces. The intercepting surface area of the vegetation is generally related to the type, density and age of the forest, density of the undergrowth, thickness and consistency of the surface litter and the season of the year (Kittredge, 1948). Direct effects of wind velocity and humidity are generally neglected while simulating interception due to their variable nature. Evaporation of intercepted water is a significant pathway of water loss and should be considered (Kittredge, 1948). Interception studies for grasses and herbs were conducted by Clark (1940). Clark (1940) found that interception for grasses and herbs was considerably higher than that for other vegetation types. But since Clark (1940) did not consider stemflow, in reality the net interception could be much lower than observed. Zinke (1967) provides a good review of the interception process and the approaches that can used for simulation. Zinke (1967) also summarized the major observations by various

researchers, some of which are listed below:

Studies by Horton (1919) indicated that -

● In general, interception storage for trees varies from 0.5 to 9mm.

● Interception evaporative loss during storms is less in forests than for isolated trees.

● Percent interception loss is greater for storms with small amounts of precipitation, ranging from 100 percent to about 25 percent as an average constant rate for most trees

● Most hardwood trees have similar interception loss during the growing season

● Stemflow is a relatively small percentage, ranging from 1 to 5 percent of the total precipitation, being zero in small storms

● Interception loss from needle-leaved trees is greater than from broad-leaved trees, both as regards interception storage and evaporation during rain

Chapman (1948) conducted studies on the effects of precipitation on throughfall (precipitation that is not intercepted and which reaches the soil surface through the gaps in the canopy) and found that:

● Median drop size of rain reaching the ground in the forest is always higher than in the open, and more constant than drop size in the open.

An important component of the total interception process is the interception by the litter layer present below the vegetation canopy (and on the soil surface). The magnitude of litter interception depends on litter storage capacity (via its depth and water retention characteristics) and on the frequency of wetting and the rate of drying (Helvey and Patric, 1965). Although the storage capacity of the litter can be high (typically around 10mm: Mader and Lull, 1968), the energy available (for evaporative purposes) below the vegetation is low. Hence, the absolute amount of litter evaporation is usually small, between 1% and 5% of the gross rainfall, but may constitute a significant (10-15%) portion of the total interception loss (Helvey, 1964; 1967; Helvey and Patric, 1965; Rutter, 1966).

3.3.1.2 Modeling approaches

Empirical models

Early attempts to simulate interception led to generation of regression equations that related

interception to precipitation via a linear function given by

$$I = a + bP \qquad\qquad 3.1$$

where I is interception , P is precipitation amount, and a and b are regression parameters. The major limitation of this approach is that in reality, interception is rarely a linear process. Horton (1919) proposed a relationship which computed interception as a linear function of the precipitation per shower and which is given by

$$I = S + \frac{KET}{P_s} \cdot P_s \qquad\qquad 3.2$$

where I is intercepted depth, S is interception storage (0.3 to 1.3mm), K is the ratio of evaporating leaf surface area to the protectional area, E is the evaporation rate in depth per hour during a rain, T is the storm duration in hrs, P_s is the amount of precipitation over the watershed divided by the number of showers for the months when the trees were in leaf. Merriam (1960) extended Horton's equation considering an exponential relationship between precipitation and interception, which is given by

$$I = S \left[1 - e^{-\frac{P}{S}} \right] + RET \qquad\qquad 3.3$$

where I is interception in inches, S is storage capacity of vegetation in inches, R is the ratio of vegetation surface to the projected area of the canopy, and P is the storm precipitation in inches. Equation 3.3 has been calibrated for various forest types.

Rutter et al. (1971, 1975) framework for interception

Rutter et al. proposed a detailed framework for interception computations which is illustrated in Figure 3.2. The model calculates a running water balance for the canopy and trunks of the forest stand using inputs of hourly rainfall and the meteorological parameters necessary to estimate evaporation. It computes the rate of evaporation of the intercepted water, and also the amount of water reaching the ground directly or in the form of drips from the canopy ('throughfall')

and down the trunks of the trees ('stemflow'). Evaporation (E_p) in the model is computed using the Penman-Monteith equation applicable under wet conditions. Other parameters required include: S the canopy capacity, p the throughfall coefficient, S_t the trunk capacity, C_t the depth of water on the trunks, p_t the proportion of the rain which is diverted to stemflow, e a trunk evaporation factor, and D_s and b which are used to describe drip from the canopy. Later, Gash (1979) used the Rutter et al. approach along with regression relationships defining the parameters to develop an analytical model.

RAINFALL INPUT
P

EVAPORATION
FROM CANOPY

$E = E_p \frac{C}{S}$

Canopy
input

Free
throughfall

Trunk
input

EVAPORATION
FROM TRUNKS

$E = E_{pt} \frac{C_t}{S_t}$

$E = E_p$

$(1-p-p_t)P$

pP

$p_t P$

$E_{pt} = e \cdot E_p$

C<S   C≥S

C_t≥S_t C_t<S_t

C $\frac{}{S}$

Drainage

$D = D_s \exp[b(C-S)]$

C_t S_t

THROUGHFALL   STEMFLOW
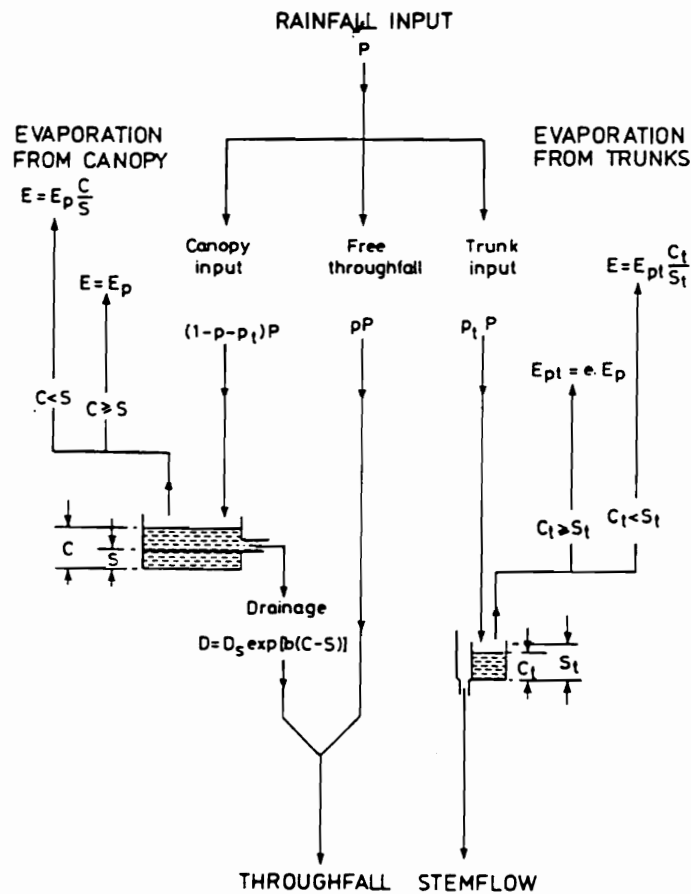
Figure 3.2: Rutter et al. model for interception

Thomas and Beasley (1986) model

Thomas and Beasley (1986) modified Merriam's (1960) equation to calculate interception as

$$INT = PIT \cdot \left[1 - e^{(-\frac{RAIN}{PIT})} \right] \cdot PER \qquad\qquad 3.4$$

where INT is the interception volume, PIT is the potential interception storage volume under maximum cover, RAIN is the rainfall volume during the period, PER is the percentage maximum canopy cover.

3.3.2 Evapotranspiration

3.3.2.1 Process description

Evapotranspiration is a combination of two distinct processes: evaporation and transpiration. Evaporation is the net rate of water transfer from the liquid to the gaseous phase. Transpiration is the transfer of water vapor by the plants through their stomatal system to the atmosphere. The importance of evapotranspiration can be underlined by the fact that approximately two-thirds of all rain falling in the continental United States is returned to the atmosphere by evapotranspiration processes. The amount of evapotranspiration at a site is generally influenced by the energy input and the moisture status. Other than the energy and moisture status the extent of evapotranspiration may be influenced by plant characteristics such as species type, canopy cover, plant height and density; soil characteristics such as soil type and soil cover; topographic features such as slope and aspect; and weather parameters such as wind speed and humidity.

Experimental evapotranspiration studies conducted on forested and grassed surfaces indicate a distinct difference (Metz and Douglass, 1959; Marston, 1962; Rowe and Reimann, 1961). These studies indicated that forest vegetation consistently used more water and from deeper depths than shallow rooted grass. The difference in water use between forest and grass was primarily attributed to the differences in rooting depth. Other factors such as differences in

vegetation growth period, density and height could also play a significant role. Studies by Patric (1961), Rowe (1963) and Rowe and Reimann (1961) suggest that early maturing of grass is another factor that could account for the evaporation difference between forest and grass cover. Studies targeted towards evaluating evapotranspiration differences within forest species (coniferous and hardwood) indicate that well stocked forests appear to use the same amount of water regardless of species (Lull and Axley, 1958; Metz and Douglass, 1959; Moyle and Zahner, 1954; Patric, 1961). There is some evidence that evapotranspiration increases with stand height in humid regions, possibly because of greater utilization of radiant energy and advective heat and increased air turbulence with increasing stand height (Patric, 1962).

3.3.2.2 Modeling approaches

Evapotranspiration computations are generally performed considering three sets of variables (Saxton and McGuiness, 1982): [a] variables related to the determination of potential ET; [b] variables related to plant and soil-water interaction; and [c] variables related to soil water characteristics. Potential ET (PET) is defined as the amount of water lost when moisture is not limiting and is a function of meteorological factors only. Methods to compute potential ET are generally classified into three major categories:

- *Aerodynamic equations*: involving measured temperatures, vapor pressure, etc.
- *Energy-budget equations*: including terms involving solar radiation, transfer of sensible heat, transfer of latent heat, in an attempt to calculate the total amount of energy available for evapotranspiration
- *Combination methods*: involving the use of both the above approaches.

Approaches commonly used in modeling crop and forest scenarios are discussed below.

Potential ET

Pan Evaporation

Pan evaporation approach uses coefficients that correlate evaporation for different vegetation to measured evaporation from standardized pans. The PET can be expressed as

$$PET = C_{ET}PE \qquad 3.5$$

where C_{ET} is the pan coefficient which is used to adjust for the higher exposure and lower reflectance of a free evaporating surface compared to a well wetted vegetated surface.

Turc's equation

Turc's (1961) equation is based on the energy-balance method. PET is computed using the relationship given by

$$PET = 0.40T \cdot \frac{R_s + 50}{T + 15}$$ 3.6

where PET is evapotranspiration in mm/month, T is mean monthly air temperature (°C), and R_s is solar radiation in langleys. Thomas and Beasley (1986) used Turc's equation in computing evapotranspiration from forested surfaces.

Penman equation

The Penman equation (1948, 1956) is an example of the combination approach in estimating PET. PET is related to temperature, humidity, wind velocity, vapor pressure, and solar radiation. The equation is expressed by

$$LE = \frac{(\Delta/\gamma)R_n + \dfrac{KLd_a u_a}{[\ln(\dfrac{z_a - d}{z_o})]^2}}{1 + (\Delta/\gamma)}$$ 3.7

where

$$K = \frac{\rho k^2 \epsilon}{P}$$ 3.8

where E is the potential evaporation rate (cm/day), Δ is the slope of psychometric saturation line (mbars/°C), γ is the psychometric constant (mbars/°C), R_n is the net radiation flux (cal/cm^2/day), L is the latent heat of vaporization (cal/g), d_a is the saturation vapor pressure deficit of air (mbars), u_a

is the wind speed at elevation z_a (m/day), z_a is the anemometer height above soil (cm), d is the wind profile displacement height (cm), z_o is the wind profile roughness height (cm), ρ is the air density (g/cm^3), K is the von Karman coefficient (0.41), ϵ is the water/air molecular ratio (0.622), and p is the ambient air pressure (mbars). Penman's equation has been observed to give good results for evapotranspiration from surfaces completely covered by short green crops under temperate conditions, where the supply of moisture is not limiting. Difficulties arise when estimates are to be made for conditions of sub-optimum moisture supply to soil and plant surfaces (Van Bavel, 1966).

Actual ET:

Actual evapotranspiration is calculated considering the effects of the other two variables (plant-water characteristics and soil-water characteristics) along with the estimates of potential ET. Actual soil evaporation and plant transpiration are generally computed separately. Ritchie's approach (1972) is the most popular method and has been used in a multitude of hydrologic models. In Ritchie's approach, soil evaporation is computed in two stages and plant transpiration is related to the leaf area index (LAI). Potential evaporation is given by

$$
E_o = \frac{0.0504 \ H_o \Delta}{0.68 + \Delta} \tag{3.9}
$$

where E_o is the potential evapotranspiration (cm), H_o is the net solar radiation (langleys) and Δ is the slope of the saturation vapor pressure curve at the mean air temperature given by

$$
\Delta = \frac{5304}{T^2} \cdot e^{(21.55 - 5304/T)} \tag{3.10}
$$

where T is the daily temperature in Kelvin.

As described earlier potential soil evaporation is simulated in two phases. In the first phase the evaporation rate is energy limited and is given by

$$E_{so} = E_o \, e^{(-0.4LAI)} \qquad\qquad 3.11$$

where E_{so} is the potential soil evaporation (cm), and LAI is the leaf area index. Soil evaporation is assumed to occur at this rate until an upper limit U which is given by

$$U = 0.9(\alpha_s - 3.0)^{0.42} \qquad\qquad 3.12$$

where U is the first stage upper limit (cm) and α_s is a soil evaporation parameter (cm/day$^{0.5}$). The second phase is considered moisture limited with the evaporation given by

$$E_s = \alpha_s(t^{0.5} - (t-1)^{0.5}) \qquad\qquad 3.13$$

where E_s is the soil evaporation rate for day t (cm/day) and t is the number of days since stage 2 evaporation started (days).

Potential plant transpiration in the model is computed in proportion to the LAI and is given by

$$\begin{aligned} E_{po} &= \frac{E_o LAI}{3} & 0 \le LAI \le 3.0 \\ E_{po} &= E_o - E_s & LAI > 3.0 \end{aligned} \qquad\qquad 3.14$$

and if soil moisture is a limiting factor the plant transpiration is further reduced to

$$E_p = \frac{E_{po} SW}{0.25FC} \qquad SW \le 0.25 \; FC \qquad\qquad 3.15$$

where E_p is the plant transpiration (cm), SW is the current soil water in the root zone (cm) and FC is field capacity (cm).

3.3.3 Infiltration

3.3.3.1 Process description

Most of the previous studies conducted in riparian and upland forests have found high infiltration rates (Lowrance et al., 1984; Rawls et al., 1976; Harr, 1977; Bonell et al., 1983). These high infiltrations rates have been primarily attributed to conditions encountered in forest soils such as porous channels due to root and animal activity, incorporated organic matter in the surface layers and possible accumulations of organic debris on the soil surface.

Due to the transmissive nature of the forest soil surface and the inherent variability involved in the occurrence of macropores, determining and simulating infiltration in forest soils has proved difficult. Existing process based infiltration models such as Green-Ampt (1911) are based on the "ponded infiltration theory" and "ideal soil" assumptions which rarely occur in forest soils. Other empirical models such as Holtan's (1961) and Horton's (1939, 1940) equations have generally been applied to upland soils and have not been tested for forested situations. Though Weirda et al. (1989) applied Mein and Larson's (1973) extension of the Green-Ampt model with reasonable success to forest soils, they encountered problems owing to an irregular wetting front from flow instability, and non-uniformity of soil porosity with depth arising from biological activity associated with the surface horizons of forest soils. Another problem that may be encountered while applying models like Green-Ampt to forest soils is the existence of lateral subsurface stormflow, which is significant on steep slopes with an impeding layer, and which violates the model's one dimensional flow assumption. Other attempts to use existing empirical models include the use of Holtan's equation to simulate infiltration in forested watersheds (Thomas and Beasley, 1986). Their (Thomas and Beasley, 1986) approach was more representative of a forest situation since they combined infiltration calculations with macropore and subsurface flow.

3.3.3.2 Modeling approaches

Green-Ampt equation

The Green-Ampt equation (1911) is a process based equation based on Darcy's Law,

which assumes a homogeneous soil profile with uniform soil moisture distribution throughout the soil profile. The infiltration process is seen as a saturation wetting front moving vertically through the soil profile, with soil moisture behind the wetting front at saturation and that ahead at the antecedent soil moisture. In its original form, infiltration with a ponded surface is given by

$$K_s t = F - N_s \ln\left[1 + \frac{F}{N_s}\right]$$

3.16

where K_s is saturated hydraulic conductivity (cm/hr), t is time (hr), F is cumulative infiltration (cm) and N_s is effective matrix potential (cm). The infiltration rate is determined by differentiating the above equation with respect to time, which leads to

$$f = K_s\left[1 + \frac{N_s}{F}\right]$$

3.17

where f represents the infiltration rate (cm/hr). Mein and Larson (1971) modified the above approach to consider infiltration as a two stage process - infiltration prior to ponding and infiltration after ponding. Prior to ponding the infiltration was assumed to be equal to the rainfall rate, and after ponding was computed using the above stated equations.

Holtan's equation

Holtan's equation (Holtan, 1961) in its modified form (Overton, 1965) is given by

$$FMAX = FC + A\left(\frac{PIV}{TP}\right)^P$$

3.18

where FMAX is the infiltration capacity with surface inundated (cm/hr), FC is the steady state infiltration capacity (cm/hr), A is the maximum infiltration capacity in excess of FC (cm/hr), TP is the total porosity within the control depth (cm), PIV is the air volume remaining in the control

depth prior to saturation (cm), and P is an empirical coefficient. Parameters that need to be defined for each soil include: total porosity, field capacity, control zone depth, steady state infiltration rate, and the two coefficients A and P. The major drawback of this equation is the difficulty in determining the parameters A and P and specifying the control zone depth. The control zone depth is used to regulate the infiltration rate and in the ANSWERS model (Huggins and Monke, 1968), which utilized the Holtan's equation, was considered equal to the depth of the A horizon. Thomas and Beasley (1986) used Holtan's equation to determine infiltration in forest soils but assumed the control zone depth to be determined by an impeding soil layer or a layer of lower permeability. ANSWERS uses a drainage function to release water from the control zone, which indirectly influences infiltration, and is given by

$$ DR = FC \left(1 - \frac{PIV}{GWC} \right)^3 \qquad \qquad 3.19 $$

where DR is the drainage rate of water from the control zone (cm/hr) and GWC is the gravitational water capacity of the control zone (cm).

Horton's equation

Horton's equation (Horton, 1940) is also an empirically based equation given by

$$ f = f_c + (f_o - f_c) e^{-kt} \qquad \qquad 3.20 $$

where f is the infiltration rate (cm/hr), f_c is the final infiltration rate (cm/hr), f_o is the initial infiltration rate (cm/hr) and K is a constant dependent on soil type and soil moisture content.

3.3.4 Depression storage and surface detention

3.3.4.1 Process description

Depression storage can be defined as that amount of water that is held in the surface depressions, none of which runs off (Horton, 1933), but which may be subsequently evaporated or infiltrated. Surface detention is that part of the rain which remains on the ground surface during

the storm, gradually moving downslope by overland flow, and either runs off or is absorbed by infiltration after the rain ends (Horton, 1933; 1937). Depression storage can represent a significant loss of water on grassed or forested slopes. Horton (1935) estimated that on moderate or gentle slopes, surface depressions can hold the equivalent of 5 to 13mm of water, and significantly more for meadow or forest land. The character of depression storage as well as its magnitude depends largely on the surface characteristics that can be generally related to the land use. The primary factors determining depression storage are surface character, roughness and slope. An accurate estimation of depression storage is difficult, thus in most hydrological models depression storage is lumped together with the interception storage.

Horton's work on surface detention arose primarily from his concern with the hydraulics of overland flow. He estimated that surface detention commonly ranges from 3 to 20mm for flat areas and somewhere between 12 to 38mm for cultivated fields and natural grassland or forests (Horton, 1935).

3.3.4.2 Modeling approaches

Beasley and Huggins (1982) developed a relationship describing the surface storage potential (depression and surface retention combined) as a function of water depth in the zone of micro-relief. This equation was based on data collected from several field surfaces and is given by

$$DEP = HU \cdot ROUGH \cdot (\frac{H}{HU})^{1/ROUGH} \qquad 3.21$$

where DEP is the volume of stored water, H is the height above the datum, HU is the height of maximum micro-relief and ROUGH is a surface characteristic parameter. Values for each of these parameters corresponding to different surface conditions were provided by Beasley and Huggins (1982). Thomas and Beasley (1986) used the same approach to simulate forested surfaces, though they adjusted the values for HU and ROUGH to better represent the surface.

3.3.5 Interflow or lateral subsurface flow

3.3.5.1 Process description

Subsurface flow seems to be the predominant pathway of water flux through riparian forests having an underlying impeding layer (Jordan et al., 1993; Peterjohn and Correll, 1984; Lowrance et al., 1983,84; Lowrance, 1992; Fail et al., 1986; Jacobs and Gilliam, 1985). Lateral subsurface flow has also been observed on hillslope forests, where most of the studies have been conducted (Lowdermilk, 1930; Hursh and Brater, 1941; Kirkby and Chorley, 1967; Calver et al., 1972). At the start of a storm, flow may occur in the vertical direction until it reaches an impeding layer. When percolation reaches a less-permeable layer (or impeding layer), which will not accept the full percolation flow, the less-permeable layer will become saturated from its surface and a saturated wetting front will slowly penetrate the less permeable layer. Simultaneously a saturated layer will develop above the interface, which will initiate lateral downslope movement of the soil moisture (Whipkey and Kirkby, 1980). This water movement is called interflow or subsurface stormflow or shallow subsurface flow. Field observations have revealed that a large portion of the runoff response from a hillslope is as a result of interflow contributions (Hursh and Brater, 1941; Roessel, 1950; Hewlett and Hibbert, 1963, 67; Mosley, 1979; Weymour, 1970, 73; Troendle and Hohfmeyer, 1978; Anderson and Burt, 1978). On forested hillslopes, interflow typically occurs via the soil micropores (soil matrix) or larger cavities or pores termed as macropores or soil pipes. Though interflow occurs as a combination of soil matrix flow and macropore/pipe flow, most field investigations indicate that macropore flow contributions are orders of magnitude larger than soil matrix contributions (Tsukamoto, 1961; Whipkey, 1965, 67; Aubertin, 1971; Chamberlin, 1972; Feller and Kimmins, 1979; DeVries and Chow, 1975; Jones, 1971, 78; Weyman, 1974; Arnett, 1974; Beasley, 1977; Pilgrim et al, 1978; Mosley, 1979, 82; Beven, 1978). Large flow contributions from macropores have been attributed to the turbulent nature of flow in these pores and the high flow velocities typically associated with flow (Mosley, 1979, 82; Aubertin, 1971; Beven, 1980; Pilgrim et al., 1978). Table 3.3 provides an estimate on the flow velocities typically observed in macropores. Though a majority of studies predict macropore flow contributions under saturated soil conditions, a small number of hillslope investigations indicate that vertical or lateral macropore flow may also occur under unsaturated soil conditions (Bouma and Dekker, 1978; Beasley, 1977; Aubertin, 1971; Bouma et al., 1977; Mosley, 1979, 82). Figure 3.3 illustrates the diverse nature of runoff mechanisms on forested hillslopes.

Table 3.3: Recorded macropore flow velocities (m/s) (from Beven and Germann, 1982)

Reference	Mode of determination	Max.	Mean	Min.
Mosley, 1982	flow observation	0.0-0.0208	0.0-0.0098	
Aubertin, 1971	flow observation	0.00508		
Beven, 1980	tracer experiment	0.005		
Pilgrim et al., 1978	flow observation			0.00025
Beasley, 1977	from lag time of hydrograph	0.00925		
Whipkey, 1965	flow observation	0.00085		
Newson and Harrison, 1978	Tracer experiments		0.06-0.2	
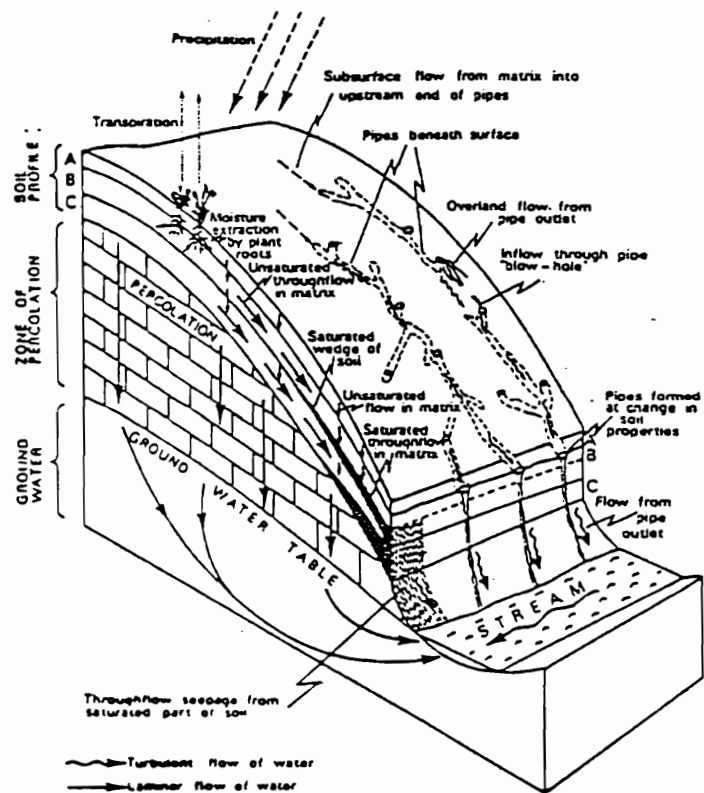
Figure 3.3: Subsurface flow types occurring on forested hillslopes (Whipkey and Kirkby, 1980)

In conditions where the soil horizon depth decreases, or where upslope contributions are sufficiently large the saturated layer building up over the impeding horizon may reach the surface. In such conditions any additional rainfall falling on the soil surface cannot be accepted by the saturated soil mass and runs off as overland flow. This runoff is called saturation overland flow (Dunne and Black, 1970a,b; Dunne et al., 1975; Beven, 1978; Bonell and Gilmour, 1978; O'Loughlin, 1986). In addition, it is also possible for upslope subsurface flow contributions which cannot be discharged via the saturated soil depth to be released to the surface. This phenomenon is called exfiltration (as opposing infiltration) or return flow (Hewlett, 1974; Dunne and Black, 1970a, b). Similar to interflow, return flow to the surface can occur either via the soil matrix or macropores. The hillslope areas where saturation overland flow occurs and where return flow emerges have been termed "variable source areas". The term "variable" being based on the fact that in plan these areas expand or contract as the subsurface saturated layer rises and falls. In addition to the subsurface saturated soil layer reaching the surface, generation of "variably saturated areas" has also been attributed to the presence of capillary fringe above shallow water tables. This mechanism is described as "groundwater ridging" (Ragan, 1968; Skalsh and Farvolden, 1979; Abdul and Gillham, 1984; Gillham, 1984). Despite some field evidence, further experimentation is needed to verify the generality of this mechanism.

In addition to soil features, favorable conditions for the generation of saturation overland flow or return flow may also be created by hillslope topography and form. Research has demonstrated that concave-convergent hillslopes provide ideal conditions for generation of saturation overland flow and return flow (Kirkby and Chorley, 1967; Burt, 1986; O' Loughlin, 1981, 86. This has been attributed to (a) the progressively decreasing soil cross section that is available at the base of the convergent hillslope, and (b) the decrease in the hydraulic gradient caused by the decrease in slope towards the base of the concave hillslope. It is very unlikely that "variable source areas" that are created at the base of the hillslope are distributed uniformly across the width. On most hillslopes these areas are widest at the base of the hillslope and slowly decrease in width as they extend upslope. This is because subsurface saturated layers first reach the surface at the lowest points or topographic depressions and then slowly expand around these depressions.

3.3.5.2 Macropore characteristics and their occurrence

Origin of macropores in soils can be attributed to soil fauna (Omoti and Wild, 1979; Ehlers, 1975; Green and Askew, 1965), plant roots (Gaiser, 1952; Aubertin, 1971), and/or to the erosive action of subsurface water (Zaslavsky and Kassif, 1965; Jones, 1971; Gilman and Newson, 1980). Though a number of field studies have supported the occurrence of macropores in structured soils, accurate quantification has been elusive. Determination of size and distribution of macropores has generally been accomplished using direct physical methods or indirect procedures. Direct physical methods include exposing and vacuuming horizontal soil planes (Edwards et al., 1988); insitu pore counts (Ehlers et al., 1983); image analysis of photographic slides of soil planes lighted to darken pores (Edwards et al., 1988); and marking outlines of macropores on plastic sheets (Logsdon et al., 1990). Indirect methods have inferred macropore diameters by measuring flow rates through soil cross sections and related macropore diameters to these flow rates. Watson and Luxmoore (1986) estimated vertical infiltration rates using tension infiltrometers and then related flow rates at different tensions to macropore diameters. The relation was based on the assumption that flow in macropores can be described using the laminar Poiseuille equation. The drawback of such procedures is that most of them are conducted on a small scale and thus do not provide an estimate of macroporosity at field or hillslope scale. Most of these procedures have yielded different macropore size definitions, some of which are reproduced in Table 3.4.

Only a fraction of the total macroporosity within a soil horizon is generally available to conduct water. This fraction is termed as the "hydrologically active" macroporosity (Wilson and Luxmoore, 1988). Procedures that associate flow rates to macropore diameters are essentially estimating the "hydrologically active" macroporosity rather than the total macroporosity. Using one such procedure Watson and Luxmoore (1986) found that macropore diameters tend to be lognormally distributed. This was inferred from the fact that infiltration rates measured using the tension infiltrometer in this study were lognormally distributed. Thus, the lognormal distribution generated in this study is applicable only to the "hydrologically active" fraction of the macropores and cannot possibly be extended to describe the complete macropore distribution constituting the total macroporosity.

Table 3.4: Macropore size estimates (modified from Beven and Germann, 1982)

Reference	Equivalent diameter (μm)
Luxmoore (1981)	> 1000
Beven and Germann, 1981	> 3000

Reeves (1980)
 	
      enlarged macrofissures
      macrofissures
	
	2000 - 10,000
	200 - 2000

Bullock and Thomasson (1979)	60

Brewer (1964)
 	
      coarse macropores
      medium macropores
      fine macropores
      very fine macropores
	
	5000
	2000 - 5000
	1000 - 5000
	75 - 1000

3.3.5.3 Soil piping and its occurrence

Soil pipes can essentially be considered a subclass of macropores. Soil pipes are essentially macropores which are larger in size and are continuous for longer lengths. Jones (1981) has provided the most comprehensive review to date regarding soil piping, and the conditions that are necessary and favorable for pipeflow to occur. Jones (1981) lists a number of factors that influence the development of pipes which include climate, geomorphology, biotic influences, and soil type. Important observations that can be derived from this review are:

- Pipes are often found in soils subject to climate variability - alternate dry and wet periods encourage soils to desiccate and crack up.
- Perpetually saturated soils (eg., wetland soils) may not be conducive to pipe formation.
- Pipe formation is most probable to occur in undisturbed forested hillslopes with an underlying impeding/restricting layer that encourages lateral subsurface flow.
- Baillie (1975) listed the main conditions for piping as:
  - a permeability contrast between upper (A horizon) and lower layers

- sufficient gradient on the impermeable layer to drain
- soil material clastic enough for particle or aggregate detachment but cohesive enough to prevent premature collapse

- Influence of soil texture: Soil piping typically occurs in soils with a moderate to high silt clay content. Piping is aided by decreasing grain size and the presence of humus and mycelia.

- Highly susceptible soils (based on existing studies) are yellow podzolic group, grey brown podzols and yellow solodics (susceptibility in high to low order).

3.3.5.4 Modeling Approaches
3.3.5.4.1 Models simulating interflow

The following discussion provides a review of hillslope models that have simulated the occurrence of interflow.

Sloan and Moore's (1984) comparison of models

Sloan and Moore (1984) provided an excellent comparison of five subsurface flow models of varying complexity by comparing their predictions to hillslope runoff measurements made by Hewlett and Hibbert (1963). These five models were - a two dimensional finite element model (Neiber, 1979; Neiber and Walter, 1981) and a one dimensional finite element model (Nieber, 1982), both based on Richard's equation; a kinematic wave subsurface flow model (Beven, 1981, 82); and two simple storage discharge models termed the kinematic storage model (based on the kinematic approximation) and Boussinesq storage model (uses the Boussinesq assumption) (Sloan et al., 1983). The following sections provide a brief description of each of the models followed by the results of model comparisons performed by Sloan and Moore.

Neiber's two and one dimensional finite element models

Both models are based on Richard's equation for flow in saturated and unsaturated porous media, which in two dimensional form is given as

$$\frac{\delta \theta}{\delta t} = C(h)\frac{\delta H}{\delta t} = \frac{\delta}{\delta x}\left[K(h)\frac{\delta H}{\delta x}\right] + \frac{\delta}{\delta z}\left[K(h)\frac{\delta H}{\delta z}\right] \qquad 3.22$$

where H is the total hydraulic head (= h+e), h is the soil water pressure head, e is the gravity head, θ is the volumetric water content, C(h) is the specific water capacity, K(h) is the unsaturated hydraulic conductivity defined by Verma and Brutsaert (1971), and x and z are the distances in the horizontal and vertical directions. The above equation is reduced to one dimension by considering flow in the direction of the slope gradient and assuming hydrostatic conditions normal to this gradient. The resulting one dimensional form of the equation is given by

$$DC(h)\frac{\delta H}{\delta t} = \frac{\delta}{\delta x}\left[K(h) \ D\cos^2\alpha \ \frac{\delta H}{\delta x}\right] + i \qquad\qquad 3.23$$

where D is the vertical soil depth, α is the angle of the impermeable to the horizontal, and i is the rate of water input to the saturated zone from the unsaturated zone normal to the surface.

A finite element approach is applied to the space domain of both models and is solved using a fully implicit backward finite difference scheme. Discretization of the flow regime is accomplished using triangular and linear elements in the two dimensional and one dimensional models, respectively.

Kinematic Wave Model

The kinematic assumptions used in the models that (a) flow lines in the saturated zone above the impermeable layer are parallel to the layer and that the hydraulic gradient equals the slope of the bed. Using these assumptions gives

$$q = K_s H_x \sin\alpha$$
$$C\frac{\delta H_x}{\delta t} = -K_s \sin\alpha \ \frac{\delta H_x}{\delta x} + i \qquad\qquad 3.24$$

where q is the discharge per unit width, H_x is the thickness of the saturated zone, and i is the rate of water input to the saturated layer. The specific water capacity at saturation C, is equivalent to Beven's (1981) effective storage coefficient. This model was assumed to be applicable in conditions where $\lambda < 0.75$, where

$$\lambda = \frac{4i \, \cos\alpha}{K_s \sin^2\alpha} \qquad\qquad 3.25$$

Sloan et al., 1983 simple storage models

The two simple storage models developed by Sloan et al. are based on water balance and consider the complete hillslope segment as the control volume. The idealized hillslope segment was considered to have an impermeable boundary at its bottom with slope α and length L, and a soil profile of thickness D. The kinematic storage model assumes that the water table has a constant slope between upslope and downslope boundaries, and that the hydraulic gradient equals the slope of the impermeable bed. The drainable volume of water stored in the saturated zone is given by

$$S = \frac{H_o \theta_d L}{2} \qquad\qquad 3.26$$

where H_o is the saturated thickness normal to the hillslope at the outlet, and θ_d is the drainable porosity. The exiting flow rate at the base is given by $q = H_o v$, where $v = K_s \sin\alpha$.

The Boussinesq storage model is based on the assumption that the water table has a constant slope and that the hydraulic gradient is equal to this slope. Under these conditions the exiting velocity is given by

$$v = K_s \sin\beta \qquad\qquad 3.27$$

where β is the angle of the water table to the horizontal. The exiting flow rate is the product of this velocity and the saturation depth. The drainable volume of water stored in the saturated zone of the hillslope is given by

$$S = \frac{D^2 \theta_d}{2\tan(\alpha-\beta)} \qquad \tan(\alpha-\beta) < D/L \qquad\qquad 3.28$$

or

$$S = L\theta_d \left[D - \frac{L}{2}\tan(\alpha - \beta) \right] \qquad \tan(\alpha - \beta) > D/L \qquad 3.29$$

The two simple storage models, the one dimensional finite model, and the kinematic wave models were solved by coupling each one of them with a model that simulated vertical water movement from the unsaturated zone to the saturated zone.

Conclusions and results from model comparisons

Results from model application to an Appalachian hillslope study (Hewlett and Hibbert, 1963) indicated that, overall, the two simple storage models performed better than the more sophisticated finite element and the kinematic wave models. It was expected that runoff from the forested hillslope was a combination of macropore and soil matrix flow. It is expected that for forested hillslopes where porous soil conditions exist, finite element models based on the Richard's equation would be expected to perform poorly because the diffusion type flow assumptions inherent in the models are violated. These results confirmed that field verification is essential because the complex models may not be very good standards for testing and validating other models.

3.3.5.4.2 Modeling approaches for macropore flow

A majority of the macropore flow models developed to date have simulated vertical macropore flow on a plot scale. There have been only a few attempts to simulate macropore flow at the field or hillslope scale. Most of the macropore flow models can be classified into three categories - [a] mechanistic models, [b] statistical models, and, [c] statistical mechanistic models. Mechanistic models assume that flow in the soil occurs through two domains - the soil matrix domain where flow is Darcian and the macropore domain where flow is predominantly non-Darcian. Examples of such models include Edwards et al. (1979); Hoogmoed and Bouma (1980) and Beven and Germann (1981). All these models simulated preferential flow in the vertical direction. The limitations of the mechanistic approaches to macropore flow led to the development of Transfer Function Models (TFM). The basis of TFM is a recognition that it may be impossible to obtain a full physical description of flow and transport processes considering the

soil heterogeneity, structure and preferential pathways. Thus, transfer function models attempt to describe preferential movement in terms of a distribution of residence times, which are derived from observations. The third type, statistical mechanistic models use procedures in which macropore occurrence or characteristics are described by stochastic methods and flow in macropores is based on mechanistic approaches. Models by Smetten and Collis-George (1985) and Beven and Clarke (1986) are examples of this category. As mentioned above, most of these models have been used to describe vertical flow on the plot scale. Only a few models exist that simulate macropore (soil pipes) contribution to lateral flow at a hillslope scale. Some of these models are descibed in the following sections.

3.3.5.4.3 Models simulating pipeflow

Existing modeling approaches for pipeflow can be categorized into three distinct groups (Jones, 1988):

- Empirical indirect models: Wilson and Smart (1984) and McCaig (1983) used experimental measurements to determine possible contributions from pipeflow for specific sites. No attempt was made to develop a model that could be applied to other sites.

- Statistical approaches: Gilman and Newson (1980) and Jones and Crane (1984) applied statistical tools to experimentally measured pipeflow hydrographs to establish causal factors and then develop predictive models.

- Physically based models: Physically based approaches were developed by Gilman and Newson (1980), McCaig (1983), Nieber and Warner (1991) and Thomas and Beasley (1986) who expressed pipeflow as a function of pipe size, pipe hydraulic properties, and spacing density.

Physically based modeling has been achieved by breaking the pipeflow problem into four major components and developing simulation procedures for each component (Jones, 1988):

- Contribution to pipes: Water contribution to pipes on a hillslope can occur via rising phreatic water, infiltrating rainfall, and overland flow captured via blow holes.

- Pipe geometry and hydraulic properties: Includes parameters used to describe the flow carrying capacity such as pipe diameter, mannings roughness, and slope.

- Structure and continuity of the pipe network: This component involves defining parameters such as pipe spacing, pipe connectivity and lengths. Only a few studies have been able to define these parameters using field measurements.

- Position of pipe outfalls relative to the channel

Of the physically based models mentioned above, most have developed simplified simulation procedures considering only the first three components. A few of the models along with their simplifying assumptions are discussed below.

Nieber and Warner's (1991) model

Nieber and Warner (1991) simulated flow through a completely saturated idealized hillslope segment considering a single soil pipe. The simplified situation is illustrated in Figure 3.4. The simplifying assumptions made in the model were:

1) Soil pipes are uniformly spaced across the hillslope (@ 2W) - thus only a representative portion of the hillslope with width W and with a single pipe was evaluated.

2) Soil pipes were assumed to be on the same slope angle as the hillsope.

3) The hillslope soil was considered uniformly thick and underlain by an impermeable layer.

4) Contribution of flow to the pipe was only via the soil matrix.

5) Soil properties were assumed uniform for the full length of the segment. Pipe length was considered same as that of the segment.

6) Pipes were assumed to flow full under a zero gradient.

The situation was represented by the equation for steady saturated flow in heterogenous media and is given by

$$\frac{\partial}{\partial x}(K_s \frac{\partial \phi}{\partial x}) + \frac{\partial}{\partial y}(K_s \frac{\partial \phi}{\partial y}) + \frac{\partial}{\partial z}(K_s \frac{\partial \phi}{\partial z}) = 0 \qquad 3.30$$

where $\phi = (h+e)$ is the hydraulic head, h is the pressure head, e is the elevation head, K_s is the

saturated hydraulic conductivity and x,y,z are the Cartesian coordinates. The boundary conditions for the flow problem are illustrated in Figure 3.4. The problem was solved using a finite difference method. The successive overrelaxation (SOR) procedure was used to solve the resulting system of difference equations. The solution yields the distribution of hydraulic head in the region, the discharge rate from the soil matrix, and the discharge rate into the soil pipe. The solution is dependent upon - slope angle (α), slope length (L_s), depth of soil matrix (d_s), hydraulic conductivity (K_s), depth of pipe in the soil matrix (d_p), length of the pipe (L_p), radius of the soil pipe (r), and the spacing between the soil pipes (2W). Parameters for these variables were provided.
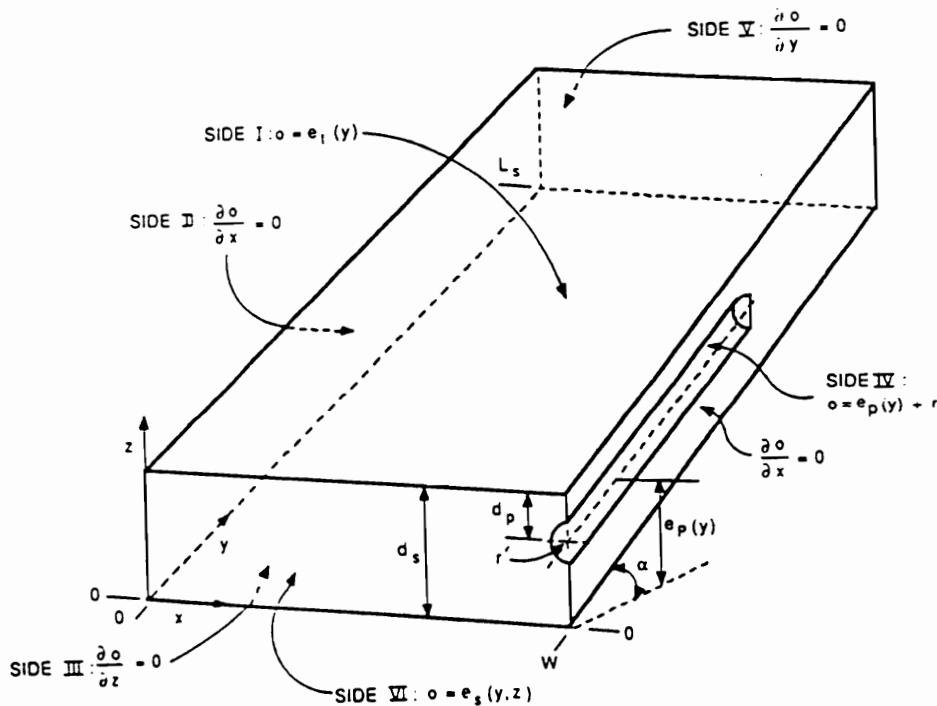
Figure 3.4: Hypothetical hillslope segment (Nieber and Warner, 1991).

Comments on the model:

1) The major limitation of the model is that the soil is assumed completely saturated and steady state conditions are assumed to prevail. These conditions will not in general prevail in the field.

2) Flow contributions to the pipe are only considered to occur from the soil matrix. In field situations, significant contributions to pipeflow will also occur due to overland flow captured via blowholes and macropores and rising phreatic surface to the pipe level.

3) The model is too mathematically intensive to be applied to long term simulation of a full riparian hillsope.

McCaig's (1983) pipeflow model

McCaig (1983) developed a much simpler model by using Chezy's equation to represent flow in pipes. For a given soil segment (similar to one illustrated in Figure 3.4) he assumed that: pipes flow half full, geometric and hydraulic properties within a segment are uniform, pipe slope is the same as hillslope (or segment slope in this case) and pipe length is equal to segment length. Though McCaig (1983) did not assume the slope segment to be saturated, he did assume that contributions to pipeflow would only initiate after a particular "threshold" soil water storage within the segment had been reached. McCaig arbitrarily established this "threshold" value for his simulations based on empirical observations made on the catchment he was simulating.

Using Chezy's equations, pipe discharge was given by

$$Q = U \ 0.5\pi r^2 \qquad\qquad 3.31$$

where U is given by

$$U = C(RS)^{1/2} \qquad\qquad 3.32$$

and

$$C = \frac{R^{1/6}}{n} \qquad\qquad 3.33$$

where R is the hydraulic radius of the pipe, S is the slope, r is the radius of pipe and n is the mannings roughness for the pipe. The above equation assumes half full pipes.

Comments on the model:

1) Some of the assumptions made in the model are too simplified. For example, Jones (1986) has found that pipe geometry and hydraulic properties vary significantly even over small distances.

2) Jones (1988) indicates that defining a "threshold" for pipeflow initiation is very difficult since pipes exist at various vertical positions within a soil column and thus are subjected to varying soil moisture levels. He classified pipes into two categories - ephemerals and perennials, according to the position within the horizons and the nature and frequency of their contributions. The two types of pipes seemed to have different "thresholds", which varied with season (Jones and Crane, 1984).

Thomas and Beasley's model (1986)

Modeling of pipeflow has also been attempted by the use of a variation of the Darcy-Weisbach equation given by

$$q^2 = \frac{8Rg}{f} \cdot \frac{d\phi}{dl} \qquad 3.34$$

where q is the discharge per unit cross-sectional area, R is the hydraulic radius, g is the acceleration due to gravity, f is the friction factor or flow resistance and $d\phi/dl$ is the hydraulic gradient for water filled pipes or the slope of the water surface in the case of uniform flow in a partially filled pipe. Although this equation has been used, parameters for the equation such as the friction factor and hydraulic radius are difficult to estimate. Thomas and Beasley (1986) attempted to simulate pipeflow using a similar variation of the Darcy-Weisbach equation.

3.3.6 Surface runoff

3.3.6.1 Process description

Typical Hortonian overland flow (Horton, 1933) has rarely been observed in forested

situations (Dunne and Black, 1970a,b; Freeze, 1972; Kirkby and Chorley; 1967). This has mainly been attributed to the porous nature of the forest topsoil where high infiltration rates occur. Surface runoff, if present, has been generally observed to take one of the following routes: over accumulated leaf debris, laterally through the surface humus/litter layers and above the mineral soil interface or in channels (Pierce, 1967). Other forms of overland flow that have been observed to occur under forested situations include (Whipkey and Kirkby, 1980):

- Saturation overland flow: Overland flow of this type is observed when receiving soil surface has already been previously saturated due to incoming upslope shallow subsurface flows. This situation especially occurs near the lower end of a forested hillslope having an impeding layer beneath the soil surface.
- Return flow or exfiltration: This form of surface flow occurs when subsurface flow is forced to the surface by a downslope thinning of permeable soil layers (Dunne and Black, 1970a,b). The partial (or variable) contributing area concept has been used by forest hydrologists to explain this phenomenon (Beven and Kirkby, 1979; Hewlett and Nutter, 1970).

Existing overland flow models are generally targeted towards simulating overland flow in upland situations where lower infiltration rates and significant surface flows are observed. Moreover, because of the nature of the runoff, most of the models are primarily concerned with simulating infiltration excess, or Hortonian type flow. Very few models exist that take into consideration the unique forms (discussed above) of surface runoff that exist in forested situations. In addition, overland flow in forest situations is rarely observed as uniform sheet flow, but is mostly present in concentrated channels whose existence is governed by surface microtopography, surface cover and slope. Though recent models have attempted to simulate this phenomenon (Lane and Nearing, 1989; Inamdar, 1993), further research is needed to better quantify the effects of channelization on overland flow transport.

3.3.6.2 Modeling approaches

Overland flow modeling has generally been attempted using approaches such as the SCS curve number (USDA, 1972) or procedures where the rainfall excess is determined after

considering abstractions for interception and infiltration.

SCS Curve number approach

The SCS procedure was developed from watershed data collected by the Soil
Conservation Service during the late 1930's and early 1940's. In its simplified form the
relationship that relates precipitation to runoff is given by

$$Q = \frac{(P-I)^2}{P-I+S}$$

3.35

where Q is the runoff (cm), P is the precipitation amount (cm), I is the initial abstraction which
could be due to interception, surface retention and detention (cm), and S is the maximum retention
(cm). From the collected data, an empirical relationship was derived which is given by

$$I = 0.2 \; S$$

3.36

where S in turn was related to another parameter called Curve Number (CN) that is given by

$$C = 2.54 \; \frac{1000}{S+10}$$

3.37

Curve number is an indicator of runoff potential from the surface and is related to soil type,
management practices, vegetation cover and density, antecedent soil moisture, and the hydrologic
condition of the watershed. Despite its simplicity, a number of major limitations of the model
make it less desirable for use in hydrologic modeling. Some of the major limitations include:

- Runoff is not related to the rainfall intensity or the duration of the storm. This could
  create a problem for discontinuous storms, or storms continuing for a duration more than a
  day.
- The method was developed using data from small agricultural watersheds, thus application
  of the procedure for forested or rangeland conditions may be inappropriate.

Process based approaches

     Overland flow routing has generally been attempted using simplified kinematic wave procedures (Woolhiser and Liggett, 1967; Lane and Nearing, 1989; Beasley and Huggins, 1982). Again, similar to determination of overland flow depth, routing procedures have generally been developed for bare to lightly covered upland slopes, and application of these procedures to upland forested slopes requires modifications to account for unique forest features such as, presence of a thick litter layer, and increased hydraulic roughness due to forest vegetation.

3.3.7 Existing "riparian" hydrology models

     The Riparian Ecosystem Management Model (REMM), a first generation continuous simulation riparian buffer zone model, is currently being developed at the USDA-ARS Southeast Watershed Laboratory at Tifton, Georgia (Altier, 1994). The primary aim of the REMM project is to develop a management oriented model that can be used by local conservation agencies to better manage, evaluate and design riparian buffer zones as a BMP. The model essentially consists of four major interactive modules - climate, hydrology, erosion and nutrient. The discussion that follows describes the hydrology module. The discussion presented below is aimed at bringing out strengths and weaknesses of the present version of the hydrology model. In addition, alternative approaches that could be used to better simulate the hydrology of the riparian system are described.

     The hydrology model is common to the three zones, namely, the grass filter zone, the managed forest zone and the undisturbed forest zone (the three zones are defined in Chapter I). Though hydrologic processes are common to the three zones, variability within the zones is represented by discretizing the full slope into three segments each having its unique inputs. The model schematic is illustrated in Figure 3.5 (Sheridan et al., 1993).

     Movement and storage of water within the riparian buffer system is simulated by a process based, two dimensional water balance operating on a daily time step. Processes simulated in the model include interception, surface runoff, vertical and lateral drainage, evapotranspiration, and deep seepage. External inputs to the model include precipitation and incoming upslope surface and subsurface flows.
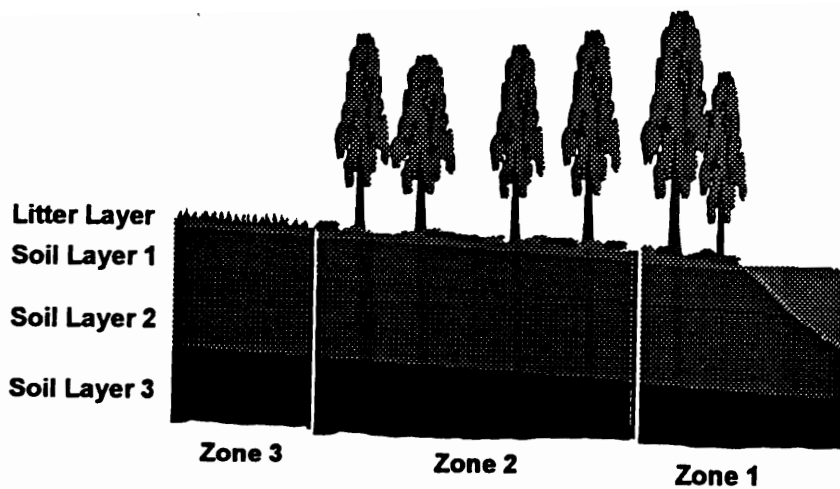
Figure 3.5: Riparian buffer simulated in REMM (Sheridan et al., 1993).

Prior to simulation the user will have to provide inputs that describe the system. These inputs include

- Site description: length, width, slope and aspect of riparian and upland contributing areas

- Daily weather data: temperature, precipitation, and solar radiation (indirectly provided by the "Climate" model)

- Soil properties: profile descriptions including layer thicknesses, porosity, permeability, and soil moisture contents at wilting point and field capacity

- Upslope inputs: daily inputs of surface and subsurface water, sediment, and nutrients from upland areas - the users are expected to utilize upland models like GLEAMS (Leonard et al., 1987) to obtain these parameters

A brief description of each of the processes follows:

Interception: Interception is simulated using Thomas and Beasley's (1986) model. In addition to canopy interception, litter interception is also simulated. Litter storage is related to the litter depth and an empirically defined litter storage capacity.

Throughfall: Daily throughfall is essentially simulated as a difference of the precipitation amount and the interception.

Surface runoff and Infiltration: Surface runoff is computed using the SCS Curve Number approach. Curve number is updated on a daily basis considering soil moisture status. The curve number approach requires total daily amount of precipitation, and break-point precipitation is not applicable. Potential infiltration is given by the difference in the net precipitation (minus interception) and the surface runoff.

Lateral and Vertical Drainage: Lateral and vertical drainage is simulated using Darcy's equation given by

$$Q = va = -K \cdot a \cdot \frac{h}{L} \qquad\qquad 3.38$$

where v is the apparent velocity, K is the soil permeability, h/L is the potential gradient and is the difference in water surface elevation over the length of the flow line, Q is the flow rate and a is the cross-sectional area. As is apparent from the above description the model does not simulate lateral flow in pipes. All the lateral flow is assumed to be matrix flow or seepage.

Evapotranspiration: Procedures for estimating evapotranspiration are based on the Ritchie (1972) and Penman Monteith equations. Evapotranspiration is considered as a sum of evaporation from the soil surface and transpiration from the plant surface. Potential ET is determined using pan evaporation data or Penman Monteith equation. Soil evaporation is determined in a two stage approach and plant transpiration is a function of leaf area index (LAI) and moisture status.

Strengths of the hydrology model include:

- A well defined model framework and a continuous simulation approach based on a daily time step. Continuous simulation can be expected to provide a better estimate of hydrologic condition in the buffer.

- Detailed representation of interception and evapotranspiration processes. Canopy

interception and evapotranspiration are related to LAI which is updated on a daily basis.

Major weaknesses of the model and alternative approaches that could be adopted include:

- A poor surface runoff simulation component (SCS Curve Number). The SCS curve approach was originally developed for small agricultural watersheds and was targeted to be used on watershed scale areas where small differences in watershed conditions could be averaged out. It was never intended to be at a scale as that of a riparian forest (width 30 - 50 m). In addition, the curve number approach may not be able to realistically distinguish between the component zones of the riparian buffer. A better approach could be determining surface runoff the using the infiltration excess method. An infiltration equation such as Holtan's equation could be used. The control zone parameter in the equation could physically represent the depth to impeding/restricting layer below a riparian forest.

- In REMM the subsurface pipeflow component is completely neglected. Depending on site conditions significant contributions from pipeflow are possible. Though granted that at present there are no sophisticated models available to describe pipeflow, models such as that developed by Thomas and Beasley (1986) can provide a first estimate of the process. The use the such a model will simulate to at least a small measure the quickflow response associated with pipes.

- The REMM model does not consider effects of surface channelization of flow. Channelization of flow can significantly influence the movement of surface runoff through the buffer and consequently affect the quantity of sediment and pollutants trapped. Channelization could be represented in a stochastic manner using procedures developed by Inamdar (1993).

3.4 Sediment Transport

3.4.1 Process description

Most of the coarse (> 100 micron) sediment washed off agricultural fields is immediately deposited at the upslope edge of a riparian zone due to reduction in surface runoff velocity and

loss of runoff to infiltration. Only fine sediment (< 50 micron) is expected to be transported downslope if surface runoff is sustained. Soil detachment/litter transport, though rarely observed, may occur if the sediment load is less than the transport capacity of flow. Sediment transport, detachment and deposition processes within riparian zones are primarily restricted to rills or channels. Most of the interrill areas have a thick litter cover which significantly reduces the possibility of soil erosion in these areas.

Some erosion and detachment may also occur at the lower edge of the riparian slope where saturation overland flow or return flow is observed. Two unique erosion conditions are possible in such locations. Soil/litter (from O, A horizon) may be made available for transport by miniature soil slumps created because of undermining of the topsoil layers (Higgins, 1984). Undermining of topsoil can occur due to return flow pore pressures and/or tractive forces created at pipeflow openings. This soil/litter and any previously deposited non-cohesive sediment will then be transported downslope by fluvial tractive forces associated with return and/or saturation overland flow. In another condition, fine soil particles (< 10 micron) may be scoured from soil pipes and introduced into overland flow by pipeflow returning to the surface (Dunne, 1988). Though these erosion phenomena have been observed by many researchers not much is known regarding the significance of these processes in terms of total soil loss/erosion from riparian slopes.

3.4.2 Sediment detachment, transport, and deposition models

Modeling soil detachment/deposition has been accomplished using both empirical and fundamental methods. Empirical methods are based on equations developed from extensive data sets and are not generally based on physical processes. In contrast, fundamental methods attempt to model the physical processes and thus are more representative of the actual physical situation. The parameters that determine the erosion process can either be defined deterministically or stochastically. A deterministic definition would require a known or assumed description of the erosion parameters. A stochastic definition would attempt to define parameters or processes that are random in nature and are difficult to predict at a given location in space or instant of time.

For determining erosion on bare soil surfaces, there exists a range of stochastic as well as deterministic models. At present, few models exist that can simulate sediment transport and

deposition in grass filters and forest buffers. This section discusses the fundamental processes behind sediment detachment and deposition and the influence of rills and channels on sediment transport. Most of the principles discussed in the following paragraphs can be extended to simulate sediment transport and deposition in grass and forested buffers. Later in this section, existing grass filter models are described.

3.4.2.1 Sediment deposition and detachment

Basic principles and concepts

Soil erosion and sedimentation occur as a result of three unique and interrelated processes, soil detachment, transport and deposition. Soil detachment is defined as the process in which soil particles are separated from parent bed material by forces of raindrop impact or flow shear. Runoff is initiated when the rainfall intensity exceeds the infiltration rate. Runoff then dislodges sediment particles when the runoff shear forces exceed the critical shear forces that hold the particles together at their point of origin. Once detached, the sediment particles are transported downslope along with the flow via a phenomenon termed sediment transport. The sediment is transported downslope until a point is reached where the runoff energy becomes less than the energy required for transport of the particles. At this point deposition occurs. Finer sediment or smaller sized particles, which require lesser energy for transport, travel farther before depositing. This phenomenon is called sediment enrichment. Runoff energy may decrease or increase downslope, depending on the amount of runoff and the surface on which it flows. If the infiltration rate goes on increasing as the flow proceeds downstream, runoff energy will be reduced as the runoff is lost to infiltration. Runoff energy or transport capacity may also decrease when flow reaches a rough surface, for example, grass media which provide resistance to the flow. Under such conditions the runoff velocity decreases and deposition occurs.

When rainfall occurs, runoff initially occurs as shallow sheet flow, but tends to concentrate as it moves downslope, leading to channelization of flow. These small flow channels are called rills, and the areas between them where shallow flow still exists are called interill areas. Rainfall splash is the major detachment mechanism in interill areas, whereas flow shear is the overriding detachment force in rills. Rills can be obliterated by tillage and are randomly located

for each storm event at points controlled by the surface microrelief. As the flow proceeds downslope, and as detachment occurs, rills become deeper and more permanently etched on the terrain. Such channels are then called ephemeral gullies. Ephemeral gullies are channels formed on the soil surface at points controlled by the macrotopography. Thus, they form at the same place for each storm event.

Foster and Meyer (1975) presented the above discussed principles of rill and interill transport in the form of an equation called the statement of continuity of mass transport. Assuming steady state conditions this equation can be given by

$$D_r + D_i = \frac{\partial q_s}{\partial x} \qquad\qquad 3.39$$

where q_s is the sediment load, x is the distance downslope, D_r is the rate of detachment/deposition in the rills and D_i is the rate of detachment/deposition in the interill areas. For non-steady state conditions the equation is given by

$$D_r + D_i = \frac{\partial q_s}{\partial x} + \rho_s \cdot \frac{\partial cy}{\partial t} \qquad\qquad 3.40$$

where ρ_s is the mass density of sediment particles, c is the concentration of sediment in the flow and y is the flow depth varying with time t.

In the development of the continuity equations, deposition or detachment was assumed to be independent of the sediment in the flow. Meyer and Monke (1965) proposed that detachment and deposition are not independent of the sediment load but are rather influenced by it. Hence considering the interdependence between detachment and deposition, Foster and Meyer (1972) then further defined detachment by the equation

$$D_r = C_1 (T_c - q_s) \qquad\qquad 3.41$$

where T_c is the transport capacity, q_s is the sediment load and C_1 is a coefficient. Foster and Meyer proposed that if the runoff impinges on an erodible layer and has sufficient transport capacity, detachment will be initiated. This detachment will increase down the slope until a point at which the sediment load in the flow is equal to the transport capacity. Any reduction in the

transport capacity beyond that point due to changes in the flow hydraulics will lead to deposition of the sediment. Thus, transport capacity and sediment load are the limiting conditions that govern deposition or detachment. The interaction between sediment load and transport can be written in equation form as

$$\frac{D_r}{C_1 T_c} + \frac{q_s}{T_c} = 1.0$$

3.42

or in alternate form can be given by

$$\frac{D_r}{D_{rc}} + \frac{q_s}{T_c} = 1.0$$

3.43

where D_{rc} is the maximum detachment rate also defined as the term $C_1 T_c$ in equation 3.42. It can be seen from Equation 3.43 that when the sediment load q_s in the flow is zero, then D_r, the detachment rate, equals the maximum detachment rate, D_{rc}, and when D_r is zero, the sediment load equals the transport capacity.

Conclusions

Sediment yield from a source area is as a result of two interdependent processes - detachment and deposition. Detachment occurs as a result of rainfall splash and flow shear. Deposition occurs when the sediment is deposited because of insufficient transport capacity. Occurrence of either of the two phenomena is linked to the amount of sediment in the flow and the transport capacity. Most of the modeling efforts consider steady state conditions. Under such conditions sediment load at any point downslope is the sum of the detachment and deposition up to that point. Similarly, in the case of flow through grass filters and forest buffers, steady state conditions are applicable and sediment continuity can be assumed. In case of flow through dense grasses rill detachment/deposition dominates and interrill contribution is small enough to be neglected.

3.4.2.2 Rill/channel processes

Rill transport is one of the major mechanisms via which sediment is transported

downslope. Soil is detached in rills when the flow shear exceeds the critical forces that hold the soil particles together. Soil detachment is also enhanced due to side wall sloughing and head wall advancement in the rills. A combination of these two mechanisms leads to the development of rill networks. The following sections discuss the generation of rill networks and the methods used to represent them.

Rill networks and their development

Rill networks develop when rills forming on the soil surface join together, or when one single rill partitions into a number of rills. This network development is random in nature and prediction of its form for a given situation is virtually impossible. Hence due to its stochastic nature, there has been a minimal understanding of the development of rill networks.

Rill network development and formation was studied in detail by Leopold et al. (1964), who suggested that cross grading and micropiracy were the two important components in the development of rill patterns. Leopold et al. observed that rill patterns are initiated in a parallel form with each rill having its own drainage area. Cross grading occurred when flow overtopped in a rill and overflowed across the ridge to a neighboring rill at a lower elevation. This phenomenon by which the flow in the larger rill increased at the expense of the smaller rill was termed micropiracy.

Sediment yield and rill density

Meyer et al.(1975) observed that rill density at a section is one of the major factors influencing sediment yield at that section. Earlier, Ellison and Ellison (1947) observed that in the case of highly erodible soils, rills were located close to each other and remained approximately the same size from top to bottom. This indicated transport limiting flow with raindrop detachment and interill transport as the more dominant processes. They also suggested that for less erodible soils the rills were spaced farther apart and the rill cross sections increased down the slope, indicating that rill incision and side wall sloughing are the dominant detachment processes. Meyer et al. (1975) proposed that the degree of rilling in a plot is dependent on runoff rate, slope steepness and soil properties.

The observation that rill density influences sediment yield was supported by studies

conducted by Hirschi and Barfield (1988b) using the KYERMO model. They stated that as the rill density across the section increased, the sediment yield also increased until a maximum value was reached, after which the sediment yield decreased for any further increase in rill density. Hirschi and Barfield attributed this decrease in sediment yield to the decrease in the flow rate in individual rills as total surface runoff was distributed in increasing number of rills.

Rill network representation

There are two major approaches that are used to represent rill networks. Methods that represent the rill network stochastically and methods that determine rill network based on topographic data using digital elevation models. Stochastic methods (Karlinger and Troutman, 1989; Howard, 1971; Leopold and Langbein, 1962) which represent the statistical properties of rill network fail to simulate the actual physical appearance (Abrahams, 1984). These models do not consider parameters such as topography, consolidation and soil erodibility when delineating rill networks.

Use of digital elevation models for determining rill networks has recently been receiving attention. In this approach, preferential flow paths are determined based on microtopographic data and soil properties. One such comprehensive model was developed at the USGS Data Center by Jenson and Dominque (1988). This model takes a raster grid of topographic elevations, divides the surface into cells of equal dimensions, and then delineates the preferential flow paths.

Rill detachment and deposition

In contrast to the limited knowledge base for models available to represent rill network patterns, rill erosion on an individual rill basis has been studied extensively. As discussed earlier, the three processes that govern rill erosion are soil detachment, transport and deposition. Each of the three processes is discussed in detail in the following sections.

Rill detachment

Rill detachment occurs when the flow shear stresses acting along the rill boundary exceed the critical binding forces by which the soil particles are held together with the parent material. The rate of soil detachment can be expressed by

$$D_{rc} = \alpha(\tau - \tau_c)^b \qquad\qquad 3.44$$

where D_{rc} is the maximum detachment rate, τ is the average flow shear stress along the rill boundary, τ_c is the critical shear stress needed to detach the soil particle and a, b are constants. The average shear τ_o for a known rill cross section is given by

$$\overline{\tau_o} = \gamma RS \qquad\qquad 3.45$$

where γ is the specific weight of the water, R is the hydraulic radius and S is the bed slope of the rill. Critical shear stress for rills can be determined using Shield's diagram (1936).

Sediment transport

Sediment transport may occur in the form of wash load, bed load or suspended load. Wash load consists of fine sized particles that do not settle easily. Bed load consists of sediment particles moving along the bed of the channel by saltation, rolling or sliding. Suspended load consists of particles in the smaller size range of bed load material. Suspended load moves for an appreciable period of time in suspension.

A number of models have been developed to simulate sediment transport in rills and overland flow. Their application to any field situation is subject to the conditions present. The most common bed load transport models being used are the Yalins Model (1963) and the unit stream power concept developed by Yang (1973). Other models include Acker's and White (1973), Laursen (1958) and Einstein's bed load equation (1950). Yalin's bed load equation and Einstein's calibrated total load equation are discussed in the following sections.

Yalins's bed load equation

Yalin's (1963) equation was developed for transport of cohesionless grains of equal size on moveable bed and is given in the form of series of equations

$$\phi = \frac{q_s \sqrt{\rho_w}}{(\gamma_s d)^{3/2}} = 0.635 s Y^{1/2} \left[1 - \frac{1}{as} \ln(1+as) \right] \qquad\qquad 3.46$$

$$a = 2.45 Y_{cr}^{1/2} S_g^{-0.4}$$ 3.47

$$Y = \frac{\rho_w U_*^2}{\gamma_s d}$$ 3.48

$$s = \frac{Y}{Y_{cr}} - 1$$ 3.49

where Φ is a dimensionless transport rate number, q_s is the sediment transport rate (N/m-s), ρ_s is the particle specific weight in water (N/m^3), d is the mean particle diameter, Y is the mobility number, Y_{cr} is the critical mobility number found from Shield's curve, S_g is the sediment specific gravity, and U_* is the bed shear velocity (m/s).

Rill deposition

Deposition of sediment in rills occurs when the sediment load exceeds the transport capacity. Deposition occurs with coarser particles settling preferentially compared to the finer sized sediment. Foster and Meyer (1972) expressed deposition by

$$D_p = \alpha(T_c - q_s)$$ 3.50

where α is a deposition coefficient and other terms are as defined before.

Conclusions

Significant progress has been made in recent years in the understanding of rill growth and development, especially for rill formation on bare soils. Much research still needs to be conducted to have a better understanding of detachment/deposition in rills under grassed and forested conditions.

Representation of rill networks is another area that needs further study and research. Because of the random nature of rill networks, defining them is difficult. At present, representation of rill networks is achieved stochastically, through the use of digital elevation models coupled with topographic data. In the case of bare soils, rill network formation may be

governed by microtopography, whereas in case of grass and forested surfaces they may be influenced by macrotopography.

Basic mechanisms of sediment deposition/detachment on bare soils and grass/forested surfaces are essentially similar. But estimation of parameters such as critical shear might be complicated by the presence of vegetal cover. Sediment transport in rills on bare soils or with surface cover has generally been modeled using Yalin's, Yang's or Einstein's equations. Under cover or grassed conditions transport capacity in significantly reduced primarily due to the reduction in flow velocity. Tollner et al. (1976) modified Einstein's equation specifically for flow through grasses taking into consideration the density of the vegetal media and its effect on flow velocity.

3.4.2.3 Previous grass filter modeling approaches

A number of models have been developed that determine sediment trapping in vegetative filter strips. Currently there are no known models that have been specifically developed for forested situations. A discussion of the major grass filter models is presented.

GRASFIL

Basic principles behind development of GRASFIL

GRASFIL was developed at the University of Kentucky by conducting basic studies of sediment transport in laboratory flumes utilizing artificial vegetative media with carefully controlled geometries (Tollner et al., 1976, 82,; Barfield et al., 1979) and projecting these results to the field via a physically based model (Hayes et al., 1979, 84). According to Hayes et al. (1979), as the sediment laden flow impinges on the grass filter, its velocity is retarded, and its transport capacity is reduced. If the transport capacity is less than the inflow sediment load, sediment is deposited at the inlet of the filter media. This deposition causes the slope to increase with a resulting increase in velocity and sediment transport capacity down the deposition face.

For simulation purposes Hayes et al. (1979) considered that the filter consists of four distinct zones. The length of each zone varies with time as sediment is deposited down the filter strip. In zone A(t) deposition of sediment has occurred until the top of the media and essentially all the incoming load is transported down to the next zone. Sediment deposition in zone B(t)

occurs in the form of a triangular wedge with the incoming sediment being uniformly deposited along the slope. The slope of the deposition wedge is referred to as the equilibrium slope. In zones C(t) and D(t), the assumption is made that the tractive force is less than the critical value for the original channel bed. In section C(t), it is assumed that sufficient sediment has been deposited on the original channel bed so that all the surface irregularities are filled, allowing the sediment to be transported as bedload. In zone D(t) it is assumed that insufficient amount of material has been deposited on the bed to fill the irregularities, thus all the sediment reaching the bed is considered to be trapped.

Significant infiltration is assumed to occur only in zone D(t). Since the model does not include an infiltration component, a uniform predefined infiltration rate is assumed. The assumptions made in the development of the GRASFIL model are:

- Erect, non-submerged filter elements.
- Incoming sediment load is greater than the transport capacity of the flow through the filter, hence deposition is the dominant phenomenon.
- The travel velocity of the sediment is considered the same as that of overland flow.

Development of equations for sediment trapping

Tollner et al. (1976) showed that flow velocity in VFS can be computed using a modified form of Manning's equation given by

$$V_m = (\frac{1.5}{xn}) R_s^{\frac{2}{3}} S_c^{\frac{1}{2}} \tag{3.51}$$

where xn is a calibrated value of Manning's roughness, S_c is the slope of the channel and R_s is the spacing hydraulic radius, given by

$$R_s = \frac{(S_s d_f)}{(2d_f + S_s)} \tag{3.52}$$

where d_f is the depth of flow and S_s is the spacing between the media. The flow per unit width is given by

$$q_w = V_m d_f \tag{3.53}$$

Equation 3.51 and 3.53 can be solved for flow depth and velocity. Given these values, sediment trapping can be determined in zone D(t) as described below.

In zone D(t) the layer of litter on the bed has not been covered with sediment thus bedload transport is assumed negligible. Trapping efficiency in this zone is assumed to be directly proportional to the fall velocity and inversely proportional to the flow Reynolds number (Tollner et al., 1976). Trapping efficiency in this zone is given by

$$T_s = \frac{(q_{sd} - q_{so})}{q_{sd}} = e^{(-1.05 \times 10^{-3} R_e^{0.82} N_f^{-0.91})} \qquad 3.54$$

where q_{sd} is the sediment load entering D(t), q_{so} is the sediment load exiting D(t), R_e is the Reynolds flow number given by

$$R_e = \frac{V_{mda} R_{sda}}{v} \qquad 3.55$$

where v is the kinematic viscosity and N_f is the fall number given by

$$N_f = \frac{V_s L(t)}{V_{mda} d_{fda}} \qquad 3.56$$

where V_s is the settling velocity, and L(t) is the total length of the zone varying with time.

In Zone C(t) it is assumed that there is sufficient deposition for bed load transport to occur but not enough to alter the bed slope. Tollner et al. (1982) developed a calibrated version of the Einstein bedload function to predict sediment transport in zone C(t) given by

$$\psi = 1.08(\phi)^{-0.28} \qquad 3.57$$

where Ψ is the Einstein shear intensity given by

$$\psi = (SG-1) \frac{d_{pd}}{S_c R_{sd}} \qquad 3.58$$

and Φ is Einstein's transport rate function given by

$$\phi = \frac{q_{sd}}{\gamma_s [(SG-1)gd_{pd}^3]^{0.5}}$$
 3.59

where SG is the particle specific gravity, γ_s is the particle weight density, and d_{pd} is the particle diameter.

Using principles of continuity the rate of advance of the deposition wedge X(t) is calculated using the incoming sediment load q_{si}, exiting sediment load from B(t) q_{sd}, height H(t) and slope of the deposition wedge with respect to the bed. The equation for X(t) prior to the deposition reaching the media height is given by

$$X(t) = \left[\frac{2fq_{si}t}{\gamma_{sb}S_e} \right]^{1/2}$$
 3.60

where γ_{sb} is the bulk density, t is the time after beginning of flow and f is the fraction of incoming sediment deposited on the wedge. The depth of deposition is assumed to reach the media height when

$$t_* = \frac{H^2\gamma_{sb}}{2fq_{si}S_e}$$
 3.61

For t > t. the rate of advance is given by

$$X(t) = \frac{fq_{si}(t-t_*)}{H.\gamma_{sb}} + X(t_*)$$
 3.62

where f is given by

$$f = \frac{q_{si} - q_{sd}}{q_{si}}$$
 3.63

For small slopes the relationship between S_e and the total deposition slope S_c was given by $S_e = S_{et}$ - S_c, where S_{et} is defined as the equilibrium slope. S_{et} is calculated in a trial and error solution technique using the equation

$$q_{ss} = \frac{K(R_{sb} \cdot S_{el})^{3.57}}{d_{ps}^{2.07}}$$ 3.64

where K is $6.242 \times 10^7 \times SG(SG-1)^{3.07}$.

Hayes et al. (1979) extended the above equations to consider non-homogeneous sediment. Particle size distribution was divided into three particle size classes or

- Coarse Fraction: Particle Sizes greater than 0.037 mm.

- Medium Fraction (silt): Particle sizes in the range of 0.037 to 0.004 mm.

- Fine Fraction (clay): Less than 0.004 mm.

Particles greater than 0.037 mm in size are assumed to be trapped in the sediment wedge. Mean particle size for each class is determined based on weight. Coarser particles are assumed to deposit at the leading edge of the filter (zone A and B of the filter). The medium and the fine size sediment is assumed to be trapped in the lower portion of the filter (zone C and D).

Inamdar's (1993) grass filter model

Inamdar (1993) developed an event based model to determine sediment trapping in grass filter strips considering channelization of flow. The model utilized a combination of stochastic and deterministic approaches. Channel networks forming in the grass filters were represented using a stochastic procedure whereas sediment detachment, transport and deposition in individual channels were simulated using deterministic methods. Along with channel density at a section, two other parameters, channel flow rate and shape, were also represented stochastically. Use of a combination of these two approaches (stochastic and deterministic) yielded an expected value of sediment trapping in the filter.

Channel density, flow rates and channel shapes in the grass filter were represented using probability density functions (pdf's). Microtopographic surface elevation measurements were performed on experimental grass filter plots which were then provided to a digital elevation model to delineate channel networks. Since flow rate in any single channel across a filter section is dependent on the total runoff and the channel density, flow rates were represented by a conditional pdf. For simplicity, channel shapes were assumed rectangular and were represented using a w/d (width to flow depth ratio) parameter. Since the w/d parameter is dependent on the flow rate it

was also represented using a conditional pdf. Thus, if 'n' was the number of channels at a particular cross section, its pdf was represented by f(n). If 'q' was the flow in any channel given 'n' number of total channels across the section the pdf associated with the flow 'q' was given by f(q|n). Using the same analogy the conditional pdf for 'w/d' was found to be f(w/d|q). Using these pdf's an algorithm was then developed to determine the expected detachment E(D$_r$) or deposition across the section, which is given by

$$E(D_r) = \sum_{i=1}^{imax} f(n_{[i]}) \left[\sum_{j=1}^{jmax} pf(q_{[j]}|n) \left(\sum_{k=1}^{kmax} pf(w/d_{[k]}|q_{[j]}) \cdot D_r(q_{[j]}, w/d_{[k]}) \right) \right] \qquad 3.65$$

where indexes i, j and k refer to the number of channels, flow rates and channel shapes considered, respectively, and D$_r$ is the deposition or detachment in any individual channel which was determined using deterministic procedures.

Parameters such as transport capacity, deposition and detachment were computed using deterministic procedures which are similar to that used in GRASFIL. Transport capacity was simulated using the modified Einstein' equation (Tollner et al., 1982). Deposition was simulated for two conditions - with no previous deposition (representing GRASFIL's zone D(t)) and with previous deposition sufficient to cover the surface irregularities (representing zone C(t)). Sediment deposition in the grass media was determined using the expression developed by Tollner et al. (1976). Detachment was simulated using Foster and Lane's (1983) approach. The sediment continuity equation was then used to rout the expected exiting sediment loads from each section down through the filter to yield the exiting sediment load at the bottom.

Summary and conclusions

Modeling of sediment trapping in grass filters, to date has been primarily restricted to a deterministic approach. In addition, models such as GRASFIL assume a uniformly distributed shallow flow across the width of the filter. Though such an approach gives a good initial estimate for constructed vegetative filter strips (sufficiently leveled) it overpredicts sediment trapping for naturally occurring vegetative filter strips located beside upland drainage channels. These models overpredict deposition, because the flow in these filters is rarely shallow and uniformly distributed,

thus violating the basic assumption or premise of these models. Channelization of flow can significantly influence the sediment trapping efficiencies of filters strips, especially on moderate to steep slopes.

Inamdar (1993) attempted to simulate sediment trapping in filters considering channelization of flow. The approach used a combination of stochastic and deterministic procedures to simulate the trapping phenomenon. Channel densities, flow rates, and channel shapes were represented by pdf's. Similar approaches need to be developed to simulate conditions in naturally occurring riparian grass filters and forest buffers. To apply such approaches at other locations, generic pdfs of channel density and channel shapes will have to be developed for a combination of slopes, soil types and surface roughnesses.

3.5 Model evaluation procedures

The following sections present the various approaches and procedures that have been used to evaluate model predictions.

3.5.1 Deviance measures

Deviance measures can be used when the observed and simulated values can be paired according to time, location or treatment. Two commonly used measures are:

1) *Mean absolute error* (MAE) given by

$$MAE = \frac{(\sum |y_{oi} - y_{si}|)}{n} \qquad 3.66$$

where y_{oi} represents observed values, y_{si} represents simulated values, and n the number of pairs.

2) *Root mean square error* (RMSE) given by

$$RMSE = \sqrt{\frac{\sum (y_{oi} - y_{si})^2}{n}} \qquad 3.67$$

A low value of both the above described parameters indicates that predicted values are close to

that observed. The problem with the procedures is defining an "acceptable limit" for MAE or RMSE. If MAE or RMSE values are greater than this "acceptable limit" the validity of the model is questionable.

3.5.2 Statistical procedures

3.5.2.1 Regression analysis of observed and predicted data

Regression analysis can be performed on the observed vs predicted data. Regression of the data will yield values of intercept and slope of the fitted line which then can be compared with line of "perfect fit" having an intercept of 0.0 and slope of 1.0. Statistical analysis can be performed to investigate whether fitted values (intercept and slope) are significantly different from corresponding values of the line of perfect fit.

3.5.2.2 Confidence intervals

Haan et al. (1993) recently proposed model evaluation procedures that could help determine the confidence associated with model predictions. To accomplish this, a probability density function (pdf) is fitted to predicted data and the 95% confidence bounds associated with this distribution are determined. Observed values are then plotted to determine if they fall within the 95% confidence bounds associated with model response. The mean of the observed data can be plotted in the form of a spike (Figure 3.6), or if sufficient observed data is available, the observed data can be expressed in the form a pdf (Figure 3.7). If the observed spike falls outside the 95% confidence bounds, it indicates that the model cannot predict the observed data at a 95% level of confidence. If pdfs for both observed and predicted data are compared, the overlap of the pdfs provides a measure of the predictive ability of the model. Alternately, it is also possible to estimate the probability that the simulated output will be within some preselected tolerance c, of an observed value m. The probability associated with this given by

$$P = prob \ (m-c \ \leq \ o \ \leq m+c) \qquad\qquad 3.68$$

which can also be written as

$$P = \int\limits_{-\infty}^{\infty} \int\limits_{m-c}^{m+c} p_o(o)p_m(m) \; do\,dm \qquad\qquad 3.69$$

where $p_o(o)$ and $p_m(m)$ are the pdfs for the observed and simulated data.
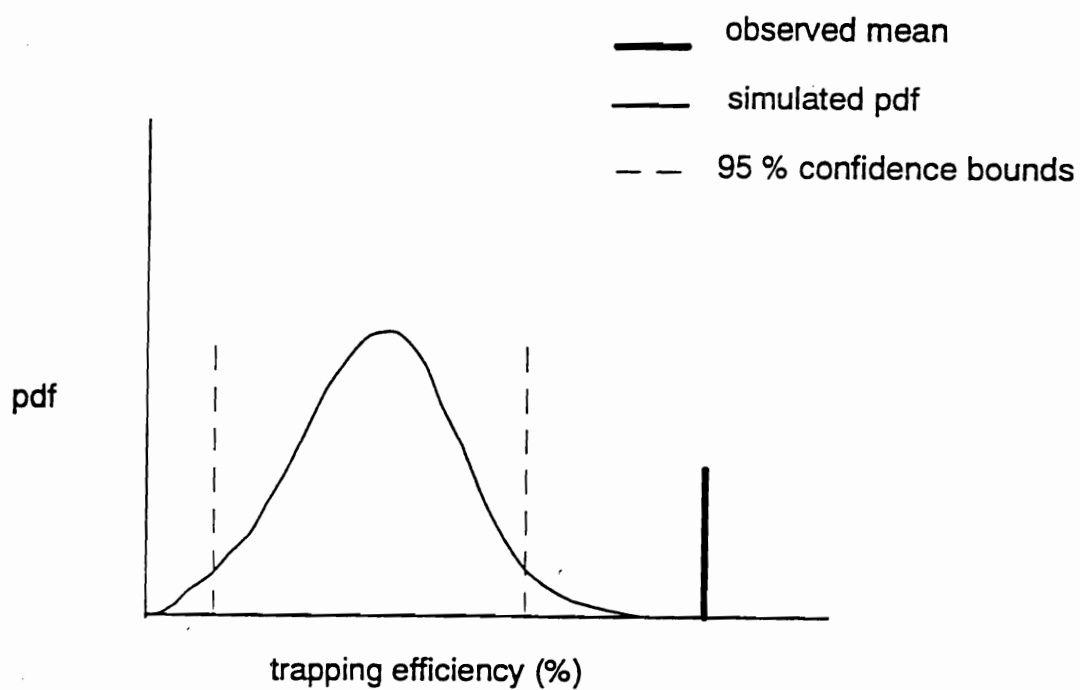
Figure 3.6: Comparison of simulated pdf and observed data.
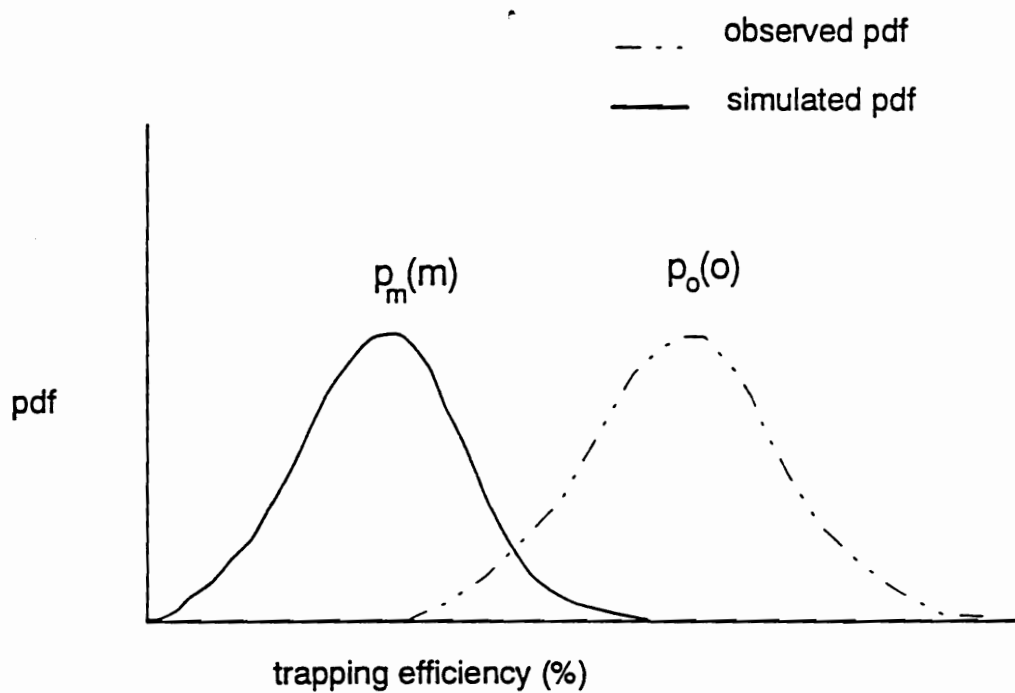
Figure 3.7: Simulated and observed pdfs.

4 HILLSLOPE SURVEYS AND DATA ANALYSIS

4.1 Rationale behind objectives/hypotheses of field surveys

The overall goal of the field surveys was to investigate the nature of and to quantify flow concentration on riparian slopes. In most circumstances, topography is the primary determinant of flow concentration. On riparian slopes this is reflected in flow concentrating along topographic depressions and drainages. This flow concentration leads to non-uniform spatial distribution of runoff as well as non-uniform runoff volume distribution as total flow is partitioned between flow channels. Flow concentration at any section along the slope can be expressed in terms of the distribution of runoff volume, and the spacing of flow channels at that section. The term channel, as defined here, includes incised rills/gullies as well as unincised depressions/valleys along which flow concentrates (Figure 4.1).

If uniform runoff generation is assumed along the hillslope, under steady state conditions the runoff at any point on the slope or in a channel is proportional to the contributing area upslope. This means that the distribution of runoff volume at any cross section can be expressed in terms of the distribution of contributing catchment areas along that section. The spacing between flow channels at any section can be determined if the exact number of channels is known. Field identification of visibly eroded incised rills/gullies is easy compared to locating unincised depressions where flow accumulation is possible. Instead of identifying the exact location of channels, this measure of flow concentration can also be expressed in terms of the catchment shape. Catchment shapes can be determined using topographic elevation data. It is expected that as catchment shape elongates, spacing between channels decreases. Hence, channel spacing can be evaluated in terms of a fundamental geomorphic attribute, namely, catchment shape.

With flow concentration being quantified in terms of catchment size and shape, the intent was to investigate if there were any distinct trends in flow concentration with slope gradient. To accomplish this, catchment size and shape were investigated over a range of slope gradients. The first objective was to determine if the runoff flow distribution varied with slope gradient.

surface channels

topographic depressions
where surface/subsurface
flow concentrates

saturation reaching
surface creates "variable
source areas"

extent of surface saturation
decided by the shape of
depression

w/d_s - surface channel
shape

w/d_b - subsurface
channel
shape

PLAN VIEW OF A HILLSLOPE
SEGMENT

SECTION A-A

w/d_s

w/d_b
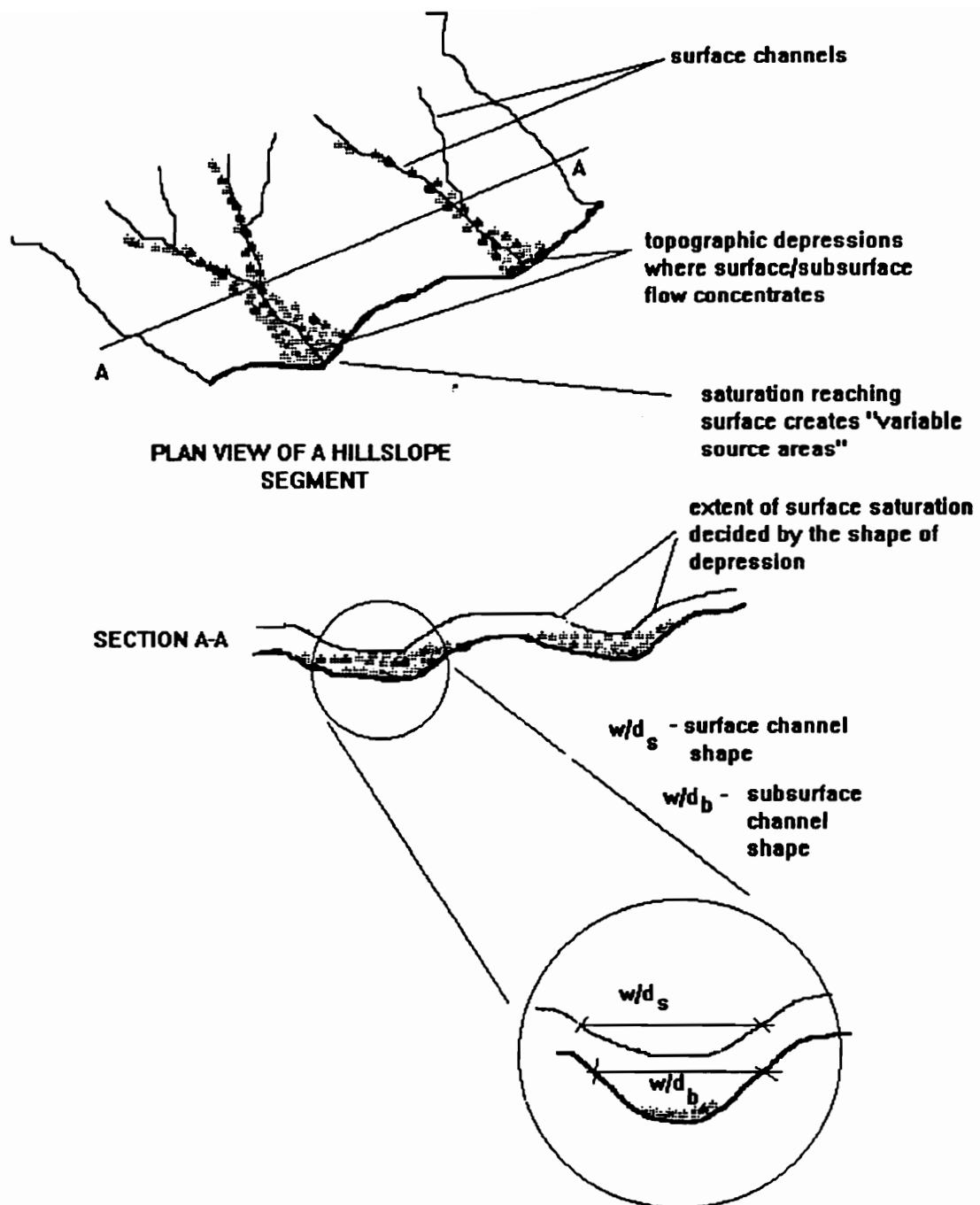
Figure 4.1: Channels and channel cross section on a hillslope segment.

The alternate hypothesis (H_a) under this objective was stated as: contributing/drainage area size decreases with increasing slope gradient. To test this hypothesis, distributions of contributing/drainage area size were compared across slope gradients. The second objective was to determine if flow channelization decreased/increased with slope gradient. The alternate hypothesis behind this objective was that contributing area shape, expressed as a ratio drainage length to drainage area, increases with increasing slope gradient. To test this hypothesis, distributions of catchment shapes were evaluated across a range of slope gradients.

In addition to flow concentration, research was also directed towards determining the distributions of drainage channel cross-sectional shapes, which route runoff on riparian hillslopes. Information on the drainage channel cross-sectional shape is important since it determines the rate of surface and subsurface flux and the spatial extent of surface and subsurface moisture distribution on a hillslope. Drainage channel shapes at the toe of a riparian slope determine the nature and spatial extent of variable source areas (Figure 4.1).

Again, similar to catchment shape and size, the intent of the field surveys was to determine if there were any distinct trends in drainage channel shape with hillslope gradient. Drainage channel shape was determined as a ratio of the drainage channel width and depth (Figure 4.1). As illustrated in Figure 4.1 every drainage channel will have two width to depth ratios, one associated with the surface and the other determined by the subsurface regime. The scope of the field surveys was limited to determining surface channel width to depth ratios. Information on distribution of drainage channel shapes is essential for routing concentrated flow in a simulation model. The alternate hypothesis behind drainage channel shape investigation was that drainage channel width to depth ratio decreases with increasing slope gradient. In other words, drainage channels tend to be more deeply incised as slope gradient increases.

4.2. Identification of hillslope sites

Hillslopes located in the Ridge and Valley Province of Virginia were targeted for topographic surveys. Surveys were performed at four major locations within this region - Virginia Tech's Whitethorne Experimental Farm in Montgomery County, Virginia Tech's Prices Fork farm

in Montgomery County, McDonald's Dairy Farm in Montgomery County and Bender Farm in Floyd County. Riparian slopes and landuse within each of the farms were typical of that in the Ridge and Valley region of Virginia. All the riparian slopes surveyed were in pasture or grass cover and were located adjacent to major field drainageways or first order channels. Hillslope gradients at the four locations ranged from 7% to greater than 25%. Hillslope sites were randomly selected within this range of slope angles.

Initial visual surveys of riparian hillslopes at these sites indicated that riparian slopes are dissected into distinct convergent, divergent or straight slope segments/units (Figure 4.2). In profile, these hillslope segments were either concave, straight, or convex. It is hypothesized that each of these units provide a unique hydrologic response and act independently of the others. The size of the segments was approximately 30-100 m along the slope and 100-300 m along the width (perpendicular to slope gradient). To capture the full topographic response of such segments, the topographic elevations were taken for the full size of each such segment/unit.

4.3 Hillslope topographic measurements and elevation interpolation

Surface point elevations for each hillslope unit were taken at an approximate grid interval of 2 m. It was expected that this resolution was adequate to capture major drainageways and depressions responsible for subsurface flow concentration and major surface flow concentration (saturation overland flow as well as infiltration excess overland flow). Point elevation measurements were taken using an Electronic instrument. A total of 26 hillslope units were surveyed. Tables 4.1 and 4.2 list slope segments with respect to slope gradient and shape, respectively. Hillslope shape classifications were made based on the classification scheme of Tsukamoto and Ohta (1988), discussed in Section 3.2.3.

Point elevation data collected at a grid resolution of 2m was then interpolated using kriging to a resolution of 1 m grid interval. The kriging was performed by SURFER (Golden Software Inc., 1990). This interpolation was performed for each of the 26 hillslope surface elevation data sets. Data files generated from SURFER were then used as input to a Digital Elevation Model (DEM) (Storm, 1991) to generate drainage area size and shape information.

---

concave convergent segment

convex divergent segment

100- 300 m

30 - 100m

response at the hillslope base determined by the topographic features of the hillslope unit
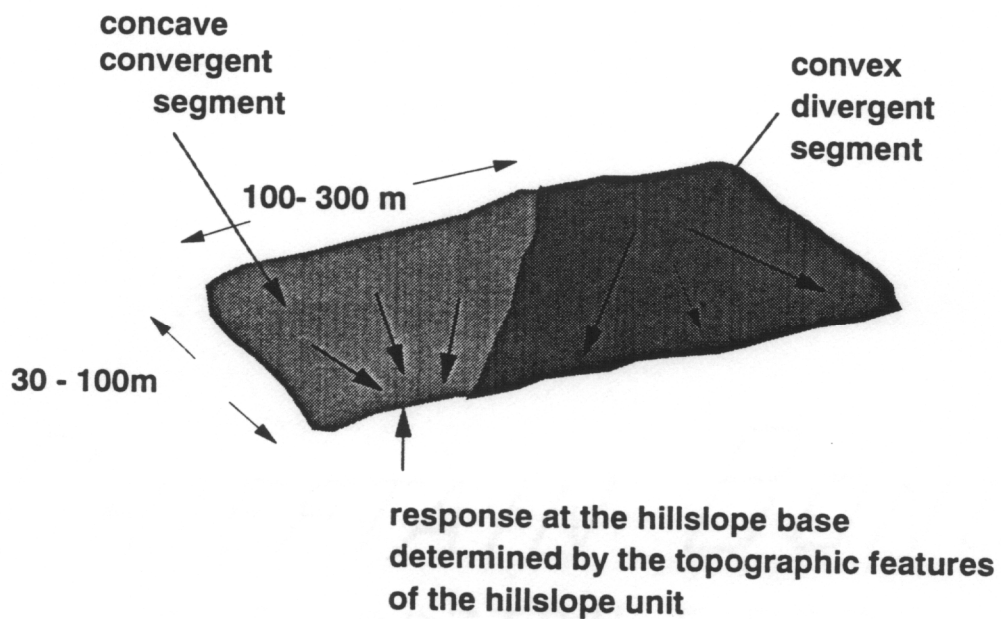
Figure 4.2: A portion of hillslope length illustrating the dissection into distinct units.

Table 4.1: Slopes of sampled hillslope segments

Hillslope gradient (%)	Number of hillslopes
0 - 10	1
10 - 15	13
15 - 20	5
20 - 25	6
> 25	1

Table 4.2: Sampled hillslope segment shapes

Hillslope shape	Number of slopes
Concave-convergent	3
Convex-convergent	5
Convex-straight	10
Convex-divergent	1
Straight-convergent	2
Straight-straight	5

4.4 Data Analysis

4.4.1 Distribution of drainage areas

Each elevation value in the interpolated elevation data files represented the elevation of a 1m x 1m cell. Using the DEM model and the interpolated elevation data, microcatchments /contributing areas/ subwatersheds were determined for each hillslope unit. Computed area was expressed as the total number of cells contributing to each catchment. Microcatchment size data

were then sorted with respect to slope gradient into three major slope categories - 7 to 15 %, 15 to 20 %, and greater than 20 %. A statistical package, VTFIT (Cooke et al., 1993), was used to fit distributions for drainage area size values within each slope category.

The comparisons of the probability distributions of drainage areas was performed for two different scenarios. These two scenarios/cases are described below:

Case I drainage area comparison:

In this case distribution of drainage areas existing within the hillslope segment were compared across slope gradients (Case I in Figure 4.3). Some of these drainage areas were subwatersheds forming a larger subwatershed on the hillslope.

Case II drainage area comparison:

In this case, drainage areas with there outlet at the base of the hillslope were compared across slope gradients (Case II in Figure 4.3). The drainage area hypotheses will be evaluated for this drainage area case, since it is expected that the distribution of drainage areas at the base of the hillslope are more representative of the slope segment (compared to Case I drainage area distribution).

4.4.2 Distribution of drainage shapes

Catchment shape was expressed as a ratio of the drainage length to the drainage area. Drainage length was determined as the distance from the catchment outlet to the furthest point on its edge along its main axis (Figure 4.4). This ratio was determined for each catchment within a hillslope unit by a FORTRAN program (attached in Appendix I). The input data required by the program included catchment identification number, its area, and the number and location of boundary cells for the catchment. This input data was generated by the DEM model. Catchment shape ratios determined using this procedure were then categorized into the three slope categories mentioned earlier. VTFIT was used to fit distributions for data within each slope category.
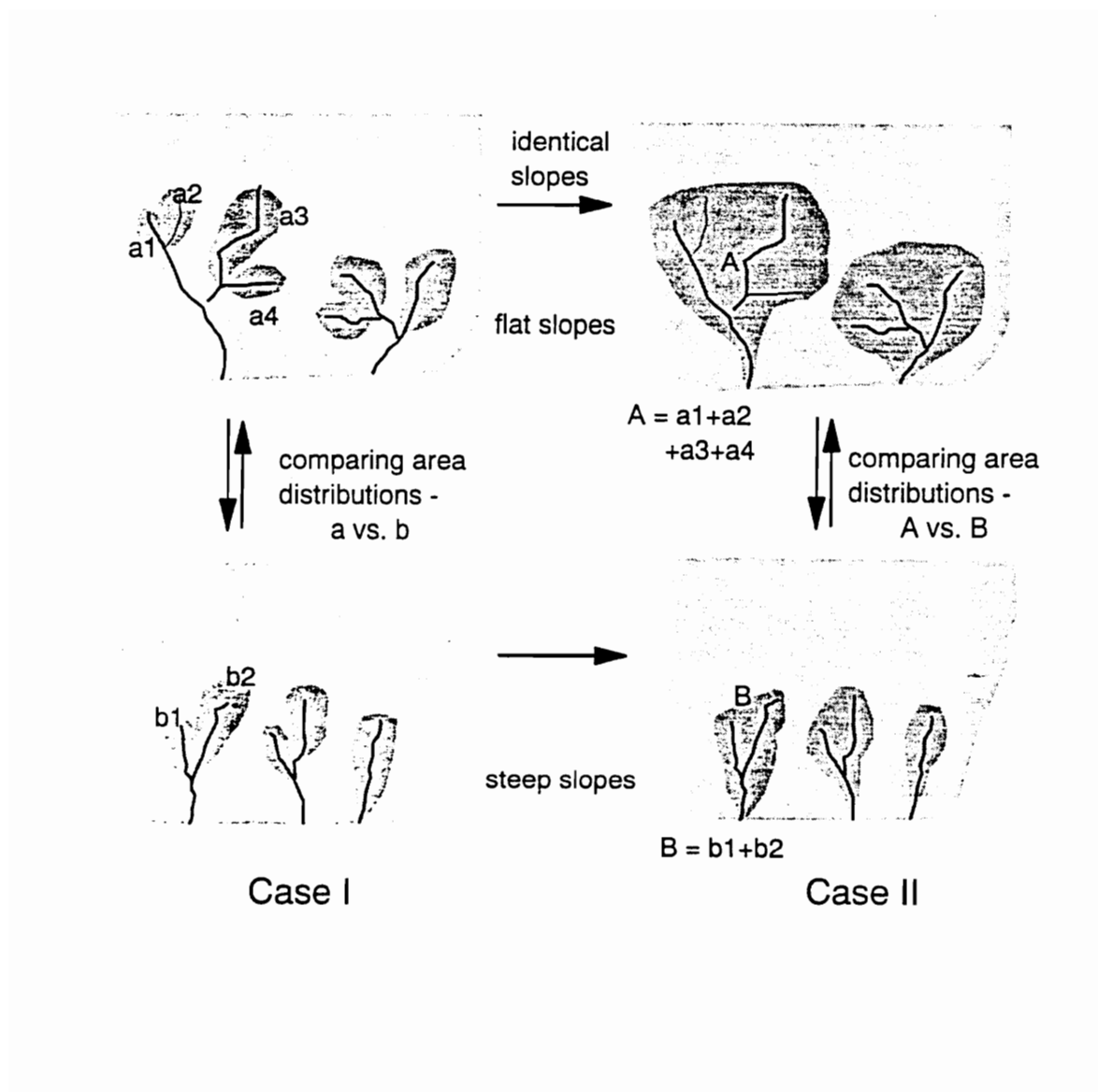
Figure 4.3: Schematic illustrating the two different approaches used to compare drainage areas on hillslopes.
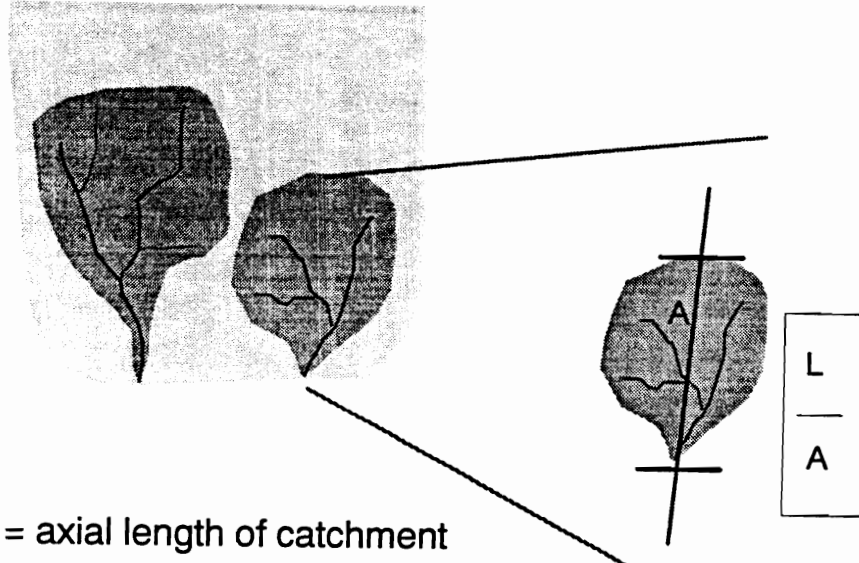
L = axial length of catchment
A = catchment area

Figure 4.4: Computation of catchment shapes

4.4.3 Distribution of channel cross section shapes

Using the 1m grid elevation data, cross sections of the hillslope were plotted. These cross-sections were selected at an interval of 5 m along the hillslope gradient. Surface width and depth of channels along such cross sections were then measured. Channel shape for each of these channels was determined as a ratio of the channel width to channel depth. Similar to drainage area size and shape, channel shape data were categorized into the three slope categories. VTFIT was used to determine channel shape distributions for each slope category.

5 HILLSLOPE SURVEY RESULTS

5.1 Representative hillslope scale

Field surveys in the Ridge and Valley region indicated that riparian hillslopes in this region are dissected into distinct hillslope segments. These slope segments were either convergent, straight, or divergent in plan, or concave, straight, or convex in section. The approximate dimensions of these hillslope segments were observed to be 30-100 m along the slope gradient and 100-300 m along the width (perpendicular to the slope gradient). Previous investigations (discussed in section 3.2) on such hillslope segments indicated that these segments provide a unique hydrologic response, which is primarily attributed to their topographic and geomorphic attributes. Contributing area sizes and shapes within each of these hillslope units are determined by the nature of the convergence/divergence and convexity/concavity of each such segment. The hydrologic response at the base of such hillslope segments/units is generated by the sum effect of all the contributing areas within the segment. Thus, evaluation of the hillslope response by considering a small portion of the hillslope segment will not be representative of the full segment. Similarly, if the portion of hillslope under investigation is larger than the size of the hillslope segment/unit, topographic features of the adjacent slope unit/segment are bound to influence the response at the base of the hillslope. If the true response of a hillslope segment is to be determined (either via field experimentation or model simulation) and related to its topographic/geomorphic features, investigation should be limited to the size of the hillslope segment. Thus, it is proposed that the size of such hillslope segments reflects the "representative hillslope scale".

Every watershed has a population of such hillslope segments through which runoff traverses prior to entering a stream or drainage channel. As mentioned in section 3.2, there are nine possible topographic forms which these hillslope segments can possess. Any one hillslope segment within a watershed with a particular topographic form (for example concave-convergent) will have a population of contributing area sizes and shapes. These contributing area size and shape values for the single segment represent only a sample from the underlying probability

distribution of these values associated with that topographic form. A more comprehensive estimate of the underlying distribution of drainage areas and shapes for a particular topographic form can be obtained by sampling additional hillslope units (existing within the watershed) having that hillslope form.

5.2 Contributing area size distributions

Probability distributions for catchment areas computed for Cases I and II were compared across the three slope categories. An analysis of variance (AOV) test was performed for the population of catchment areas for the three slope categories. Fitted lognormal distributions to contributing/catchment area size for Case I do not indicate any perceptible trend with slope gradient (Figure 5.1). But, distributions of catchment areas for Case II revealed a trend of decreasing catchment area with increasing slope gradient (Figure 5.2). The AOV test indicated that catchment area data in the three slope categories for Case II are significantly different at the 95% level. This was not so for Case I. A comparison of the mean catchment area (Case II) sampled for each slope category is provided in Table 5.1. Based on the results from Case II, the null hypothesis that catchment area does not decrease with increasing slope gradient can be rejected. The question that follows is, why did catchment area distributions for Case II show different results than those from Case I? Does this indicate scale dependency of catchment area distributions? One of the reasons could be that Case II catchment area distributions (which sampled catchment areas with their outlets at the base of the hillslope) were more representative of the full hillslope segment, in that the catchment areas were sufficiently large so as to sample the influences of slope gradient and slope convergence/divergence.

In Section 3.2.2, two contrasting contributing/catchment area evolution studies were discussed. Both studies (Dietrich et al., 1986; Kirkby, 1987) postulated that for steep hillslopes catchment area was inversely correlated to slope gradient, but the latter study (Kirkby, 1987) predicted that for low slope gradients, where overland flow was the dominant flow mechanism, catchment area was positively correlated to slope gradient. Most of the hillslopes surveyed for this field study were in the moderate slope range (10-20 %), where shallow subsurface flow as well as surface runoff (saturation and/or infiltration excess) can be expected to influence hillslope form. It

is possible that some of the hillslopes sampled in this field study reflect hillslope forms which lie somewhere in the middle of the spectrum bounded by the two case studies mentioned above.

It is also possible that determination of drainage areas in this study could have been influenced by the limitations of the DEM model. The DEM model used in the analysis can only simulate converging dendritic type channel networks and cannot realistically represent conditions where channel bifurcation is expected. Such a DEM model can reasonably simulate drainage scenarios on a convergent/straight hillslope segment but will fail to simulate the drainage form expected on a divergent-convex hillslope segment. A number of hillslopes surveyed in this study were either convex-straight or convex-divergent in form (Table 4.2). In this study, the distinction between convex-straight and convex-divergent hillslope forms was made based on visual observations. It is possible that some of the hillslopes that were identified as convex-straight could have had some divergence in plan.
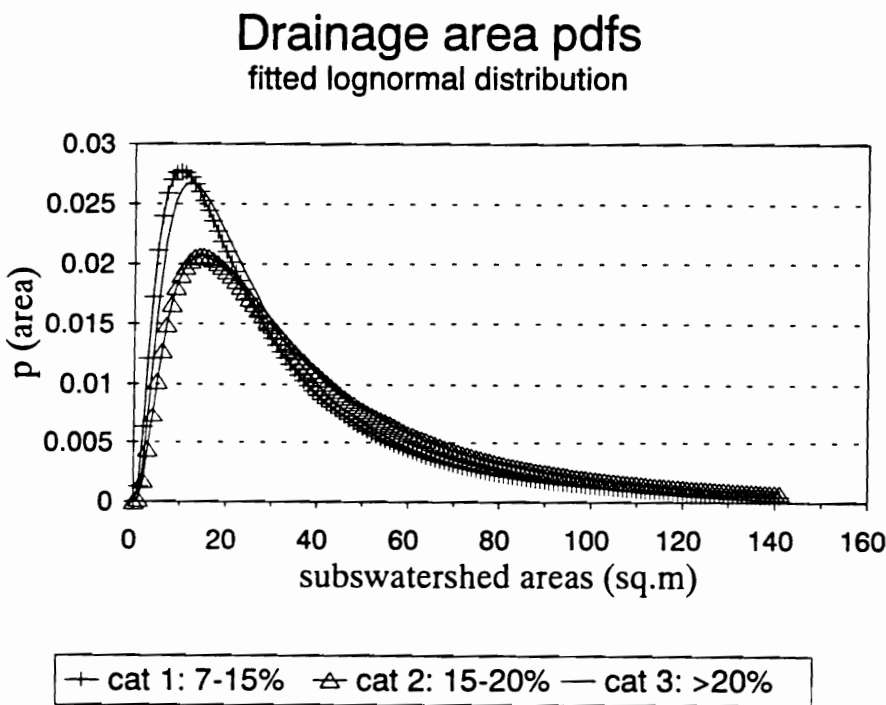
Figure 5.1: Comparison of fitted distributions for drainage areas for Case I across three slope categories.

Table 5.1: Mean values of catchment area, catchment shape (length/area), and drainage channel shape (width to depth ratio) for the three slope gradient categories (Case II).

Parameter	Slope category		
	I: 7 - 15%	II: 15 - 20%	III: greater than 20%
Catchment area (case II) m^2	296	145	118
Catchment shape (length/area) (m^{-1})	0.67	0.73	0.77
Channel shape (w/d) (m m^{-1})	114	104	55

Drainage area pdfs
fitted lognormal distribution
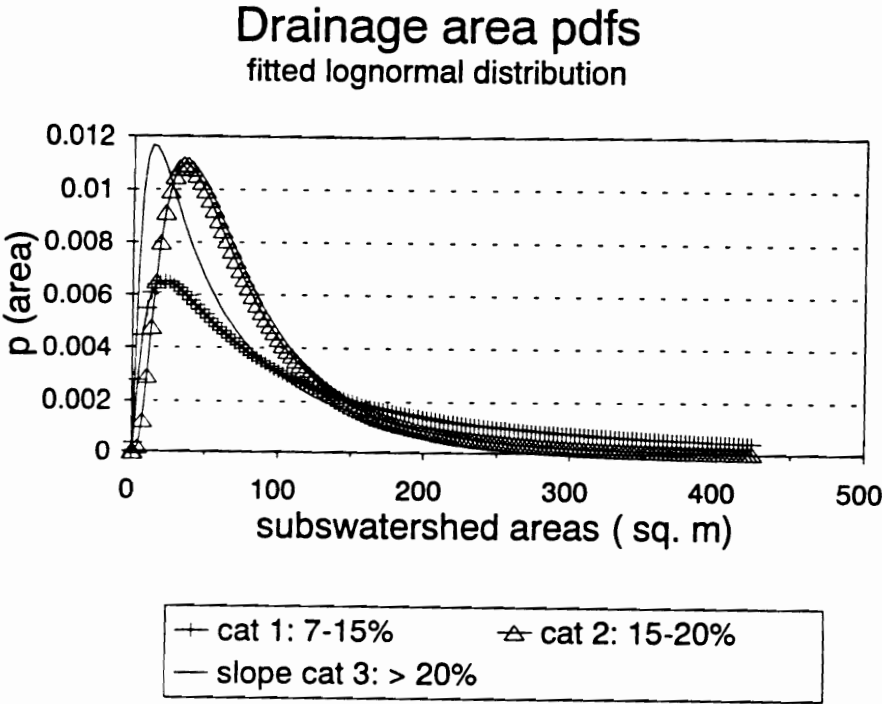
Figure 5.2: Comparison of fitted distributions for drainage areas for Case II across three slope categories.

This analysis provided an approach which can be used to quantify the distribution of runoff volumes on hillslopes. If accurate data on the contributing area size are available for a hillslope, distribution of contributing area size can provide a reasonable approximation of the runoff distribution. Such information can be effectively used while simulating runoff in hillslope models.

5.3 Contributing area shape distributions

Fitted Weibull distributions to catchment shape values for the three slope categories are provided in Figure 5.3. AOV test on the data indicate that the distributions are significantly different at the 95% level. A comparison of the mean length to area ratio of the sampled catchments for the three slope categories is provided in Table 5.1. From Figure 5.3 it is evident that catchment length to area ratio increases with increasing slope gradient, indicating catchment shape elongation with increasing gradient. This means that the average width of contributing areas on the slope decreases with increasing gradient. Extending the above argument, for a given width, steep slopes accommodate a larger number of catchments compared to moderate or low gradient slopes which results in greater flow concentration/partitioning.

At present, modeling approaches simulating flow concentration on hillslopes require the number of channels at a section as input. Estimating the number of channels, especially in cases where flow concentrates along topographic depressions and unincised drainages is difficult, if not impossible. Use of catchment shape distributions provides an estimate of flow concentration (surface as well as subsurface) based on the basic topographic features of the hillslope. In addition, using catchment shape distributions precludes the need for identifying and providing the number of channels. The number of catchments at any section along the slope can be determined using an average catchment shape value and shape distribution applicable to the slope. Total flow can then be partitioned among the expected number of catchments for a given hillslope width.

Drainage shape (l/a) pdfs
fitted weibull dist.
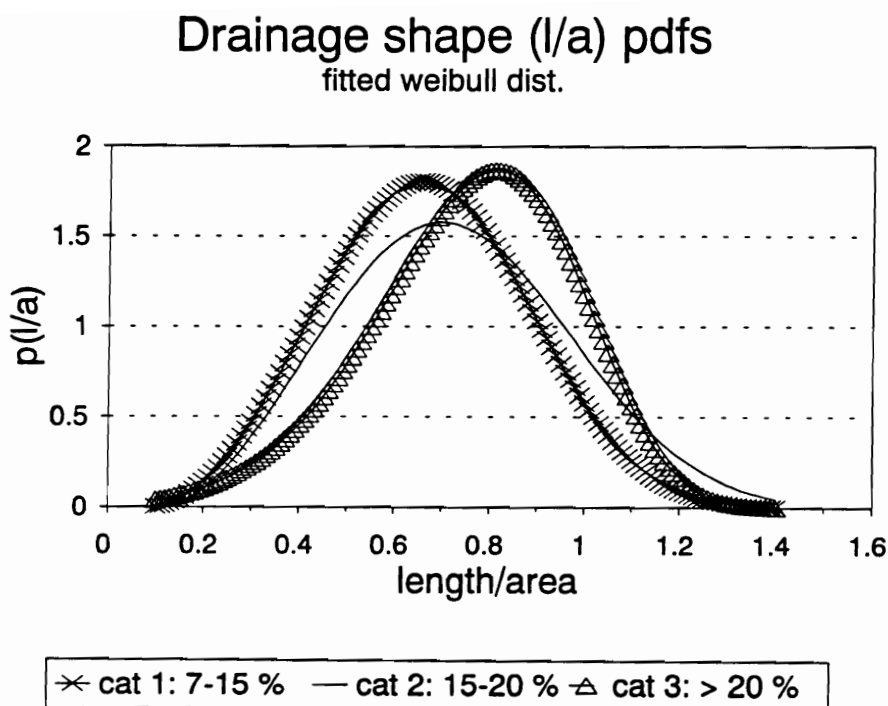
Figure 5.3: Comparison of fitted distributions of catchment shape across slope categories.

5.4 Drainage channel shape distributions

Fitted Lognormal distributions of drainage channel shape data indicate a decreasing trend in width to depth ratio with increasing slope gradient (Figure 5.4). AOV test on the data indicate that shape values for the three slope categories are significantly different at the 95 % level. A comparison of the mean channel width to depth ratios for the three slope categories is provided in Table 5.1. Deeper channels on steeper slopes (compared to moderate or flat slopes) are the result of long-term influences of greater flow concentration and higher erosion potential of runoff associated with steep slope gradients.

This analysis indicates that there is a distinct variation and trend in channel shape with increasing slope gradient. Results from this study also demonstrate that drainage channel shapes

can be quantified in terms of width to depth ratio distributions. Since channel shapes influence the rate of surface and subsurface runoff movement, spatial distribution, and production, it is imperative that they be considered in hillslope runoff models. This can be accomplished by including channel shape (width to depth ratio) distributions which vary with slope gradient, similar to those generated by this study.

w/d pdfs
fitted lognormal distributions
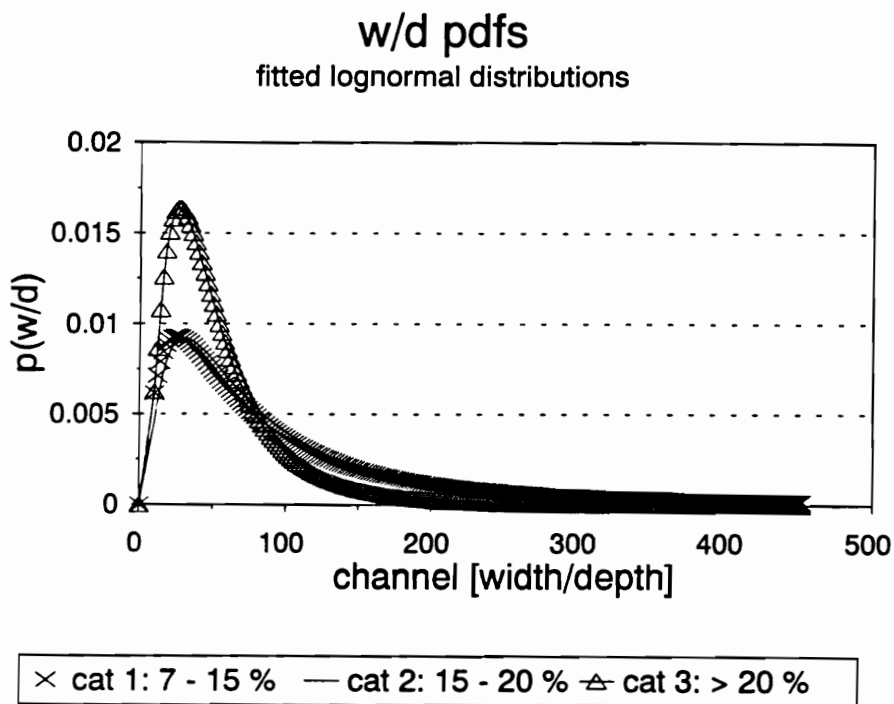
Figure 5.4: Comparison of fitted distributions of drainage channel shape across slope categories.

6 MODEL SCOPE AND OVERVIEW

6.1 Model Scope

6.1.1 Model applicability

Riparian site, soil and vegetative conditions vary significantly from one physiographic region to another. Riparian conditions may also vary within a region with stream order. For example, riparian zones in the Ridge and Valley region, in general, have moderate to steep slopes where the dominant water flux is rapid downslope subsurface flow over an impeding layer. In contrast, riparian zones in the Atlantic Coastal Plain are typically flat with high water table conditions and slow water movement through the zone. Accommodating these two completely different scenarios within a single simulation model can be difficult since the physics of water movement is entirely different for the two cases mentioned. The intent of this research was to develop a simple yet detailed model that could provide an insight into the dynamics of water and sediment movement. To accomplish this goal the model scope was limited to simulating riparian conditions similar to those typically observed on riparian hillslopes adjacent to first order streams in the Ridge and Valley region. The fundamental assumptions with regard to these riparian slopes were:

- riparian hillslopes have moderate (greater than 5%) to steep slope gradients, such that topography is primary determinant of surface and subsurface water movement,
- stream flow influences (such as bank flooding and seepage from streams towards the hillslope) on the riparian zone are negligible,
- perched water table formation may occur over an impeding soil layer, but because of its transient nature capillary effects associated with the water table are insignificant and can be neglected.

It is expected that the riparian hillslope model is applicable over a wide range of site, soil and vegetative conditions, provided, the assumptions mentioned above are satisfied.

6.1.2 Model Structure

The riparian hillslope model is a hillslope scale, continuous simulation model. The
hillslope scale is the "representative hillslope scale", defined by the size of segments into which
the hillslope is dissected (referred to earlier in Chapter 5). Continuous simulation requires that the
model simulate runoff events and non-runoff event processes such as evapotranspiration.
Hydrology and sediment transport processes within the riparian hillslope model are simulated
using process based approaches/algorithms to avoid model calibration. The physical situation
simulated within the model is illustrated in Figure 6.1. As shown in Figure 6.1, the riparian
hillslope is located between an upland contributing area (which may be farmland or pasture) on its
upslope edge and a first order stream/field drainageway at its downslope edge. Water and
sediment loadings to the riparian slope can occur from upland contributing areas and rainfall. The
spatial extent of the riparian hillslope in the model is described by including information on
riparian width (distance perpendicular to slope), length and gradient along the slope. Surface and
subsurface flow concentration on the hillslope is simulated by providing information on the
number and shape features of the drainage channels. Vegetation on the hillslope can be grasses,
shrubs or trees or combinations of the three. The soil profile is described in the model by
including a complete description of the soil horizons, their depths and properties required to
simulate water movement. Water and sediment loads leaving the slope at the lower edge are
estimated after routing incoming water and sediment loading through the riparian slope.
Simulations are performed with a minute time step during runoff events and on a daily basis
during non-runoff event periods.

6.2 Model Overview

The riparian hillslope model is composed of three major components which together
simulate water and sediment movement on the hillslope. These components include a climate and

upland loading component, a hydrologic component and a sediment component. Each of these components are described in the following sections.

6.2.1 Climate and upland loading

This component is concerned with generation of daily weather information such as precipitation amount and duration, air temperature, solar radiation, and wind velocity. This component also transforms incoming upland water (surface as well as subsurface) and sediment loadings into appropriate form for the riparian hillslope model. Upland contributions are expected to be generated by an upland model such as WEPP.

6.2.2 Hydrologic component

This component simulates the movement, rate, and spatial distribution of surface and subsurface water as it traverses the riparian hillslope. Processes simulated include - rainfall interception by vegetation canopy and litter, infiltration, Hortonian overland flow, vertical drainage, saturated downslope Darcian and preferential macropore flow, saturation overland flow, return flow or exfiltration, deep seepage losses and evapotranspiration. Figure 6.1 illustrates some of these processes.

Hydrologic phenomena unique to riparian hillslopes are specifically targeted. These phenomena include:

- subsurface flow concentration on main drainages on the hillslope;
- surface runoff concentration in rills/channels;
- variation in cross-sectional shapes of surface channels and subsurface colluvial channels;
- initiation and build up of perched water tables/saturated layers on restricting soil horizons;
- slow Darcian soil matrix flow and quick non-Darcian macropore flow in the saturated soil layer;
- the variable source area mechanisms - generation of saturation overland flow and return flow caused by subsurface flow influences;

interception &
evapotranspiration

precipitation

infiltration

surface
runoff

& sediment loading

overland flow

return flow

Subsurface
flow

matrix &
macropore flow

UPLANDS

STREAM

Deep Seep
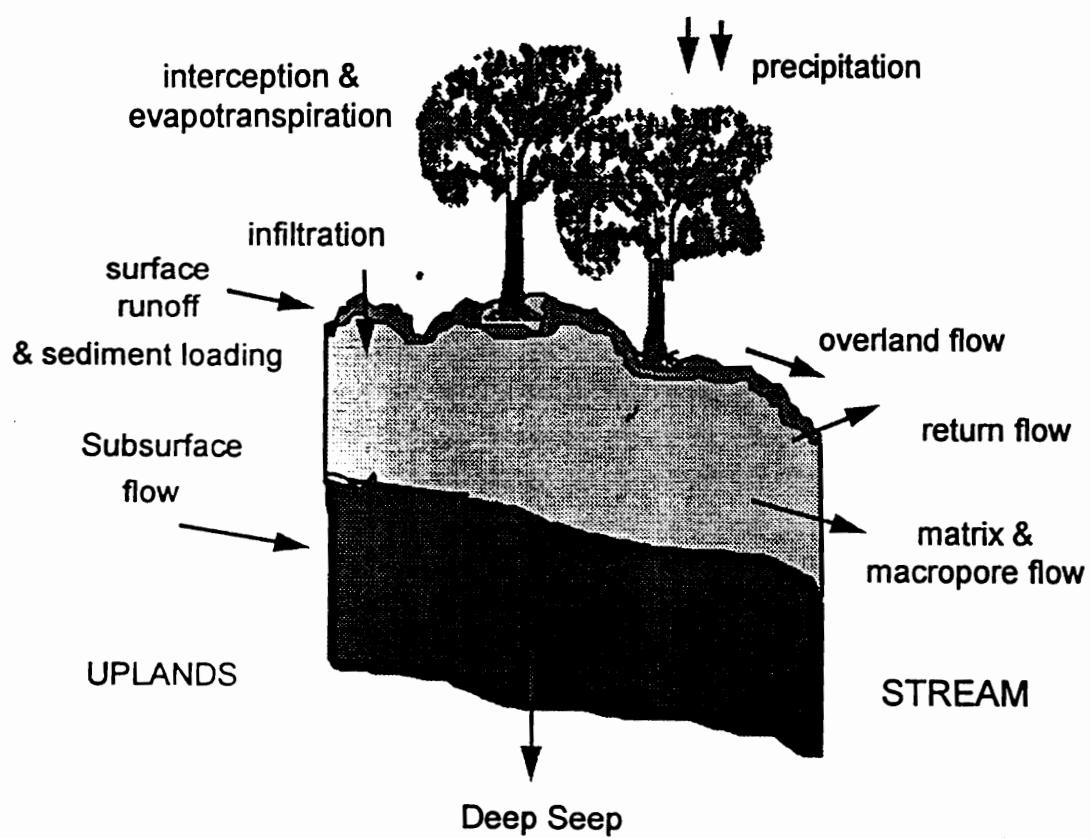
6.1: Riparian hillslope conditions simulated in the model.

- simulation of hydrologic influences associated with topographic effects of convergence/divergence and concavity/convexity of hillslope.

Specific details on the procedures and the equations used to simulate these phenomena are discussed in the following chapters on Model Development and Model Framework.

6.2.3 Sediment component

This component simulates the transport, detachment, and deposition of sediment on riparian hillslopes. Sediment contributions can occur by upland contributing areas or may be generated within the riparian area due to tractive forces associated with overland flow. Sediment transport, detachment, and deposition is simulated to occur only in the rill or channel areas. Effects of flow concentration on sediment delivery are simulated. Sediment generation in interill areas is not simulated. The specific equations and procedures used to simulate these phenomena are discussed in the following chapters on Model Development and Model Framework.

7 MODEL DEVELOPMENT

This chapter describes the basic theory, assumptions, and equations applicable to deterministic processes simulated in the riparian hillslope model. An overview of the major components and processes was provided earlier in the chapter on Model Scope and Overview. The application of the equations and the computational scheme is described in the following chapter.

7.1 Climate and upland loading component

The climate model generates climatic records required by the riparian hillslope model. An existing model CLIGEN (Nicks, 1985), is used for generation of climate parameters. These parameters include - daily precipitation, storm duration, peak storm intensity, air temperature, solar radiation, dew point temperature and wind speed and direction.

Water and sediment loads from upslope contributing areas are generated by a stand alone upland model such as WEPP (Flanagan and Livingston, 1995). This loading includes surface runoff, sediment, and lateral subsurface flow.

7.2 Hydrology component

7.2.1 Interception

Canopy interception is simulated using the relationship developed by Thomas and Beasley (1986) where the rainfall volume intercepted at any time is related to the canopy cover and is given by

$$INT_{can} = PIT \cdot (1 - e^{[-\frac{RAIN}{PIT}]}) \cdot PER \qquad 7.1$$

where INT_{can} is the volume of interception (m), PIT is the potential interception storage under

---

maximum canopy cover (m), RAIN is the rainfall amount (m), and PER is the percentage of canopy cover. Litter layer interception is related to litter layer depth and storage capacity, and is given by

$$INT_{lit} = MINT \cdot d_{lit} \qquad\qquad 7.2$$

where INT_{lit} is the intercepted moisture in the litter layer (m), MINT is the litter layer storage capacity per unit litter layer thickness (m) and d_{lit} is the litter depth (m). Throughfall, THF (m), is the difference between the rainfall and the interception depth

$$THF = RAIN - [INT_{can} + INT_{lit}] \qquad\qquad 7.3$$

7.2.2 Infiltration

Infiltration is estimated using the explicit form of the modified Green-Ampt equation (Stone et al., 1994). The total infiltration depth F(t) (L) for time t is given by

$$F(t) = \psi(\eta - \theta) \, F_q^*(t_c^*) \qquad\qquad 7.4$$

where ψ is the average wetting front capillary potential (L), θ is the soil moisture content, η is the effective porosity, and $F_q^*(t_c^*)$ is the dimensionless infiltration depth, which is given by

$$F_q^*(t_c^*) = t_c^* + \sqrt{2t_c^*} - 0.2987 t_c^{*0.7913} \qquad\qquad 7.5$$

where t_c^* is the dimensionless time computed using

$$t_c^* = \frac{K_s(t + t_s - t_p)}{\psi(\eta - \theta)} \qquad\qquad 7.6$$

where K_s is the saturated vertical conductivity (L/T), t_p is the time to ponding (T), and t_s is time shift parameter (T) given by

$$t_s = \frac{F_{pp} - \left(\psi \, \ln \left[1 + \frac{F_{pp}}{\eta - \theta} \right] \right)}{K_s} \qquad\qquad 7.7$$

where F_{pp} is the infiltration depth (L) prior to ponding given by

$$F_{pp} = R \cdot t_p \qquad\qquad 7.8$$

where R is the rainfall rate (L/T). The time to ponding t_p is given by

$$t_p = \frac{K_s \, \psi \, (\eta - \theta)}{R(R - K_s)} \qquad\qquad 7.9$$

7.2.3 Hortonian and saturation overland flow

Rainfall/runoff depth greater than infiltration depth is considered Hortonian overland flow and is routed downslope. Saturation overland flow is assumed to occur when the topmost surface soil layer is completely saturated. In conditions when the topmost soil layer is saturated, infiltration at the surface is controlled by the rate of drainage from the surface layer, which in turn is controlled by the rate of movement of the wetting front into the lower layer. The movement of the wetting front in the lower layer is simulated by applying the infiltration equation at the surface of the lower layer. Surface runoff depth generated due to Hortonian or saturation overland flow conditions is routed downslope using Manning's equation in combination with the mass-continuity equation.

7.2.4 Surface runoff concentration

Surface runoff on riparian hillslopes typically concentrates along topographic depressions and channels as it moves downslope. This flow concentration, in most conditions, results in greater delivery of water down the hillslope, since water losses to infiltration are restricted to channel areas only. The amount and rate of movement of total surface runoff at any section across the hillslope is determined by the number of channels and their cross-sectional shapes. Deep channels generally have higher runoff depths and flow velocities compared to shallow wide channels. On riparian hillslopes a population of channel shapes generally occurs which varies from shallow wide channels to narrow deeply incised channels.

In the riparian hillslope model, surface flow concentration along any hillslope section is simulated by considering the number of channels and the possible channel shapes at that section. The range of possible channel shapes is represented by a probability distribution. If n is the number of channels at any flow section, and p_s is the probability distribution representing the channel shapes, the expected total runoff at the section is given by

$$E[q_{tot}] = n \int p_s[s] \cdot q_f[s] \, ds \qquad \qquad 7.10$$

where $E[q_{tot}]$ is the expected total surface runoff at the section (m^3 min^{-1}), $p_s[s]$ is the probability associated with the discrete channel shape s, and $q_f[s]$ is the flow associated with channel shape s (m^3 min^{-1}). Surface channel shapes are quantified in terms of channel width to channel depth ratio. Numerical procedures used to compute and route runoff through surface channels are discussed in the following chapter.

7.2.5 Vertical drainage

Vertical drainage from a soil layer is assumed to occur when soil moisture exceeds the field capacity. The vertical hydraulic conductivity is varied from the saturated conductivity K_s value at saturation to zero at field capacity (Williams et al., 1985), and is given by

$$K_{sai} = K_{si} \left[\frac{\theta_i}{\theta_s} \right]^{B_i} \qquad \qquad 7.11$$

where K_{si} is the saturated conductivity for layer [i] (m min^{-1}), K_{sai} is the adjusted hydraulic conductivity (m min^{-1}), and B_i is the parameter that causes K_{sai} to approach zero as soil moisture, θ_i (m^3 m^{-3}), approaches field capacity. B_i is computed using

$$B_i = \frac{-2.665}{\log\left[\frac{FC_i}{\theta_s}\right]} \qquad \qquad 7.12$$

where the constant -2.665 forces K_{sai} to a value of $0.002K_{si}$ at field capacity FC_i.

Drainage from a soil layer may be restricted by an underlying layer of lower conductivity. In such a condition, the conductivity of the lower layer determines the rate of drainage from the upper layer.

7.2.6 Subsurface downslope flow

Subsurface downslope flow is assumed to occur only under saturated soil conditions. No subsurface lateral/downslope flow is assumed to occur within the unsaturated zone. Subsurface downslope flow is assumed to be the sum of Darcian flux through the soil matrix and non-Darcian flow via soil macropores. Subsurface flow is initiated when a perched water table (saturated layer) develops over a restricting soil horizon. The slope of the water table is assumed equal to the slope of the impermeable soil layer (the kinematic assumption), which is assumed to be equal to the surface gradient (Sloan and Moore, 1984). The depth of the perched water table within a layer is determined from the water in excess of field capacity for that layer. Specific equations that are used to simulate soil matrix and macropore flow are discussed below. The full scheme that is used to simulate the sum of Darcian soil matrix and non-Darcian macropore flux for a given water table depth and the procedures to route the water down the hillslope are discussed in the Model Framework chapter.

Darcian matrix flow

The Darcian soil matrix component of subsurface flow is given by

$$q_m = K_h \cdot A(d) \cdot S \qquad\qquad 7.13$$

where q_m is the soil matrix flux (m^3 min^{-1}), K_h is the saturated lateral hydraulic conductivity (m min^{-1}), $A(d)$ is the saturated flow cross-section as a function of d the depth of saturation (m), and S is the slope gradient (m m^{-1}).

Non-Darcian macropore flow

Flow in a single macropore is simulated using Manning's pipe flow equation given by

$$q_{mac} = a_{mac} \cdot \left[\frac{1}{n} R^{(2/3)} \sqrt{S} \right] \qquad 7.14$$

where q_{mac} is macropore flow (m³ min⁻¹), a_{mac} is macropore cross-sectional area (m²), n is the inner macropore roughness, and R is the macropore hydraulic radius (m). For simplicity, macropores are assumed circular in cross section and are assumed to flow full.

Within any soil horizon it is assumed that a distribution of macropore sizes exists and that the total macropore flow (for a given water table depth) is the probabilistic sum of flow conducted by through these macropores. The total expected macropore flow $E[q_{tot}]$ (m³ min⁻¹) is given

$$E[q_{tot}] = \int p(m) \cdot q_m(m) \, dm \qquad 7.15$$

where p(m) and $q_m(m)$ are the probability and flow rate, respectively associated with discrete macropore sizes, respectively. The numerical procedure for determining the total flow considering the distribution of macropore sizes is discussed in the Model Framework chapter.

7.2.7 Subsurface downslope flow concentration

Similar to surface runoff, though not as apparent, subsurface downslope flow on riparian hillslopes also concentrates along the colluvium of topographic depressions and channels (Figure 7.1). This subsurface flow concentration occurs when a restricting soil layer limits vertical drainage and gravitational gradient causes water to move towards depressions. In addition to the above mentioned phenomenon, subsurface soil moisture conditions in the colluvium of depressions and channels are also enhanced by infiltration from concentrated surface runoff. Figure 7.1 illustrates the accumulation of water in the colluvium of drainages and depressions. Similar to surface runoff concentration, subsurface flow concentration in these "colluvial channels" leads to quicker (compared to uniform distribution of subsurface flux) subsurface flow movement, and greater perched water table or saturated flow depths. Elevated saturated conditions within these "colluvial channels" also provide greater opportunity for preferential flow via soil macropores. Higher saturation depths associated with concentrated subsurface flows also increase

the possibility of saturation reaching the surface, and consequently the occurrence of saturation overland flow or return flow (variable source area phenomenon).

Similar to surface runoff, the rate of movement of subsurface flux across any hillslope section is determined by the number of "colluvial channels" and their cross-sectional shapes (Figure 7.1). Hence, subsurface flow in the riparian hillslope model is represented using a stochastic scheme similar to that used for surface runoff, where total expected subsurface flow at a section is given by

$$E[qs_{tot}] = n_s \int ps_s[s] \cdot qs_f[s] \ ds \qquad 7.16$$

where $E[qs_{tot}]$ (m^3 min^{-1}) is the total expected subsurface downslope flow at any section, n_s is the number of "colluvial channels" at that section, $ps_s[s]$ is the probability associated with a "colluvial channel" with shape ratio s, and $qs_f[s]$ is the subsurface flow in the "colluvial channel" (m^3 min^{-1}). As can be seen in Figure 7.1, the shape of the "colluvial channel" is defined by the soil surface at the top and the restricting soil layer at the bottom. For simplicity it is assumed that the restricting layer profile is identical to the soil surface profile (Figure 7.1). Using this assumption the "colluvial channel" shape can be quantified in terms of the width to depth ratio of the surface profile. In reality, the colluvium depth tends to increase towards the center of the depression/channel, a result of erosion/deposition phenomena over time (Figure 7.1). The numerical procedures that describe subsurface flow routing along these "colluvial channels" are discussed in the next chapter.

7.2.8 Return flow or seepage

Return flow is assumed to occur when the upslope subsurface water contributions to the topmost soil layer for a hillslope segment exceed the sum of the storage capacity, vertical drainage and downslope subsurface flow for that layer. Excess water is transferred to the surface and is considered overland flow.

surface channels

main drainages where subsurface
flow concentrates

A

A

**PLAN VIEW OF A HILLSLOPE
SEGMENT**

saturation reaching
surface creates "Variable
source areas"

SECTION A-A

impeding soil surface

subsurface flow concentration
along main drainageways

s- subsurface flow
towards depression

i - infiltration
from concentrated
runoff

s

i

shape of subsurface
"colluvial channel"
as assumed in the
model

Figure 7.1: Subsurface flow concentration on a hillslope and its representation in the model.

7.2.9 Evapotranspiration

Potential evapotranspiration in the model is computed using the Penman-Monteith equation given by (Monteith, 1965)

$$\lambda E = \frac{s}{(s+\gamma)} A + \frac{\rho c_p [D_i - D_{eq}]}{(s+\gamma)r_a + \gamma r_c} \qquad 7.17$$

where λ is the latent heat of vaporization (MJ kg^{-1}), E is the potential evapotranspiration (m day^{-1}), A is the net incident radiation (MJ m^{-2} day^{-1}), s is the slope of the saturation vapor curve (kPa C^{o-1}), γ is the psychometric constant (kPa C^{o-1}), ρ is the density of air (kg m^{-3}), c_p is the specific heat (= 1.013 kJ kg^{-1} K^{-1}), D_i is the vapor pressure deficit (kPa), D_{eq} is the vapor pressure deficit at equilibrium (kPa), r_a is the aerodynamic resistance (sec m^{-1}), and r_c is the surface resistance (sec m^{-1}). The equilibrium saturation deficit D_{eq} is computed using the equation

$$D_{eq} = \frac{s}{(s+\gamma)} \cdot \frac{\gamma r_c}{\rho c_p} A \qquad 7.18$$

The slope of the saturation vapor pressure curve, s, is given by

$$s = \frac{4098 \, e_s}{(237.3+T)^2} \qquad 7.19$$

where T is the temperature (C^o), and e_s is the saturation vapor pressure given by (Tetens, 1930)

$$e_s = 0.6108 \, e^{(17.27T)/(237.3+T)} \qquad 7.20$$

Vapor pressure deficit is computed using

$$D = \frac{[e_s T_{max} + e_s T_{min}]}{2} - e_s T_d \qquad 7.21$$

where T_{max} is the maximum daily temperature ($C°$), T_{min} is the minimum daily temperature($C°$), and T_d is the dew point temperature ($C°$). The latent heat of vaporization is computed using (Harrison, 1963)

$$\lambda = 2.501 - 0.002361T \qquad 7.22$$

The psychometric constant is computed using

$$\gamma = 0.0016286 \frac{P}{\lambda} \qquad 7.23$$

where P is the atmospheric pressure (kPa). The aerodynamic resistance which reflects the influences of wind velocity on the vapor pressure deficit is given by

$$r_a = \frac{b}{u_r} \qquad 7.24$$

where

$$b = \frac{(\ln[(z_r - d)/z_o])^2}{V_k^2} \qquad 7.25$$

where u_r is the wind velocity (m s^{-1}), z_r is the height at velocity is measured (m), z_o is 0.01h, h is the height of vegetation (m), d is 0.75 h (m), and V_k is the von Karman's constant (0.41).

Potential soil and plant components of total evapotranspiration are computed using Ritchie's (1972) partitioning factor and the Penman-Monteith equation described above. Potential soil evaporation is given by

$$E_{sp} = E_{p[r_c = 0]} \cdot e^{-0.4LAI} \qquad 7.26$$

where E_{sp} is the potential soil evaporation, LAI is the leaf area index of the vegetation on a given day, and $E_{p[rc=0]}$ is value of potential evaporation assuming no surface resistance at the soil surface. Potential plant evapotranspiration is given by

$$E_{tp} = E_p \cdot [1 - e^{-0.4LAI}] \qquad 7.27$$

where E_{tp} is the potential plant evapotranspiration, and E_p is the potential evapotranspiration for an appropriate value of r_c (function of vegetation type).

7.2.10 Distribution of soil evaporation

Soil evaporation losses on a given day are first satisfied from litter moisture storage at a rate defined by potential soil evaporation. After litter moisture storage has been exhausted, evaporation losses occur from the topmost mineral soil layer until soil moisture reaches the wilting point, θ_w, after which soil evaporation is assumed zero.

7.2.11 Distribution of evapotranspiration losses

Soil moisture losses to plant transpiration occur only after all intercepted water in the vegetation canopy is lost. Hence, plant transpiration adjusted for intercepted moisture is given by

$$E_{tp} = E_{tp} - INT_{can} \qquad 7.28$$

Evapotranspiration losses are distributed in the root zone based on the procedures used in WEPP (Savabi et al., 1989) and given by

$$U_{Pi} = \frac{E_{tp}}{1 - e^{-V}} \left[1 - e^{\left(-V\frac{h_i}{RZ} \right)} \right] - \sum_{j=1}^{i-1} U_j \qquad 7.29$$

where U_{pi} is the potential water uptake from layer [i] (m day^{-1}), and V is a use rate-depth parameter assumed equal to 3.065 (based on the assumption that 30 percent of the total water comes from the top 10% of the root zone), h_i is the depth of the soil layer, RZ is the root zone depth, and U_j is the water loss from the soil layer above the layer [i].

The actual water loss from any soil layer will be limited by the moisture present in the soil layer and given by

$$U_i = U_{Pi} \qquad \theta_i > \theta_w$$
$$U_i = U_{Pi} \cdot \frac{\theta_i}{\theta_w} \qquad \theta_i \leq \theta_w \qquad\qquad 7.30$$

where θ_i is the soil moisture content of layer [i], and θ_w is the wilting point water content.

7.3 Sediment component

7.3.1 Sediment continuity

The sediment component uses the steady state sediment continuity equation to describe sediment deposition, detachment and transport down the hillslope, given by (Foster and Meyer, 1975)

$$\frac{dq_s}{dx} = D_r + D_i \qquad\qquad 7.31$$

where q_s is the sediment load (kg s⁻¹ m⁻¹), dx is distance downslope (m), D_r is the rill/channel erosion rate (kg s⁻¹ m⁻²) and D_i is the interill erosion rate (kg s⁻¹ m⁻²). Sediment movement down the hillslope is simulated using a combination of stochastic and deterministic processes. Occurrence of rills/channels and their shapes are represented using stochastic procedures whereas sediment deposition, transport and erosion processes in individual rill/channels are simulated using deterministic procedures. The stochastic scheme for representing channels is discussed in the chapter on Model Framework.

For grassed and litter covered forested hillslopes, interill erosion is considered negligible and is not simulated. Rill/channel processes that are simulated using deterministic procedures include :

- Deposition
- Detachment
- Sediment transport capacity

- Change in sediment particle size distribution down the slope
- Sediment enrichment

Total sediment is divided into six particle size classes and sediment deposition, detachment, and transport computations are performed for each particle class. A description of each of these processes follows.

7.3.2 Deposition

Deposition of sediment load in rill/channels occurs when the sediment load exceeds the transport capacity of flow. Deposition is simulated using Foster and Meyer's (1972) equation and is given by

$$D_{p[i]} = \frac{\beta V_{s[i]}}{q} (q_{t[i]} - q_{s[i]}) \qquad 7.32$$

where the subscript [i] represents the particle class, $D_{p[i]}$ is the deposition rate per unit width and channel length (k s^{-1} m^{-2}) for particle class [i], β is a deposition coefficient generally assumed to be 0.5, $V_{s[i]}$ is particle settling velocity defined using Stoke's law (m s^{-1}), q is the channel flow rate per unit channel width (m^2 s^{-1}), $q_{t[i]}$ is the transport capacity (kg s^{-1} m^{-1} channel width) and $q_{s[i]}$ is the sediment load in the flow (kg s^{-1} m^{-1} channel width).

For discrete quiescent settling, the settling velocity of an individual particle $V_{s[i]}$ is computed by Stokes's Law

$$V_{s[i]} = \frac{1}{18} \left[\frac{d_{[i]}^2 g}{v} (S_{g[i]} - 1) \right] \qquad 7.33$$

where $V_{s[i]}$ is the settling velocity (m s^{-1}), $d_{[i]}$ is the particle diameter (m), g is the acceleration due to gravity (m s^{-2}), v is the kinematic viscosity (m^2 s^{-1}), and $S_{g[i]}$ is the particle specific gravity. The Reynold's number corresponding to the settling velocity is computed using

$$R_e = \frac{V_{s[i]} d_{[i]}}{v} \qquad 7.34$$

Stoke's equation is only valid up to a Reynold's number of 0.5 (Barfield et al., 1981). When Reynold's number exceeds 0.5 , Wilson et al. (1983) developed the following equation for computing settling velocity of spherical particles with a S_g of 1.65 in water

$$\log_{10}(100V_{s[i]}) = -0.34246272[\log10(1000d_{[i]})]^2 \\ + 0.98912185\log_{10}(1000d_{[i]}) + 1.146128$$

7.35

To account for varying specific gravity, the settling velocity computed above is multiplied by the ratio $(S_g-1)/1.65$.

7.3.3 Detachment

Rill/channel detachment occurs when sediment load in the flow is less than the flow transport capacity and the flow shear stresses acting along the rill boundary exceeds the critical binding forces by which soil particles are held together. This detachment rate $D_{r[i]}$ is computed using the equation (Foster and Meyer, 1975)

$$D_{r[i]} = D_{rc}\left[1 - \frac{q_{s[i]}}{q_{t[i]}}\right]$$

7.36

where $D_{r[i]}$ is the detachment rate per unit width and channel length, D_{rc} (kg s^{-1} m^{-2}) is the maximum detachment rate per unit channel width and length (kg s^{-1} m^{-2}) and other parameters are as explained above. The maximum detachment rate is calculated as a difference between the shear stress acting along the rill/channel boundary and the critical shear stress of the soil and is given by (Foster and Lane, 1983)

$$D_{rc} = K_{ch}(\tau_s - \tau_c)$$

7.37

where K_{ch} is the soil erodibility factor (s m^{-1}), τ_s is the flow shear (Pa) and τ_c is the critical shear stress (Pa). The average channel flow shear stress is given by

$$\tau_{avg} = \gamma RS$$

7.38

where γ is the specific weight of water (kg m^{-3}), R is the flow hydraulic radius, and S is the

channel slope. Critical shear stress as a function of surface cover can be estimated using (Foster et al., 1980)

$$\tau_c = \frac{\tau_b}{[n_b/n_c]^{0.9}}$$ 7.39

where τ_b is the critical shear stress for bare soil (Pa), n_b is the mannings roughness for bare soil, and n_c is the Manning's roughness corresponding to surface cover.

7.3.4 Transport capacity

Two options are provided for determining channel/rill sediment transport capacity. In most conditions, riparian hillslope surfaces have a thick vegetative cover in the form of grass or litter layer. For such surfaces, little bedload transport is expected and any sediment reaching the surface is assumed to be trapped. Under such conditions, sediment transport, if any, occurs primarily in the form of suspended load. Hence, sediment transport in this case can be adequately simulated using a suspended load equation.

In contrast, where the soil surface is exposed, or where previously deposited sediment has sufficient depth to cover the litter layer, suspended load as well as bedload transport can occur. For these conditions, the transport capacity is simulated using a total load equation.

7.3.4.1 Bagnold's (1966) suspended load equation

Bagnold's suspended load transport equation (1966) is used for conditions where no bedload transport is expected and sediment transport occurs primarily in suspension. Bagnold's sediment transport equation, based on the stream power concept, is given by

$$T_{c[i]} = \eta_{[i]}\kappa\tau \frac{V_c^2}{V_{s[i]}}$$ 7.40

where $T_{c[i]}$ is the sediment transport capacity (kg m^{-1} s^{-1}), η is an effective transport factor, κ is the transport capacity factor, τ is flow shear stress (Pa), V_c is the flow velocity (m s^{-1}), and $V_{s[i]}$ is the particle settling velocity (m s^{-1}). The transport capacity factor is given by

$$\kappa = (1-e_b) \cdot e_s \cdot \left(\frac{\gamma_w}{\gamma_s - \gamma_w} \right)$$

7.41

where e_b is the bedload transport efficiency, e_s is the suspended load transport efficiency, γ_s is the sediment specific weight (kg m^{-3}), and γ_w is the specific weight of water (kg m^{-3}). The combined efficiency term $(1-e_b)e_s$ was found to be 0.01 for sands (Simons and Senturk, 1977). To adjust this term for other particle sizes Young et al. (1986) introduced the term η

$$\eta_{[i]} = 0.74 E_{f[i]}^{-1.98}$$

7.42

where E_f is an entrainment function given by (Simons and Senturk, 1977)

$$E_{f[i]} = \frac{\tau}{(\gamma_w - \gamma_s) d_{[i]}}$$

7.43

7.3.4.2 Einstein's total load equation

Einstein's total load equation is used for conditions where sediment transport is expected to be a combination of bed and suspended load. Transport capacity is determined using the calibrated version of Einstein's equation (Tollner et al., 1982) which is given by

$$\psi = 1.08(\phi)^{-0.28}$$

7.44

where ψ is the Einstein's shear intensity factor given by

$$\psi = (S_{g[i]} - 1) \frac{d_{[i]}}{SR_s}$$

7.45

and ϕ is the transport rate factor, given by

$$\phi = \frac{q_{sd[i]}}{\gamma_s \sqrt{(S_{g[i]} - 1) g d_{[i]}^3}}$$

7.46

where $q_{sd[i]}$ is the transport capacity (kg m^{-1} s^{-1}), S is the ground slope (m m^{-1}), $S_{g[i]}$ is the particle specific gravity, γ_s is the particle weight density (kg m^{-3}), $d_{[i]}$ is the particle diameter (m), and R_{sd} is the spacing hydraulic radius (m), which is a function of vegetative media spacing (Tollner et al., 1982).

7.3.4.3 Transport capacity for a sediment mixture

Both Bagnold's and Einstein's equations compute transport capacity for sediment composed of a single uniform particle size. Hirschi (1985) proposed a procedure to compute the transport capacity of a sediment mixture. This procedure is given as:

1) Compute transport capacity $T_{c[i]}$ using the transport equation for each individual particle class.

2) Determine the sum of transport capacities $\sum_{i=1}^{np} T_{c[i]}$, where np is the number of particle classes in the sediment mixture.

3) Determine d_{65} for the mixture - particle diameter for which 65% of the sediment is finer.

4) Compute transport capacity T_{c65} corresponding to d_{65} using the transport equation.

5) The transport capacity $T_{[i]}$ for particle class i in the sediment mixture is then given by

$$T_{[i]} = T_{c65} \cdot \left[\frac{T_{c[i]}}{\sum\limits_{i=1}^{np} T_{c[i]}} \right] \qquad 7.47$$

7.3.5 Particle size distribution

Particle size distribution of the sediment mixture is updated after sediment deposition or detachment. The sediment fraction for any particle size class is simply the ratio of the sediment load in the class to the total sediment load.

7.3.6 Sediment enrichment

Enrichment of sediment due to deposition/detachment is determined using procedures developed in WEPP (Foster et al., 1989). The enrichment ratio is expressed by

$$ER = \frac{SSA_{sed-in}}{SSA_{sed-out}}$$ 7.48

where SSA_{sed-in} is the specific surface area of the incoming sediment, and $SSA_{sed-out}$ is the specific surface area of the exiting sediment. The specific surface area of the sediment is computed using

$$SSA_{sed} = \sum_{i=1}^{np} f[i] \; [frsnd[i] \cdot ssasnd + frslt[i] \cdot ssaslt + frcly[i] \cdot ssacly]$$ 7.49

where np is the number of particle size classes, f[i] is the fraction of the particle class in the sediment, frsnd[i], frslt[i], and frcly[i], are the fractions of sand, silt, and clay comprising each particle class, respectively, and ssasnd, ssaslt, and ssacly are the specific surface area of sand, silt and clay, respectively.

8 MODEL PARAMETERS AND COMPUTATIONAL FRAMEWORK

8.1 Physical representation of the riparian hillslope

Spatial variability along the hillslope is represented in the model by discretizing the hillslope into segments and providing information for each segment. Figure 8.1 illustrates the hillslope in discretized form. Input variables that are used to describe the hillslope and the hillslope segments include slope and topographic features, soils information, vegetative data, channel shape distributions, and channel dimensions. These variables are discussed in detail below.

8.1.1 Slope and topographic features

Table 8.1 provides a listing of the variables used to describe the slope and topographic features of the hillslope. This includes the number of segments the hillslope is dicretized into, and length (distance along the slope gradient), width (distance perpendicular to slope gradient), and slope gradient for each segment. For simplicity, the model assumes equal length segments. The segments that constitute the hillslope are assumed to have a slope gradient only in the length direction (Figure 8.1). Flow concentration (surface as well as subsurface) within each hillslope segment is simulated by providing information on channels along which surface and subsurface flow concentrates. Henceforth, channels which represent surface runoff concentration will be referred to as surface channels, whereas, channels which simulate subsurface flow concentration will be referred to as main drainage elements. Channel (which includes both surface channels as well as main drainage elements) information required for each segment includes the expected number of channels at each segment, the average w/d ratio for the population of expected channels at the segment, the channel shape distribution identifier, the number of discrete channels shapes to be simulated (out of the given distribution), and the incremental w/d value (Table 8.1). The distribution identifier is used to select the required set of distribution parameters from a distribution input file (Table 8.4).
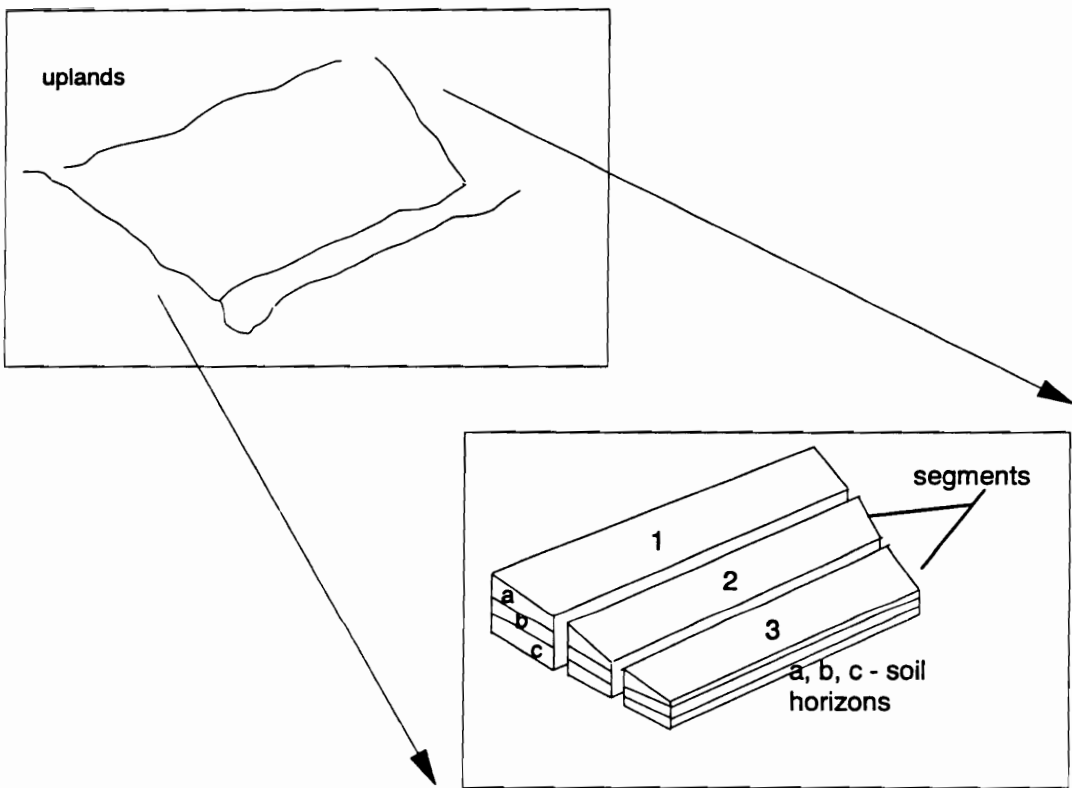
Figure 8.1: Hillslope representation in discretized form in the model.

Since cross slopes within a segment are not considered, it is assumed that convergence/divergence (in plan) along the hillslope is simulated by providing appropriate input values for slope width and channel numbers and shape distribution. For example, convergent hillslopes are simulated by reducing the segment width down the hillslope, reducing the number of channels down the hillslope, and changing the channel shape distribution appropriately. The underlying assumption behind this is that slope convergence/divergence can be represented through slope attributes such as width and drainage channel information. Hillslope concavity/convexity in section is considered by providing appropriate slope gradient values for each segment constituting the hillslope.

Table 8.1: Slope and topographic information

•   Number of segments
•   Segment characteristics (for each segment)
length, width, slope gradient
number of main drainage channels, number of w/d values, w/d average, increment
number of surface channels, number of w/d values, w/d average, increment

8.1.2 Soil information

The parameters necessary to describe the soil within each segment are listed in Table 8.2. The model can simulate variability in the number of soil horizons, horizon depths and their properties along the slope. Information on vertical and horizontal saturated soil matrix conductivity is required to simulate the drainage in the vertical and downslope directions. Field capacity, as defined here, is the moisture content of the soil measured at the matric potential of -33 kPa. Macroporosity as defined here is the fraction of the total porosity that is occupied by pores larger than 0.01 mm. Macroporosity is used to estimate the macropore flow component of lateral subsurface flow (described in detail in section 8.3.2). Minimum and maximum macropore

diameters provide the bounds of macropore size distribution expected in the soil horizon. Antecedent soil moisture content provides an estimate of the soil moisture content within each soil layer at the start of event simulation. A capillary potential parameter is required for the surface layer only and is used in infiltration computations. Rill erodibility, critical tractive force, and Manning's roughness for bare soil are parameters that are used in erosion computations.

Table 8.2: Hillslope soil description

• number of soil horizons	
• Soil characteristics (for each soil horizon):	
horizon depth	total porosity
macroporosity	field capacity
vertical saturated conductivity	horizontal saturated conductivity
moisture content at saturation	antecedent soil moisture content
number of discrete macropore	macropore roughness
dia. selected from pdf	
minimum macropore diameter	maximum macropore diameter
• capillary potential parameter	
• rill/channel erodibility	
• critical tractive force	
• Manning's roughness for bare soil	

8.1.3 Vegetative data

Vegetative parameters are required to describe the influence of vegetation on processes such as interception, evapotranspiration, and surface runoff. The required input parameters are listed in Table 8.3. Since vegetative growth is not simulated in the model, information on the maximum leaf area index (LAI) and its variation within a growing year is required as input. The surface resistance term provides a measure of the leaf resistance offered to evapotranspiration (used in the Penman-Monteith equation). Manning's n value provides a measure of the resistance of vegetation to overland flow.

Table 8.3: Vegetative data

•	number of vegetation types
•	Vegetation characteristics (for each vegetation type):

maximum canopy interception capacity	litter interception capacity
maximum LAI	LAI (by day)
surface resistance	Manning's n value

8.1.4 Channel shape distributions

Channel shapes (surface channels as well as main drainage channels) are represented in the model in the form of probability distributions of normalized channel width (w) to depth (d) ratio given by

$$[(w/d)_{norm}]_i = \frac{(w/d)_i}{w/d_{avg}}$$ 8.1

where $(w/d)_i$ is the discrete w/d value, and w/d_{avg} is the average w/d for the population. Normalization of the individual w/d values with the average w/d value for the population results in the population distribution parameters (parameters that describe distribution shape) being independent of the discrete w/d values. This allows application of the distribution to different w/d_{avg} values. Channel shape distribution can be provided as one of the three distribution types - Lognormal, Gamma and Weibull. To evaluate channel shape distribution at a hillslope section, input information is required in the form of the distribution type, values for each of the distribution parameters (Table 8.4), and the average w/d value (w/d_{avg}) for the hillslope section. Equations describing each distribution type are listed in Appendix II.

Table 8.4: Input data for channel shape distribution

Distribution Identifier (refer to Table 8.1)	
•	Distribution type (Lognormal/Gamma/Weibull)
•	Mean, variance (if Lognormal); Location, shape parameters (if Gamma/Weibull)

8.1.5 Channel dimensions

Figure 8.2 provides a physical characterization of how a distribution of surface and main drainage channels at a hillslope segment are considered in the model. To route water and sediment through these channels, actual width and depth values are required. Actual channel (surface as well as main drainage) width and depth values are determined by assuming that the sum of widths of all probable channels (defined by the distribution) across a section is equal to the total width for that section. The computational procedure is:

- assume an initial channel depth value d_{ini}

- using d_{ini}, w/d_{avg}, and the normalized distribution, determine the sum of widths of all possible discrete channels at the section. This sum is expressed as

$$SW = n \sum_{i=1}^{s} p_s[i] \cdot ([w/d]_i \cdot d_{ini}) \qquad 8.2$$

  where SW is the sum of all channel widths, n is the number of channels at the section, s is the number of possible channel shapes for each channel, $p_s[i]$ is the probability associated with a single discrete channel shape expressed as $[w/d]_i$. The assumption behind this is that though channel widths differ for each discrete w/d value, all channels possess the same depth. In reality, channels would differ both in depth as well as width.

- If SW is less than the hillslope section width W_{tot}, d_{ini} is incremented and SW computed again. This iterative procedure is continued until SW is nearly equal to W_{tot}.

- This procedure is followed for each individual segment the hillslope is discretized into.

8.2 Water and sediment loading

Event loadings provided to the model include rainfall, surface runoff, subsurface flows, and sediment loads from upslope contributing areas. Rainfall loading is provided in the form of breakpoint data for each event. Runoff hydrographs in discretized form provide the surface and subsurface loadings. Runoff hydrographs are generated using an upland model. Similarly, sedigraphs associated with runoff provide sediment loadings.
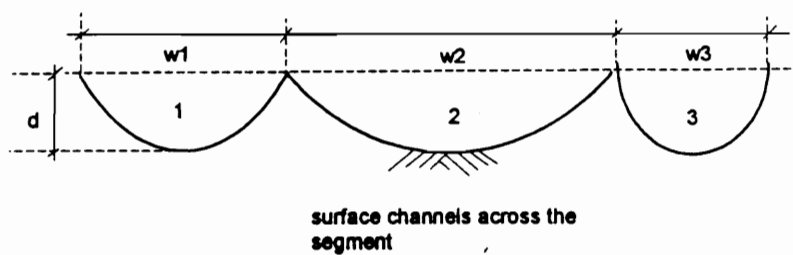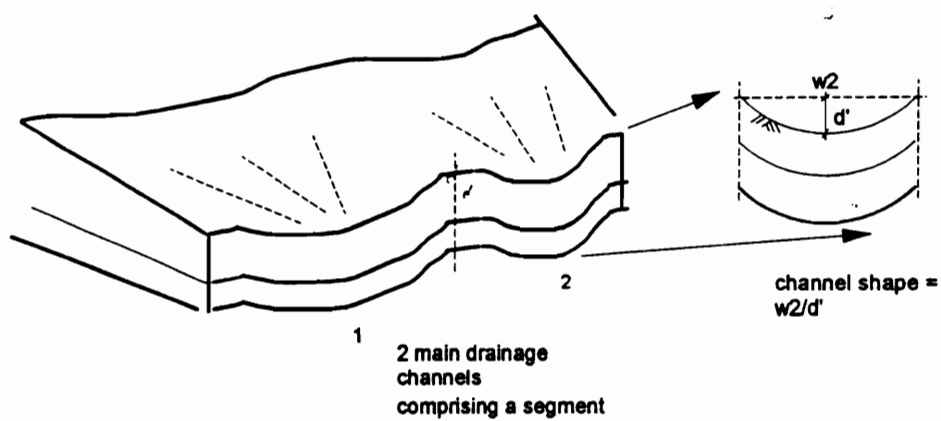
Figure 8.2: Characterization of surface and subsurface channels in the model.

Thus, for every 1 minute event time step, the loadings are:

- rainfall depth (m min^{-1})
- total upslope surface runoff (m^3 min^{-1})
- total subsurface flow (m^3 min^{-1})
- total sediment load (kg min^{-1})

8.3 Water and sediment routing

Surface and subsurface water volumes are routed based on simple mass balances applied to each segment down the hillslope. These mass balances are computed for each time step (1 minute) during an event.

8.3.1 Subsurface flow routing

Water loading to a segment occurs via rainfall and/or upslope surface and subsurface flows. Subsurface flow within a segment is assumed to concentrate and move in main drainage channels. Infiltration of rainfall and/or incoming surface runoff adds to the subsurface flow in the main drainage channels. To compute infiltration losses, incoming surface runoff and rainfall volume are assumed to be uniformly distributed over the surface of main drainage channel elements. Runoff in excess of infiltration is considered as surface runoff for the segment and is routed through surface channels. Routing procedures for surface runoff are described in a following section.

Loadings to a main drainage channel within a segment are illustrated in Figure 8.3. These loadings include infiltration and upslope subsurface flow contribution along each soil horizon. Water movement within each soil horizon/layer of the main drainage channel is based on a simple mass continuity equation given by

$$\frac{dS}{dt} = I - O \qquad\qquad 8.3$$

where dS is the change of storage in time dt, I is the sum of inflows, and O is the sum of outflows.

q sub -A = upslope subsurface flow
q surf = surface runoff entring main drainage
rain = rainfall addition
drain = vertical drainage to lower layer
q ext - A = lateral flow exiting horizon A
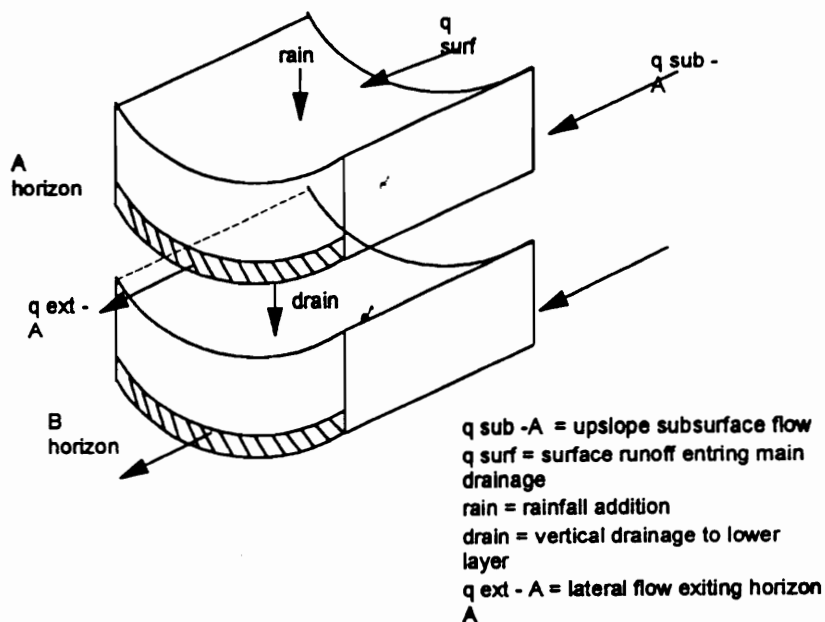
Figure 8.3: Loadings to a main drainage channel within a hillslope segment.

The computational procedure for each main drainage channel is:

1)   Determine the vertical inflow (infiltrating water volume for the surface layer) and upslope subsurface flow input for the soil horizon. The upslope subsurface flow volume for a soil layer within a main drainage channel element is computed by

$$q_{sub-in[i,j,k]} = q_{sub-in[i,k]} \cdot \left(\frac{a_{[i,j,k]}}{a_{f[i,k]}} \right) \qquad 8.4$$

where the subscripts [i, j, k] indicate the segment, main drainage channel element, and the soil layer respectively, $q_{sub-in[i,j,k]}$ is the incoming subsurface flow (m^3 min^{-1}), $q_{sub-in[i,k]}$ is the

total subsurface flow for layer [k] entering the segment from an upslope segment (m^3 min^{-1}), $a_{[i,j,k]}$ is the cross sectional area of the main drainage element (m^2), and $a_{t[i,k]}$ is the total cross sectional area for layer [k] and segment [i] (m^2). The infiltration volume in case of a surface layer is also determined by similar proportioning with respect to surface area.

2) If the initial water content of the soil layer is less than the field capacity and if the sum of the incoming flow is less than the field capacity storage (water volume required to bring the soil moisture to field capacity) all water is assumed to be stored within the layer.

3) If inflows exceed the storage volume, excess water is available for vertical and lateral drainage. The moisture content that determines the rate of vertical drainage is given by :

$$\theta_d = \frac{\theta_o + \theta_n}{2} \qquad 8.5$$

where θ_o is the moisture content for the soil layer at the start of the time step, θ_n is the moisture content due to added inflows, and θ_d is the average moisture.

4) The volume of water lost to vertical drainage/percolation for the current time step is computed using equations 7.11 and 7.12.

5) If the soil moisture after vertical drainage is still in excess of the field capacity, it is assumed that the excess water forms a perched water table/saturated layer at the base of the current soil layer. The depth of the water table is determined by distributing the excess water uniformly within the drainage element (Figure 8.3).

6) Lateral subsurface flow from a layer is assumed to be initiated with the formation of the saturated layer. Lateral subsurface flow is assumed to occur simultaneously via the soil matrix and macropores. For the saturated soil layer depth d_{sat}, the total lateral subsurface flux is given by

$$q_{sub-out[i,j,k]} = \left(K_{s[i,k]} S_{[i]} \, d_{sat[i,j,k]} w_{[i,j]} \right) + \left(por_{mac[i,k]} d_{sat[i,j,k]} w_{[i,j]} V_{mac[i,k]} \right) \qquad 8.6$$

where: $q_{sub-out[i,j,k]}$ is the sum of matrix (first term on the right hand side of the equation) and macropore subsurface flow (second term) from layer [k], drainage channel [j] and segment [i] (m^3 min^{-1}); $K_{s[i,k]}$ is the lateral saturated conductivity for layer k (m min^{-1}); $S_{[i]}$ is the slope of the segment; $por_{mac[i,k]}$ is the macroporosity for the soil horizon; $d_{sat[i,j,k]}$ is

the depth of saturation (m); and $w_{[i,j]}$ is the width of the main drainage channel element [j] (m). The computation of macropore flow is described in additional detail later.

7) If the saturated layer exceeds the soil horizon depth, and if the current layer is the surface layer, all the water volume contributing to the excess depth is assumed to be return flow and is added to the total surface runoff generated from the colluvial channel element. If the saturated depth exceeds the horizon depth in the case of a lower layer, the excess water is assumed to be return flow to the upper soil layer in the downslope segment.

8) After vertical and lateral exiting flows are computed and routed to a lower layer and a downslope segment, respectively, soil moisture is updated for the current soil horizon/layer. The new soil moisture value then becomes the initial moisture content for the next time step.

9) During drainage (when no inflow occurs to a layer) lateral subsurface flow is assumed to occur until a saturated layer does not exist within the horizon. Vertical drainage is assumed to cease when soil moisture reaches field capacity.

10) The total subsurface (lateral) flow exiting a soil layer from a segment is the probabilistic sum of the flows exiting from the main drainage channels and is expressed by

$$E(q_{sub-out[i,k]}) = n_{[i]} \sum_{j=1}^{s} P_{[i,j]} \cdot q_{sub-out[i,j,k]} \qquad 8.7$$

where $E(q_{sub-out[i,k]})$ is the expected total subsurface flux exiting from soil layer [k] and segment [i] ($m^3\ min^{-1}$), $n[i]$ is the number of main drainage elements for the segment, $p[i,j]$ is the probability associated with drainage element [j], and $q_{sub-out[i,j,k]}$ is the subsurface flow from drainage element [j] ($m^3\ min^{-1}$).

8.3.2 Macropore flow component of subsurface flow

The fraction of the total porosity occupied by macropores for a soil horizon area is represented by the parameter por_{mac} for each soil horizon (Table 8.2). It is assumed that this macroporosity is populated with macropores of varying sizes (diameters) and that this size variation can be quantified in terms of a probabilistic Lognormal distribution bounded by a

---

minimum ($dmac_{min}$) and maximum ($dmac_{max}$) macropore diameter. The bounding diameters are required inputs for a soil layer (Table 8.2). The minimum and maximum diameters are assumed to provide the 90% bounds for the Lognormal distribution. Macropores are assumed to be cylindrical in shape, uniformly distributed within the soil horizon, and continuous for the full length of the segment. It is also assumed that macropores are aligned such that macropore gradient can be approximated by the slope of the segment.

Using the assumptions mentioned above, flow in a single macropore flow is approximated with Manning's pipe flow expression (equation. 7.14). For a distribution of macropores bounded by $dmac_{min}$ (m) and $dmac_{max}$ (m), the total expected macropore flow rate $E(Q_{mac})$ (m^3 min^{-1}) is given by

$$E(Q_{mac}) = \sum_{i=1}^{n_{mac}} p_{mac}[i] \cdot q_{mac}[i] \qquad 8.8$$

where n_{mac} is the number of discrete macropore diameters selected from the distribution, $p_{mac}[i]$ is the probability associated with macropore [i], and $q_{mac}[i]$ is the flow in macropore [i] computed using Manning equation (m^3 min^{-1}) . The expected flow rate occurs through an expected macropore cross sectional area $E(A_{mac})$ (m^2) or macroporosity given by

$$E(A_{mac}) = \sum_{i=1}^{n_{mac}} p_{mac}[i] \cdot a_{mac}[i] \qquad 8.9$$

The macropore flux V_{mac} (m min^{-1}) associated with this macropore size distribution is given by

$$V_{mac} = \frac{E(Q_{mac})}{E(A_{mac})} \qquad 8.10$$

For the total macropore cross sectional area determined by por_{mac}, the depth of saturation within the horizon d_{sat}, and the width of the drainage element, the total macropore flow $Q_{mac[i,j,k]}$ (m^3 min^{-1}) is given by

$$Q_{mac[i,j,k]} = por_{mac[i,k]} w_{[i,j]} d_{sat[i,j,k]} V_{mac[i,k]} \qquad 8.11$$

8.3.3 Surface runoff routing

Water in excess of infiltration is considered surface runoff and is routed through surface channels. Surface runoff generated on a segment is partitioned into surface channels in proportion to the channel width, and is given by

$$q_{surf[i,l]} = Q_{surf[i]} \cdot \left(\frac{w_{[i,l]}}{W_{[i]}} \right)$$ 8.12

where $q_{surf[i,l]}$ (m^3 min^{-1}) is the runoff in surface channel [1], $Q_{surf[i]}$ (m^3 min^{-1}) is the total runoff on segment [i], $w_{[i,l]}$ (m) is the width of surface channel [l] and $W_{[i]}$ (m) is the segment width. Flow depth and velocity associated with $q_{surf[i,l]}$ are then determined using Manning's equation. Assuming a rectangular surface channel cross section and hydraulic radius approximated by the flow depth, the flow depth $d_{f[i,l]}$ (m) is computed as

$$d_{f[i,l]} = \left(\frac{q_{surf[i,l]} \, n_{mann[i]}}{\sqrt{S_{[i]}} \, w_{[i,l]}} \right)^{3/5}$$ 8.13

where $n_{mann[i]}$ is the Manning's surface roughness for the segment and other terms are as defined earlier. The exact hydraulic radius, $R_{h[i,l]}$ (m), for the rectangular channel is then computed as

$$R_{h[i,l]} = \frac{w_{[i,l]} \, d_{f[i,l]}}{w_{[i,l]} + 2d_{f[i,l]}}$$ 8.14

Flow velocity $v_{f[i,l]}$ (m min^{-1}) for the channel is then given by

$$v_{f[i,l]} = \frac{1}{n_{mann[i]}} \cdot R_{h[i,l]}^{2/3} \sqrt{S_{[i]}}$$ 8.15

8.3.4 Sediment routing

Sediment movement down hillslope segments is simulated using the continuity equation. Sediment transport, deposition, and detachment is limited to concentrated overland flow in surface

---

channels. Sediment load entering a channel at the upslope edge of the segment is proportioned according to the ratio of the flow in the channel to the total surface runoff across the segment, and is given by (Lewis et. al. 1994)

$$q_{s[i,l]} = Q_{s[i]} \cdot \left(\frac{q_{surf[i,l]}}{Q_{surf[i]}} \right)$$ 8.16

where $q_{s[i,l]}$ (kg min^{-1}) is the sediment load in channel [l], and $Q_{s[i]}$ (kg min^{-1}) is the total sediment load on the segment.

For the given sediment loading, $q_{s[i,l]}$, and channel flow rate, $q_{surf[i,l]}$, computations for sediment transport, deposition, and detachment for each surface channel are performed as illustrated in Figure 8.4. Once exiting sediment loads for all channels within the segment are determined, the total expected sediment exiting the segment $E(Q_{s\text{-}out[i]})$ (kg min^{-1}) is computed by

$$E(Q_{s\text{-}out[i]}) = n_{[i]} \sum_{l=1}^{s} P_{s[i,l]} \cdot q_{s\text{-}out[i,l]}$$ 8.17

where $q_{s\text{-}out[i,l]}$ (kg min^{-1}) is the sediment exiting from channel [l] after deposition/detachment, and other terms are as defined earlier.

8.3.5 Linkage of event hydrology and sediment components

The subsurface runoff component, the overland flow component, and the sediment component are all linked together in the model. Overland flow can be generated due to infiltration excess, saturation overland flow, and/or, return flow. Subsurface moisture conditions are required to determine the occurrence of the mechanisms and are computed in the subsurface component. If runoff exists, then sediment loading from upslope, is routed down the segment. Figure 8.5 illustrates how surface and subsurface runoff computations during an event are linked to the sediment component of the model.

for segment i, and surface channel l

determine sediment load
corresponding to channel flow

determine sediment load
in each particle class

compute transport capacity
for each particle class

compare transport capacity with
sediment load

transport > sediment load   transport < sediment load

compute maximum detachment
rate

compute deposition

compute detachment rate

compute expected exiting sediment loads
for each particle class

sum sediment loads across all channels
for each particle class

compute total sediment load and
particle size distribution leaving
segment

compute sediment enrichment
for segment

Figure 8.4: Flow chart for sediment computations

event
simulation
initiated

(AA) →

(1)

→ initiate time step t = t1

If rainfall > 0, compute interception,
throughfall

(2)

→ initiate segment, s=1

(3)

→ initiate main drainage elements, mele =
1

compute
infiltration

compute runoff
excess

compute vertical drainage
and lateral subsurface flow from each
horizon

(3)

← all main drainage elements
evaluated

no,
mele=mele+1   ↓ yes

compute total expected lateral subsurface
flow
exiting the segment from each horizon

(6)

(6)

compute total runoff excess for
segment

runoff excess > 0 (5) →

no

↓ yes

(4)

→ initiate surface channels, surch = 1

compute velocity for channel
flow

perform sediment
computations

(4)

← all surface channels
no,   evaluated
surch=surch+1   │ yes

compute exiting total sediment (5)
load and particle size distribution ←

(2) all segments
← evaluated
no,
s=s+1   ↓ yes

(1) all time steps
← evaluated
no,
t=t1+1

Figure 8.5: Flow chart illustrating the linkage of hydrology and sediment components.

8.3.6 Flowchart for complete model simulation

Since the model is a continuous simulation model, simulation duration is composed of event and non-event periods. During events, surface and subsurface flows and sediment routing are simulated with a one minute time step. During non-event periods water losses from the hillslope occur through evapotranspiration. Evapotranspiration losses are assumed to occur from intercepted moisture if any, and the soil moisture storage. The equations used to describe evapotranspiration losses and their redistribution in the soil were discussed in the chapter on Model Development. Figure 8.6 illustrates how evapotranspiration computations performed within the model and how event and non-event simulation processes are integrated.
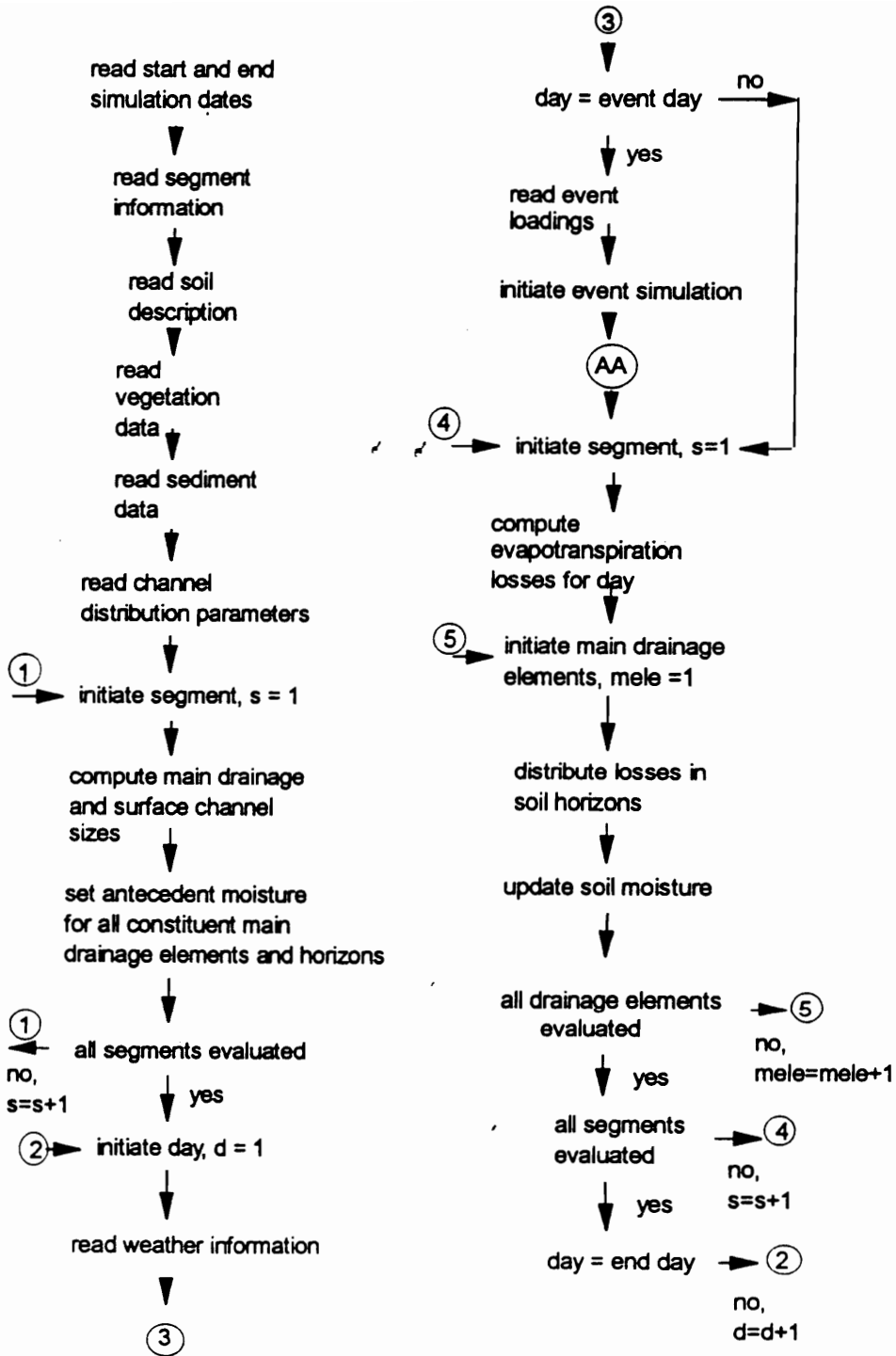
Figure 8.6: Linkage of event and non-event components of the model.

9 EXPERIMENTAL DATA FOR MODEL EVALUATION

To test and evaluate the riparian hillslope model, measured field data from riparian/hillslope studies were required. Since no single study had the complete data set required to test the model in its entirety, major phenomena simulated in the model were tested individually. The phenomena targeted for evaluation were subsurface downslope flow (Darcian soil matrix flow and non-Darcian macropore flow), variable source area generation mechanisms, and sediment transport. Experimental datasets collected to test these phenomena are listed in Table 9.1, followed with a brief description of each study.

Table 9.1: Model components and experimental studies

Model component	Experimental study
Subsurface flow	Canadian Shield basin
	Melton Branch hillslope catchment
Variable source area mechanism	Hachioji Basin, Japan
Sediment transport	Kentucky Grass Filter study

9.1 Canadian Shield Basin hillslope study

9.1.1 Investigators and objectives

The Canadian Hillslope Study was initiated in May 1991 by D.L. Peters and J.M. Buttle at Trent University, Peterborough, Ontario, Canada (Peters, 1994; Peters et al., 1995). The primary objective of this experimental study was to investigate and quantify subsurface flow and its contribution to storm flow in a headwater basin. The hypotheses behind the study were: (1) on shield slopes with thin soil cover, most flow occurs at the soil-bedrock interface; (2) a significant portion of the event water moves via preferential flow pathways vertically to the bedrock surface and laterally along the soil-bedrock interface; (3) the relative pre-event water contribution to subsurface flow is a function of the soil thickness; (4) a significant portion of event water flux in

storm flow from forested basins with shallow soil cover is supplied via subsurface flow along the soil bed-rock interface. A brief description of the study is provided below. A comprehensive description can be found in Peters (1994).

9.1.2 Site location and description

The study was conducted in the Plastic Lake basin 1-08 (PC1-08) located on the Canadian Shield 20 km south of Dorset, Ontario, Canada. The basin is underlain by granitic gneiss and amphibolite. Weakly developed orthic humo-ferric and orthic humo-ferric podzols have formed on the thin sandy basal till. Soil thickness varies from 0 to 1.5 m, averaging 0.29 m. In some areas the mineral B horizon has not developed and the bedrock is covered by an A horizon and/or a humus layer. Vegetation is dominated by coniferous species (white pine, eastern hemlock, and white cedar).

Rainfall at the site was monitored using a tipping bucket rain gage. Throughfall was found to be 90% of the open area totals. Subsurface hillslope flow was monitored for four hillslope segments. Two of the slopes (1B and 2B) had shallow soil consisting of an organic layer overlying the bedrock. The deeper slope sites (1A and 2A) consisted of an organic-Ae horizon and mineral B horizon above the bedrock. Subsurface flow exiting each constituent horizon was measured at the soil trench located downslope of each slope segment (Figure 9.1). Streamflow from the catchment was also monitored using a 90^0 V-notch weir. Twenty nine rainfall events were monitored from May 1 to June 21, 1991, and from September 22 to November 15, 1991. Of the monitored storms, 12 yielded no flow (A events), 8 produced only hillslope flow (B events), and 9 produced both hillslope and streamflow (C events).

9.1.3 Description of selected data used for model testing

Of the four hillslope segments instrumented, only the deeper segments (1A and 2A) were used for model evaluation. The largest of the 29 rainfall events, the C events, produced the most significant runoff at the 1A and 2A hillslope segments and thus were selected for model testing.
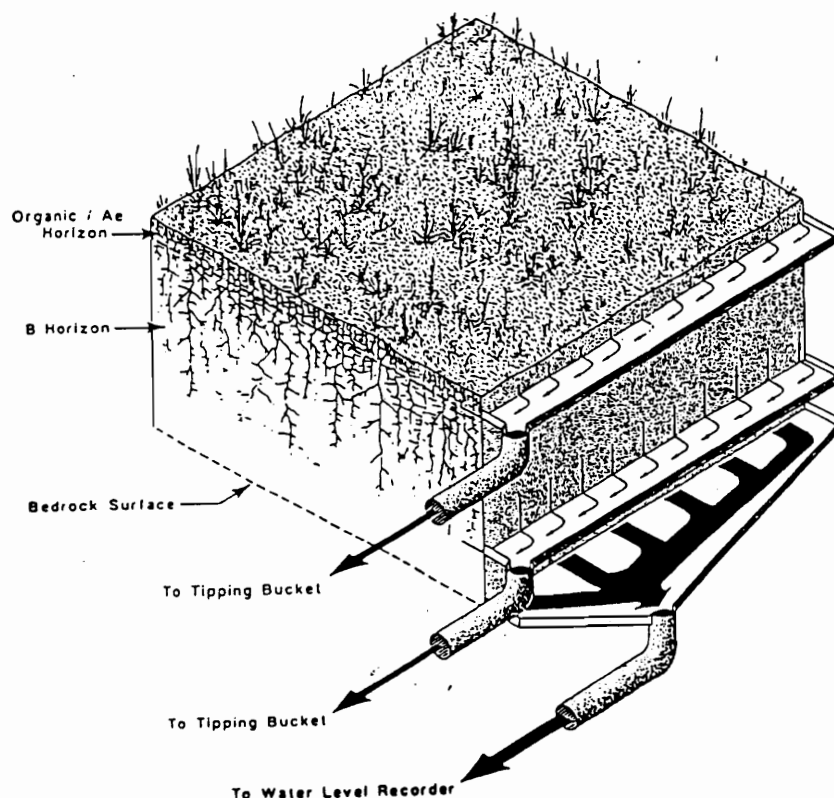
Figure 9.1: Flow measurement facility located at base of the hillslopes (Peters, 1994).

Other data that were used to generate model input included -

•   Hillslope dimensions and topographic information: Table 9.2 provides the dimensions and drainage areas of hillslopes 1A and 2A. Topographic maps for the hillslopes are provided in Figures 9.2 and 9.3.

Table 9.2: Dimension and drainage area for hillslopes 1A and 2A

Segment	Length (m)	Avg. width (m)	Slope (%)	Drainage area (m^2)
1A	46.5	9.0	15	397
2A	70.0	13.1	18	822
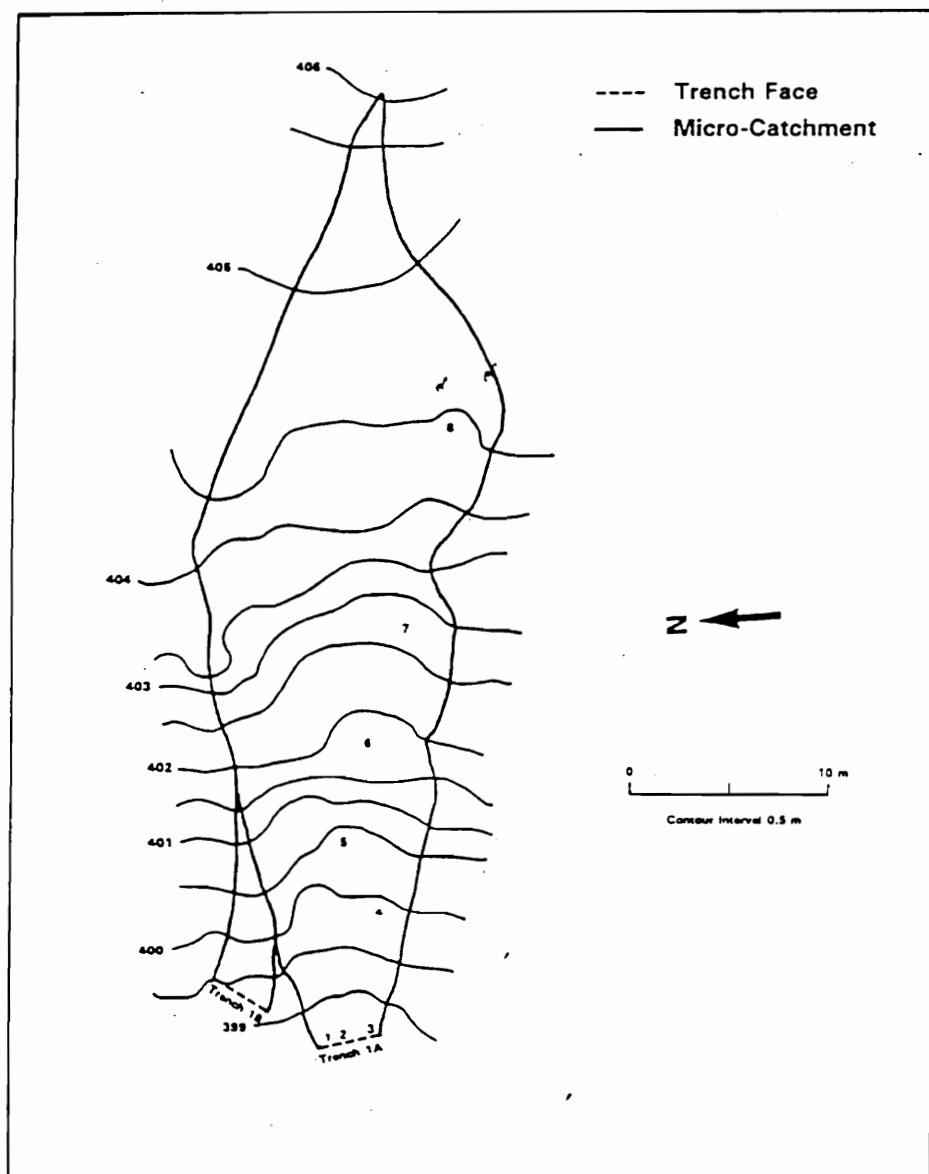
Figure 9.2: Topographic map of hillslope 1A (Peters, 1994)
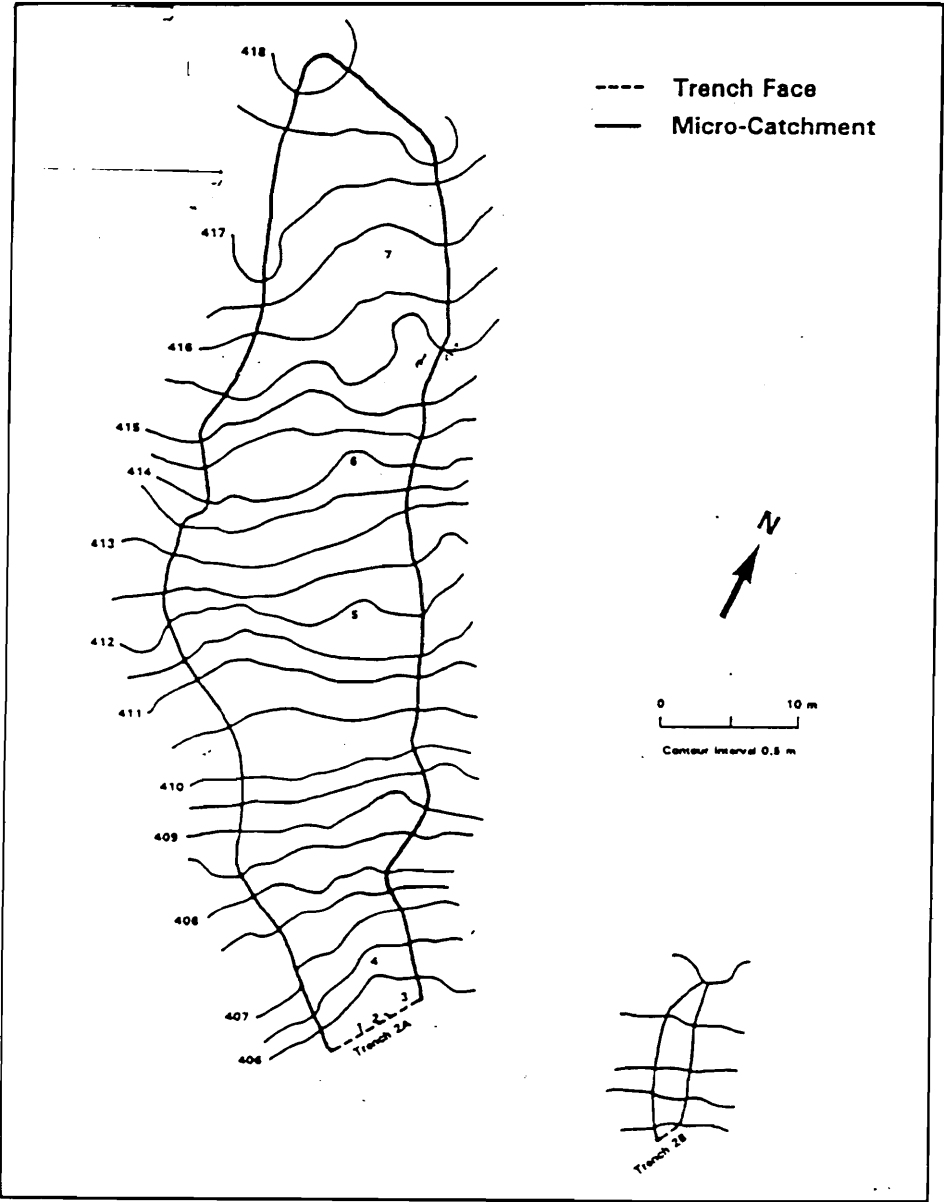
Figure 9.3: Topographic map of hillslope 2A (Peters, 1994).

- Soil horizon description : For hillslopes 1A and 2A, information was available on soil horizon thickness, total porosity, vertical and horizontal conductivity. A tabular description of these data is provided in Appendix III. Soil moisture release curves from core samples collected for each hillslope provided information on the porosity distribution in different pore size classes (Appendix III).

- Rainfall event information: Rainfall information (C events) for each hillslope included total rainfall, peak rainfall intensity, duration, rainfall hyetograph, and antecedent soil moisture condition prior to precipitation. Antecedent soil moisture conditions were expressed in the form of antecedent precipitation indexes API_7 and API_{14}, antecedent seven and 14 day precipitation, respectively. Rainfall information is provided in Appendix III.

- Hillslope runoff response: Data on hillslope response to rainfall events were available in terms of lateral subsurface flow runoff hydrographs for each soil horizon measured at the base of the hillslope (at the trench), and total runoff and peak runoff from each horizon. Mean lag to peak (time between the center of mass of rainstorm and peak runoff was also measured for each rainfall response. Runoff ratios (ratio of total rainfall to total runoff) were also computed for each hillslope. Tensiometers installed on the hillslopes provided an estimate of the depth and development of the saturated layer (forming over the restricting soil layer) during the rainfall event.

9.2 Melton Branch subwatershed data

9.2.1 Investigators and objectives

Melton Branch subwatershed investigations were initiated in 1991 by G.V. Wilson, P.M. Jardine, J.D. O'Dell, and M. Collineau at the Oak Ridge National Laboratory (Wilson et al., 1993). Objectives of the study included investigation and quantification of lateral subsurface flow,

investigation of the nature of contaminant flux with lateral subsurface flow, and creation of a database of field measurements that could be used for model testing and evaluation. A brief description of the study is provided below. Comprehensive descriptions of the study and site can be found in Wilson et al. (1993) and Luxmoore and Abner (1987).

9.2.2 Site location and description

Investigations were conducted within the Melton Branch watershed, located on the Oak Ridge Reservation in eastern Tennessee. The experimental area within the Melton Branch watershed is underlain by Maryville limestone, which is a limey shale formation. The weathered parent material is close to the surface, ranging from 0.5 to 5 m in depth. The Montevallo (Inceptisol) and Apison (Ultisols) soils formed on Maryville limestone are shallow soils (<5 m to bedrock) that occur on slowly weathering parent material. Landuse in the watershed is primarily forests. The vegetation is eastern deciduous forest species (oak, hickory and yellow poplar). The sites contain second regrowth forest which is 40 years old and approximately 20 m high.

A 0.67 ha hillslope subcatchment located within the Melton Branch watershed was instrumented to monitor and measure subsurface lateral flow (Figure 9.4). The hillslope subcatchment can be classified as a convergent slope with convex upper slopes that transcend into concave lower slopes. The subcatchment has developed within the Conasauga geologic formation. The Conasauga group weather to a shallow (< 1m) soil overlying saprolite that retains the bedding and structure of the original limey shale rock. Subsurface flow is measured at a 2 m deep by 16 m deep long trench located at the outflow region of the subcatchment. The scheme of trench collection pans and H flumes is illustrated in Figure 9.5. Subsurface lateral flow exiting from A and B horizons (0 - 0.6 m) is collected by the upper flume, whereas flow exiting from the C horizon (0.6 - 1.0 m) is collected in the lower flume. A Belfort rain gage located less than 50m from the site in a cleared area is used to monitor rainfall intensity and total rainfall. Estimates of rainfall interception for the region are available from an earlier study. Perched water tables within the subcatchment are monitored using tensiometers and wells.
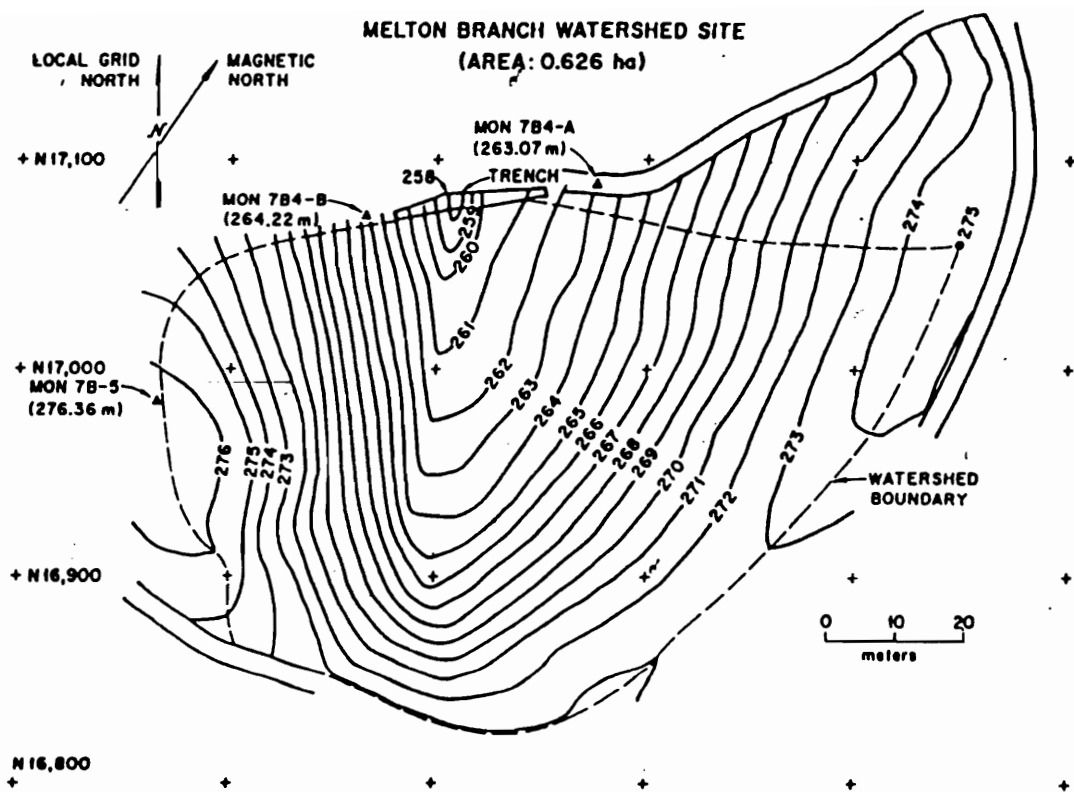
Figure 9.4: Topographic map of Melton Branch hillslope catchment (Luxmoore and Abner, 1988).
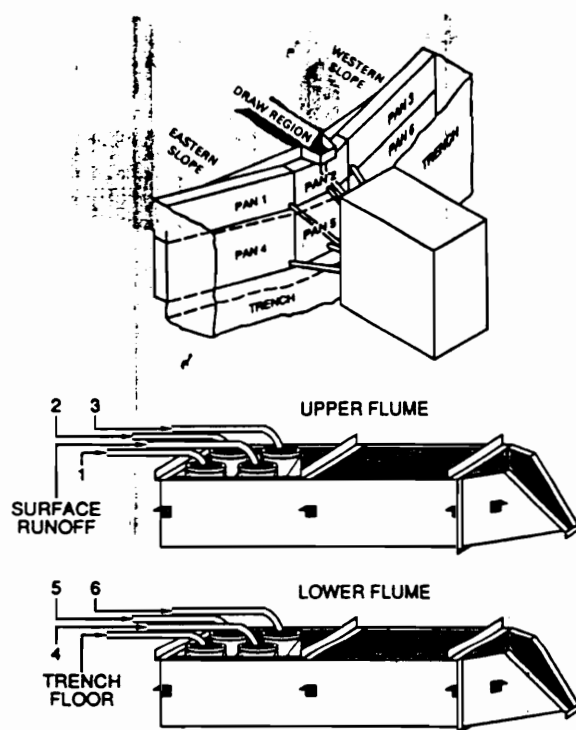
Figure 9.5: Pan facility located at the base of the hillslope catchment to monitor subsurface flow (Wilson, et al., 1993).

9.2.3 Description of selected data used in model testing

* Hillslope dimensions and topography: Figure 9.4 provides a topographic map of the Melton Branch subcatchment at a 1 m contour resolution. The slope length was 78 m and the average gradient was approximately 25%.
* Soil horizon description: Soil moisture release curves, saturated conductivity, and macroporosity measurements were available for the A, B, and C soil horizons. Soil moisture release curves are attached in Appendix IV.
* Rainfall event information: Rainfall events extending over the period January to December 1991 were monitored. Six rainfall events that occurred during this period were selected for model evaluation. Rainfall hyetographs for the six events are included in Appendix IV.
* Hillslope subcatchment response: Subcatchment response to rainfall events was measured and is available in terms of lateral subsurface flow hydrographs from the upper (A and B horizon contribution) and lower (C horizon) H flumes.

9.3 Hachioji catchment study

9.3.1 Investigators and objectives

The Hachioji catchment study was conducted during the period 1980-83 by T. Tanaka, M. Yasuhara, H. Sakai and A. Marui at the Institute of Geoscience, University of Tsubaka, Ibaraki, Japan. The study objectives were: (1) to elucidate by intensive field observations the physical processes of storm generation and to identify the main source of storm runoff, and (2) to explain the generation mechanism of the main component. A brief description of the study is provided below. A comprehensive description can be found in Tanaka et al. (1988).

9.3.2 Site location and description

The study was conducted in the Hachioji Experimental Basin, which is located in the western suburbs of Tokyo. The experimental basin is a 0.022 km² forested basin (Figure 9.6). The topography is typical of a dissected hill having a valley floor slope of about 12% and a steep hillside slope of 50%. The valley floor covers a major portion of the basin. The basin lies within the Tama hills which are underlain by the Pliocene Miura and the Pleistocene Narita groups. The upper 2 m of the surficial deposits are broadly classified as clay loam and silty clay. Under these soils, impermeable clay or compacted clayey sand deposits, which constitute the upper part of the Renkoji Alternation belonging to the Pliocene Miura group are present over almost the entire basin. The vegetation consists of dense deciduous trees approximately 15 m in height, sparse bamboo 1-2 m high, and a dense ground cover of ferns and small shrubs.

A hillslope segment within the experimental basin was instrumented to study runoff generation (Figure 9.6). Precipitation at the site was measured using a tipping bucket recording rain gage. Discharge from the basin was automatically recorded at three sites using a 90° V notch weir and two parshall flumes. Pressure heads of soil water were measured using tensiometers. Ground water potential was measured using peizometers.

9.3.3 Description of selected data used in model testing

- Dimensions and subcatchment topography: A topographic map of the subcatchment is shown in Figure 9.6. The valley floor and hillside slopes were 12 and 50%, respectively.
- Soil horizon description: Data on soil horizon depths and conductivity were available and are reproduced in Figure V.1, Appendix V. Values of conductivity ranged from 10^{-4} to 10^{-7} cm/s. Information on total porosity, field capacity values, and soil moisture release curves was not available for these soil horizons.
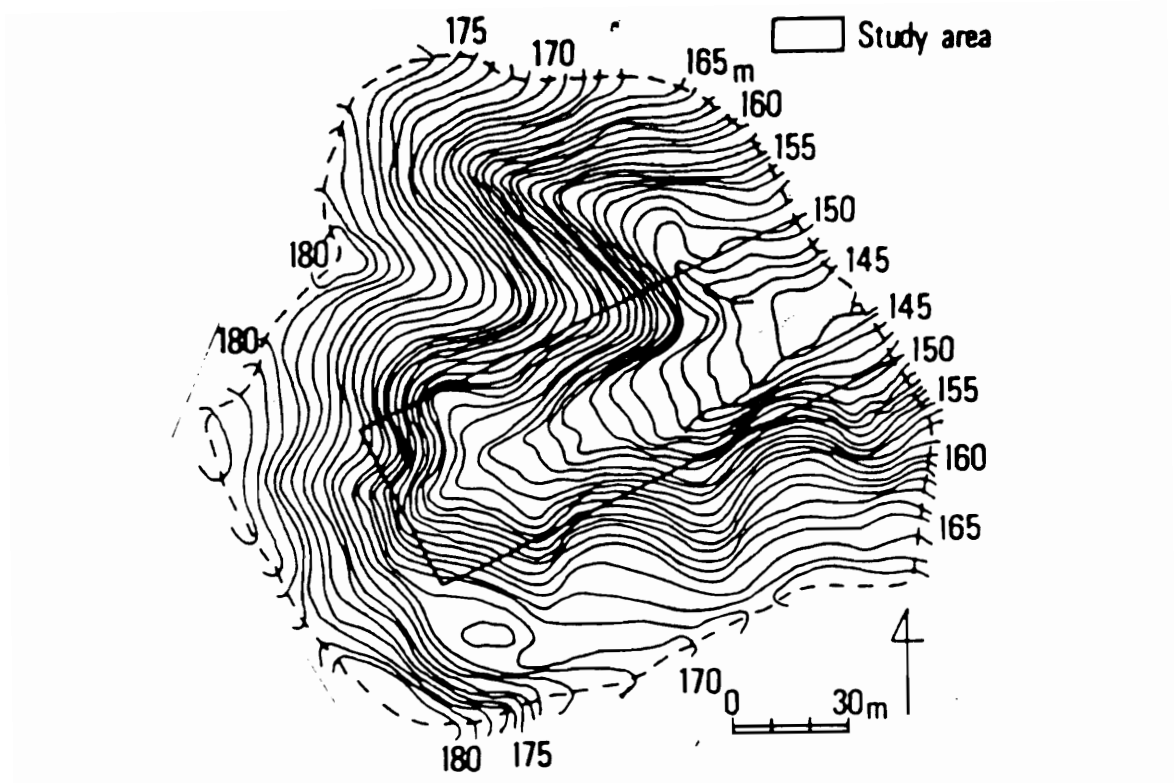
Figure 9.6: Topographic map of Hachioji Experimental Basin and the plan view of instrumented hillslope section (Tanaka et al., 1988).

- Rainfall event information: Intensive data on eight storms with a rainfall total greater than 50 mm are available. Out of these, one storm was selected for model evaluation. Rainfall information was in the form of rainfall hyetographs and total rainfall estimates (Appendix V). Estimates of antecedent moisture conditions prior to storm events were not available.

- Hillslope/subcatchment response: Hillslope response for each rainfall event was available in terms of total discharge volume at the main weir, direct runoff ratio, peak discharge rates, and the subsurface and surface soil saturation profiles caused by runoff.

9.4 Kentucky grass filter data

9.4.1 Investigators and objectives

The Kentucky Grass Filter study was conducted from May to August 1992 by S.P. Inamdar, B.J. Barfield, A.W.Fogle, and D.I. Carey at the University of Kentucky, Lexington. The primary objective of the experimental investigations was to determine the amount of sediment trapped in naturally occurring grass filter strips of variable length. A brief description of the site and experimental investigations is provided below. A comprehensive description of the study can be found in Inamdar (1993) and Fogle et al. (1994).

9.4.2 Site location and description

Experiments were conducted at the University of Kentucky Agricultural Experiment Station Farm at Lexington, Kentucky. The grass strips were located on Maury silt loam, a deep well drained soil on an area with a general slope of 8.7%. The grass was primarily a mixture of dense fescue and bluegrass. The grass strips had a constant width of 4.57m and lengths of 4.57, 9.6, and 13.1 m. Each length was duplicated once (Figure 9.7). Sediment loading to the grass strips was provided by erosion plots 4.57 m wide and 22.1 m long, located upslope of the grass strips (Figure 9.7). Rainfall was applied artificially on the erosion plots at the rate of 66mm/hr.

Figure 9.7: Plan view of erosion plots and grass filters strip used in the Kentucky study (Inamdar, 1993).

9.4.3 Description of selected data used for model testing

- Grass filter strip dimensions and topographic information: Figure 9.7 provides the dimensions for each grass filter strip. Point elevations were taken within each of the grass strips at a grid interval of approximately 0.3 m to determine the density and cross-sectional shape of flow channels within the filter. A detailed description of the grass filter surface topography is given by Inamdar (1993).
- Event information: Each grass strip was subjected to two runoff events. For each event information was available on runoff rate and sediment concentration entering and leaving the grass strip and particle size distribution of the incoming and exiting sediment.

10 MODEL EVALUATION

10.1 Introduction

The goal of model evaluation was to compare observed and predicted data, and more importantly, determine the confidence associated with model predictions. To accomplish this, model results were evaluated using statistical procedures developed by Haan et al. (1995) (discussed in section 3.5). Such approaches are more realistic in that they consider the uncertain nature of the model/simulated mechanisms as well as the inherent variability in the measured/observed data. Expression of the model results with associated confidence bounds also provides a better estimate of model performance compared to procedures that determine absolute and relative error between point values (observed and predicted).

Specific procedures that were used to compare observed and model predicted data included:

- Visual comparisons
- Regression analysis: Statistical analysis to evaluate whether parameters (slope, intercept) of the line of perfect fit are significantly different from the parameters of the line generated by regression of observed and predicted data.
- Probability distributions: Comparison of probability distribution functions (pdfs) of predicted and observed data with their associated confidence bounds.

A description of field measured data available to test model predictions was provided in an earlier chapter. The model components that were targeted for evaluation were:

- Subsurface flow
- Variable source area generation mechanism
- Sediment transport and fate

The extent to which each of these model components were evaluated was decided by the amount and type of information (quantitative/qualitative) that was available from each of the field studies. The sections that follow describe for each component which specific hillslope responses were

evaluated and why, the selection/extraction of parameters values needed for model simulation from field measured data, and finally the discussion comparing model predictions and observations.

10.2 Subsurface flow component evaluation

Data from two experimental field studies was available to test the subsurface lateral flow component of the model. A discussion on the two studies follows.

10.2.1 Canadian Shield hillslope

10.2.1.1 Scope of evaluation

The Canadian Shield data set was the most detailed data set available for model testing. A brief description of this data was provided earlier in section 9.1. Extensive quantitative information collected in this study allowed a comprehensive quantitative comparison between observed and predicted hillslope responses. The hillslope responses that were compared included:

- runoff hydrographs from each horizon
- event subsurface runoff totals
- peak subsurface runoff values
- lag times to peak runoff values

10.2.1.2 Input data selection

The specific parameters required to describe and simulate hillslopes in the riparian hillslope model were discussed earlier in the chapter on Model Framework. Values corresponding to some of the hillslope parameters (e.g., vertical and horizontal conductivities) were extracted directly from field measurements, whereas, others (e.g., field capacity) were estimated from the observed data. The following paragraphs describe how the values were extracted/estimated.

10.1.1.2.1 Segment information

Hillslopes 1A and 2A were both discretized into six segments each. Topographic maps of hillslopes 1A and 2A (shown in Figures 9.2 and 9.3) were used to determine the total hillslope

length, and individual segment lengths, widths, and slope gradients. Information on these parameters is listed in Table 10.1. To determine drainage channels and drainage shape information, the topographic maps were digitized and converted to point elevation data. This was accomplished using the IDRISI software. A DEM model was then used to determine the flow concentration along the hillslope. Since no surface runoff was observed during field studies, the emphasis was to determine depressions and their shape attributes along which subsurface flow might concentrate. A surface map of the two hillslopes was generated using SURFER (Figures 10.1 and 10.2). Figures 10.1 and 10.2 and the DEM analysis indicated a single major channel along the full length of the hillslope along which subsurface flow might be expected to concentrate. Cross sections of the hillslope were then extracted at every 5 m down the hillslope and drainage channel width to depth ratios determined. These width to depth ratios were normalized to the average w/d value. The best fitting distribution to the population of normalized w/d values was then determined using VTFIT. A Lognormal distribution seemed to best fit the data. Distribution parameters for the drainage shape data are listed in Table 10.2.

Table 10.1: Segment input

	Hillslope 1A	Hillslope 2A
# of segments	6	6
length of segments (m)	7.75 (46.5 m) [a]	11.56 (69.36m) [a]
width of segments (top to bottom) (m)	2.06, 10.00, 13.23, 12.06, 9.41, 5.88	10.21, 13.19, 14.89, 18.30, 13.19, 8.94
slope gradient of segments (%)	10.30, 9.00, 19.30, 11.61, 23.20, 20.6, (16.00 [b], 9 [c])	14.70, 10.38, 21.62, 21.62, 19.89, 23.35, (18.64 [b], 10.56[c])
# main drainage elements	1	1
average main drainage w/d	25	25

Note: [a] total hillslope length
        [b] average hillslope gradient (%)
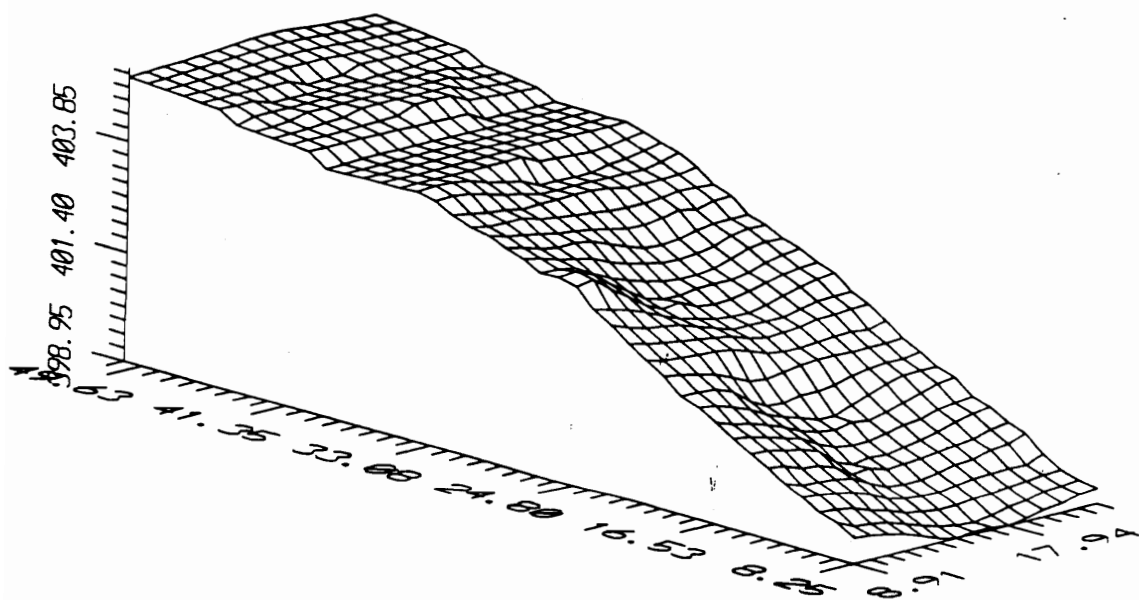   [c] slope gradient in degrees.

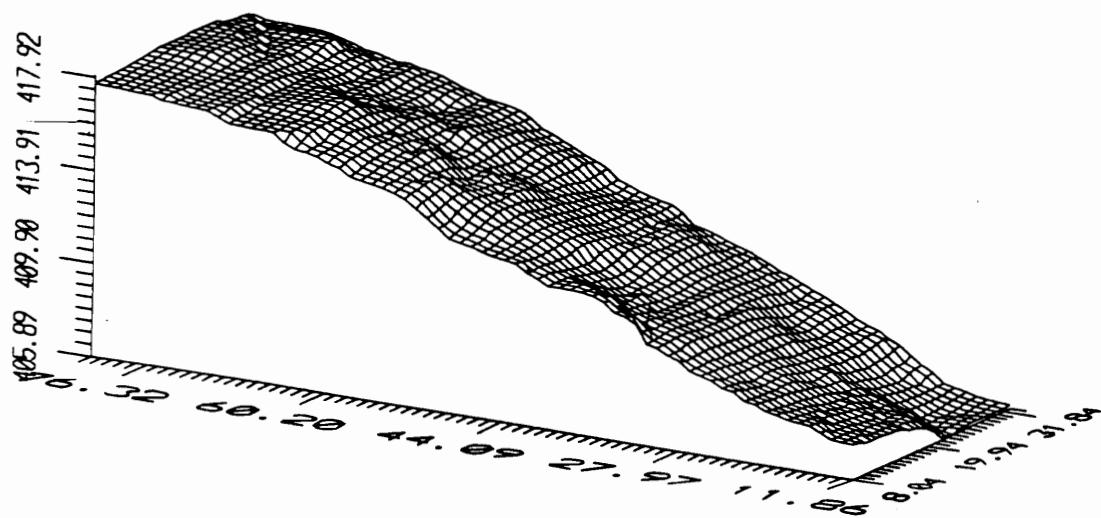Figure 10.1: Three dimensional surface of hillslope 1A.

Figure 10.2: Three dimensional surface of hillslope 2A.

Table 10.2: Channel w/d distribution parameters

Hillslope	Distribution type	Mean	Variance
1A	Lognormal	-0.0356	0.0682
2A	Lognormal	-0.0964	0.1984

10.2.1.2.2 Soil description:

A general description of the soil horizons and their thicknesses, and soil texture found at the two hillslope sites is provided in Table III.1 and III.2, Appendix III. Depths of the soil horizons specifically at hillslopes 1A and 2A were not measured during field experiments, but an average depth to bedrock was measured at both sites (Appendix III). The soil horizon depths used in model simulation were determined by partitioning the depth to bedrock (measured at each site) in proportion to the general soil horizon depths listed in Table III.1 and III.2. As illustrated in Table 10.3, hillslopes 1A and 2A were discretized into two and three soil horizons, respectively. No parameter estimates (such as conductivity and porosity) were available for the bedrock that was assumed to underlay these soil horizons. In the absence of measured values, very low values for conductivity were assumed. Porosity, and vertical and horizontal soil horizon conductivity values for soil horizons were measured for both the hillslopes, and were used without modification (Table 10.3). Soil moisture release curves for each of the hillslopes were experimentally measured (Appendix III). The size of micropores (constituting the soil matrix) is generally limited to that below 0.01 mm (Luxmore, 1981). Using this assumption, the percentage of the total porosity occupied by pores below 0.01mm dia was estimated to be 45 and 57% for hillslope 1A and 2A, respectively. At field capacity, it is expected that all micropores are saturated. Thus, the field capacity values for the hillslopes corresponded to the porosity associated with the pores below 0.01mm. Using the percentages computed above, and the total porosity values for each of the horizons (experimentally measured), field capacity values were determined for each horizon

(Table 10.3). Maximum macropore diameter observed at the site was 30 mm. Based on Luxmoore's (1981) classification, minimum macropore diameter was assumed to be 0.15 mm. Although maximum macropore diameters of 30 mm were observed, field investigations did not indicate in which horizons they occurred. Also, in most cases only a fraction of the total macroporosity is assumed to conduct water. This fraction is called the "hydrologically active" macroporosity (discussed earlier in section 3 of the Literature Review). Measurements for determining the "hydrologically active" macroporosity for the two hillslope sites were not made. In the absence of specific information, it was assumed that the 30 mm diameter macropores were limited to the A horizon only. For lower horizons the maximum macropore diameters corresponding to the "hydrologically active" macroporosity were estimated using calibrations performed for the hillslopes using event C1. Calibration procedures are discussed in a later section. Since Manning's equation was used to describe macropore flow, macropore roughness was a required parameter. No field measurements were performed to estimate this parameter. Mannings roughness values for macropores in forest soils estimated elsewhere show a wide range from 0.036 to 1.36 (Kitahara, 1989). Considering the soil was high in organic material, an approximate value of 0.5 was selected.

Table 10.3: Hillslope soil description

Slope	Soil horizon	Horizon depth (m)	Porosity	Field capacity (m^3/m^3)	$K_{v\,sat}$ (mm/hr)	$K_{h\,sat}$ (mm/hr)
1A	A	0.102	0.79	0.35	720	7200
	BF_1	0.170	0.58	0.38	252	720
	BF_2	0.157	0.58	0.38	288	108
2A	A	0.159	0.79	0.30	720	720
	BF_1	0.150	0.65	0.37	720	720

10.2.1.2.3 Event loadings:

Rainfall data for the C events were available in the form of hyetographs. Rainfall loadings

to the model were provided by converting the hyetographs into discrete break point rainfall values. A summary of the rainfall information for the C events is provided in Table 10.4. Rainfall depths were adjusted for forest canopy interception. Interception at the site was estimated as approximately 4.5% of the rainfall depth. There were no upslope surface or subsurface loadings to either hillslope 1A or 2A. The runoff response measured at the base of the hillslopes was attributed only to rainfall on the hillslope catchments.

Table 10.4: Summary of rainfall events

Event	C1	C2	C3	C4	C5	C6
Tot. Rain (mm)	44.5	29.2	8.0	30.5	16.8	71.2
Peak intensity (mm/hr)	18.3	13.8	3.0	27.6, 3.0*	10.7, 6.1*	15.2, 12.0*
Duration (h)	17.5	13.0	4.0	16.0, 9.0*	3.0, 7.0*	11.5, 18.5*

Note : * events with two distinct rainfall pulses.

10.2.1.2.4 Values for antecedent soil moisture and macroporosity:

The model required soil moisture contents for each of the soil horizons the hillslope was discretized into. These moisture contents express the initial state of soil water at the start of the event. Soil moisture content values at the start of the event were not measured during the experiment. However, some information was collected on 7 and 14 day antecedent precipitation (API). The 7-day API values for each event are listed in Table 10.5. The API_7 was chosen as a reference and the API_{14} was not considered because it was assumed that since the hillslope had high hydraulic conductivity (Table 10.3), a 7day period would be more than sufficient to drain the hillslope and bring it to a quasi-steady state condition prior to occurrence of a subsequent event. To convert the API_7 information to estimated soil moisture contents for each horizon, a calibration run was performed. Event 1 was used for the calibration run. Keeping all other hillslope parameters constant, the soil moisture contents for the soil layers were varied until the subsurface runoff hydrograph and the subsurface runoff total from the B horizon best matched the observed. It was expected that the antecedent soil moisture contents for the horizons would be near field capacity since field observations had indicated that the lag time between the rainfall and hillslope

subsurface response was small. Once, the best fitting soil moisture contents for both hillslopes corresponding to event 1were determined, no further calibration was performed. For all other events, soil moisture contents were adjusted in proportion to the API_7 values for the events. The proportioned soil moisture contents for all events are listed in Table 10.5.

Table 10.5: Antecedent soil moisture conditions

Slope	Soil horizon	Event 1*	Event 2	Event 3	Event 4	Event 5	Event 6
API_7 (mm)		2.6	0.4	11.5	10.7	17.8	6.2
1A	A	0.22	NR	0.32	0.30	0.33	0.26
	BF1	0.33	NR	0.37	0.36	0.37	0.335
	BF2	0.33	NR	0.37	0.36	0.37	0.33
2A	A	0.23	0.22	0.28	0.28	0.285	0.25
	BF1	0.34	0.34	0.36	0.36	0.36	0.345

Note: NR - No observed runoff.
* - event used for calibration of the soil moisture content values

Estimates on "hydrologically active" maximum macropore diameter and "hydrologically active" macroporosity for the B horizon also were not available. Hence, it was decided to determine values for these parameters using calibrations. Sensitivity analysis (described in section 11.1.1) indicated that peak subsurface runoff rates were sensitive to macroporosity and macropore diameters. This was because a predominant portion of flow contribution to peak runoff occurred from preferential macropore flow. During the calibrations conducted for determining antecedent soil moisture contents, "hydrologically active" macroporosity values were simultaneously varied from 1 - 10% of the total porosity. Maximum macropore diameters for the B horizon were varied between 1 - 5 mm. To determine the value of macroporosity and maximum macropore diameter, observed and predicted peak runoff values and runoff hydrograph shapes were compared. Results of the calibration indicated that macroporosity values of (expressed as a fraction of total porosity) 10% and 5% for A and B horizons provided the best fit response for both hillslopes 1A and 2A for event C1. The maximum macropore diameter for B horizon corresponding to 5% macroporosity

was selected as 1 mm. Values of macroporosity and maximum macropore diameter obtained using calibrations represent only the "hydrologically active" fraction of the total macroporosity and should not be considered a measure of total macroporosity.

10.2.1.3 Results and discussion
10.2.1.3.1 Runoff hydrographs

Observed and predicted subsurface runoff hydrographs for hillslopes 1A and 2A across the six C events are presented in Figures 10.3 through 10.8. Evaluation of runoff hydrographs was limited to visual comparisons only. Except for event C1, for which calibrations were made for antecedent moisture and macroporosity, the observed hydrographs tend to be more flashy than those simulated. For event four, predicted runoff from hillslope from 1A was considerably more than what was observed. The small amount of observed runoff for this event and hillslope is surprising considering the relatively wet antecedent conditions and high rainfall for this event (refer Tables 10.4 and 10.5). Observed hydrographs seem to peak earlier and have smaller recession flows (quicker drainage) compared to simulated ones. This flashiness and quick drainage of observed hydrographs could be the result of:

- Vertical preferential flow via macropores: Dissolved carbon investigations (targeted towards delineating preferential flow) indicated that vertical preferential flow via macropores was occurring on the hillslopes. This phenomenon resulted in flow being transferred from the surface to lower horizons, bypassing the intermediate horizons. This process was not simulated in the model. The model sequentially routes water through each horizon.
- Seepage through the bedrock: Field investigations revealed that some water from the perched water table above the bedrock was lost to seepage through cracks in the bedrock. The losses were non-uniformly distributed along the length of the hillslope. Since estimates of bedrock permeability or seepage distribution were not available, the model could not represent this variability.
- Nonuniform soil thickness across the slope: Field observations indicated that the hillslope soil thickness varied along the width. Especially for hillslope 2A, the bedrock was exposed at a number of locations. The discretization scheme used in the model required a

uniform soil thickness for the full width of the segment. In addition, exact horizon depths along the hillslope length were not measured. The model inputs for horizon depths were estimated based on the average horizon depths for the soil type corresponding to that found on the hillslopes, and the depth to the bedrock for each hillslope.

- Underestimation of maximum macropore diameter: It is also possible that calibrations based on event C1 underestimated the maximum macropore diameter for horizon B. Larger macropore diameters would have decreased simulated drainage and recession periods.

During field monitoring, flashy runoff responses were observed at the A horizon runoff collector. The model did not predict any lateral subsurface flow from the A horizon. Field investigations attributed A horizon responses primarily to flow occurring at the junction of the O and A horizon over leaf litter. The model did not simulate flow retention and movement over leaf litter. The only way the model could predict flow from the A horizon was when the saturated layer building up over the bedrock extended into the A horizon. Overall, the observed and simulated runoff responses compared well considering the high hydraulic conductivity, variable and relatively shallow soil thickness, and porous nature of the soil.

10.2.1.3.2 Rainfall -runoff totals

To estimate the confidence associated with model predictions, total rainfall and corresponding total predicted runoff responses for events C2 - C6 were plotted in Figures 10.9 and 10.10. Event C1 was not included since it was used to calibrate some of the hillslope parameters. Figures 10.9 and 10.10 provide the model response relationships for the Canadian Shield hillslopes. Ninety-five percent confidence bounds were then generated for these relationships and the observed responses values were included. Typically, for evaluating model predictions, 95% prediction bounds are chosen. But considering the small number of events available for comparison of the observed and the simulated values, a more strict criterion of 95% confidence bounds was selected.

Figure 10.3: Observed and predicted runoff for Event 1.

Figure 10.4: Observed and predicted runoff for Event 2.

Figure 10.5: Observed and predicted runoff for Event 3.
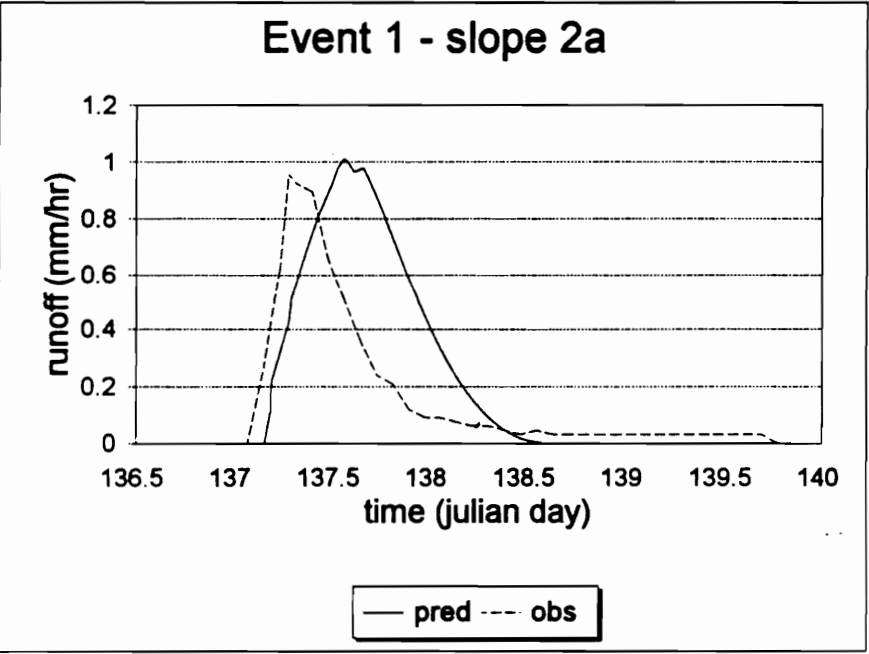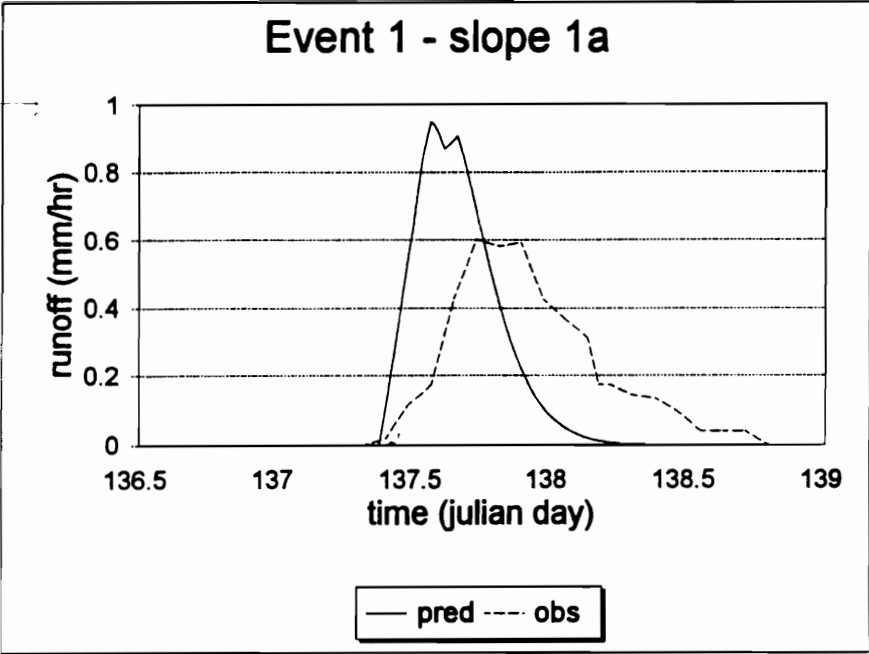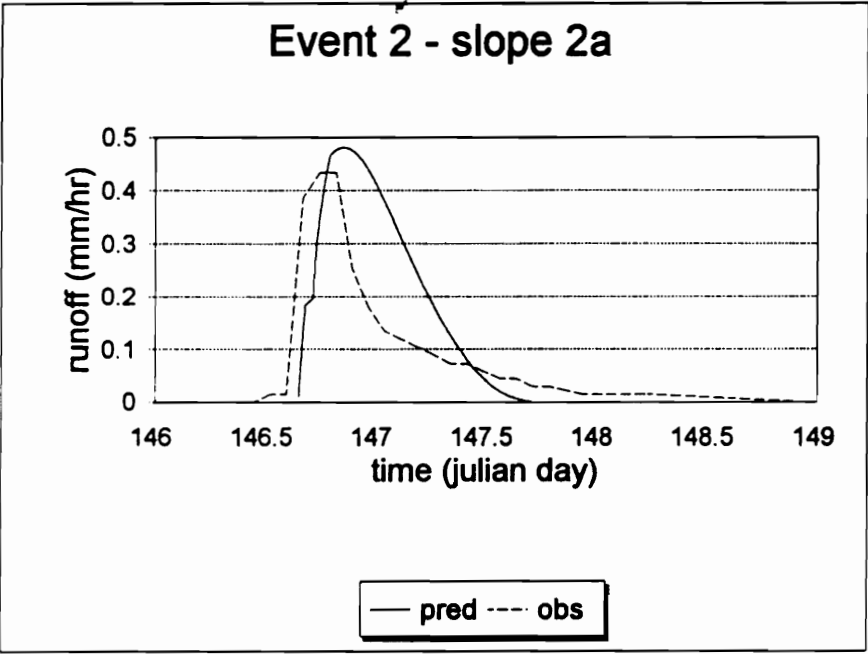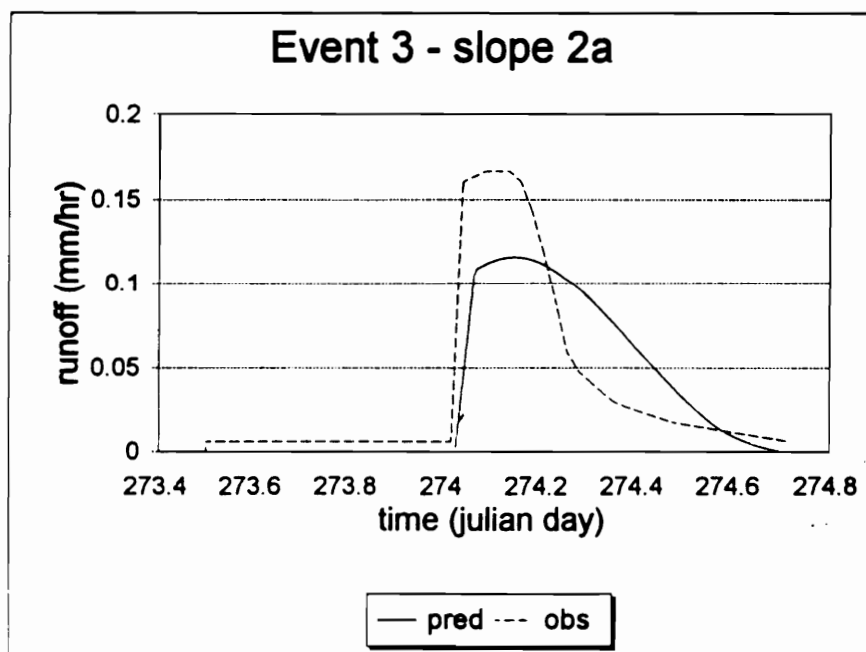
Figure 10.6: Observed and predicted runoff for Event 4.
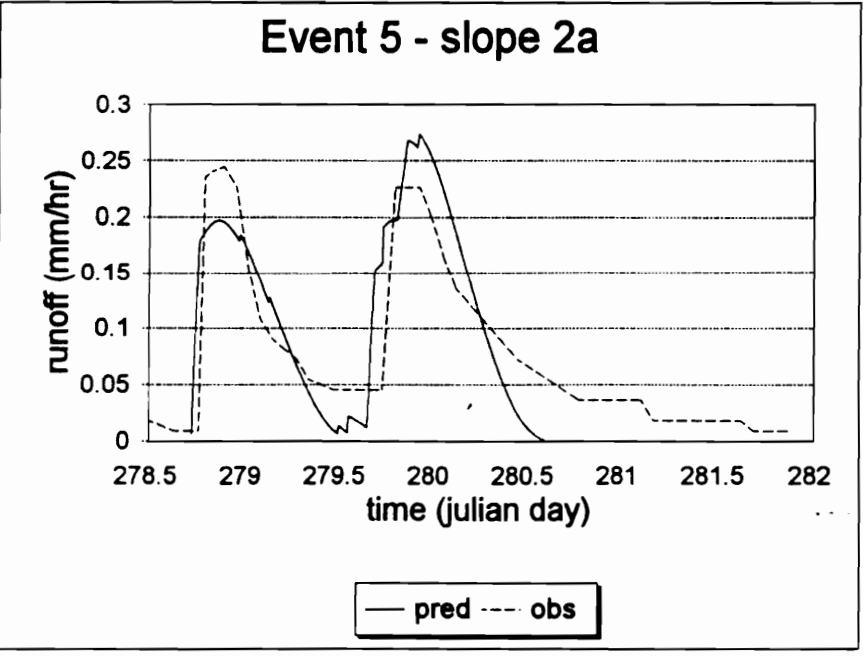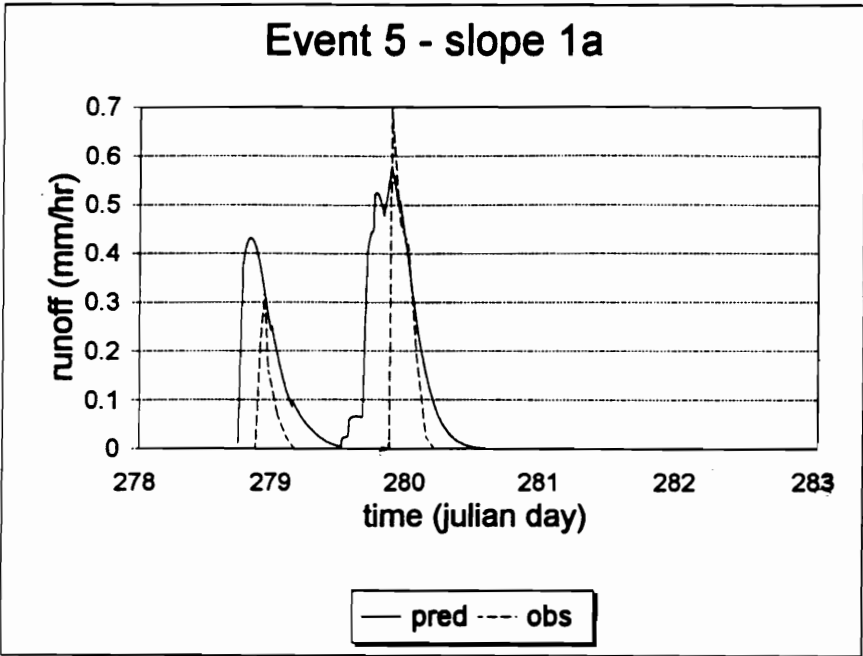
Figure 10.7: Observed and predicted runoff for Event 5.
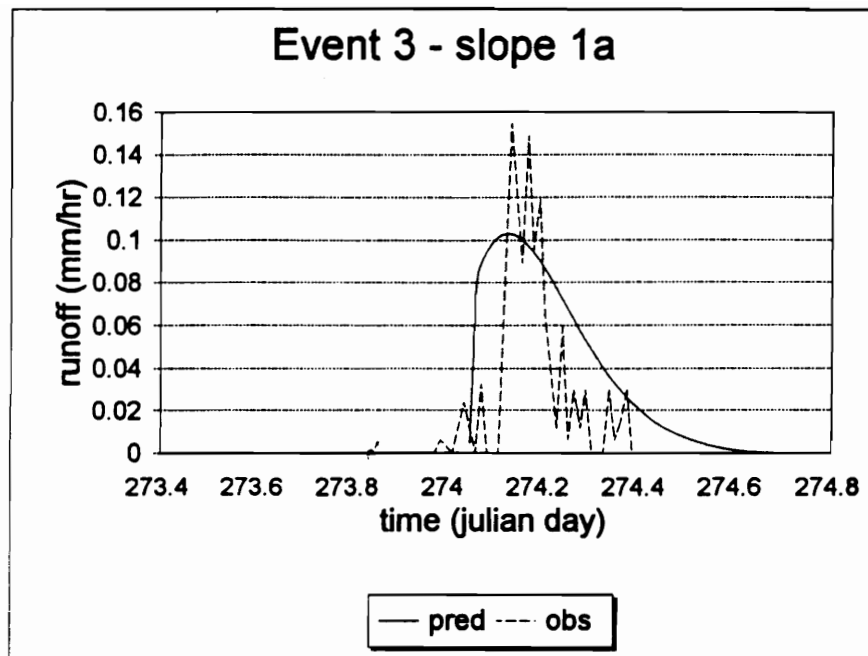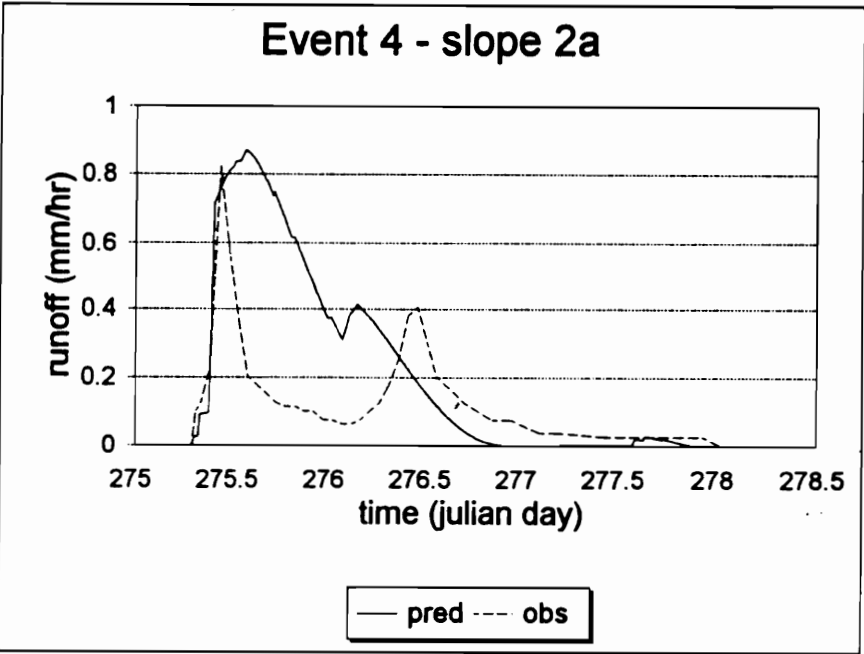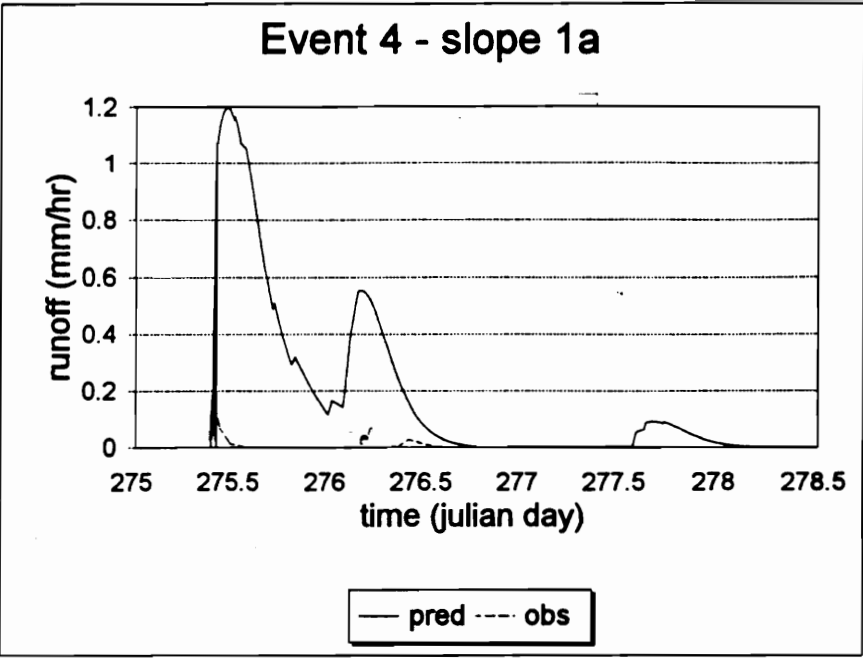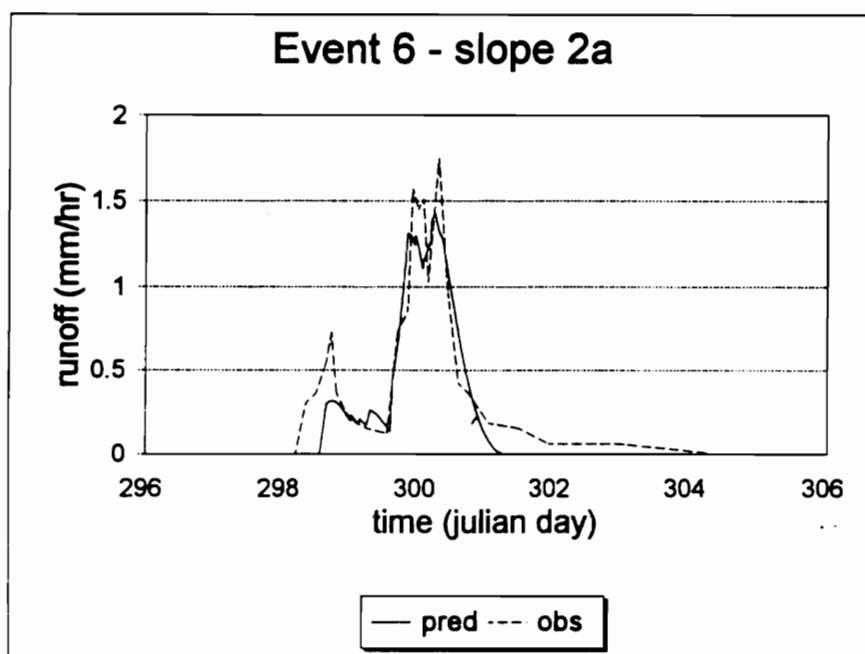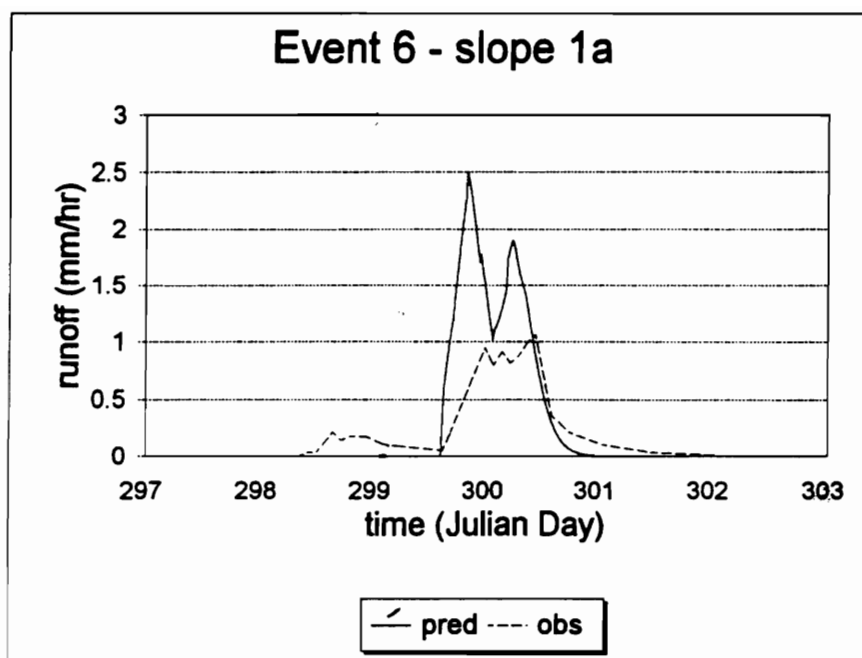
Figure 10.8: Observed and predicted runoff for Event 6.

Rainfall -Runoff totals
slope 1a
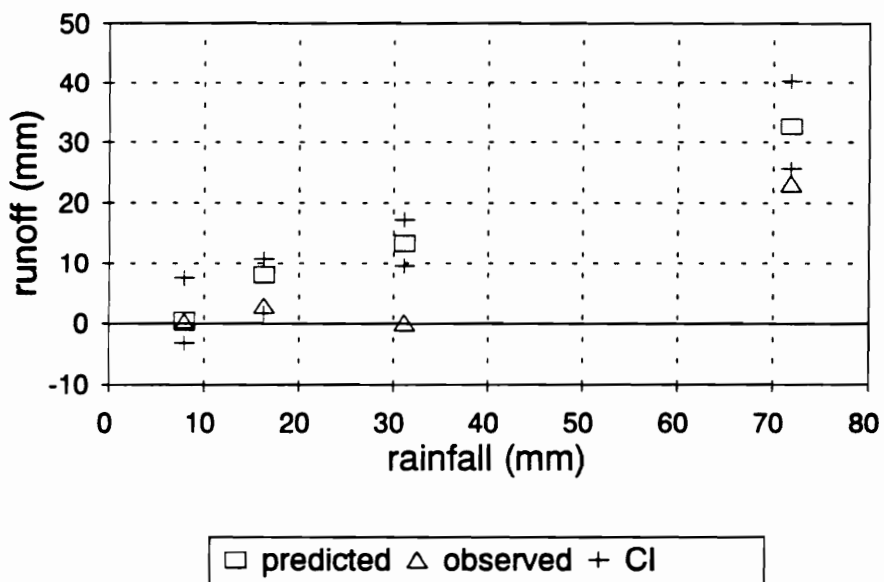
Figure 10.9: Comparison of observed and predicted total runoff values for hillslope 1A.
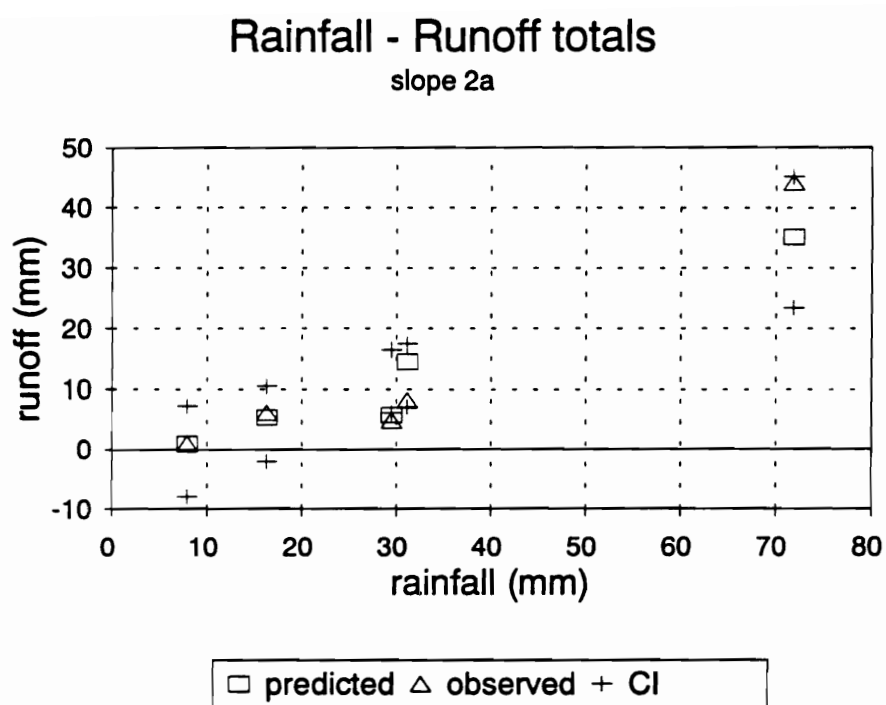
Figure 10.10: Comparison of observed and predicted total runoff values for hillslope 2A.

From Figures 10.9 and 10.10, one can determine if the model predicts the observed response at a 95% level of confidence. Of the four events evaluated for hillslope 1A, the model predicted two events at the 95% level. For hillslope 2A, four of five events were predicted at the 95 % level. Thus, if prediction at 95% level was considered a criterion for model evaluation, the model seemed to do well for hillslope 2A with a success rate of 80% (4 of 5 events) whereas for hillslope 1A the model did not fare well with prediction rate of 50%.

10.2.1.3.3 Peak runoff values, lag times to peak

Statistical evaluation of observed and predicted peak runoff values for the two hillslopes across events C2-C6 is illustrated in Figures 10.11 and 10.12. Results for hillslope 1A indicated that at a 95% confidence level, the slope and intercept values of the regression line between observed and predicted peak runoff are significantly different than the corresponding values for the equal value line (dashed line in Figures 10.11 and 10.12). For hillslope 2A, the slope and intercept of the regression line were not significantly different from the equal value line. Identical results were obtained for the plots of observed and simulated lag times to peak (Figures 10.13 and 10.14).
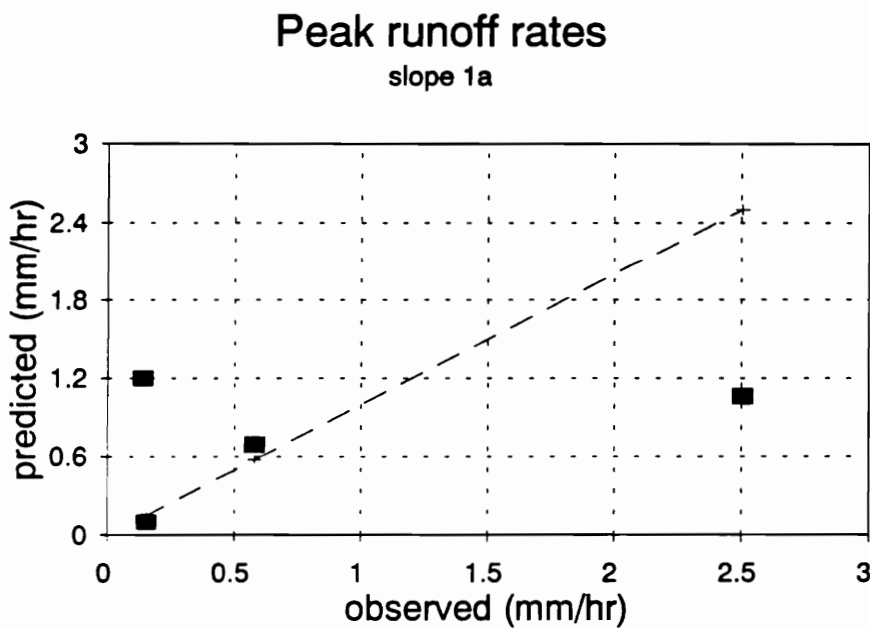
Figure 10.11: Observed and predicted peak runoff values for hillslope 1A.

Peak runoff rates
slope 2a
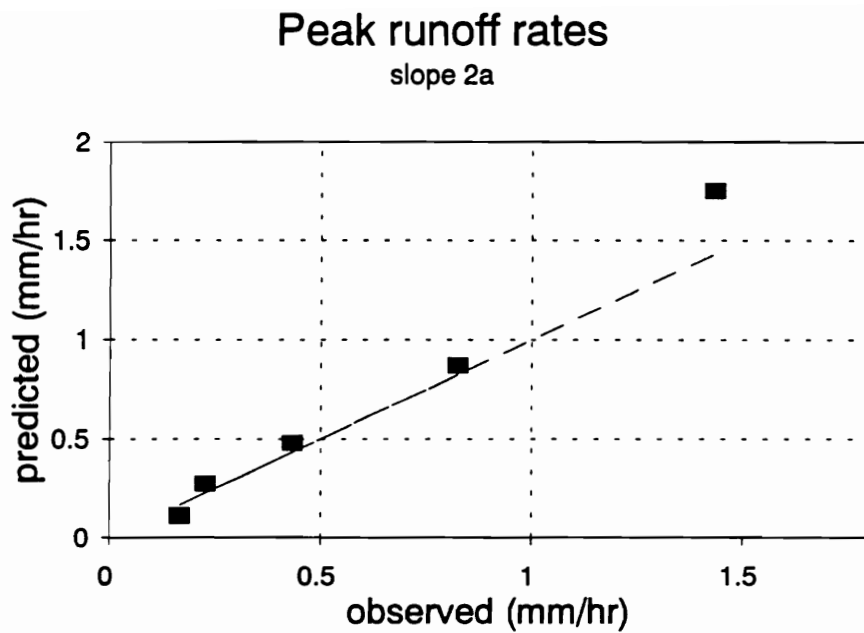
Figure 10.12: Observed and predicted peak runoff values for hillslope 2A.

Lag to peak runoff
slope 1a
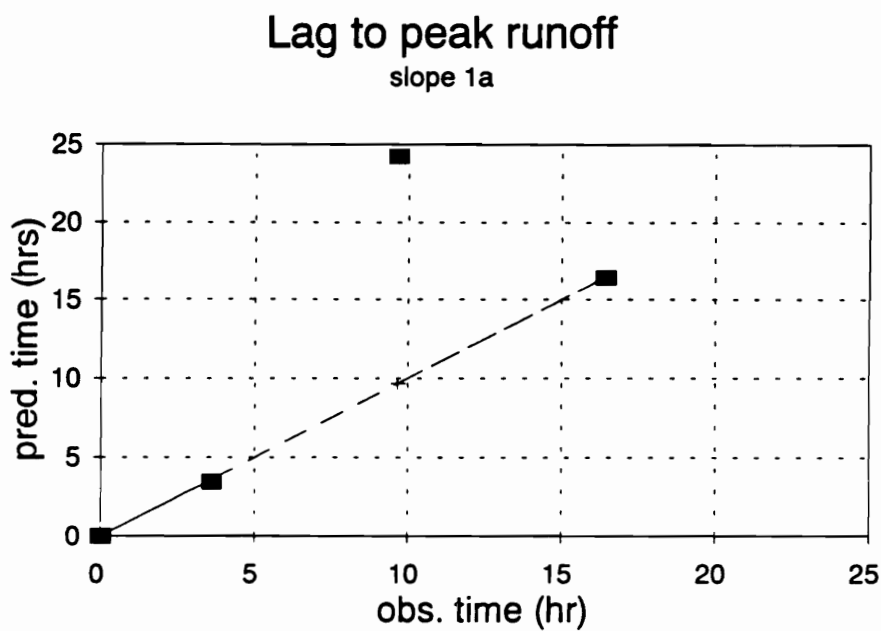
Figure 10.13: Observed and predicted lag times for hillslope 1A.

Lag to peak runoff
slope 2a
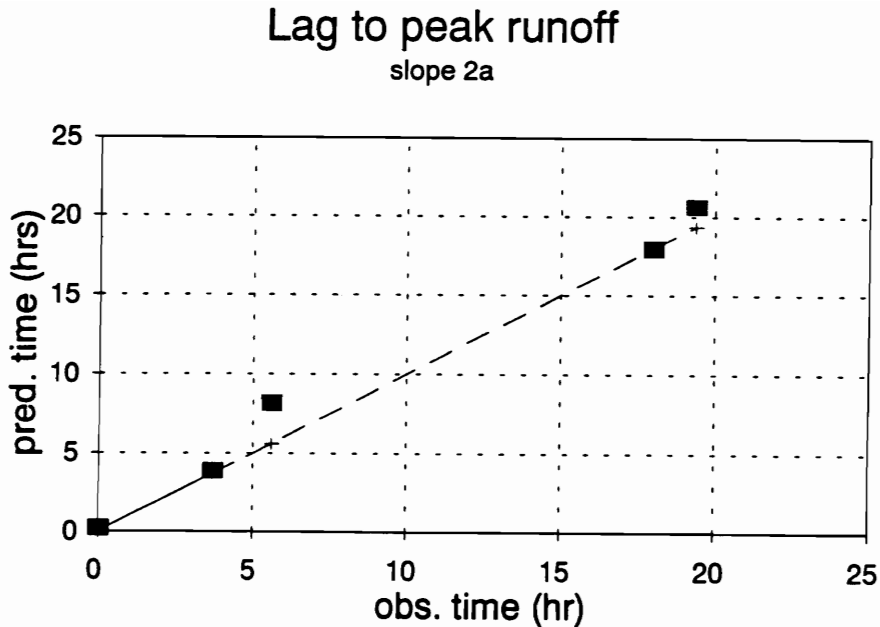
Figure 10.14: Observed and predicted lag times for hillslope 2A.

10.2.2 Melton Branch Subwatershed

10.2.2.1 Scope of evaluation

Similar to the Canadian Shield study, detailed quantitative field measurements were also available for the Melton Branch hillslope study. This allowed a detailed quantitative comparison between predicted and observed hillslope responses. The responses that were compared include:

- runoff hydrographs from each horizon
- event subsurface runoff totals
- peak subsurface runoff values
- lag time to peak runoff values
- runoff ratios (ratio of rainfall to runoff) for each horizon

10.2.2.2 Data selection

10.2.2.2.1 Segment information

The Melton Branch investigations were conducted on a single hillslope catchment. A topographic map of the catchment is given in Figure 9.4. The hillslope was discretized into six equal length segments. Segment length, widths, and slope gradients were determined using the topographic map of Figure 9.4 and are listed in Table 10.6. To determine main drainageways and their shape distribution, the topographic map was converted to a raster point elevation format and drainageways were delineated using a DEM model using procedures similar to those used for the Canadian Shield hillslopes. Channel w/d distribution was determined by extracting w/d ratios at cross sections down the hillslope. The distribution parameters are listed in Table 10.7. Since field observations indicated that the runoff was limited to the subsurface only, emphasis was placed on determining the number and shape distribution for main drainage channels along which subsurface flow concentration was expected. A three dimensional surface plot of the hillslope catchment is provided in Figure 10.15. Figure 10.15 indicates that the hillslope catchment is convergent in plan and concave in slope, with flow concentrating towards the center of the hillslope. Hence, a single main drainage channel was assumed.

Table 10.6: Segment information for the Melton Branch hillslope

Number of segments	6
Length of segments (m)	12.89 (77.34 m) [a]
Width of segments (m)	42.67, 73.33, 92.00, 104.88, 112.00, 86.20
Slope gradients (%)	31.03, 32.5, 25.5, 19.85, 15.32, 23.41, (24.60) [b]
Number of main drainage channels	1
Main drainage channel average w/d ratio	15

[a] total hillslope length
[b] average hillslope gradient
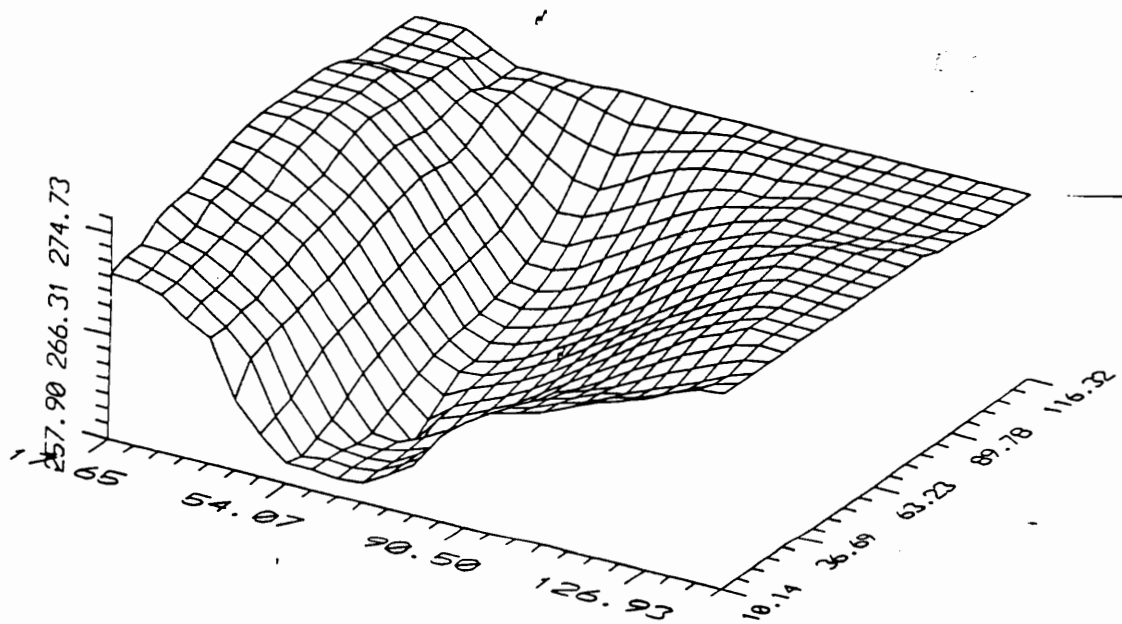
Figure 10.15: Three dimensional surface plot of the Melton Branch hillslope catchment.

Table 10.7: Channel w/d distribution parameters

Distribution type	Mean	Variance
Lognormal	-0.0356	0.0682

10.2.2.2.2 Soil description

Soil depth above the bedrock at the Melton Branch hillslope was discretized into three soil horizons - A, B, and C. The O horizon was included within the A horizon. Depths for the B and C horizons were available from the pan collector facility installed at the base of the hillslope to measure subsurface flow exiting the horizons (Appendix IV). Observations at the site indicated an A horizon depth of approximately 0.08 m (including the O horizon). The thicknesses of the individual horizons are provided in Table 10.8. Porosity and field capacity values for each of the horizons were estimated from the soil moisture release curves (Appendix IV) and are listed in Table 10.8. Vertical hydraulic conductivity was measured on site for each of the horizons (Table 10.8). Field measurements for horizontal conductivity were not performed. In the absence of measured values, horizontal saturated conductivity was assumed to be equal to the vertical conductivity for each soil horizon. Similar to the earlier study no measurements were available on macropore roughness, thus an approximate value of 0.5 based on literature was chosen.

Table 10.8: Hillslope soil description.

Soil horizon	Horizon depth (m)	Porosity	Field capacity (m^3/m^3)	$K_{h\,sat}$ (mm/hr)	$K_{v\,sat}$ (mm/hr)
A	0.08	0.56	0.39	344	344
B	0.53	0.45	0.35	344	344
C	1.22	0.39	0.35	27.36	27.36

10.2.2.2.3 Event loadings

A total of eight events were used to test the subsurface component of the model for Melton Branch hillslope conditions. A summary of the events with event dates, and total rainfall amounts is provided in Table 10.9. Measurements for the site indicated that approximately 15% of the rainfall depth was lost to interception (Johnson and VanHook, 1989). Water loadings to the hillslope catchment were from rainfall only.

Table 10.9: Summary of events simulated for Melton Branch hillslope catchment

	Event 2	Event 3	Event 4	Event 5	Event 6	Event 7	Event 8	Event 9
Day (1991)	Feb 13	Feb 17	Mar 01	Mar 22	Mar 27	Apr 15	Jun 23	May 27
Total rain (mm)	37.76	158.7	46.93	24.15	70.53	14.91	55.72	56.96

10.2.2.2.4 Values for antecedent moisture and macroporosity

Similar to the Canadian Shield data, no antecedent soil moisture values or macroporosity information was available. Thus, using procedures described previously, antecedent soil moisture was calibrated using a single event and proportioned with respect to the 7 day antecedent precipitation API_7 for other events. The event used for calibration in this case was event E2 (Feb 13, 1991). The antecedent moisture values determined for the eight events are listed in Table 10.10. Using procedures similar to those used for the Canadian Shield data, "hydrologically active" macroporosity and maximum macropore diameters were estimated for each soil horizon. The lower macropore diameter was fixed at 0.15 mm for all (A, B, and C) horizons. Calibration results yielded a "hydrologically active" macroporosity (expressed as a percentage of the total porosity) of 1.0, 0.6, and 0.6% for horizons A, B, and C, respectively. The maximum macropore diameters that corresponded to this macroporosity were 5, 1, and 1 mm for the A, B, and C horizons, respectively.

Table 10.10: Estimated antecedent soil moisture (m^3/m^3)

	Event 2	Event 3	Event 4	Event 5	Event 6	Event 7	Event 8	Event 9
API$_7$ (mm)	23.37	40.64	8.89	13.97	24.63	27.68	34.8	8.382
A horizon	0.36	0.375	0.33	0.34	0.36	0.365	0.368	0.33
B horizon	0.33	0.34	0.35	0.32	0.33	0.335	0.338	0.315
C horizon	0.35	0.35	0.35	0.35	0.35	0.35	0.35	0.35

10.2.2.3 Results and discussion

10.2.2.3.1 Runoff hydrographs

Observed and predicted runoff hydrograph responses from upper and lower flumes of the Melton Branch hillslope catchment are plotted in Figures 10.16 through 10.22 As described in section 9.2, the upper flume collects lateral subsurface flow exiting from the A and B horizons, while the lower flume collects flow from the C horizon. The higher runoff peaks in Figures 10.16 through 10.22 are associated with runoff from the lower flume (C horizon response). The model predicted the lower flume responses reasonably well for most of the events except Event 5 on March 22. For Event 5, model runoff response is considerably less than the observed. The model seems to underestimate runoff for events for which antecedent soil moisture conditions are low. For large rainfall events and relatively wetter antecedent moisture conditions (events 2, 3, 6, and 8) model predictions seem to be good. Compared to the observed lower flume runoff volumes, observed upper runoff volumes are too small to provide a resonable comparison with the model predictions.

10.2.2.3.2 Rainfall -runoff totals

Figures 10.23 and 10.24 provide the total rainfall and predicted total runoff response with the 95% confidence bounds for the lower and upper flumes, respectively. Observed runoff responses are also included in these figures. For the lower flume, the model predicted the observed responses at a 95% confidence level for five of seven events. For the upper flume, three of four event events were predicted at the 95% level.

Figure 10.16: Observed and predicted subsurface runoff for Event 2 (Feb. 13).

Figure 10.17: Observed and predicted subsurface runoff for Event 3 (Feb. 17).
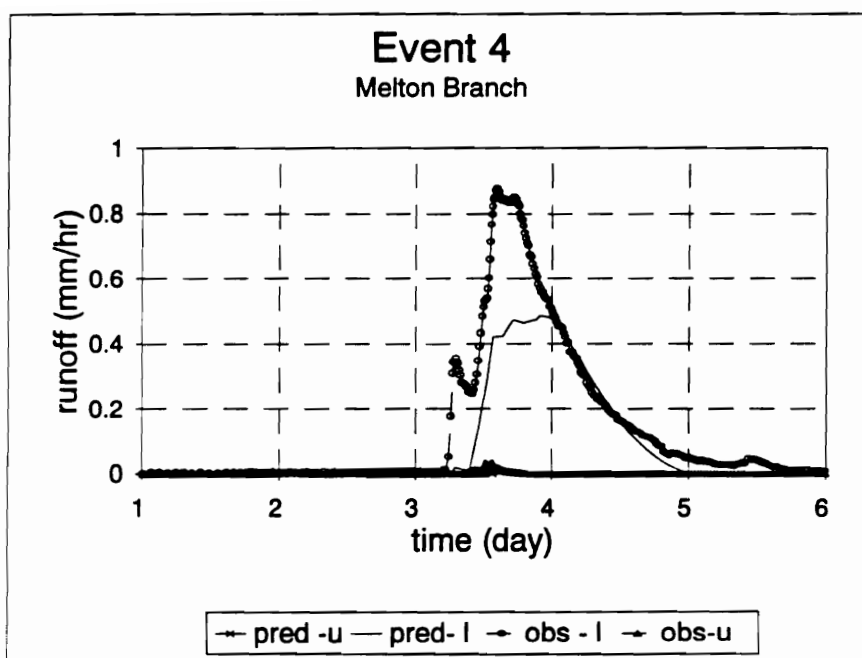
Figure 10.18: Observed and predicted subsurface runoff for Event 4 (Mar. 01).
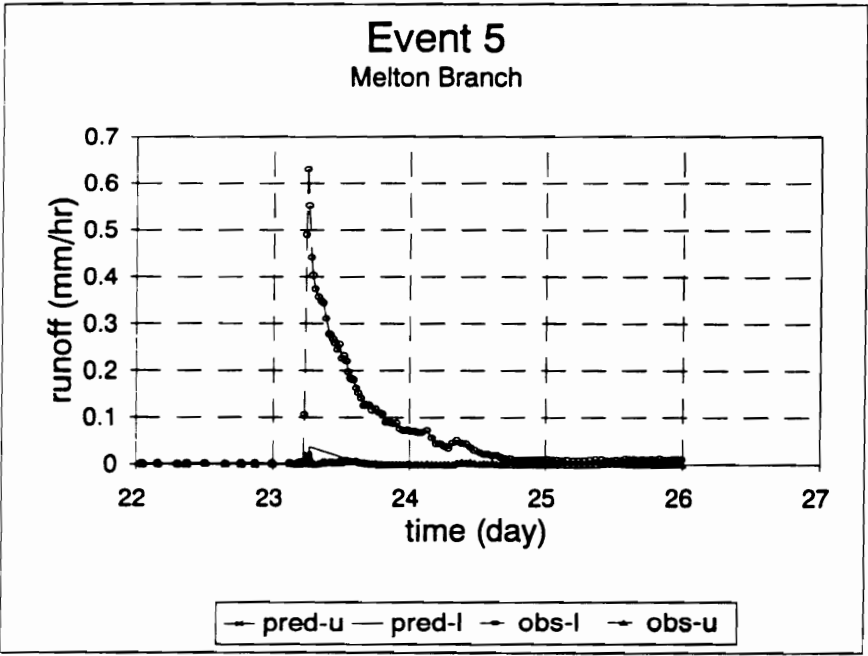
Figure 10.19: Observed and predicted subsurface runoff for Event 5 (Mar. 22).
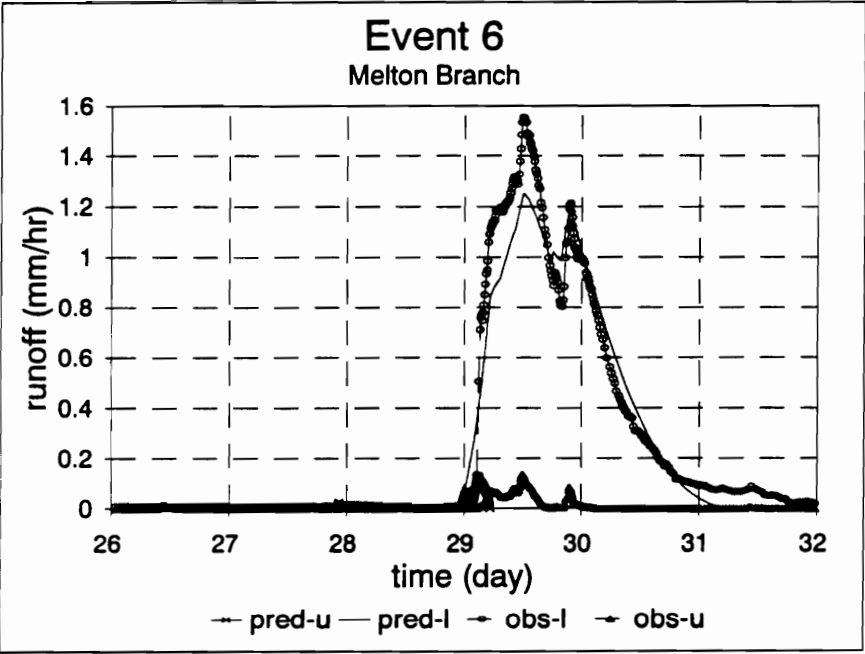
Figure 10.20: Observed and predicted subsurface runoff for Event 6 (Mar. 27).
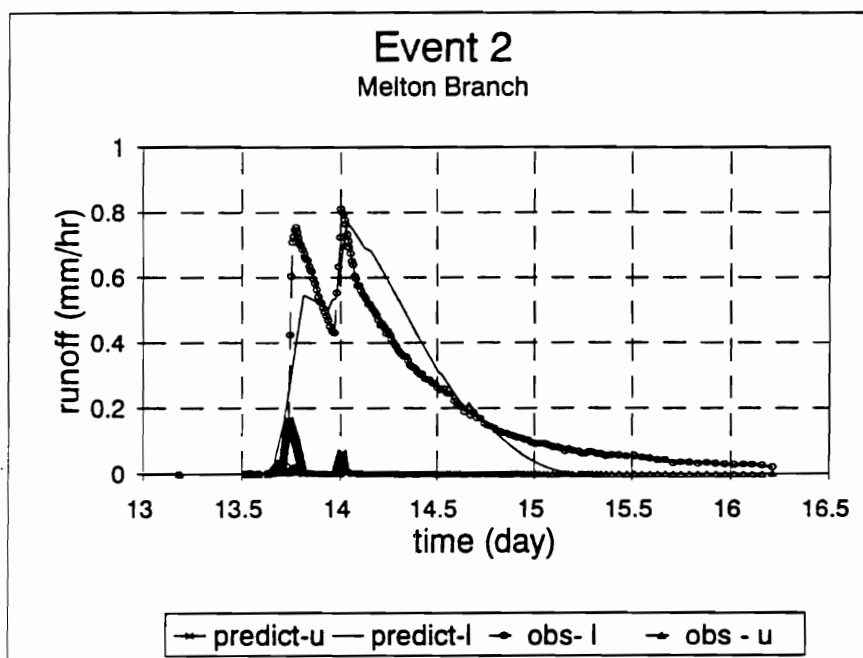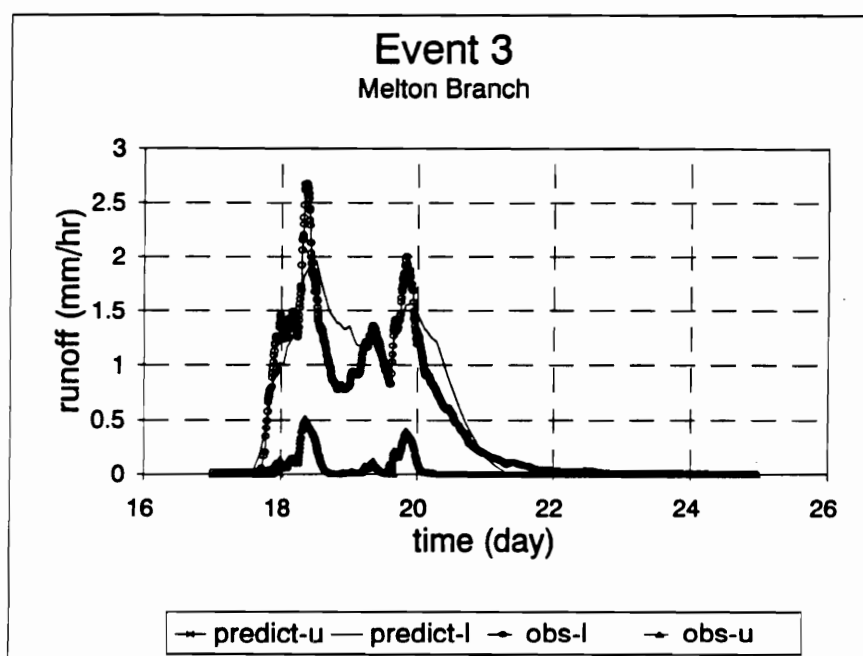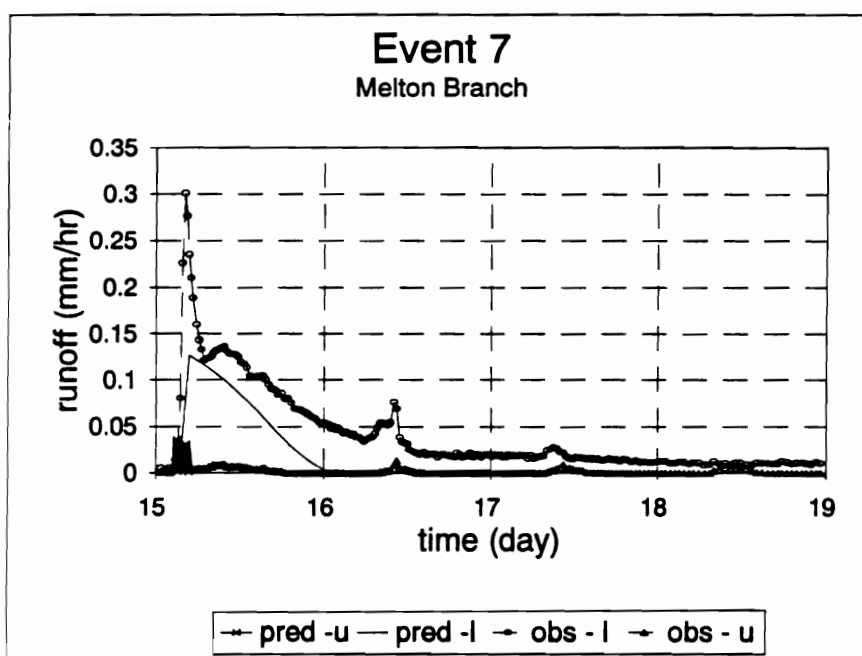
Figure 10.21: Observed and predicted subsurface runoff for Event 7 (Apr. 15).
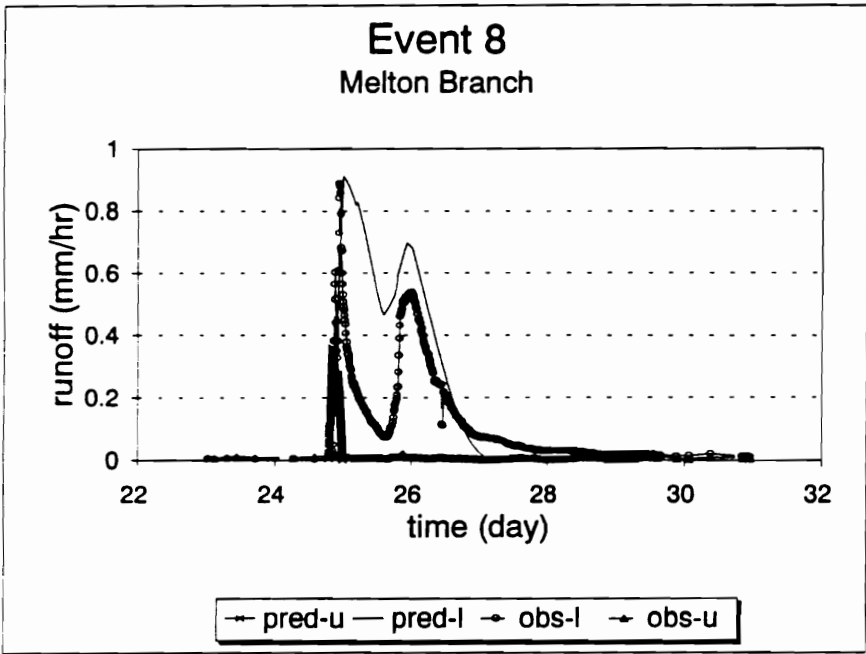
Figure 10.22: Observed and predicted subsurface runoff for Event 8 (Jun. 23).

Figure 10.23: Observed and predicted runoff totals for lower flume of Melton Branch.

Rainfall-runoff totals
Melton Branch - upper flume
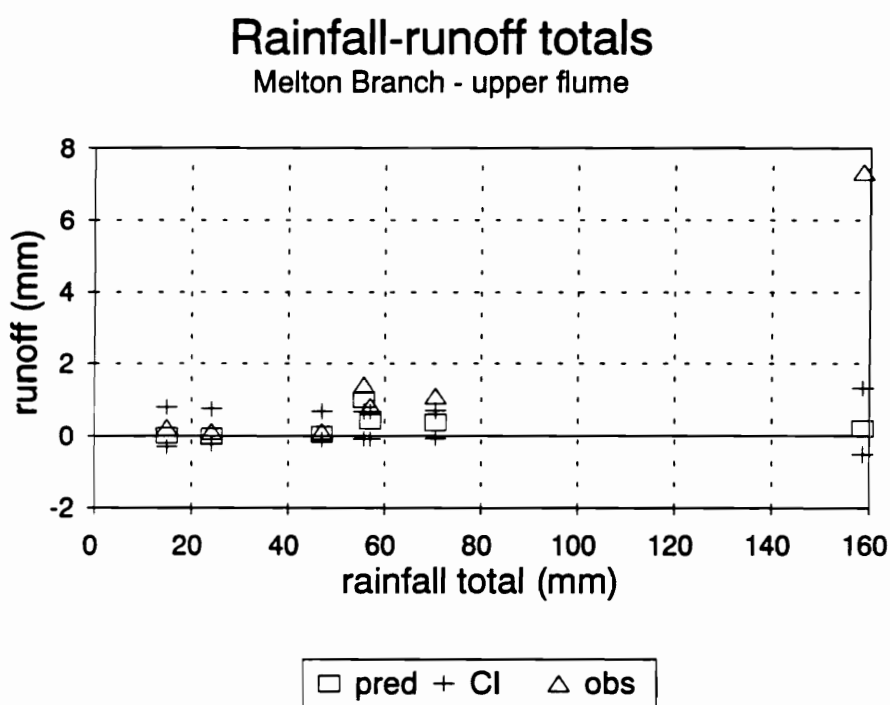
Figure 10.24: Observed and predicted runoff totals for upper flume of Melton Branch.

10.2.2.3.3 Peak values and lag time to peak

Since observed and predicted runoff from the upper flume was significantly less than that from the lower flume, comparisons of peak values and lag times to peak were generated for the lower flumes only. These results are plotted in Figures 10.25 and 10.26. Statistical analyses of these results indicate that the intecept and slope values of the regression lines are not significantly different from the equal value line.

10.2.2.3.4 Runoff ratios

Comparison of observed and predicted runoff ratio distributions was performed for events 3, 4, 6 and 8. The runoff ratio value was defined as the ratio of the hillslope runoff (mm/hr) measured at the lower flume to the rainfall rate (mm/hr), at any instant of time during the event. For events 3, 4, 6, and 8 these values were generated at one minute time intervals. Probability distributions were fitted to these data using VTFIT. The distributions of observed and predicted runoff ratio values were then compared. Figures 10.27 through 10.30 present the results for events 3, 4, 6, and 8, respectively. All of the observed runoff ratio distributions fall within the 95% confidence bounds of the predicted runoff ratio distributions. This indicates that the model does an excellent job in predicting the runoff within the duration of an event.

10.3 Hachioji Basin study - Variable source area phenomenon

10.3.1 Scope of evaluation

In comparison to the Canadian Shield and Melton Branch studies, limited field data were available for the Hachioji Basin Study. A description of the data was provided earlier in section 9.3. Information was available on the size, slope and topography of the hillslope catchment, event loadings and runoff hydrographs, and soil thickness and conductivity, but very little information was available for critical soil parameters such as total porosity and field capacity. Thus, considering the missing critical input information, a quantitative evaluation of observed and predicted results was not feasible.

Peak runoff rates
Melton Branch - lower flume
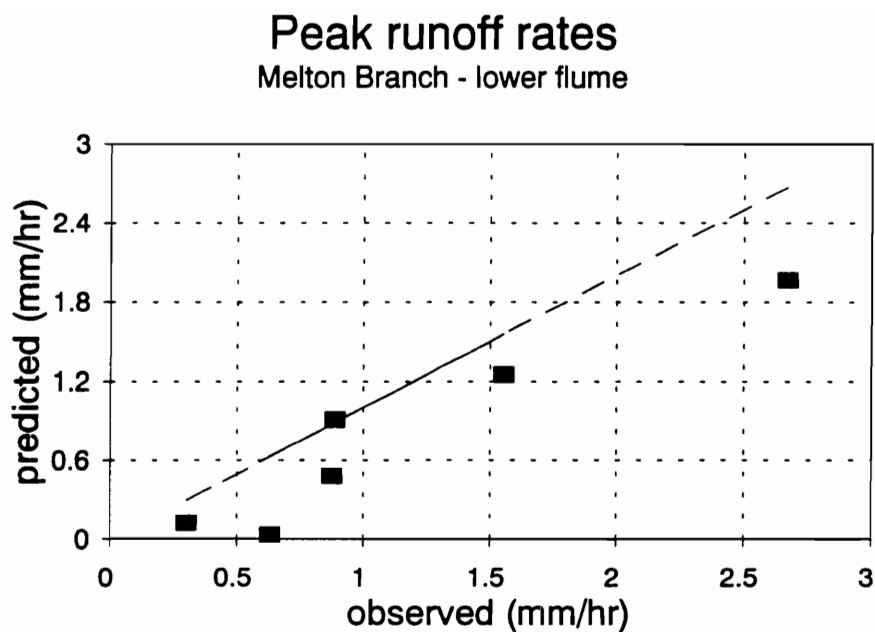
Figure 10.25: Observed and predicted peak runoff values for lower flume of Melton Branch.

Lag time to peak
Melton Branch - lower flume
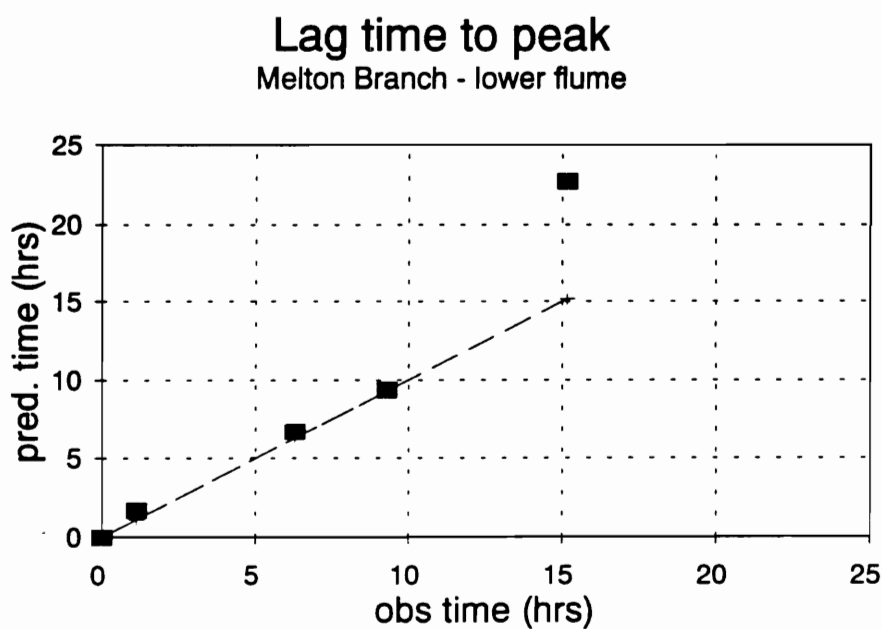
Figure 10.26: Observed and predicted lag times for lower flume of Melton Branch.

Runoff Ratio pdf- lognormal
Melton Branch - event 3
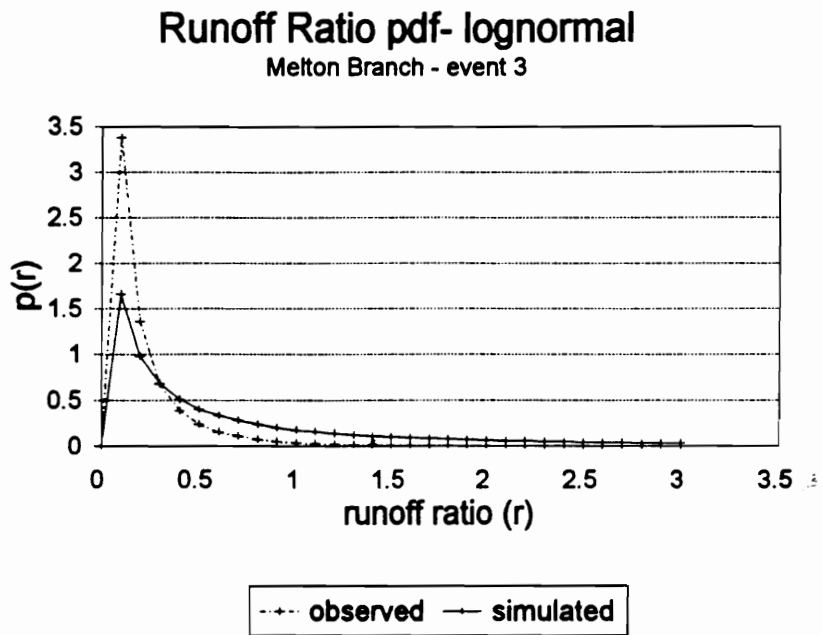
Figure 10.27: Comparison of runoff ratios probability density functions (pdfs) for Event 3.

Runoff Ratio pdf- lognormal
Melton Branch - event 4
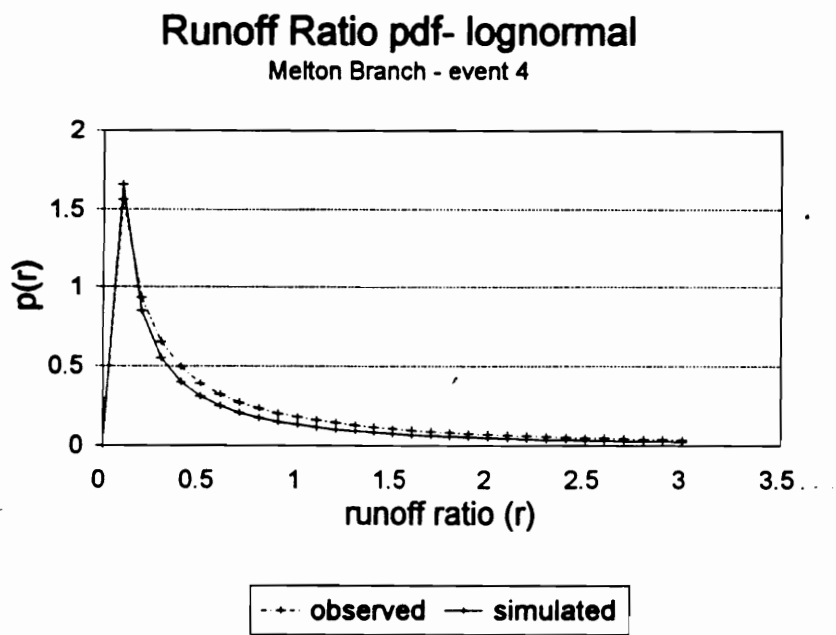
Figure 10.28: Comparison of runoff ratio pdfs for Event 4.

Runoff Ratio pdf- lognormal
Melton Branch - event 6
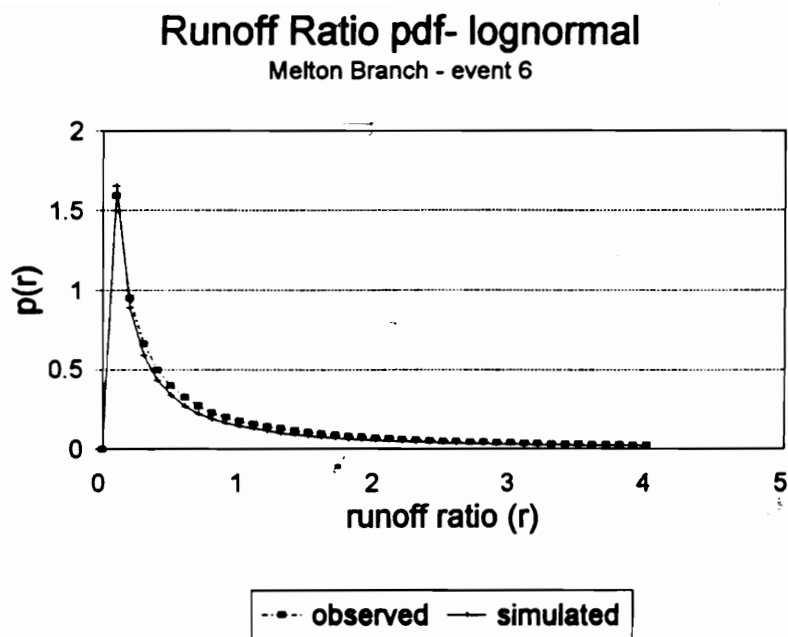
Figure 10.29: Comparison of runoff ratio pdfs for Event 6.

Runoff Ratio pdf- lognormal
Melton Branch - event 8
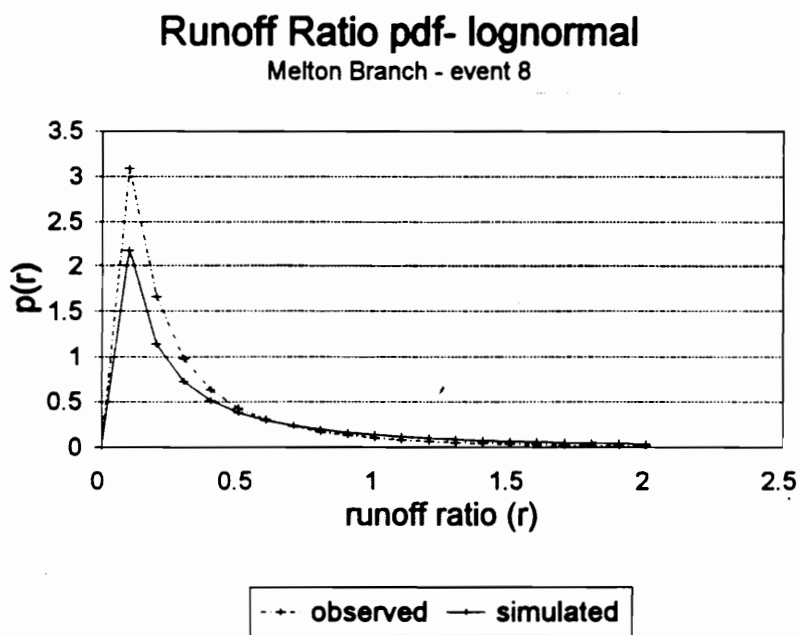
Figure 10.30: Comparison of runoff ratio pdfs for Event 8.

The salient feature of this experimental study was that the hillslope catchment generated significant variable source areas which were mapped in detail by the investigators. The surface saturation responsible for generation of the variable source areas occurred in the central lower portion of the hillslope catchment. Figure 10.31 illustrates the surface saturation within the instrumented portion of the catchment for the rainfall event of October 7-9, 1982. A cross section through the instrumented hillslope illustrating the general subsurface flow directions under high rainfall conditions is shown in Figure 10.32. As can be seen from Figure 10.32, surface saturation occurred due to the thinning of soil layers towards the lower portion of the hillslope and the resulting upwelling of soil moisture. Field measurements indicated that surface saturation first occurred at the location where the soil was thinnest. The intent in using this study was to determine if the subsurface flow component of the model could simulate the initiation and expansion of surface saturation observed in this study. Thus, evaluation of observed and predicted results was limited to a qualitative comparison of subsurface saturation conditions and the location of the initiation of surface saturation.
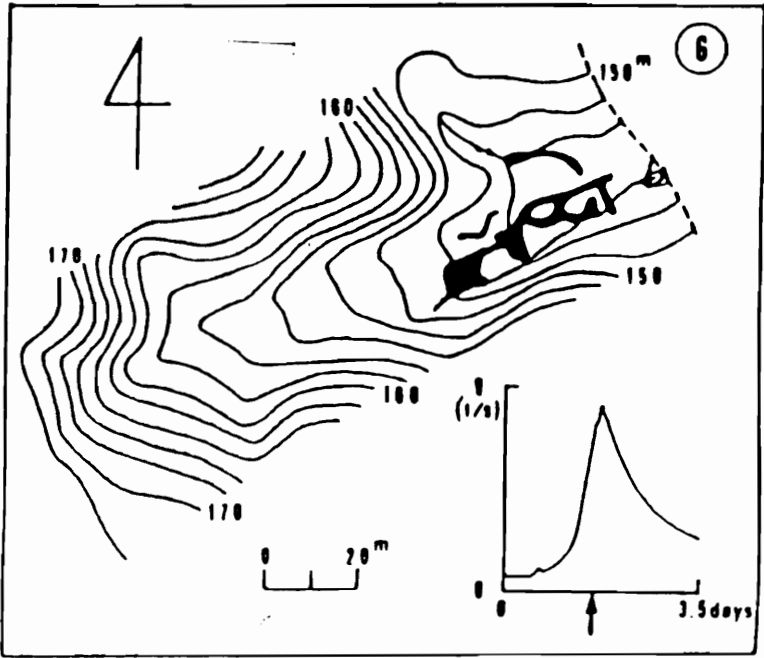
Figure 10.31: Instrumented hillslope segment illustrating surface saturation.
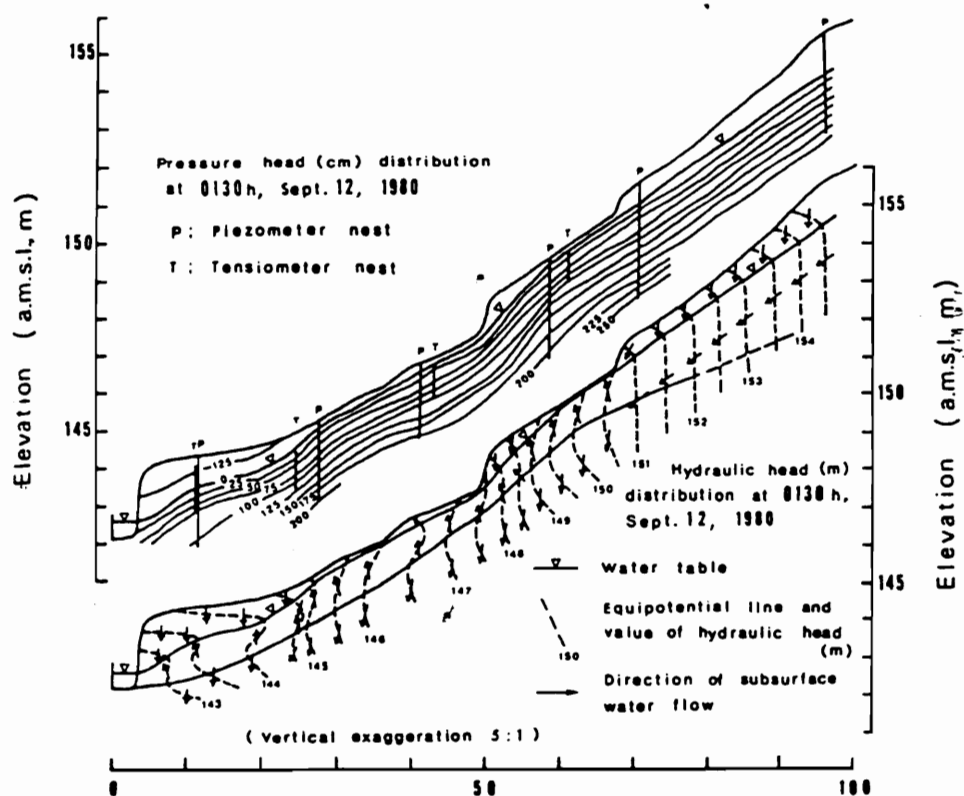
Figure 10.32: Section along slope gradient showing subsurface flow directions.

10.3.2 Data selection

10.3.2.1 Segment information

The hillslope catchment was discretized into six segments. Segment lengths, widths and slope gradients were determined using the topographic map of the catchment (Figure 9.6). Main drainages were determined using procedures similar to those described earlier. The number of main drainages for each segment and the average w/d value are listed in Table 10.11.

Table 10.11: Segment input information

Parameters	Hachioji Basin hillslope catchment
Number of segments	6
Length of segments (m)	42.5 (255.0 m) [a]
Width of segments (m)	150.0, 186.0, 246.0, 252.0, 225.0, 207.0
Slope gradients (%)	16.47, 32.94, 14.11, 14.11, 12.93, 4.70, (15.87)[b]
Number of main drainage channels (from top to bottom segment)	1, 1, 1, 2, 2, 1
Main drainage channels w/d ratio	14

Note: [a] total hillslope catchment length
[b] average hillslope gradient

Table 10.12: Channel w/d ratio distribution parameters

Distribution	Mean	Variance
Lognormal	-0.1329	0.2417

10.3.2.2 Soils description

Soil thickness varied down the length of the hillslope. To simulate the variation in soil thickness, hillslope soils were divided into two categories. Values of horizon depth and conductivities were extracted from measured field data. Since, no estimates were available on porosity and field capacity, these values were estimated from suggested literature values for soils of similar texture (Rawls et al., 1985). Parameters for the two soil categories and the segments for which the soil category was applicable are listed in Table 10.13. From Table 10.13 it is seen that hillslope segments 1, 2, and 6 have thicker soil layers than segments 3, 4, and 5. For the two studies described earlier, antecedent soil moisture values were derived from their 7 day antecedent precipitation values. For this study, no information was available on the 7-day antecedent precipitation. Field studies only indicated that the central lower portion (segments 3, 4, and 5) of

the instrumented hillslope tended to be wetter than other areas, but no moisture estimates were provided. In the absence of information on antecedent moisture conditions it was assumed that horizons in the central lower portion (segments 3, 4, and 5) of the hillslope were slightly above field capacity, whereas in other locations (segments 1, 2, and 6) they were assumed to be at field capacity. No estimates were available on "hydrologically active" macroporosity or diameters of macropores for soil horizons, but field observations indicated numerous pipe cavities in the upper two soil horizons. Considering the pipes observed for the upper soil horizons, "hydrologically active" macroporosity was estimated at 5% (percentage of the total porosity) and maximum macropore diameters were set at 30 and 20 mm for A and B horizons, respectively. The maximum macropore diameters for the clayey C horizon was set at 1 mm. The lower bound of the macropore distribution was maintained at 0.15 mm.

Table 10.13: Soil horizon description

Soil ID	Slope segment	Soil horizon	Horizon thickness (m)	Porosity	Field capacity (m^3/m^3)	K_{hsat} (mm/hr)	K_{vsat} (mm/hr)
Type 1	1, 2 , 6	A	0.36	0.55	0.35	9.42	9.42
		B	1.45	0.45	0.38	0.85	0.85
		C	1.27	0.45	0.38	0.0036	0.0036
Type 2	3, 4, 5	A	0.27	0.55	0.35	9.42	9.42
		B	0.545	0.45	0.38	0.85	0.85
		C	1.27	0.45	0.38	0.0036	0.0036

10.3.2.3 Event information

Model simulations was performed for the storm event of Oct. 7-9, 1982. Total rainfall for this event was 61 mm. Water loadings to the catchment were from rainfall only. Field investigations revealed that a major portion of the subsurface runoff measured at the outlet of the catchment was contributed through a large pipe cavity. The size of the pipe was 0.10 m along its

minor axis and 0.30 m along the major axis. The flow from the pipe was approximated at 65% of the total subsurface flow. In model simulations performed for the storm event of Oct 7-9, 1982, the occurrence of this pipe was not included. Thus, for comparing predicted runoff to the observed, the expected pipe contribution was subtracted from the total subsurface runoff. The adjusted observed subsurface runoff hydrograph which was used for comparison with model predictions is shown in Figure 10.33.

10.3.3 Results and discussion

10.3.3.1 Hillslope soil moisture response

Figure 10.33 illustrates the measured and predicted total subsurface flow response of the hillslope catchment. Considering that porosity and field capacity values were estimated from the literature and that antecedent soil moisture conditions were arbitrarily set, the subsurface flow predictions were reasonable. Figure 10.34 illustrates the fraction of the soil thickness saturated for each hillslope segment. Soil thickness was least for segment five and gradually increased thereafter for segments in upslope (4, 3, 2, 1) and downslope (6) directions. During the peak rainfall period, surface saturation was reached first for segment five (Figure 10.34). The observed hillslope saturation shown in Figure 10.31 also indicates surface saturation at the location which corresponds to segment five. After segment five, hillslope segment four, which is immediately upslope, reaches surface saturation (Figure 10.34). Upwelling of soil moisture in segment four could have been due to the soil moisture backing upslope of the saturated soil in segment five. Segment six, which has deeper soil than segment five, reaches saturation later, but its saturation depth is sustained for longer periods by recession flows. This qualitative comparison indicates that the subsurface component of the model can adequately simulate soil moisture buildup and the consequent occurrence of surface saturation.
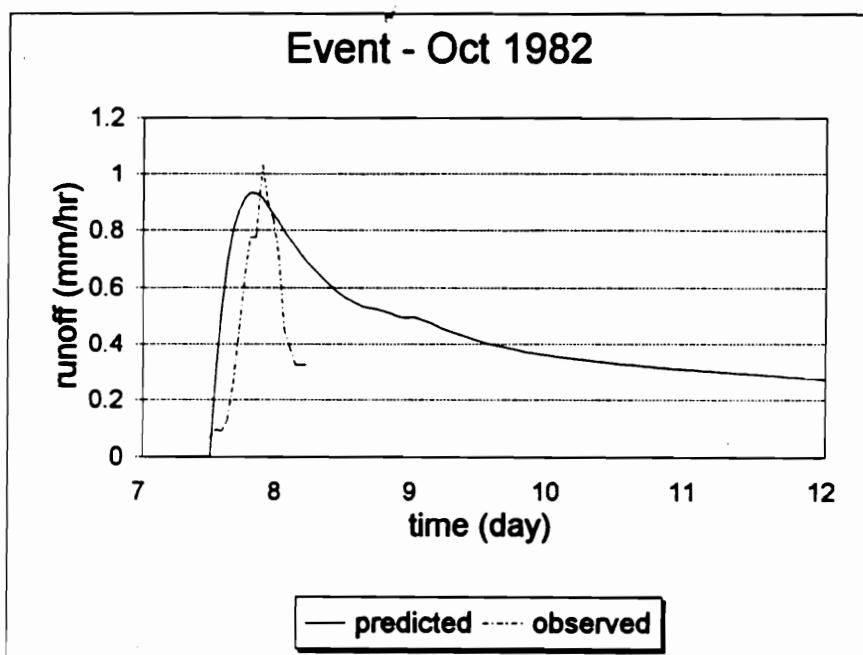
Figure 10.33: Observed and predicted subsurface runoff from the Hachioji Basin hillslope catchment.
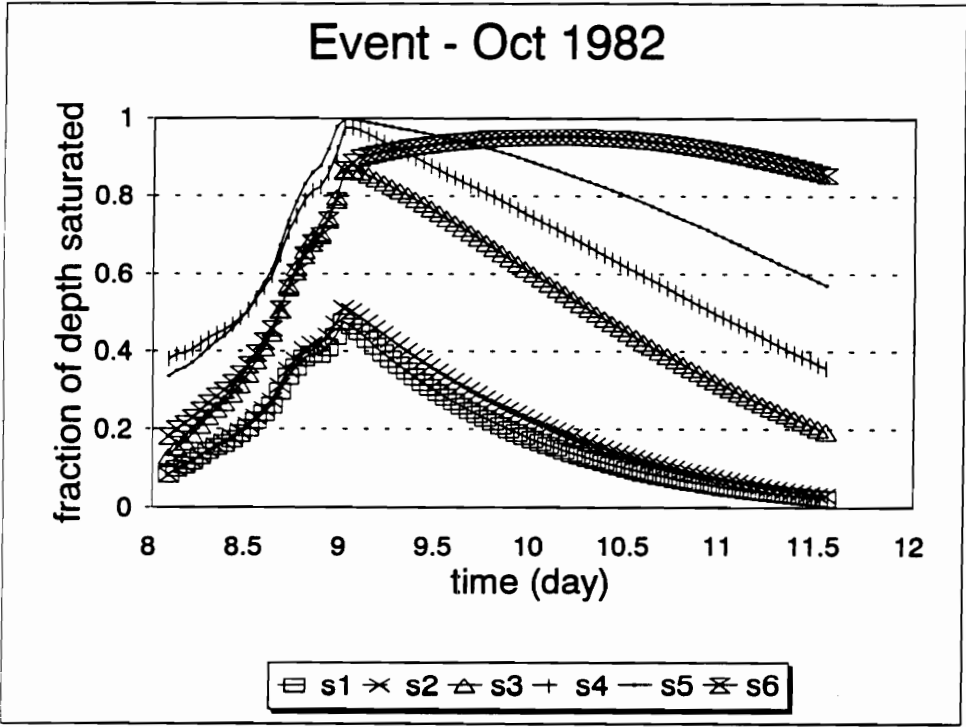
Figure 10.34: Saturation in the surface layer for different hillslope segments of the Hachioji Basin hillslope catchment.

10.4 University of Kentucky - Sediment component

10.4.1 Scope of evaluation

Detailed information on the amount and size distribution of the sediment entering and exiting riparian grass zones of variable length was available from the University of Kentucky grass filter studies. A complete description of the experimental data was provided earlier in section 9.4. Information available from this study allowed a quantitative evaluation of the sediment component of the hillslope model. Though runoff entering and exiting the grass filters was monitored, infiltration parameters were not. In the absence of infiltration parameters, it was not possible to evaluate the surface runoff component of the model using these data. Thus, measured runoff data were used to route sediment within the grass filters. The specific responses that were evaluated included:

- sedigraphs and particle size distributions exiting the grass filter
- total sediment trapping

10.4.2 Data selection

10.4.2.1 Segment information:

Sediment transport simulations were performed for 15, 30, and 45 m length filters. For simulation, each of the filters was discretized into 0.381 m segment lengths. The choice of this particular segment length was determined after performing sensitivity analysis of the sediment model to segment lengths and the rationale is provided in the following chapter on Sensitivity Analysis. The width of each filter plot was a constant 4.575 m for the full length of the filter, thus each segment had a width of 4.575 m. Topographic measurements were performed on the filter to delineate the surface channel networks and to determine their shape distribution. Topographic measurements were conducted prior to the commencement of each event. Hence, an estimate on the number of channels within the grass filter was available for each event. For details on the topographic measurements and the procedures used to determine the number of channels along the

filter, the reader is referred to Inamdar (1993). Information on the number of channels at different distances down the filter is summarized in Table 10.14. The parameters for the channel shape distribution are provided in Table 10.15. A Manning's roughness value, n, quantifying the surface resistance provided by grass was required as input. An estimate of n = 0.35 applicable to dense turf grass was selected from literature (Barfield et al., 1981). This Manning's n was assumed to be constant for the full length of the filter. For detachment conditions within the filter, estimates of the bare soil's critical tractive force and rill erodibility were required. Estimates for these values were obtained from an experimental study conducted on similar soils (Lewis, 1990). The values for critical tractive force and rill erodibility used were 3.2 Pa and 0.00125 s/m, respectively.

Table 10.14: Channel density along the length of the grass filters.

	G1'E2[b]	G3E2	G4E1	G4E2	G5E1	G5E2	G6E1	G6E2
Grass filter length L (m)	30	45	15	15	15	15	45	45
0- L/4*	2	2	2	3	2	2	3	3
L/4 - L/2	2	1	2	3	2	2	1	1
L/2 - 3L/4	1	1	2	2	1	2	1	1
3L/4 - L	1	1	1	2	1	2	1	1

* indicates the length segments for which the channel densities are applicable
[a]grass filter number; [b]event number

Table 10.15: Gamma distribution parameters for normalized w/d

Scale	Shape	Location
0.50	0.20	0.00

10.4.2.2 Sediment information:

Experimental analysis of sediment particle size distribution indicated that eroded aggregate particle sizes ranged from a maximum of 2 mm to a minimum of 0.005 mm. The sediment model routes sediment by particle class. Simulations were performed for six particle classes. Particle diameters and specific gravities for each particle class are provided in Table

10.16. Specific gravities for each particle class were estimated from literature values (Foster et al., 1985).

Table 10.16: Sediment particle classes

Aggregate size class	Particle diameter (mm)	Specific gravity
1	2.0 - 0.125	1.64
2	0.125 - 0.063	1.81
3	0.063 - 0.10	1.81
4	0.10 - 0.05	2.15
5	0.05 - 0.01	2.65
6	0.01 - 0.005	2.65

10.3.2.3 Event information

Each grass filter was subjected two events, which included runoff and sediment loading from an upslope contributing area. No rainfall was applied on the filter surface. Incoming sedigraphs are illustrated in the simulation results presented in Figures 10.35 through 10.42.

10.4.3 Results and discussion

10.4.3.1 Sedigraphs and particle size distributions

Comparisons of observed and predicted effluent sedigraphs and their particle size distributions are provided in Figures 10.35 through 10.42. In all cases, exiting sediment loads are orders of magnitude smaller than incoming sediment loads indicating deposition of sediment in the filters. Incoming and exiting runoff volumes indicated infiltration losses of water as high as 80-90%.

In nearly all the cases except filter six and event two of filter five, the predicted exiting sediment loads exceed those observed. The particle size distributions indicate that most of the

over prediction can be attributed to finer particle size classes. The model does not seem to simulate trapping of finer sediment fractions observed in experimental measurements. Experimental studies conducted in the past have indicated that a significant portion of the fine particles is entrapped in the soil matrix/litter layer as sediment is carried to the soil surface with infiltrating water (Hayes, 1979). Some fine sediment may also be deposited along with the mass settling of large sediment particles typically occurring just upslope or in the upper portion of the grass filter. Most of the fine sediment trapped in this manner cannot be considered discrete settling. The model simulates particle trapping for sizes primarily based on discrete settling. Thus, it is expected that the model will underestimate fine sediment deposition.

It is also possible errors might be associated with the approach used in the model to partition sediment load into surface channel flows entering segments. The model computes sediment concentration for a segment using total sediment load and total runoff and then computes sediment load for each channel based on the runoff in the channel. Field observations have shown that sediment concentrations in channels are rarely uniform across a segment (Inamdar, 1993). Errors may also be associated with the Bagnold transport equation used in the model. Coefficients for the equation were originally developed for flow depths much greater than those typically observed for grass filters.

In the absence of infiltration parameters and thus the ability to simulate infiltration, infiltration losses were computed as the difference between the measured incoming and exiting runoff. Surface runoff (which was used to route sediment) for each segment was then computed by distributing infiltration losses uniformly throughout each segment. In nature, infiltration is not uniform as assumed here.

10.4.3.2 Total sediment trapping

A summary of the observed and predicted sediment trapping efficiencies is provided in Table 10.17. Figure 10.43 provides a statistical comparison of the two results. At the 95% confidence level, the intercept and slope of the regression line between observed and predicted trapping is not significantly different from the equal value line.

Table 10.17: Summary of total trapping efficiencies

Filter Number	Event	Observed trapping, %	Predicted trapping, %
G1	E2	99.6	99.7
G3	E2	100.0	97.7
G4	E1	98.4	93.1
G4	E2	98.0	94.0
G5	E1	99.6	97.1
G5	E2	94.0	96.9
G6	E1	99.3	99.4
G6	E2	99.3	99.4
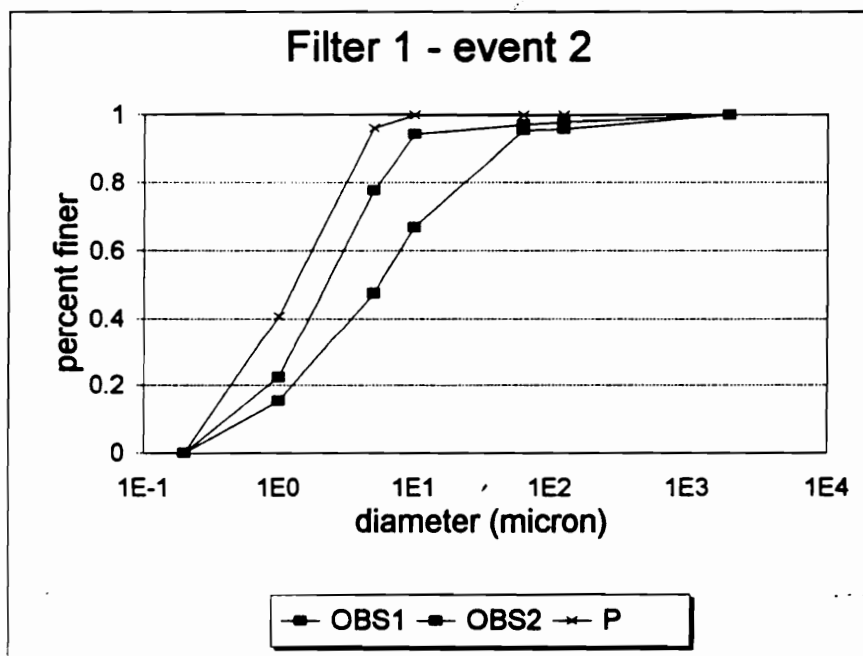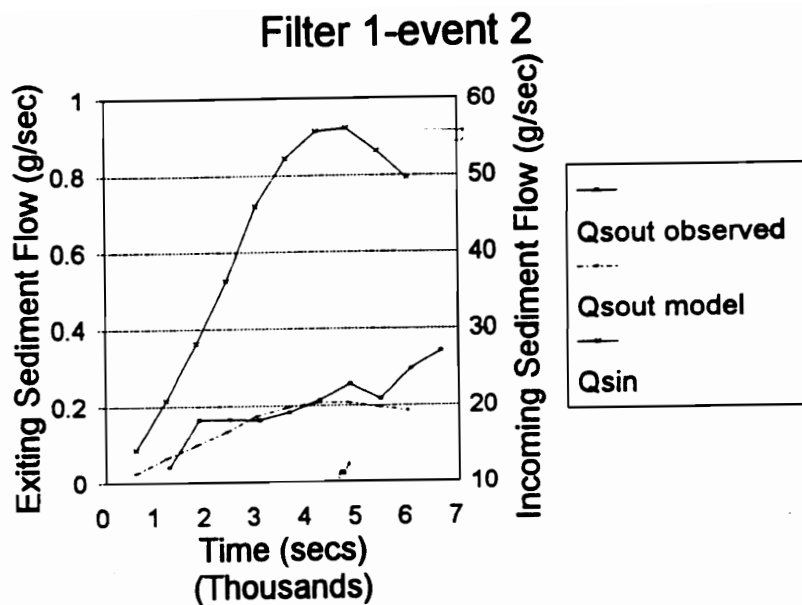
Figure 10:35: Exiting sedigraph and particle size distribution for filter G1 and Event 2 (OBS1 &
OBS2 indicate observed particle size distributions (psd); P is predicted psd .
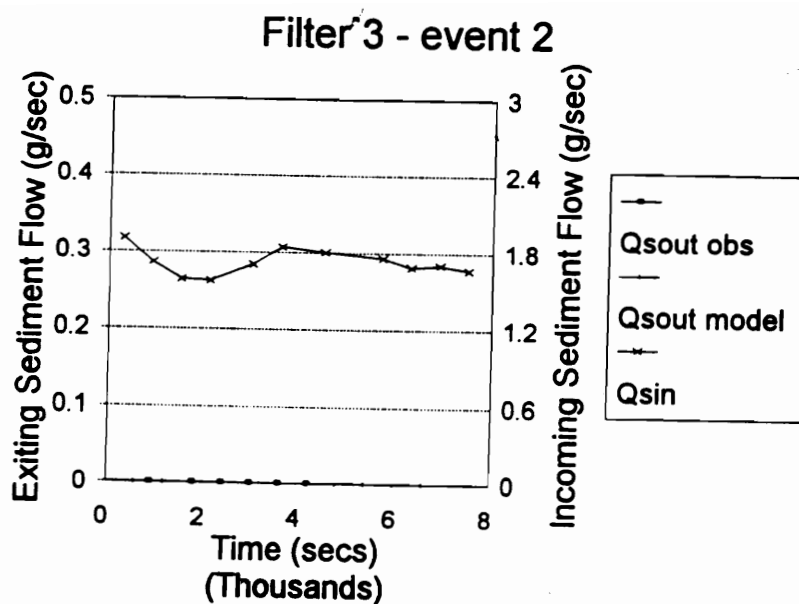
Figure 10.36: Exiting sedigraph for filter G3 and Event 2 (particle size comparisons were not made since observed distribution was not available for the lack of sediment).
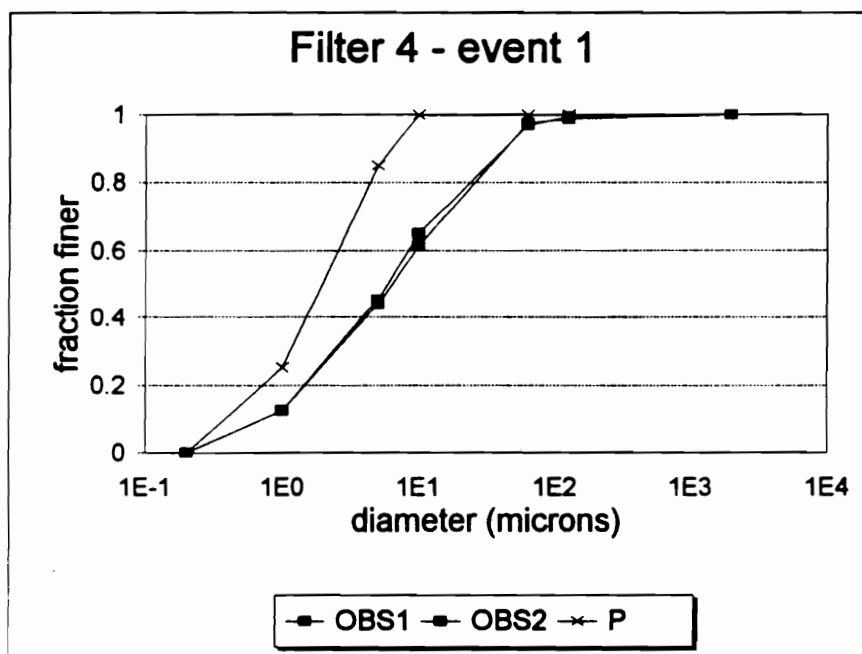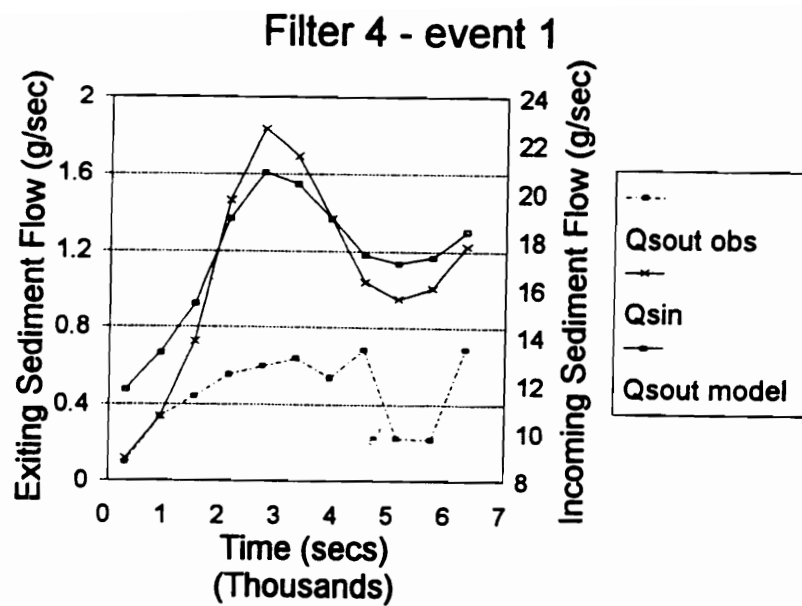
Figure 10.37: Exiting sedigraph and particle size distribution for filter G4 and Event 1.
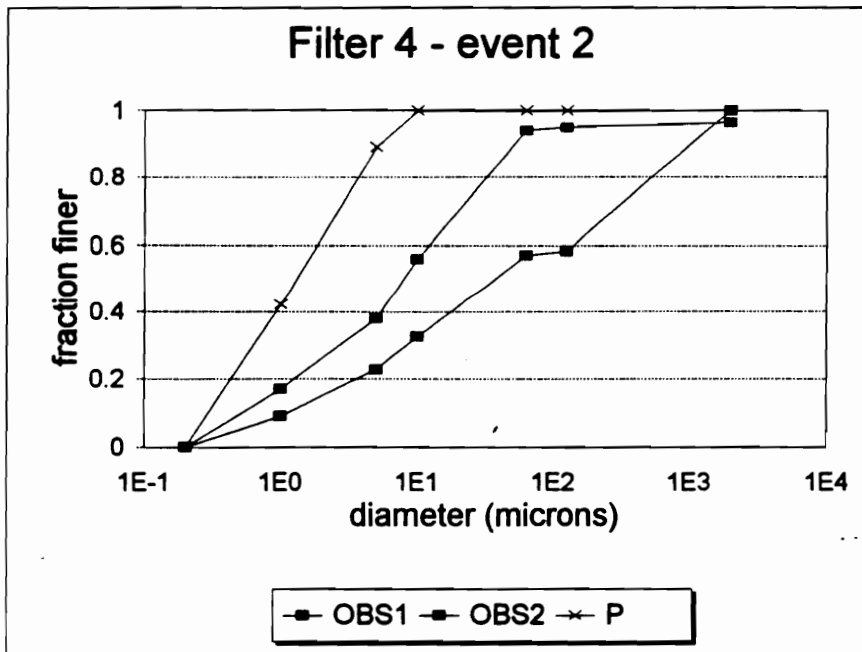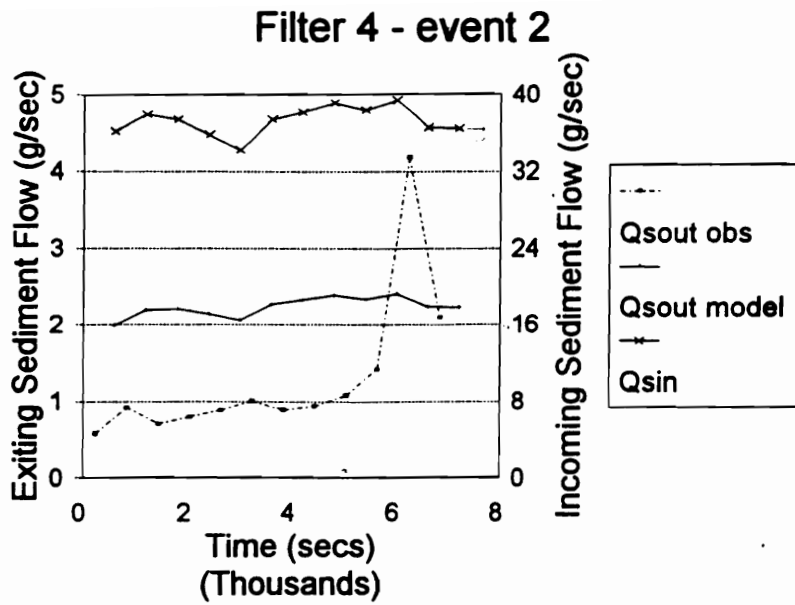
Figure 10.38: Exiting sedigraph and particle size distribution for filter G4 and Event 2.
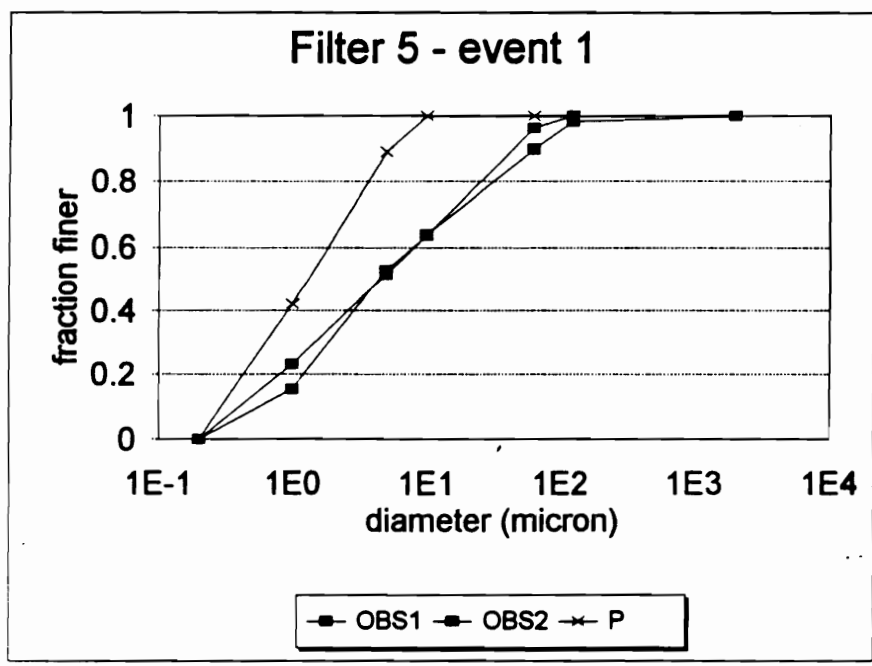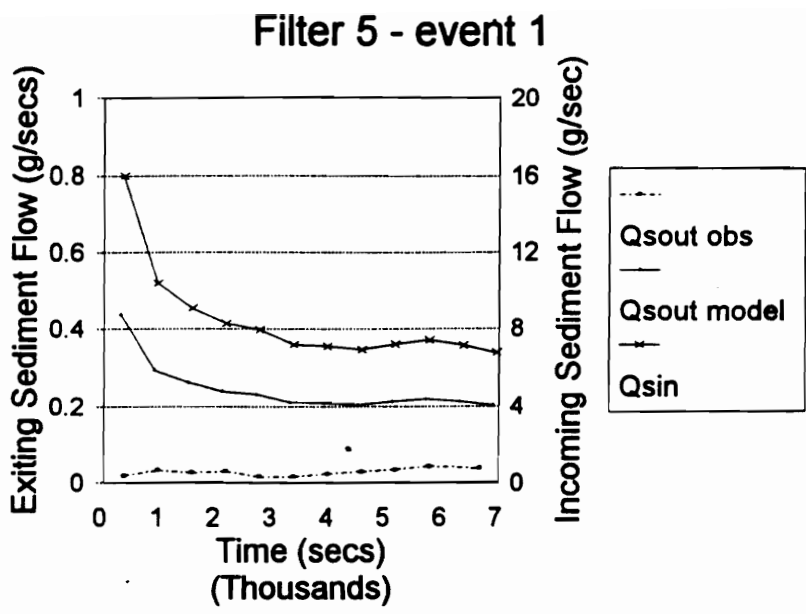
Figure 10.39: Exiting sedigraph and particle size distribution for filter G5 and Event 1.
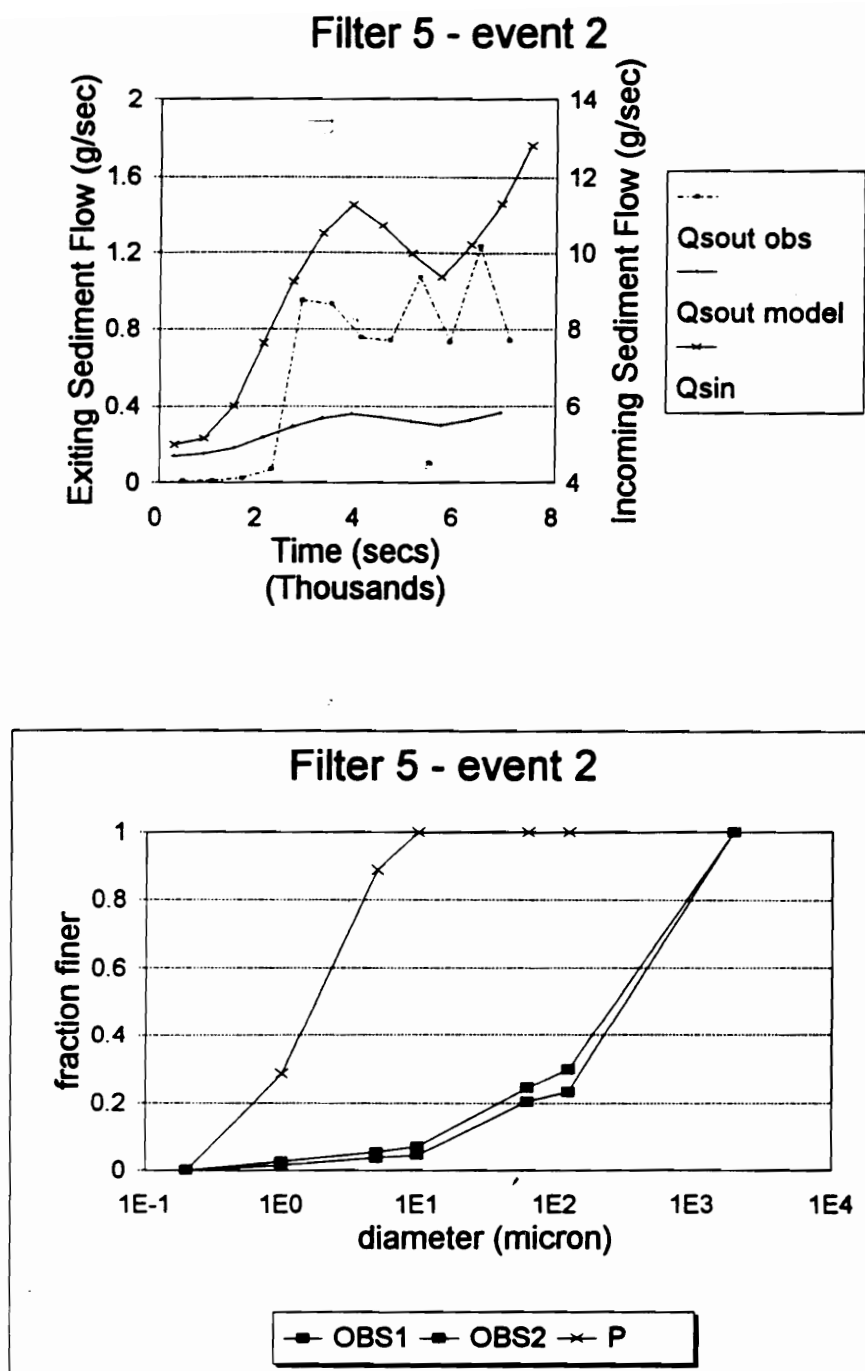
Figure 10.40: Exiting sedigraph and particle size distribution for filter G5 and Event 2.
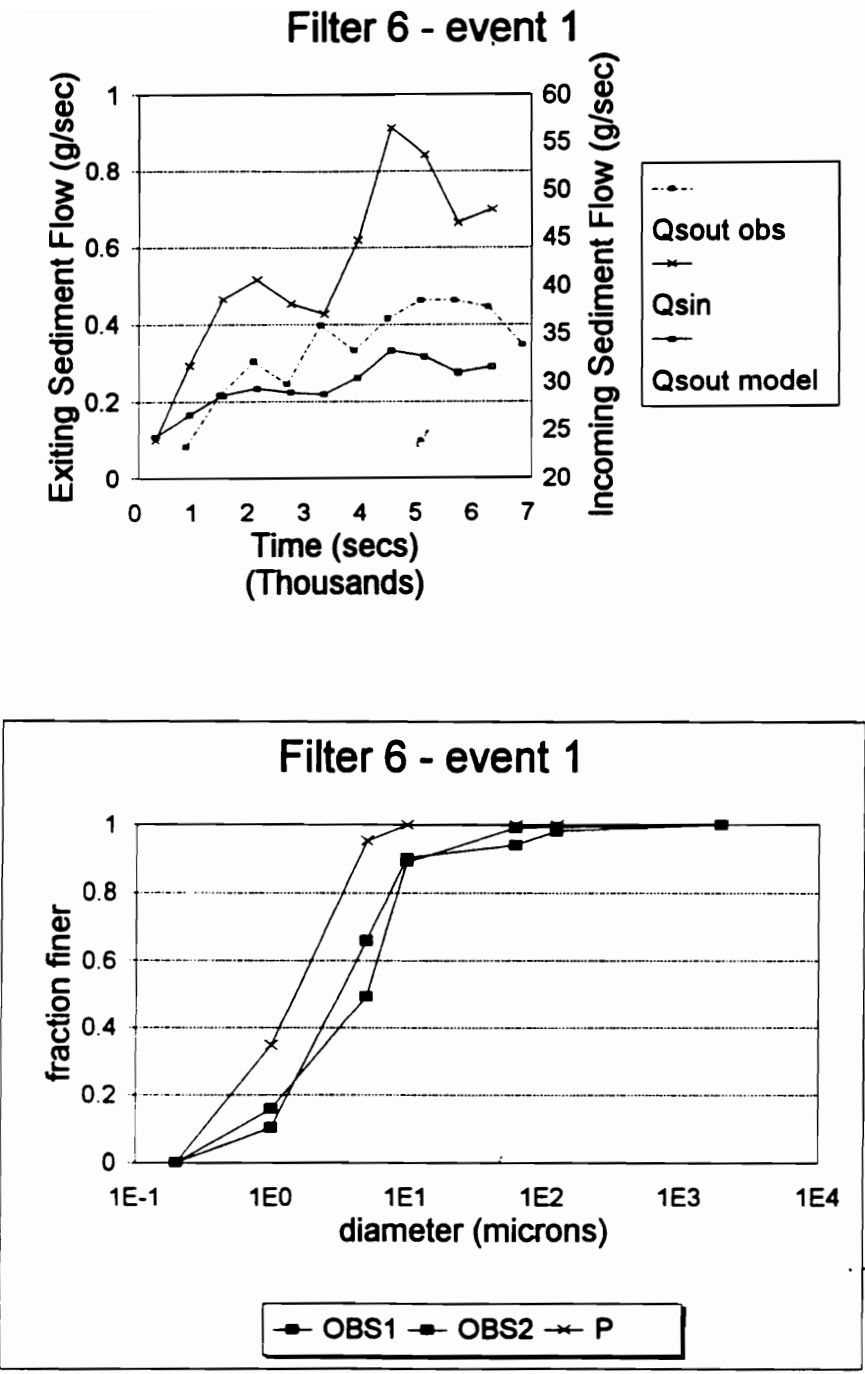
Figure 10.41: Exiting sedigraph and particle size distribution for filter G6 and Event 1.
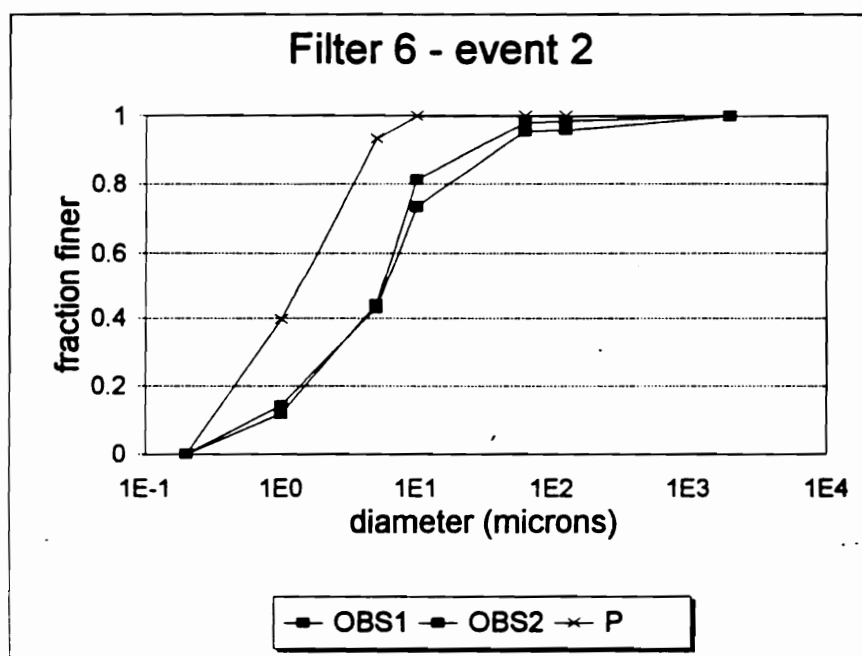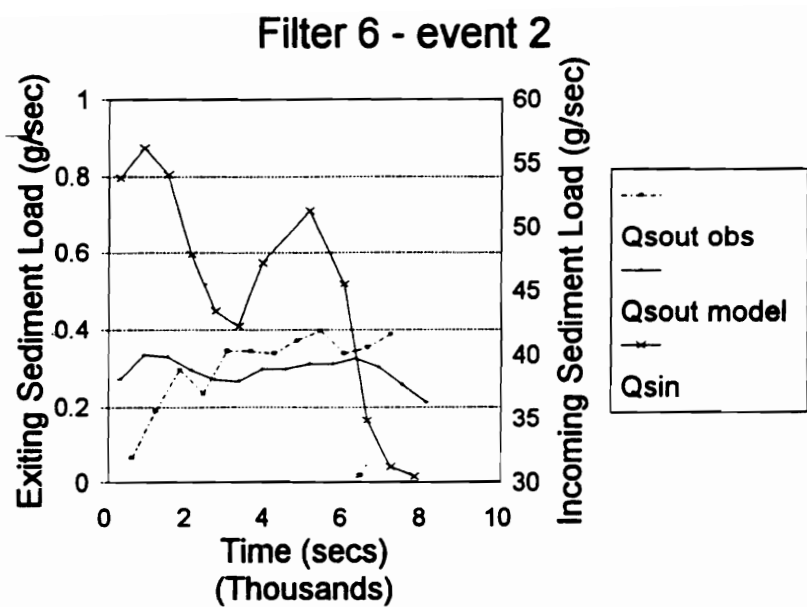
Figure 10.42: Exiting sedigraph and particle size distribution for filter G6 and Event 2.
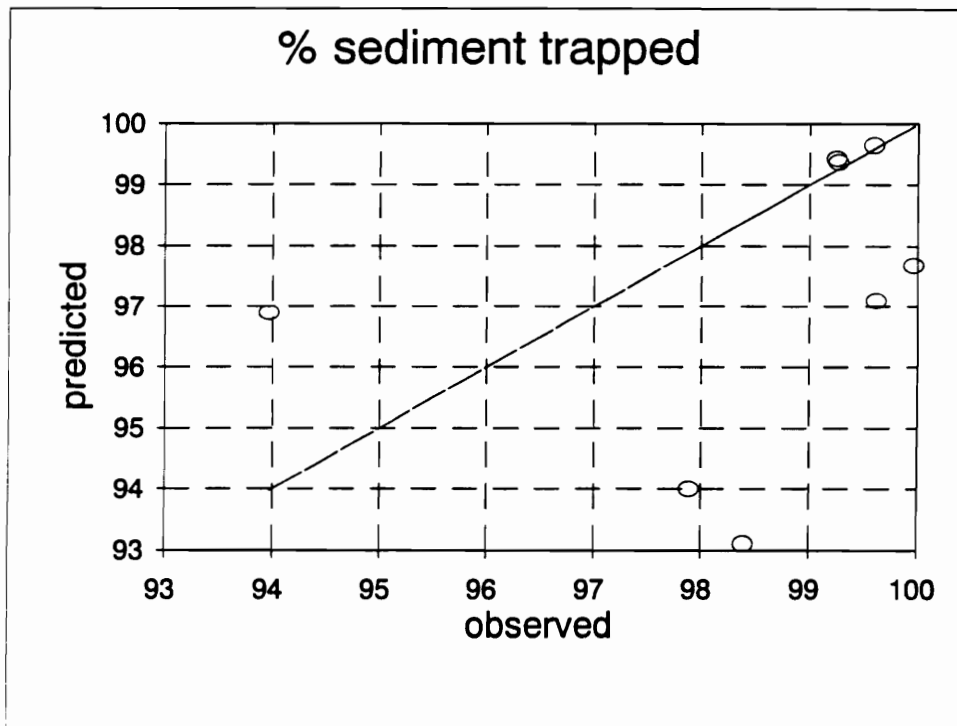
Figure 10.43: Comparison of total observed and predicted sediment trapping across all filters and events.

11 SENSITIVITY ANALYSIS AND PROCESS INVESTIGATIONS

11.1 Introduction

This chapter describes the sensitivity analysis and hypotheses testing procedures conducted to evaluate the model. Sensitivity analysis was performed to evaluate the sensitivity of model responses to predefined changes in model parameters. Model parameters that influence model responses the most are generally given greater attention while selecting input values. In addition to identifying critical parameters, sensitivity analysis also provides a means to check and evaluate model responses. In addition to sensitivity analysis, model runs were also performed to investigate if the model simulated processes unique to riparian hillslopes. These unique processes and phenomena have been observed in past field investigations and model studies.

For sensitivity analysis, model parameters were varied by ±10% about the base parameter value and the changes in model responses were then compared. Model sensitivity was evaluated using

$$S_r = \frac{\delta O}{\delta I} \cdot \frac{I}{O} \qquad\qquad 11.1$$

where S_r is relative sensitivity, δO is the change in the model output, δI is the change in model input, and O and I are the base output and input values, respectively. Since S_r is dimensionless, parameters were directly compared. Sensitivity analysis and process investigations were performed for the subsurface flow and sediment components of the hillslope model.

11.2 Subsurface flow component

11.2.1 Parameter sensitivity

Melton Branch hillslope catchment input data was used as the baseline scenario for

parameter sensitivity analysis. Site features and event information were described previously in the chapter on Model Evaluation. Values for input parameters describing segment and soil parameters for this hillslope were varied ± 10% and the corresponding hillslope responses compared to the baseline response. Parameter values were varied one parameter at a time with other parameters held at their baseline values. The parameters selected for sensitivity analysis and their baseline values are listed in Table 11.1. The model outputs that were evaluated for relative sensitivity were:

- subsurface lateral flow totals from the C soil horizon of Melton Branch (the major portion of the subsurface runoff was discharged from this horizon),
- peak runoff values for the C horizon,
- lag time to peak for the C horizon.

Table 11.1: Parameters and baseline values used for sensitivity analysis

Parameter	Identifier*	Units	Baseline values*
Horizon thickness	DEPTH	m	0.08, 0.53, 1.22
Total porosity	POROSITY	$m^3 m^{-3}$	0.56, 0.45, 0.39
Macroporosity	MACPOR	$m^3 m^{-3}$	0.005, 0.0027, 0.0023
Field capacity	FCAP	$m^3 m^{-3}$	0.39, 0.35, 0.35
Antecedent soil moisture	ASM	$m^3 m^{-3}$	0.36, 0.33, 0.35
Macropore diameter	MACDIA	mm	5, 1, 1
Macropore roughness	ROUGH	--	0.5
Vertical sat. conductivity	VSAT	$mm\ hr^{-1}$	344, 344, 27.36
Horizontal sat. conductivity	HSAT	$mm\ hr^{-1}$	344, 344, 27.36
main channel average w/d	WDRAT	$m\ m^{-1}$	15

Note: * Base values listed are for each of the three soil horizons; A, B, and C, respectively.
*identifiers used in Figures 11.1, 11.2, and 11.3

Relative sensitivities of total runoff, peak runoff, and lag time to peak runoff for the selected parameters are illustrated in Figures 11.1, 11.2, and 11.3, respectively. The upper and lower horizontal bars associated with each parameter in Figures 11.1 to 11.3 express the relative sensitivity for a +10% and -10% change in the parameter value, respectively. Identifiers used in the figures are described in Table 11.1. Antecedent soil moisture, field capacity, and porosity seem to be the parameters to which all three model outputs are highly sensitive. Antecedent soil moisture is the preexisting soil moisture in the soil layers and thus strongly influences the total runoff generated, its peak, as well as the time to peak. Field capacity is similar to a "threshold storage" beyond which excess moisture is available for vertical drainage or lateral flow. Since total subsurface runoff is the amount that exceeds the "threshold storage", it understandably is sensitive to the field capacity. Also, since the time to peak runoff includes the time taken to satisfy field capacity or the "threshold storage", the lag time to peak is also sensitive to field capacity as is obvious from Figure 11.3. In contrast, peak runoff rate is not as sensitive to field capacity as to antecedent soil moisture and porosity. This could be because once field capacity storage is satisfied, and a saturation layer formed, the peak runoff value is determined to a greater extent by macropore characteristics (model investigations indicated that a major portion of the peak flow occurs via macropores). Total porosity seems to play a greater role in influencing peak runoff rates and lag time to peak compared to the total runoff response. An increase in total porosity allows more water storage, and thus reduces the amount that can contribute to peak runoff. This phenomenon is well illustrated in the runoff hydrograph of Figure 11.4. Similar results were obtained from a sensitivity analysis performed by Kirkby (1986) on his hillslope model. Kirkby (1986) found that an increase in porosity led to a distinct decrease in the peak subsurface runoff value.

Results also indicate that although total runoff and peak runoff rates are not sensitive to the vertical saturated conductivity, lag time to peak is (Figure 11.3). Vertical conductivity influences lag time since it controls the time taken for water to traverse the unsaturated zone to reach the saturated layer. For similar reasons, the thickness of the soil horizon also influences the lag time. Figure 11.5 describes the influence of horizon thickness on the runoff hydrographs. Though the difference in peak values due to different horizon thicknesses is noticeable, the shift in lag time is not obvious in Figure 11.5. Smith and Hebbert's (1983) hillslope simulation results

indicate that the thickness of the soil layer, vertical conductivity, and total porosity influence the lag time to peak since they all influence the travel time to the saturated layer.

Macropore characteristics also influence peak runoff rate and lag time to peak runoff. Macropore roughness through Manning's equation determines the macropore flow velocity and thus the lag time to peak runoff. The sensitivity of peak runoff to macropore roughness is a cause of concern considering the large variability and limited information associated with this parameter. Investigations by Kitahara (1989) on naturally occurring soil macropores and pipes on forested slopes indicate roughness values ranging from 0.036 to 1.36. Peak runoff is also sensitive to the macroporosity, which is a measure of the total macropore cross-sectional area within a soil horizon.
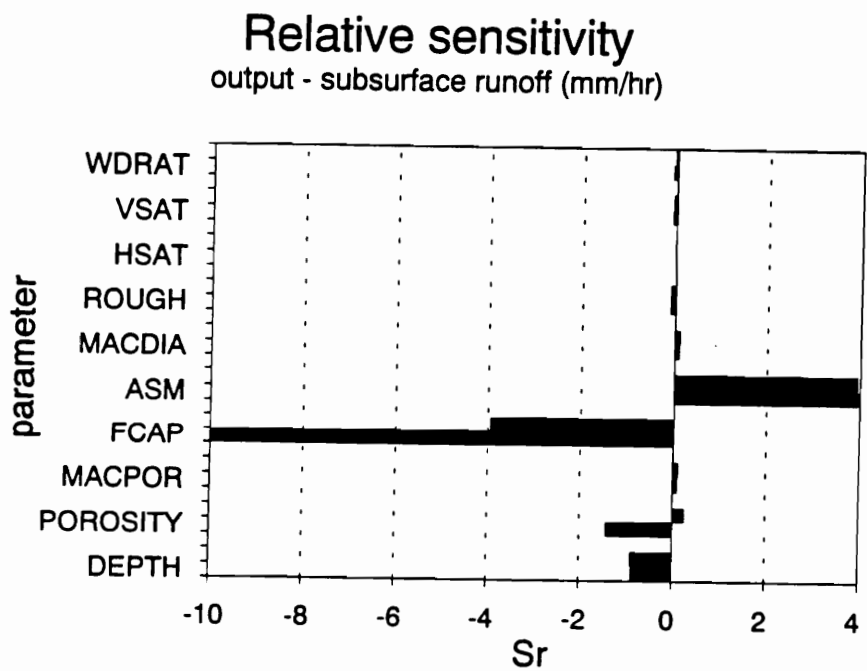
Figure 11.1: Relative sensitivity values for total runoff (the upper and lower horizontal bars correspond to +10% and -10% change in base parameter value, respectively).

Relative sensitivity
output - peak runoff rate (mm/hr)
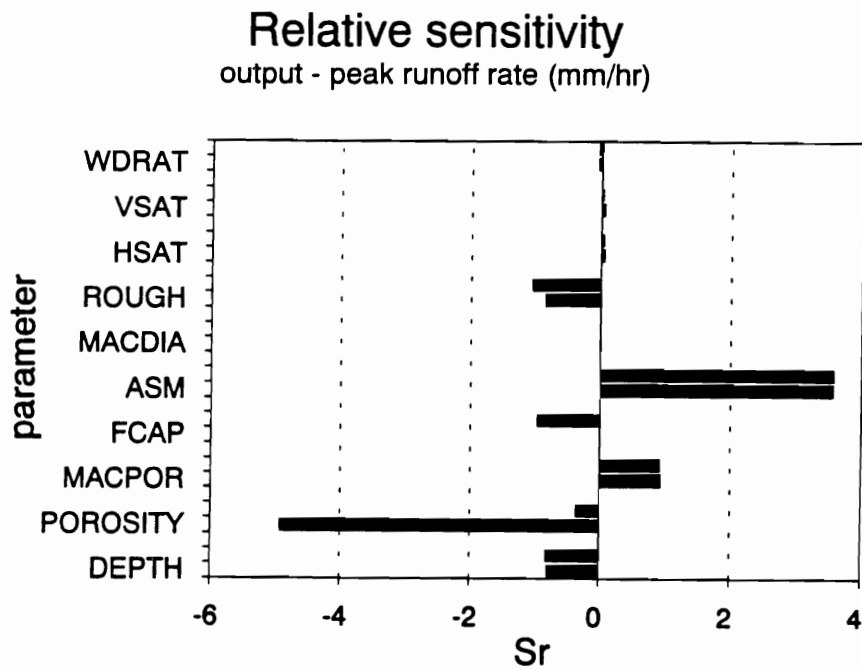
Figure 11.2: Relative sensitivity values for peak runoff.

Relative sensitivity
output - lag time to peak (min)
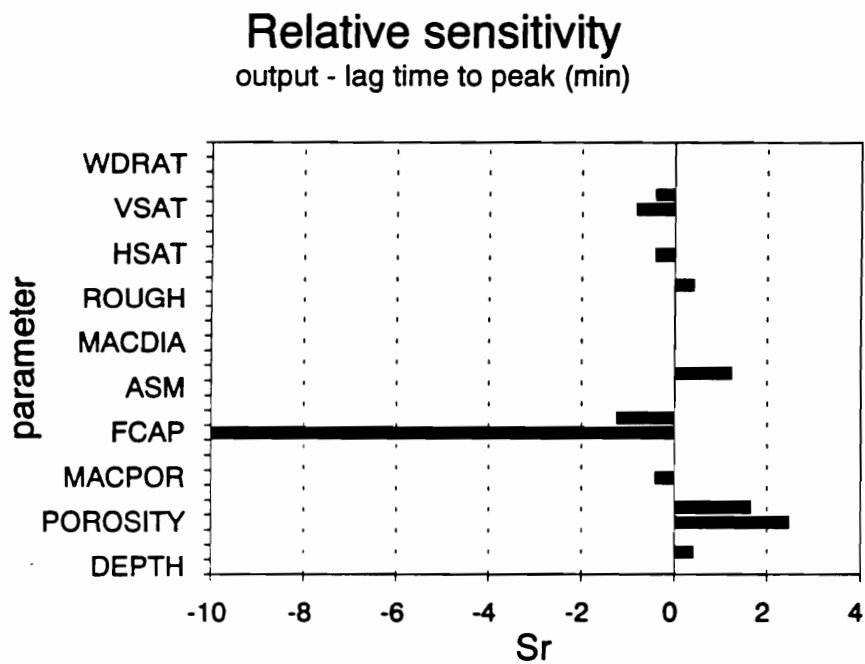
Figure 11.3: Relative sensitivity values for lag time.
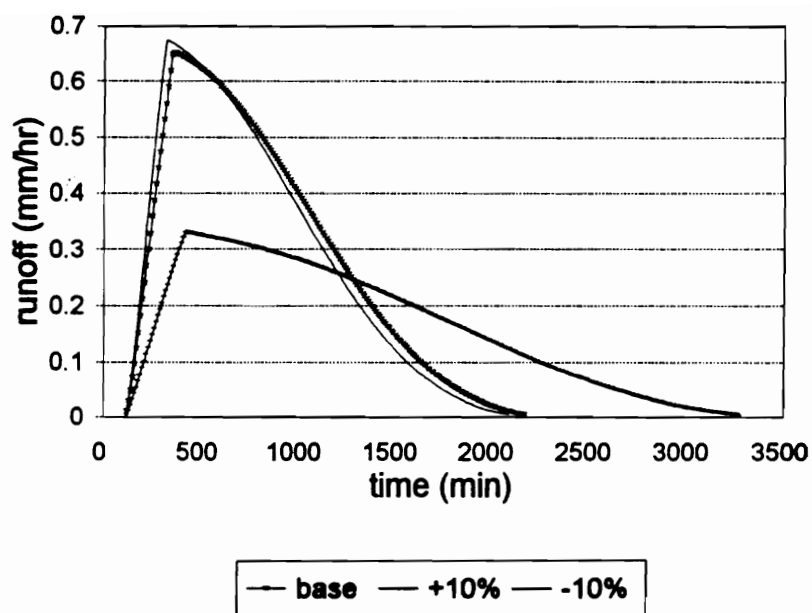
Figure 11.4: Influence of porosity on subsurface runoff.
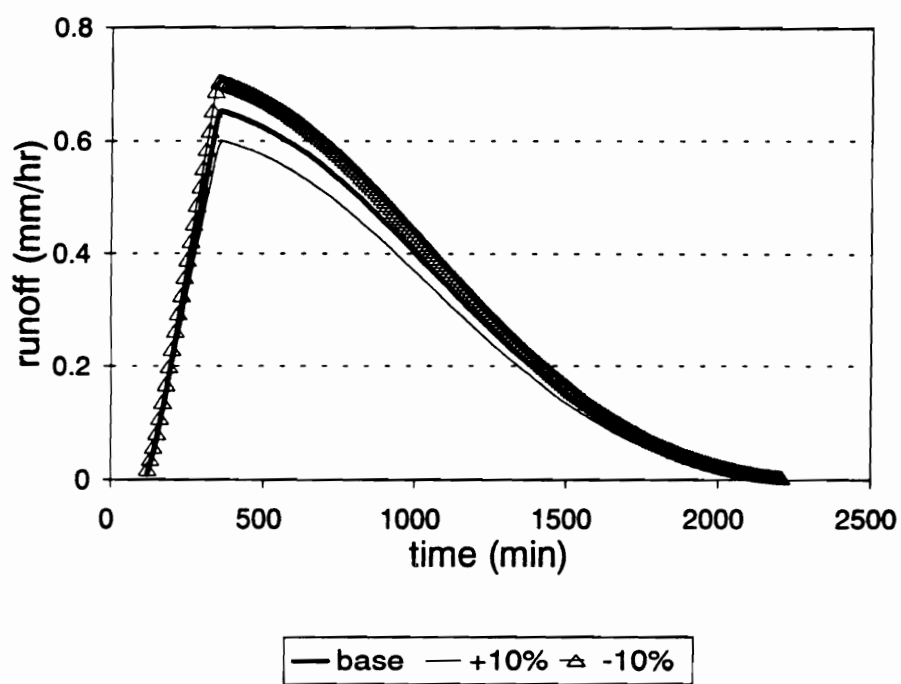
Figure 11.5: Influence of horizon depths on subsurface runoff.

11.2.2 Sensitivity to choice of segment length

As described in the Model Framework chapter, subsurface flow routing is performed by computing water balances for each hillslope segment with a one minute time step. This scheme is based on the assumption that simulations performed at an appropriate spatial and temporal discretization can approximate the smooth nature of the runoff hydrograph. For a given time step, it is expected that as the size of hillslope segment is reduced the runoff responses will change. This change in results will continue until a "critical" segment size is reached beyond which any further increase in spatial resolution will not influence model responses. It is at this "critical" spatial resolution that simulated hydrographs come closest to approximating the smooth nature of the runoff hydrograph. To determine this "critical" hillslope segment size, computations were performed using the data from hillslope 2A and event 2 from the Canadian hillslope study. This hillslope was chosen since subsurface flow response on this hillslope was the quickest of all the experimental hillslopes available (this hillslope had the shallowest soil depth, and saturated conductivities were the highest). The model parameters for this hillslope were described earlier (Chapter on Model Evaluation). Hillslope width and slope were changed to constant values of 10 m and 15%, respectively. This was done so that width and slope values would be the same for the entire hillslope and would not differ for individual segments with change in segment length. Simulations were performed for four discrete segment lengths: 23.12 m (3 segments in a total hillslope length of 69.36 m), 11.56 m (6 segments), 7.709 (9 segments), and 5.78 m (12 segments). Runoff ratios (ratio of total event rainfall to total subsurface runoff) for the B horizon (soil layer immediately above the bedrock) were determined for each of the segment lengths and are plotted in Figure 11.6. As can be seen from Figure 11.6, the largest change occurred when the slope segment length was reduced from 23.12 m to 11.56 m. The change in runoff ratio progressively decreases with decrease in segment length. The change in runoff ratio values between the 11.56 m segment length and the 5.78 m segment length was approximately 9%.
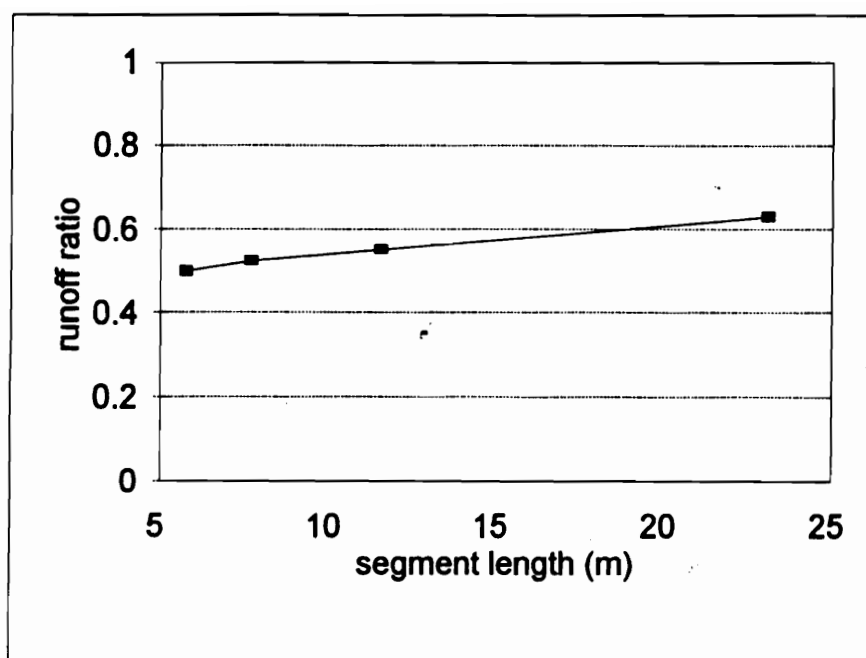
Figure 11.6: Sensitivity to segment length.

This sensitivity analysis was performed prior to model testing procedures described in the Model Evaluation chapter. For model testing, the segment length selected was 11.56 m (or six segments). The choice of this segment length seemed appropriate considering the additional computational time and efforts required to perform simulations at a higher resolution. This analysis indicates that, when comparing simulated and observed responses, error bounds associated with discretization should also be considered in addition to the bounds (in this case the 95% confidence bounds) associated with model response.

11.2.3 Process investigations

I) *For riparian hillslopes with a subsurface restricting soil layer, subsurface lateral flow is the major runoff contributor.*

Field investigations on riparian hillslopes located in humid temperate catchments have revealed that in the presence of a restricting layer, interflow seems to be the major runoff contributor (Hewlett and Hibbert, 1963; Whipkey (1965); Weyman (1973); Hewlett and Nutter (1970); Anderson and Burt (1978); Weymour (1970, 73). Corbett (1979) estimated that subsurface stormflow provided 75 to 97% of the total stormflow response. A recent investigation by Tsuboyama (1994) found that 70-93% of the total discharge from a hillslope was attributed to subsurface downslope flow over an impeding layer. Field investigations on the Canadian Shield hillslopes (used in this research to evaluate the subsurface component of the model) also demonstrated that subsurface flow occurring over an impeding layer contributed 91 to 99.9% of the total hillslope response (Peters et al., 1995).

Model simulations performed using the Canadian Shield and Melton Branch hillslope data support this observation. Model simulations for the Canadian hillslopes indicated that more than 95% of the total event water (subsurface lateral flow plus vertical seepage) leaving the hillslopes was contributed by subsurface downslope occurring over the bedrock. Similar results were observed from Melton Branch hillslope simulations. Moreover these simulations also showed that most of the lateral subsurface stormflow occurred at the junction of the most restrictive soil horizon and not at an upper or intermediate soil horizon (see runoff hydrograph results presented in the chapter on Model evaluation).

II) *Time to initiation of lateral subsurface flow is controlled by the depth of the unsaturated zone.*

Simulations by Smith and Hebbert (1983) using a finite difference hillslope model indicated that the lateral subsurface flow initiation and the lag time to peak were both strongly influenced by the depth of the unsaturated zone. Their results indicated that for a large value of unsaturated depth, the lateral flow was significantly delayed. To determine if this result was also supported by the riparian hillslope model, simulations were performed . Two scenarios of

differing unsaturated soil thicknesses were created by changing the base Melton Branch antecedent soil thickness values by ±10%. Both hillslope cases were subjected to identical rainfall events. Simulations of these two cases are illustrated in Figure 11.5. Though not noticeable in Figure 11.5, the increase in unsaturated soil thickness caused the initiation of lateral subsurface flow to be delayed by approximately ten minutes compared to the case for which the soil thickness was decreased by 10%.

III) *Under saturated conditions, macropore flow is orders of magnitude greater than soil matrix flow.*

Field investigations have revealed that on most forested hillslopes a major portion of the subsurface stormflow is routed via macropores (Aubertin, 1971; Beven, 1980; Whipkey, 1965, 67; Mosley, 1979, 82; Beasley, 1977; Pilgrim et al., 1978; Tsukamota, 1961). This flow is considered to be primarily non-Darcian based on the high velocities observed (Mosley, 1979; 82). Only a limited number of studies, though, have provided quantitative estimates on macropore flow contribution to subsurface stormflow. Tsukamoto and Ohta (1988) observed that 85.5-99.5% of all subsurface flow from a soil profile occurred through soil macropores on Pliocene slopes in Japan. Sidle et al.'s (1995) laboratory experiments on a soil pedon indicated that macropores/soil pipes contributed 21 to 83% of the total subsurface flow.

In the subsurface component of the riparian hillslope model, subsurface flow is simulated as a combination of Darcian soil matrix flow and non-Darcian macropore flow (described in detail in the Model Development chapter). Results from this model for the Canadian hillslopes indicate that macropore flow contributed 85-90% of the total subsurface flow exiting at the base of the hillslopes. For the Melton Branch hillslope catchment, macropore flow contributions to subsurface flow from the B and C soil horizons were approximately 65% and 95% , respectively. As the saturated lateral hydraulic conductivity of the horizon decreased, the model simulated greater contributions from macropore flow, thus simulating the dynamic interaction between soil matrix and macropore flow. This is obvious from the results of Melton Branch hillslope where the B horizon had a much higher conductivity compared to the C horizon. In addition, to simulating the dynamic partitioning between soil matrix flow and macropore flow, the model also successfully predicted the lowering of saturation depths and consequent reduction in recession

flow periods with increasing soil macroporosity and decreasing macropore roughness. Investigations by Montgomery and Dietrich (1995) suggest that macropore distributions influence the peizometric potentials in the soil profile. Sidle et al. (1995) found that peizometric profiles along the hillslope are depressed when macropore roughness values are decreased.

IV) *Concave-convergent slopes provide more favorable conditions for build up of the saturation wedge compared to straight or convex slopes.*

Original data for the Melton Branch hillslope indicated a concave convergent hillslope shape. The straight-straight (in plan and section) and convex-divergent hillslopes were simulated by changing the segment widths and gradients for the original Melton Branch hillslope such that the total hillslope contributing area remain unchanged. The slope gradient for the straight-straight hillslope was determined by averaging the gradients of all segments in the concave hillslope. The slope gradients for the convex hillslope were the mirror image of the those used for the concave case. The shapes of the three hillslopes in plan and section are illustrated in Figure 11.7. This combination of plan and slope profile (convergent plan with concave slope, and divergent plan with convex slope) was selected because it represents the most commonly observed hillslope shapes in humid temperate catchments (Kirkby, 1986). The values of segment width and gradient for all the three shape scenarios are listed in Table 11.2.

Table 11.2: Attributes for the three hillslope shapes*

Parameter	Concave-convergent (C)+	Convex-divergent (B)+	Straight-straight (A)+
Segment length (m)	12.89	12.89	12.89
Segment widths (m)	118.17, 104.97, 91.78, 78.58, 65.38, 52.18	52.18, 65.38, 78.58, 91.78, 104.97, 118.17	85.18 for all segments
Slope gradients (%)	35, 30, 25, 20, 15, 10	10, 15, 20, 25, 30, 35	22.5 (all segments)

Note: * contributing hillslope areas for all the three hillslopes was the same.
       + identifiers used in Figure 11.8

A STRAIGHT-STRAIGHT

B CONVEX-DIVERGENT

impeding soil layer

C CONCAVE-CONVERGENT

PLAN VIEWS   SLOPE PROFILES
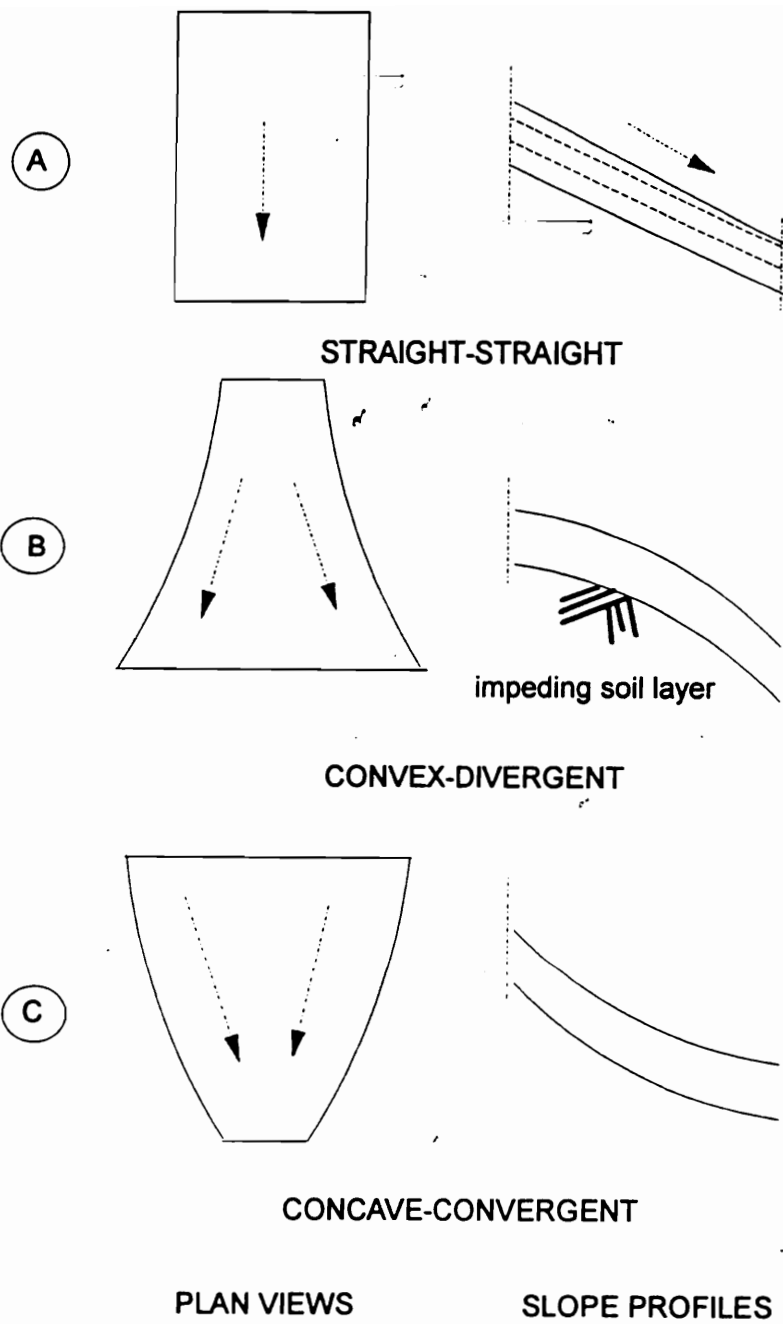
Figure 11.7: Hillslope shapes used for runoff response comparisons.

Subsurface runoff hydrographs from the C horizon of the three hillslope shapes are shown in Figure 11.8. The development of the saturated layer in the C horizon for the concave-convergent case and the convex-divergent case is illustrated in Figure 11.9. Figure 11.8 indicates that convex-divergent hillslopes provide the highest peak runoff and drain quicker compared to straight-straight and concave-convergent hillslope profiles. Very similar results were observed by Smith and Hebbert (1983) for their hillslope simulation. The depression in the subsurface runoff peak for the concave- convergent slope can be attributed to a decrease in hydraulic gradient as the slope decreases towards the base, and a progressively decreasing soil cross-sectional area that is available to flush runoff from the saturated layer. This decreasing cross-sectional area is also instrumental in generating higher saturation depths in the lower hillslope positions of the concave-convergent slopes compared to convex-divergent slopes. The higher saturation depths at the base of the concave-convergent slopes results in recession flows that are maintained for a longer periods compared to those for the other two hillslope scenarios (Figure 11.8). Though, for small duration rainfall events, the peak subsurface flow response of concave-convergent hillslopes is much smaller than that of the convex-divergent hillslope, it is possible that for storms of extended duration, concave-convergent slopes may create higher total runoff peaks. It is expected that these high runoff peaks will be primarily associated with generation of saturation overland flow and return flow (Figure 11.10). Since saturation occurs earlier and is maintained for longer durations at the base of the concave-convergent hillslopes compared to convex-divergent hillslopes (as demonstrated by Figure 11.9), it is expected that concave-convergent slopes provide more favorable conditions for the occurrence of saturation overland flow and return flow. Field investigations support the hypothesis that concave-convergent slopes provide greater opportunity for saturation overland flow and return flow (Beven, 1977; Beven and Kirkby, 1979; O'Loughlin, 1981). Using runoff hydrograph results for the two hillslope shapes presented above, it can be hypothesized that in catchments where convex-divergent hillslopes occupy a major portion of the hillslope area, one can expect a quicker catchment response to rain events compared to catchments where concave-convergent hillslopes dominate.
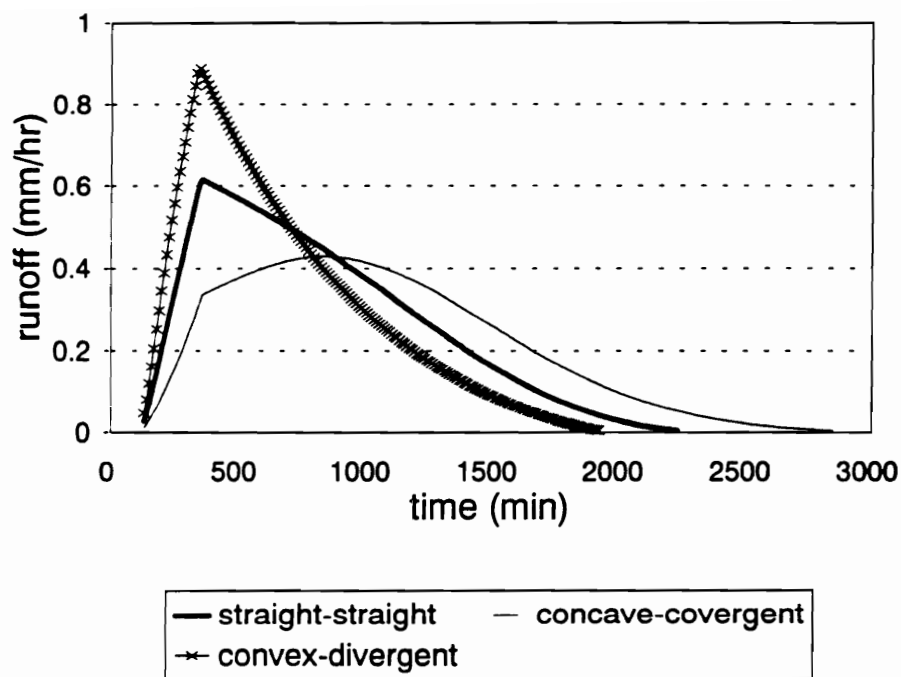
Figure 11.8: Comparison of runoff hydrographs from different hillslope forms.
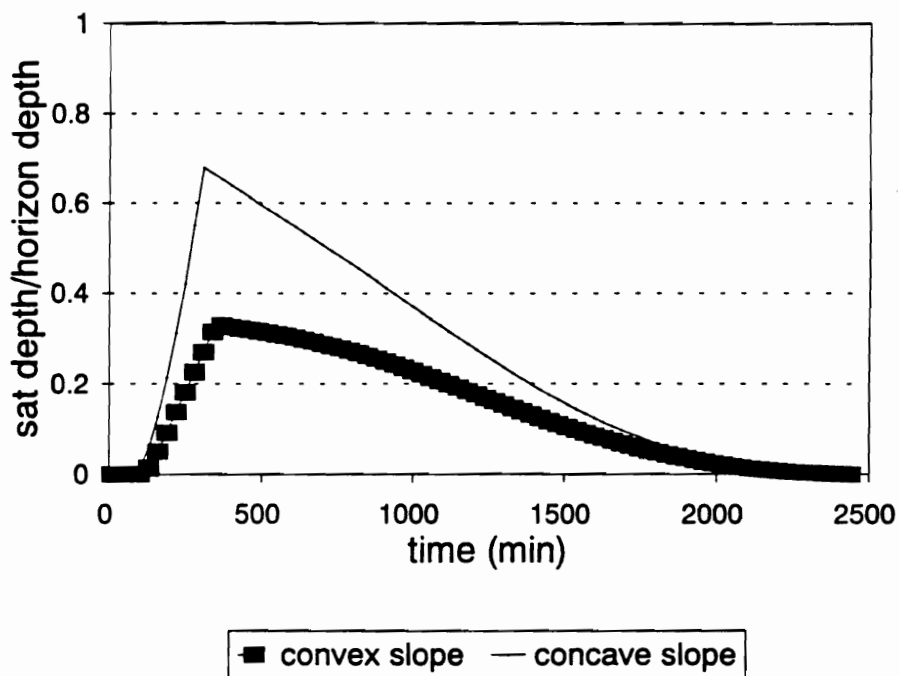
Figure 11.9: Comparison of saturation in the surface layer at the base of the hillslope for cocave-convergent and convex-divergent hillslope forms.

saturation wedge developing
over the restricting layer

shorter duration events

interflow

overland flow

longer duration events

interflow
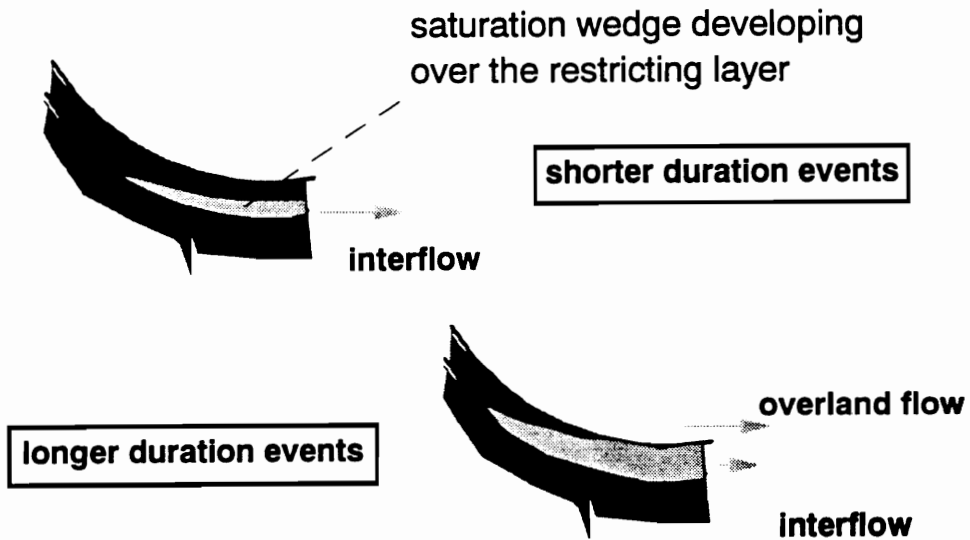
Figure 11.10: Schematic illustrating the build up of saturation wedge for long duration events and the consequent high peak flows associated with saturation overland flow.

In addition to the topographic features described above that influence subsurface flow response, soil characteristics may also be involved in shaping the subsurface runoff hydrograph. Field investigations have found that soils in the lower concave region of the slope tend to have a less permeable B horizon compared to upslope locations or similar locations in convex hillslopes (Hammermeister et al., 1982; Zaslavsky and Rogowski, 1969). Essentially, this means that the restricting soil surface moves closer to the surface for lower concave regions in the hillslope (even though the total soil horizon depth may increase towards the base). In an attempt to investigate soil horizon influences, simulations were repeated for the two concave-convergent and convex-

divergent hillslopes described above but with a variation in the depth to the restricting soil layer along the slope. A cross section through the slope profile illustrating the soil depths simulated is shown in Figure 11.11. For the concave-convergent hillslope, the depth to the restricting soil layer progressively decreases (slope section A in Figure 11.11), whereas for the convex-divergent hillslope it progressively increases (slope section B in Figure 11.11). Runoff hydrographs from these two hillslope scenarios are provided in Figure 11.12. Model results indicate that the runoff hydrographs shapes are similar to those observed earlier in Figure 11.9. Hydrographs in Figure 11.12 show higher peaks than those in Figure 11.9, but this is attributed to the shallower soil depths. The shallower soil depths result in less water storage. The intent in this analysis was to see if the variation in soil depth along the slope exaggerated the difference in hydrograph shapes between concave-convergent and convex-divergent hillslopes (compared to the shapes observed where the soil depth for both cases was the same). The model did not simulate any perceptible change in hydrograph shapes.
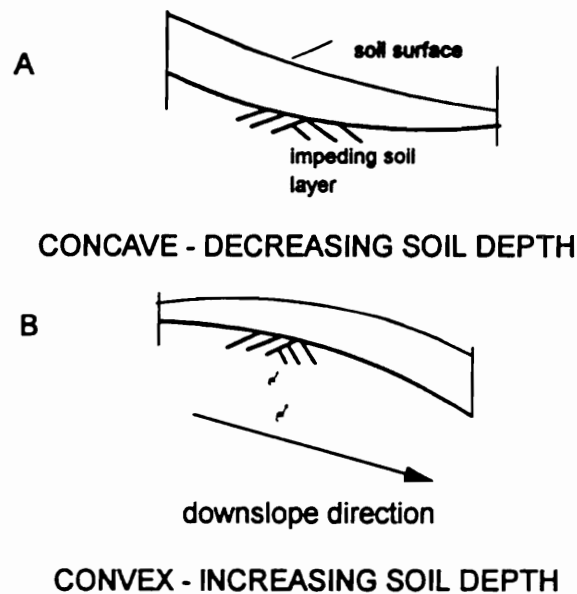
Figure 11.11: Schematic illustrating the decreasing and increasing soil depths used for the concave and convex hillslope shapes.
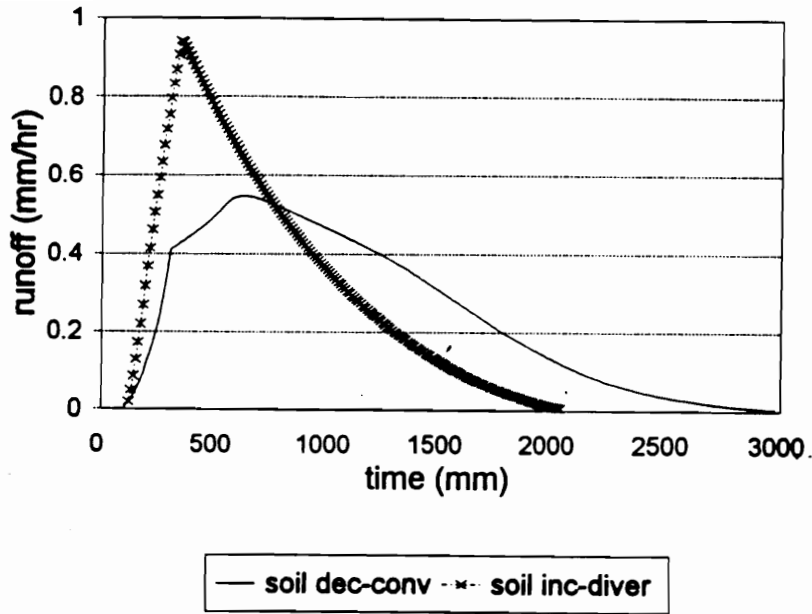
Figure 11.12: Runoff response corresponding to decreasing and increasing soil depths.

11.3 Sediment component

11.3.1 Parameter sensitivity

Site and event data from the Kentucky grass filter study (grass filter five and event two) were selected as a baseline. For sensitivity analysis procedures, the varying channel density (along the filter length) in the original data was changed to a constant value of four. Since initial simulation runs indicated sediment deposition as the major phenomenon, parameters that could influence sediment deposition were targeted. These parameters included - slope gradient, Manning's roughness for vegetation, sediment size distribution, and specific gravity for different particle size classes. In addition to these parameters, investigations were also performed to determine how changes in runoff volume along the filter length affected sediment transport and deposition.

The output chosen to compute relative sensitivity was the percentage of total sediment

trapped for each event. Each of the parameters was varied ±10% of the base values and the sediment trapping was computed. For sediment size distribution, the percent finer values were shifted by 10%.

Results from the sediment model sensitivity analysis are provided in Figure 11.13. Results indicate that the sediment size distribution, or the size of sediment load fractions in each particle class, and the specific gravity for each particle class had the greatest influence on model results. Sediment trapping was sensitive to runoff to some extent, but was less sensitive to Manning's n. Model responses were insensitive to slope gradient. Sediment deposition in grass filters has generally been attributed to the loss in transport capacity caused by infiltration losses and flow velocity reduction (a consequence of increased surface roughness provided by vegetation). Simulated sediment trapping or deposition in the grass filters was primarily a result of high infiltration losses. Approximately 90% of the incoming flow was lost to infiltration. With such high infiltration losses, it is difficult to evaluate the role of surface roughness or slope gradient in influencing deposition. It is expected that influence of surface roughness will be more obvious in cases where infiltration losses are less.

The grass filters used for this investigation had dense fescue vegetation and a thick mat of litter layer covering the soil surface. There was no previously deposited sediment extending above the litter layer. Thus, in addition to high infiltration losses, there was virtually no sediment that could be transported as bedload. Hence, the sediment transport capacity simulated in the model was primarily sediment that could be transported as suspended load. With this scheme, any sediment particle that reached the surface of the soil, was assumed to be trapped. In such an extreme scenario it is very unlikely that influences of parameters such as Manning's n, slope gradient, or runoff can be fully evaluated. It is also expected that such conditions may not fully reveal the influences of flow concentration (discussed in a following section) on sediment trapping.
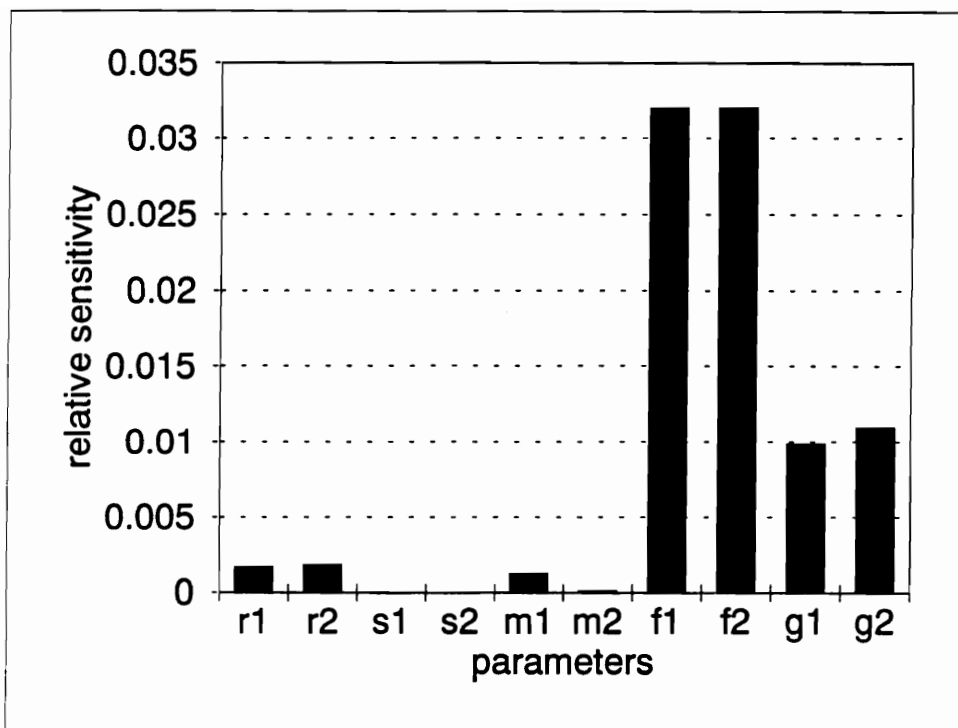
Legend

r1 - runoff +10%	r2 - runoff -10%
s1 - slope +10%	s2 - slope -10%
m1 - Manning's n +10%	m2 - Manning's n -10%
f1 - particle distribution +10%	f2 - particle distribution -10%
g1 - specific gravity +10%	g2 - specific gravity 10%

Figure 11.13: Relative sensitivity values corresponding to sediment trapping (%).

The sediment model included an algorithm that computed sediment enrichment as a result of sediment deposition. A limited investigation was performed to determine how sediment enrichment results were influenced by changes in primary particle size fractions (sand, silt, and clay) composing the sediment. Three cases representing sediment eroded from a silt loam (case 1), sandy loam (case 2), and silty clay (case 3) soil were investigated. Primarily particle size fractions composing various particle classes for the three soil texture cases are listed in Table 11.3. The values for the primary particle size fractions were selected based on the USDA soil textural triangle. Values for surface areas of each primary particle size class were selected from the literature and are provided in Table 11.2 (Savabi et al., 1989).

Sediment enrichment results for the three cases are included in Table 11.3. Sediment enrichment primarily occurs when primary clay fractions in the sediment (which have a high surface area - e.g., see values listed in Table 11.3) are not deposited. Previous research has indicated that sandy soils tend to have high enrichment ratios (Foster et al., 1985). This was because most of the sediment eroded from sandy soils is poorly aggregated, with a major portion of the clay being in fine sediment size fractions, which rarely get deposited. In contrast, for soil high in clay, the primary particles are more evenly distributed and a major fraction of the clay gets deposited when large aggregate sediment particles are deposited (Foster et al., 1985). Model simulations of enrichment ratios provided in Table 11.3 tend to confirm these observations. Simulated enrichment ratios are highest for sediment eroded from sandy loam parent soil (case 2)and lowest for the sediment eroded from silty clay soil material (case 3). For all three soil textures, most of the primary particle fractions in the large and small aggregate class (2.00 - 0.010 mm) are assumed to be trapped since these particle classes are easily deposited within the grass filters.

Enrichment results presented here are the ratios of specific surface areas of the sediment entering and exiting the grass filter. The enrichment values could be considerably higher if comparisons were made between the surface areas of the parent soil material (at the point of detachment/erosion) and the sediment exiting the grass filter. On the other hand, model simulations could be overpredicting the enrichment to some extent, since the model does not simulate the phenomenon of fine fractions being carried into the soil matrix with infiltrating water.

Table 11.3: Primary particle size fractions in each sediment class.

Aggregate class (mm)	fraction	Case 1 Silt Loam			Case 2 Sandy Loam			Case 3 Silty Clay		
		sand	silt	clay	sand	silt	clay	sand	silt	clay
2.00 - 0.125	0.571	0.3	0.5	0.2	0.6	0.3	0.1	0.1	0.4	0.5
0.125 - 0.063	0.052	0.1	0.7	0.2	0.2	0.6	0.1	0.0	0.5	0.5
0.063 - 0.010	0.268	0.0	0.7	0.3	0.0	0.8	0.2	0.0	0.5	0.5
0.010 - 0.005	0.022	0.0	0.7	0.3	0.0	0.8	0.2	0.0	0.5	0.5
0.005 - 0.001	0.061	0.0	1.0	0.0	0.0	1.0	0.0	0.0	1.0	0.0
0.001 - 0.0005	0.026	0.0	0.0	1.0	0.0	0.0	1.0	0.0	0.0	1.0
Surface area * $m^2 g^{-1}$		0.05	4.00	20.0						
Enrichment		1.033			1.167			0.8489		

Note: * specific surface area the same for all three cases

11.2.2 Sensitivity to choice of segment length

Similar to segment sensitivity analysis performed for the subsurface component, the influence of choice of segment length on sediment trapping was investigated. Simulations were again performed using site and event data from grass filter five and event two at Kentucky. Sediment trapping was determined for four segment lengths - 0.7625 m (6 segments for a total filter length of 4.575 m), 0.508 m (9 segments), 0.381 m (12 segments), and 0.305 m (15 segments). The results from this analysis are provided in Figure 11.14. From Figure 11.14 it can be seen that the percentage trapping tends to stabilize for segment lengths 0.381 m and smaller. A segment length of 0.381 m was thus selected for the model evaluation procedures described earlier in the Model Evaluation chapter.
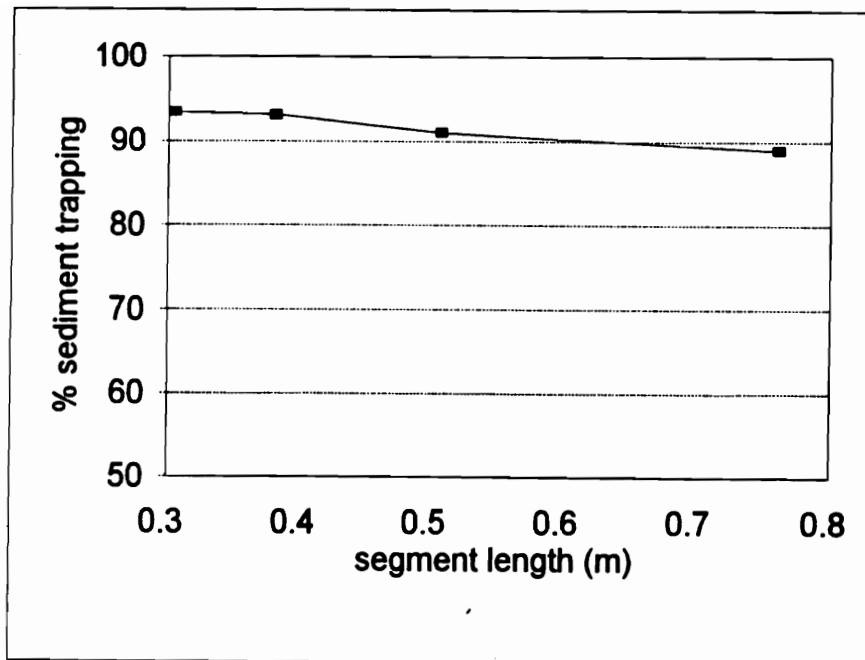
Figure 11.14: Sensitivity of sediment trapping (%) to segment length.

11.3.3 Process investigations

V)   *Sediment delivery increases with increasing runoff concentration, or sediment trapping decreases with increasing flow concentration*

Field investigations of naturally occurring riparian grass filter strips has revealed that flow concentration reduces sediment trapping in grass filter strips (Dillaha et al., 1989). This reduction in trapping is due to increased sediment transport capacity associated with concentrated flow (Dillaha et al.,1989). Increase in sediment transport capacity for concentrated flow can in turn be attributed to [a] higher runoff depths and flow velocities in channels compared to uniformly distributed sheet flow; [b] reduced infiltration losses, as infiltration is limited to channel areas; and [c] over the long term, greater availability of previously deposited sediment for detachment and transport as sediment deposition is localized in channel areas.

Simulations were performed to test the hypothesis that sediment trapping decreased with increasing flow concentration. Base information on filter size, event and sediment loading was from filter five and event two. In the model, flow concentration can be simulated by increasing the number of channels at each segment and by appropriately changing the cross-sectional shape. A channel density of one for a segment simulates uniformly distributed sheet flow. To simulate concentrated flow, the number of channels for each segment was increased to 10. Channel shape (expressed as width to depth ratio) was assumed to be the same for the concentrated flow and uniformly distributed flow case (though in reality, channels shapes associated with concentrated flow tend to be more incised).

The concentrated flow case yielded a sediment trapping of 89.0%, compared to 96.9% for the uniformly distributed flow case. These results tend to support the hypothesis that sediment delivery increases with flow concentration. The difference between the two results was less because other aspects/phenomena that typically accompany flow concentration were not included in the simulation. These other phenomena include:

- Increased runoff for each segment, since infiltration losses are reduced due to flow concentration. For model simulations it was assumed that infiltration losses and thus runoff along the filter length was identical for both cases.

- Change in channel shape associated with concentrated flow. Typically filters that have had concentrated flow for some time tend to have more incised channels shapes compared to filters with uniform flow distribution.

- Difference in surface roughness. Flow concentration leads to localized sediment deposition. Localized deposition may provide sufficient sediment to cover the litter layer and thus alter the surface roughness within the channel areas. This localized deposition also causes surface sealing as pores in the channel areas are covered and filled by sediment particles. This further reduces infiltration losses.

12 SUMMARY AND CONCLUSIONS

Research was focused on two major areas - [a] field investigations of riparian hillslopes and [b] development of a riparian hillslope model to simulate hydrologic and sediment transport processes. There were two major objectives behind the field investigations. The first objective was to identify the "representative hillslope scale" for investigating and simulating riparian hillslope processes. The second objective was to characterize and quantify geomorphic features of riparian slopes that could be used to quantify surface and subsurface flow concentrations on these hillslopes. The geomorphic features that were targeted for investigation were catchment area, catchment shape, and drainage channel cross-sectional shape. The alternate hypotheses that were proposed for each of these features were - [a] catchment area decreases with increasing slope gradient, [b] catchment shape elongates with increasing slope gradient, and, [c] drainage channel shape values expressed as width to depth ratios decrease as slope gradient increases.

The objective of the modeling effort was to develop a detailed process-oriented model that could provide insight into the dynamics of riparian hillslope processes and which could be used to investigate the influence of site conditions on riparian hillslope responses. Prior to performing detailed investigations, the model was evaluated using field measured data, and confidence bounds were established for model predictions.

Field investigations were performed on riparian hillslopes located in the Ridge and Valley region of Virginia. Field surveys of hillslopes in this region revealed that these hillslopes were dissected into distinct convergent, divergent, or straight slope segments/units. In profile, these hillslope segments/units were either concave, straight, or convex. Contributing area sizes and shapes within each of these hillslope units are determined by the nature of the convergence/divergence and convexity/concavity of each such segment. The hydrologic response at the base of such hillslope segments/units is generated by the sum effect of all the contributing areas within the segment. Thus, evaluation of the hillslope response by considering a small portion of the hillslope segment would not be representative of the full segment. Similarly, if the portion of hillslope under investigation is larger than the size of the hillslope segment/unit,

topographic features of adjacent slope units/segments influence the hillslope response. If the true response of a hillslope segment is to be determined (either via field experimentation or model simulation) and related to its topographic/geomorphic features, investigation should be limited to the size of the hillslope segment. Hence, it was proposed that the size of such hillslope segments represents the "representative hillslope scale".

A detailed field survey was conducted at a 2 m interval to determine catchment area, catchment shape, and drainage channel shapes at the identified "representative hillslope scale". Distributions for catchment area, catchment shape, and drainage channel shapes were extracted from the topographic data using a digital elevation model (DEM) and a statistical package. Distributions for each of these parameters were computed for three slope gradient categories - 7 to 15%, 15 to 20%, and greater than 20%.

Distributions of catchment area showed that catchment area decreases with slope gradient. The data in the three slope categories were significantly different at the 95 % level. Based on this information, the null hypothesis that catchment area does not decrease with increasing slope gradient can be rejected. Previous studies have revealed contrasting results regarding drainage area size. For steep hillslopes where subsurface stormflow was dominant, catchment area was inversely correlated to slope gradient. For low slope gradients, where overland flow was the dominant flow mechanism, drainage area size was positively correlated to slope gradient. It is possible that some of the hillslopes sampled in this field study reflect hillslope forms which lie somewhere in the middle of the spectrum bounded by the two case studies mentioned above. It is also possible that determination of catchment areas could have been influenced by the DEM, model, which can simulate only converging dendritic type channel networks and cannot realistically represent conditions where channel bifurcation is expected. This analysis provided an approach that can be used to quantify the distribution of runoff volumes on hillslopes. If accurate data on the catchment areas are available for a hillslope, distribution of catchment areas could provide a reasonable approximation of the runoff distribution. Such information can be used effectively to simulate runoff in hillslope models.

Distributions of catchment shape data across the three slope categories were found to be significantly different at the 95% level, thus rejecting the null hypothesis. This indicates that catchment length to area ratio decreases with increasing slope gradient, indicating catchment shape

elongation with increasing gradient. This means that the average width of contributing areas on the slope decreases with increasing gradient. At present, modeling approaches simulating flow concentration on hillslopes require the number of channels at a section as input. Estimating the number of channels, especially in cases where flow concentrates along topographic depressions and unincised drainages, is difficult, if not impossible. Use of catchment shape distributions provides an estimate of flow concentration (surface as well as subsurface) based on the basic topographic features of the hillslope.

Distributions of drainage channel shape data indicated a decreasing trend in width to depth ratio with increasing slope gradient. These distributions were found to be significantly different at the 95 % level, thus rejecting the null hypothesis. Deeper channels or low width to depth ratios for steeper gradients are attributed to the long-term influences of greater flow concentration and higher erosion potential of runoff associated with steep slope gradients. Since channel shape influences the rate of surface and subsurface runoff movement, spatial distribution, and production, it is imperative that they be considered in hillslope runoff models. This can be accomplished by including channel shape (width to depth ratio) distributions which vary with slope gradient.

Modeling efforts were directed towards the development of a hillslope scale, continuous simulation model. The hillslope scale was the "representative hillslope scale" defined by the size of the converging/diverging hillslope segments. Model scope was limited to simulating riparian hillslopes typically observed in the Ridge and Valley region. The riparian hillslope was assumed to be located downslope of an upland contributing area. Hydrologic and sediment transport processes that were simulated include rainfall interception, evapotranspiration, infiltration, infiltration excess and saturation overland flow, vertical drainage, interflow or subsurface stormflow, return flow, and sediment deposition, detachment, transport, enrichment. These phenomena were simulated using process-oriented modeling approaches.

Special attention was given to simulating unique riparian phenomena such as subsurface lateral flow or interflow occurring over different soil horizons and its concentration along depressions and drainages. Interflow was simulated as a combination of Darcian soil matrix flow and non-Darcian macropore flow. Preferential macropore flow movement was simulated using a combination of a stochastic description of the population of macropores within each soil horizon,

and a description of flow in individual macropores via Manning's equation. Surface saturation and consequent generation of variable source areas due to the saturated water layer reaching the surface within these concentrated interflow drainages were also simulated. Surface runoff concentration in rills/channels was included. Flow concentration along subsurface and surface routes was represented in the model by providing a stochastic description of the population of drainages and surface channels on the hillslope.

Model predictions of interflow, generation of surface saturation (a key component of the variable source area mechanism), and sediment transport and fate were evaluated by comparisons with field observations. Evaluation results were expressed with the confidence associated with model predictions. Interflow, or the subsurface lateral flow component of the model, was evaluated using detailed quantitative field data from two hillslopes from the Canadian Shield Basin study and a hillslope catchment from the Melton Branch subwatershed study in Tennessee. The ability of the model to predict surface saturation was evaluated qualitatively using observed data from the hillslope catchment of Hachioji Basin study in Japan. The sediment transport component of the model was tested using detailed quantitative data on sediment trapping in vegetative grass filters conducted at the University of Kentucky.

The interflow/subsurface lateral flow component was evaluated for total subsurface lateral flow, peak flow, lag time to peak, and ratio of runoff to rainfall during different times within events. The response relationship between model predicted runoff totals and rainfall totals alongwith the 95% confidence bounds was compared to observed runoff totals. For most sites and events, the model predicted the observed runoff totals at a 95% level of confidence. The model predictions were not as good for the upper horizon of the Melton Branch watershed. The model also could not predict lateral runoff from A horizons, which occurred on the Canadian Shield hillslopes, and which was attributed to runoff over leaf litter. Procedures to simulate runoff over leaf litter were not included in the model. Observed and predicted peak runoff values and lag times to peak were regressed, and the slope and intercept of the regression line were compared to that of the equal value line. Statistical analysis indicated that the regression line parameters (slope and intercept) were not significantly different from the equal value line parameters for all sites. For the Melton Branch hillslope, comparison of within event observed and predicted runoff/rainfall depth ratio probability density functions yielded excellent results. Visual

comparisons of observed and predicted subsurface runoff hydrographs of contributing soil horizons were also conducted for each event. In general, observed hydrographs tended to be more flashy and had lower recession periods than predicted hydrographs. For the Canadian hillslopes, this was attributed to variable seepage through the bedrock, vertical macropore flow bypassing intermediate horizons, and exposed bedrock conditions that were not simulated by the model.

Qualitative comparisons between observed and predicted surface saturation along the length of the Hachioji hillslope catchment yielded good results. The model predicted the field observed hillslope location where surface saturation was initialized. Surface saturation was attributed primarily to the thinning of soil horizons towards the central lower portions of the hillslope.

Evaluation of the sediment component using the Kentucky data indicated sediment deposition as the primary phenomenon. Statistical analysis of the sediment trapping results revealed that the parameters of the regression line between observed and predicted values were not significantly different at a 95% level from those of the equal value line. Comparison of observed and predicted sedigraphs and exiting particle size distribution indicated that the model tended to underestimate fine sediment trapping. Experimental studies have indicated that a significant portion of the fine particles are entrapped in the soil matrix/litter layer as sediment is carried to the soil surface with infiltrating water. Some fine sediment may also be deposited along with the mass settling of large sediment particles typically occurring just upslope or in the upper portion of the grass filter. Most of the fine sediment trapped in this manner cannot be considered discrete settling. The model simulates particle trapping for all sizes based on discrete settling and thus does not account for trapping due to other mechanisms.

Sensitivity analysis was performed to reveal sensitive parameters that influenced model results. This was done by computing relative sensitivity values for selected outputs. For the subsurface flow component, total subsurface runoff, peak runoff, and lag time to peak runoff were the selected outputs. Sensitivity analysis results indicated that total porosity, field capacity, and antecedent soil moisture were the parameters which influenced all three outputs. In addition to the three parameters mentioned, peak runoff rates were sensitive to macropore roughness, macroporosity, and horizon thickness. Model simulations revealed that a major portion of the interflow, especially during peak flows, occurred through macropores. Similarly, in addition to

antecedent moisture, porosity, and field capacity, lag time to peak was sensitive to vertical saturated conductivity and horizon depth. Sensitivity analysis for the sediment component found that sediment size distribution (or the fraction in each particle class), specific gravity for each particle class, and runoff rate were the three parameters that influenced sediment deposition the most. Simulation results from the Canadian Shield hillslopes and the Melton Branch hillslope catchment revealed that with a subsurface restricting soil layer, subsurface lateral flow was the major runoff contributor. Nearly 95% of the total runoff for the Canadian Shield hillslopes was discharged as interflow at the junction of the B horizon and bedrock. Simulations with the Melton Branch data demonstrated that as the depth of the unsaturated zone increased, the initiation and peak of interflow was delayed. Comparisons of soil matrix and macropore flow contributions to subsurface flow revealed that macropore flow rate was disproportionately higher than soil matrix flow. The model also simulated the dynamic interaction between soil matrix flow and macropore flow by simulating proportionately reduced macropore contributions in cases where the lateral soil matrix conductivity was high. The decrease in saturation depths with increase in macroporosity and decrease in macropore roughness was also simulated by the model.

Comparisons of concave-convergent and convex-divergent hillslope scenarios revealed that convex slopes have higher peak flows and shorter recession periods. Simulations also showed that concave-convergent hillslopes provide more favorable conditions for saturation overland flow and return flow than convex-divergent hillslopes because of greater saturation depths at the base of the concave-convergent hillslope. It is possible that for longer duration events saturation overland flow or return flow initiated at the base of the concave-convergent slopes could yield higher peak flows than those observed for convex-divergent hillslopes subjected to similar events.

Results from the sediment simulations showed that sediment delivery increased with increase in flow concentration, and consequently sediment trapping was reduced. The difference in trapping predicted for the concentrated flow scenario and the uniformly distributed flow condition was not large because phenomena such as change in channel shape, reduced infiltration, and decreased surface roughness that typically accompany flow concentration were not included in the simulation. It is expected that more realistic (compared to the situation above) results will be obtained if information to simulate these process mechanisms is included.

In summary, the major conclusions of this research are:

- Riparian hillslopes are dissected into distinct convergent/divergent and convex/concave hillslope units. Geomorphologic features used to characterize flow concentration on these hillslope units revealed distinct trends with slope gradient. These results suggest that hillslope topographic and geomorphologic attributes are not uniform and their variability should be accounted for when investigating hillslope responses via field experimentation or models.

- Site conditions such as slope gradient, slope convergence and divergence, slope concavity and convexity, soil thicknesses and their characteristics, and flow concentration play a significant role in shaping the hydrologic and sediment phenomena on these hillslopes. These results underscore the need for site specific evaluation of riparian zones. If riparian zones are to be utilized as BMPs, a model like the one developed in this research could provide an initial estimate of their effectiveness (based on hydrologic and sediment transport response) for a given set of site conditions.

In addition to these major conclusions, some of the salient conclusions regarding riparian hillslope processes include:

- Interflow is the dominant runoff mechanism on riparian hillslopes. This indicates that the effectiveness of riparian zones in mitigating pollution will be determined primarily by the dynamics, pathways, and the rate of water moving as interflow.
- A large fraction of the interflow occurs via macropores. Water moving through macropores is orders of magnitude quicker than that moving through the soil matrix. Thus, it is important to have an accurate estimate on the macroporosity.
- Infiltration excess overland flow rarely occurs on riparian hillslopes. Overland flow if any will generally occur due to saturation overland flow or return flow, typically at the base of the hillslope. The occurrence of these flow mechanisms is strongly influenced by site features such as slope gradient, slope shape, upslope contributing area, and soil horizon

thickness and its characteristics.

- Considering the overall results from the subsurface and sediment components, it is expected that most of the sediment entering riparian areas will be trapped due to high infiltration losses. Sediment transport, if it occurs, will primarily be limited to concentrated flow channels where overland flow is sustained by a combination of infiltration excess, saturation excess, and /or return flow.

13 LIMITATIONS OF RESEARCH AND
RECOMMENDATIONS FOR FUTURE WORK

In the scope of this research, a number of simplifying assumptions were made. The discussion presented below describes some of the assumptions and limitations of this research and how they can be addressed in future research. Limitations and recommendations associated with field investigations and modeling studies are discussed separately.

13.1 Field investigations into geomorphologic features of riparian hillslopes

- When investigating the distribution of drainage areas and shapes it was assumed that slope gradient was the overriding determinant in the formation of drainage features. With this assumption, drainage features from concave-convergent, convex-divergent, straight-straight, and other hillslope forms were lumped together to compare them for different slope gradient categories. It is possible that within a slope category, drainage features may vary with hillslope form. This variation needs to be investigated.
- The DEM used to delineate drainage features in this research could not simulate diverging flow networks. This means the DEM could not have realistically represented drainage features typical of divergent hillslopes. Drainage features for different hillslope forms should be investigated with a DEM that can accommodate divergent topography.
- The scope of this research involved comparing distributions of drainage features across slope gradients. Future research should be targeted towards determining if there is a unique distribution of drainage features (area, shape) associated with a topographic form (e.g., concave-convergent, convex-divergent) for a fixed slope range within a watershed. Such information would immensely help in modeling of flow concentration and distribution on such hillslopes. Also, if the population of drainage features for a given topographic form follow similar trends, it would help confirm the hypothesis that the size of such hillslope forms define the "representative hillslope scale".

- In the Ridge and Valley region of Virginia, hillslopes were dissected into distinct convergent or divergent forms. It was hypothesized that the size of such hillslope segments reflected the "representative hillslope scale". What happens in regions where the slopes are flat and the riparian slopes are not dissected into such distinct features (for e.g., the riparian slope in the Atlantic Coastal Plain)? How doe one determine the "representative scale" for such slopes? How can flow concentration and distribution on such hillslopes be quantified? Future research needs to address some of these fundamental issues.

13.2 Model studies

- The model assumed rainfall/throughfall input to the surface as uniformly distributed. This is very unlikely in forested conditions where stem flow and canopy drip create localized saturated areas. These localized saturation patterns further encourage vertical preferential flow through macropores. Future modeling studies should somehow determine this non-uniform rainfall distribution by considering tree and canopy architecture.
- Vertical macropore flow was not simulated in the model. It could be important since it allows water to bypass intermediate horizons and reach lower horizons.
- The model simulated vertical drainage using the field capacity soil moisture storage concept. This is a simple concept and appropriate considering the variability and porous nature of forest soils (conditions which do not support assumptions of more mathematically sophisticated unsaturated models). The problem with the field capacity routing is determination of the representative field capacity value for soil horizons. Field capacity estimates derived from soil cores can not be representative of actual site conditions.
- In model simulations, perched water tables forming over restricting soil horizons are assumed transient and are drained quickly. Thus capillary influences associated with water tables were assumed to be negligible and not simulated. For flat slopes where water tables are maintained for extended periods, capillary effects associated with the perched water could influence the vertical drainage. Such a condition could occur at the base of a

concave-convergent hillslope. This situation could typically occur only for lower horizons, since upper forest soil horizons are too porous for capillary effects to be significant. Capillary influences associated with the water table may not allow a layer to drain to field capacity.

- In model simulations, perched water table losses were assumed to occur to vertical and lateral matrix flow, and lateral macropore flow. It is expected that in nature, a considerable amount of perched water is also lost through vertically aligned macropores.

- The model indicated that peak values were sensitive to macropore roughness. This is a cause of concern because of the high variability associated with this parameter.

- Macropores were assumed to be aligned parallel to the slope of the soil horizon. This may or may not be true, depending on their origins. Macropores whose origins are root cavities might run parallel to the surface of the impeding layer.

- Since the model was simulating the "hydrologically active" fraction of macroporosity, macropores were assumed circular in cross-section and to assumed to flow full. It is highly unlikely macropores will be circular considering their origins. In addition, macropores in most cases would be filled with organic debris.

- Due to limited topographic information on the experimental data sets which were used to evaluate the model, the probability distribution to simulate surface and subsurface drainage channel shapes was generated by lumping together all drainage channel w/d values for the hillslope segment. It is expected that channel w/d values will tend to change along the hillslope length, a consequence of erosion and deposition processes. Thus for an accurate representation of drainages, separate w/d distributions representing changing w/d values along the slope should be used. This would require detailed topographic information. The model has the capability to include variation in channel shape distributions along the hillslope length.

- To simulate subsurface interflow concentration, the shape (w/d value) of the subsurface drainageway was assumed to follow the surface profile. In nature, this is generally not the case. Research indicates that the depth of the colluvium increases towards the center of the drainageway.

- Surface topography was assumed to define the location of colluvial drainages. This

assumption precludes the consideration of permeable colluvial seams which may not be located in depressions.

- For computational simplicity, we assumed that the perched water table surface is distributed uniformly across the width of the subsurface colluvial drainage channel. Thus, the surface of the water table was defined by the w/d value of the drainageway. This assumption may not hold for colluvial drainages that have low width to depth ratios. In such drainages, subsurface water will concentrate towards the center of the drainageway and the water table building up over the impeding layer will enter the upper layer, prior to the lower layer being completely saturated.

- In the model, total surface runoff at a section was partitioned into channels at that section in proportion to the channel widths. This was done since accurate information on the distribution of upslope contributing areas was not available. Flow partitioning should be based on the probability distribution of upslope contributing drainage areas (provided runoff is generated uniformly in upslope areas).

- Previous research has indicated that other than the phenomenon of subsurface saturated layer reaching the surface, saturation overland flow may also be generated in conditions where the capillary fringe associated with a shallow water table is close to the surface. This is called the "groundwater ridging hypothesis" and is generally assumed to occur only in near-stream areas. This condition was not simulated in the model. Future investigations should be conducted to verify the occurrence of such a phenomenon, and modeling approaches should be developed thereafter.

- The evapotranspiration component of the model was not evaluated in this research. Future research should attempt to test the validity of this model for longer durations.

- This model was developed for and tested primarily on moderate to steep riparian hillslopes. Riparian conditions may be very different for flat slopes neighboring streams in areas such as the Atlantic Coastal Plain where shallow water table influences predominate. Under these circumstances, "field capacity" is not a fixed variable but is influenced by the position of the water table. In these situations, the physics of evapotranspiration losses in the soil will also change, since there will be an upward flux from the water table to meet upper evapotranspiration losses. Stream influences such as

bank flooding and stream recharge may also play a larger role. These scenarios need to be considered to expand the scope of the model.

- In the absence of forest sediment data, the sediment component was primarily evaluated for deposition on grassed surfaces. Future research should be directed towards investigating sediment detachment, deposition and transport processes under forest canopy and the influences of litter layer on this movement.

- The sediment model should be modified to include fine sediment trapping due to infiltration.

- The model includes suspended load and total load submodels but it is uncertain when one or the other should be used, especially for grassed surfaces.

14 REFERENCES

Abdul, A. S., and R. W. Gillham, 1984. Laboratory studies of the effects of the capilliary fringe on streamflow generation. *Water Resour. Res.* Vol. 10(6):691-698.

Abrahams, A. D. 1984. Channel Networks: A geomorphological prospective. *Water Resour. Res.* Vol. 20(2): 161-168

Ackers, P. and W. R white. 1973. Sediment Transport: New Approach and Analysis. *J. of Hydraul. Div. ASCE* 99(HY11):2041-2060.

Altier, L. S. 1994. *REMM: Riparian Ecosystem Management Model.* Unpub. Users Manual, S. E. Watershed Research Laboratory, USDA-ARS, Tifton, GA.

Anderson M. G. and T. P. Burt. 1978. The role of topography in controlling throughflow generation. *Earth Surface Processes and Landforms.* Vol. 3: 331-344.

Arnett, R. R. 1974. Environmental factors affecting speed and volume of topsoil interflow. *Institute of British Geographers. Special Publication No.* 6:7-22.

Aubertin, G. M. 1971. Nature and extent of macropores in forest soils and their influence on subsurface water movement. *For. Sev. Res. Pap. NE(US)* 192PS, 33pp.

Bagnold, R. A. 1966. An approach to the sediment transport problem from general physics. *Prof. Paper 422. J. U.S. Geol. Surv.* Reston, VA.

Barfield, B. J., R. I. Barnhisel., J. L Powell, M. C Hirchi and I. D Moore. 1984. Erodibilities and eroded size distribution of Wester Kentucky mine spoil and reconstructed topsoil. *1984 Symposium on Surface Mining, Hydrology, and Sedimentology and Reclamation.* Pp. 179-189. University of Kentucky, Lexington, KY.

Barfield, B. J., and S. Albrecht. 1982. Field evaluation of the effectiveness of vegetative filters for controlling sediment from strip mines. *Proceedings 1982 National Symposium on Surface Mine Hydrology, Sedimentology and Reclamation.* College of Engineering, University of Kentucky, Lexington, KY.

Barfield, B. J., R. C Warner and C. T Haan. 1981. *Applied Hydrology and Sedimentology for Disturbed Watersheds.* Oklahoma technical Press, Stillwater, OK 74074

Barfield, B. J., I. D Moore and R. G Williams. 1979. Prediction of the sediment yield in surface mined watersheds. *Proceedings Symposium on Surface Mining Hydrology, Sedimentology and Reclamation,* University of Kentucky, Lexington, Kentucky. Pp. 89-92.

Barfield, B. J., E. W. Tollner, and J. C. Hayes. 1977. Prediction of sediment transport in grasses media. *ASAE paper no. 77-2023.* ASAE St. Joseph, MI.

Beasley, R. S. 1977. Contribution of subsurface flow from the upper slopes of forested watersheds to channel flow. *Soil Sci. Am. J.* Vol 40: 955:957.

Beasley, D. B., and L. F. Huggins. 1982. ANSWERS: Areal nonpoint source watershed environment response simulation: Users Manual. *U.S. EPA-905/9-82-001.* U.S. Environmental Protection Agency Region V.

Beasley, D. B., L. F. Huggins, and E. J. Monke. 1980. ANSWERS: A model for watershed planning. *Trans. ASAE.* Vol. 23(4):938-944.

Bell, G. I. 1968. Piping in the badlands of North Dakota. *Proceedings 6th Annual Engineering Geology and Soils Engineering Symposium,* Boise, Idaho, 242-257 pp.

Beven, K. 1991. Scale considerations. In *Recent Advances in the Modeling of Hydrologic Systems.* Eds. D.S. Bowles, and P.E. O'Connel. Pp. 357-371.

Beven, K. 1982. On subsurface stormflow: Predictions with simple kinematic theory for saturated and unsaturated flows. *Water Resour. Res.* Vol. 18(6): 1627-1633.

Beven, K. 1981. Kinematic subsurface stormflow. *Water Resouces Res.* Vol. 17(5):1419-1424.

Beven, K. 1980. Underwood field drainage experiment. *Rep. 65, 30pp. Instl. Hydrol. Wallingford,* U.K.

Beven, K. 1978. The hydrological response of headwater and sideslope areas. *Hydrol. Sci. Bull.* *Vol.* 23:419-437.

Beven, K. 1977. Experiment with a finite element model of hillslope hydrology - The effect of topography. In *Surface and Subsurface Hydrology.* Eds. H.J Morel Seytoux et al., pp. 37-51. Water Resources Publication, Fort Collins, CO.

Beven, K. And R. T. Clarke. 1986. On the variation of infiltration into a homogenous soil matrix containing a population of macropores. *Water Resour. Res.* Vol. 22:383-388.

Beven K. and P. F. Germann. 1982. Macropores and water flow in soils. *Water Resour. Res.* Vol.18: 1311- 1325.

Beven, K., and P. F. Germann. 1981. Micro-, meso, macroporosity in and channeling flow in soils. *Soil Sci Soc. Am. J.* Vol. 45:1245.

Beven, K., and P. F. Germann. 1981. Water flow in soil macropores. II. A combined flow model. *J. Soil Sci.* Vol. 32:15-29.

Beven, K., and M. J. Kirkby. 1979. A physically based variable contributing area model of basin hydrology. *Hydrol. Sci. Bull.* Vol. 24:43-69.

Beven, K., E. F. Wood, and M. Sivapalan. 1988. On hydrological heterogeniety-catchment morphology and catchment response. *J. Hydrol.* Vol. 100:353-375.

Baillie, I. C. 1975. Piping as an erosion process in the uplands of Sarawak. *Journal of Tropical Geography.* Vol 41: 9-15.

Blong, R. J. 1965. Subsurface water as a geomorphic agent with special reference to Mangakowhiriwhiri catchment. *Auckland Student Geographer (N.Z.),* Vol 1(2): 82-95.

Bonell, M., D. A. Gilmour, and D. S. Cassells. 1983. A preliminary survey of hydraulic properties of rainforest soils in tropical north-east Queensland and their implication for the runoff process. *Catena,* Suppl.,4:57-78.

Bonell, M., and D. A. Gilmour. 1978. The development of overland flow in a tropical rainforest catchment. *J. Hydrol.* Vol. 39: 365-382.

Bouma, J., and L. W. Dekker. 1978. A case study on infiltration into dry clay soil, 1, Morphological observations. *Geoderma.* Vol. 20:27-40.

Bouma, J., A. Jongerius, O. Boersma, A. Jager, D. Schoonderbeek. 1977. The functions of different types of macropores during saturated flow through four swelling soil horizons. *Soil Sci. Soc. Am. J.* Vol.41:945-950.

Brewer, R. 1964. *Fabric and mineral analysis of soils.* John Wiley, NY.

Brinson, M. M., H. D. Bradshaw, and E. S. Kane. 1984. Nutrient assimilative capacity of an alluvial floodplain swamp. *J. Appl. Ecol.* Vol. 21(3):1041-1057.

Brown, G. W. 1961. *Some physical and chemical soil properties associated with piping erosion in Colorado.* Unpub. MSc Thesis, Colarado State University, Fort Collins, Colorado.

Brown, G. W. 1962. Piping erosion in Colorado. *J. Geol.* Vol 27: 552-561.

Buckham A. F. and W. E. Cockfield. 1950. Gullies formed by sinking of the ground. *American Journal of Science.* Vol 248: 137-141.

Bullock, P., and A. J. Thomasson. 1979. Rothamstead studies of soil structure, 2, Measurement

and characterization of macroporosity by image analysis and comparison with data from water retention measurements. *J. Soil Sci. Vol.* 30(3): 391-414.

Burt, T. P. 1986. Runoff processes and solutional denudation rates on humid temperate slopes. In *Solute Processes.* Eds. S.T. Trudgill. John Wiley, Chicester. Pp. 193-250.

Calver, A., M. J. Kirkby, and D. R. Weymann. 1972. Modeling hillslope and channel flow. In R. J. Chorley, eds. *Spatial Analysis in Geomorphology,* Methuen, London. pp 197-218.

Chamberlin, T. W. 1972. Interflow in a mountainous forest site in coastal British Columbia, in *Mountain Geomorphology,* eds. H.O. Slaymaker, and H.J. McPhearson, pp: 121-126.

Cooke, R. A., S. Mostaghimi, and F. E. Woeste. 1993. VTFIT: A microcomputer based routine for fitting probability distribution functions to data. *Applied Engineering in Agriculture.* Vol. 9(4):401-408.

Corbett, E. S. 1979. *Hydrologic evaluation of the stormflow generation process on a forested watershed.* Univ. Microfilms Int. Ann Arbour, MI.

Cooper, J. R. and J. W Gilliam. 1987. Phosphorous redistribution from cultivated fields into riparian areas. *J. Soil Sci. Soc. Am.* 51(2):416-420.

Czeppe, Z. 1960. Suffosional phenomena in slope loams of the Upper San darinage basin. *Instyut Geologiczny Biul.* (Warsaw) Vol 9:297-332.

Delgado, A. M., T. A. Dillaha, J. W. Gilliam, F. Bouraoui, and J. E. Parsons. 1992. Nitrogen transport and cycling in vegetative filter strips. *ASAE Paper No. 92-2624.* ASAE, St. Joseph. MI.

DeVries, J. and T. L. Chow. 1978. Hydrologic behaviour of a forested mountain soil in Coastal British Columbia. *Water Resour. Res.* Vol 5:935-942.

Dietrich, W. E., C. J. Wilson, and S. L. Reneau. 1986. Hollows, colluvium, and landslides in soil mantled landscapes. In *Hillslope Processes.* Eds. A.D. Abrahams, pp. 361-388. Allen and Unwin, London.

Dillaha, T. A. Water quality impacts of vegetative filter strips. 1989. *ASAE Paper no. 89-2043.*

Dillaha, T. A., and J. C. Hayes. 1991. A procedure for the design of vegetative filter strips. Final *Report prepared for the US Soil Conservation Service.* Department of Agricultural Engineering, Virginia Tech, Blacksburg, Virginia.

Dillaha, T. A., R. B. Reneau, S. Mostaghimi, and V. O. Shanholtz. 1989. Vegetative filter strips for nonpoint source pollution control. *Trans. ASAE.* Vol. 32(2):491-496.

Dillaha, T. A., J. H Sherrard., D. Lee., S. Mostaghimi and V. O Shanoltz. 1988. Evaluation of vegetative filter strips as best management practices for feed lots. *J. Water Poll. Cont. Fed.* 60:1231-1238; 1988.

Dillaha, T.A., R.B Reneau., S. Mosthaghimi., V. O Shanoltz and W. L Magette. 1987. Evaluating Nutrient and Sediment Losses from Agricultural Lands: vegetative filter strips. Annapolis, MD. USEPA. CBP/TRS 4/87.

Dillaha, T. A., J. H Sherrard and D. Lee. 1986. Long term effectiveness and maintenance of vegetative filter strips. Blacksburg, VA. Virginia Water Resources Research Center. VPI-VWRRC-BULL 153.

Dooge, J. C. I. 1982. Parameterization of hydrologic processes. In *Land Surface Processes in Atmospheric General Circulation Models.* Eds. P.S. Eaglson, Cambridge University Press, London. Pp.243-288.

Dooge, J.C.I. 1986. Looking for hydrologic laws. *Water Resources Res.* Vol. 22:46S-58S.

Doyle, R. C., G. C. Stanton, and D. C. Wolf. 1977. Effectiveness of forest and grass buffer filters

in improving the water quality of manure polluted runoff. *ASAE paper no. 77-2501*. ASAE, St. Joseph, MI.

Dunne, T. 1988. Hydrology and mechanics of erosion by subsurface flow. In *Hydrogeology*. Eds. W. Back, J.S. Rosenshein, and P.R. Seaber, Geological Society of America, Boulder, CO.

Dunne, T. and R. D. Black. 1970a. An experimental investigation of runoff production in permeable soils. *Water Resour. Res.* Vol 6:478-490.

Dunne, T., and R. D. Black. 1970b. Partial area contributions to storm runoff in a small New England watershed. *Water Resour. Res.* Vol 6:1296-1311.

Dunne, T., T. R. Moore, and C. H. Taylor. 1975. Recognition and prediction of runoff producing zones in humid regions. *Hydol. Sci. Bull.* Vol. 20:305-327.

Eastman, J. R. 1992. *IDRISI User's Guide: Version 4.0 (Rev. 1)*. Clark Iuniversity, Graduate School of Geography, Worcester, MA.

Edwards, W. M., and L. D. Norton, and C. E. Redmond. 1988. Characterizing macropores that affect infiltration into nontilled soil. *Soil Sci. Soc. Am. J.* Vol. 52:483-487.

Edwards, W. M., R. R. van der Ploeg, and W. Ehlers. 1979. A numerical study of the effects of non-capilliary sized pores upon infiltration. *Soil Sci. Soc. Am. J.* Vol. 38:157-172.

Ehlers, W. 1975. Observations on earthworm channels and infiltration in tilled and untilled loess soils. *Soil Sci. Vol.* 119(2):242-249.

Ehlers, W., U. Kopke, F. Hesse, and W. Bohm. 1983. Penetration resistance and root growth of oats in tilled and untilled loose soil. *Soil Tillage Research.* Vol 3:261-275.

Einstein, H. A. 1950. The bed load function for sediment transportation in open channel flows. *USDA-SCS Technical Bulletin* No. 1026, 78pp.

Ellison, W. D., and O. T. Ellison. 1947. Soil erosion studies - Part IV: Soil detachment by surface flow. *Agricultural Engineering.* Vol. 28(5):402-405.

Fail, J. L., B. L. Haines and R. L Todd. 1986. Riparian forest communities and their role in nutrient conservation in an agricultural watershed. *American Journal of Alternative Agriculture.* Vol II.No. 3. Pg. 114-121.

Feller, M. C., and J. P. Kimmins. 1979. Chemical characteristics of small streams near Haney in Southwestern British Columbia. *Water Resourc. Res.* Vol. 15:247-258

Flanagan, D. C., and S. J. Livingston. 1995. USDA-Water Erosion Prediction Project (WEPP): Technical Documentation. NSERL Report no. 10, NSERL, West Lafayette, IN.

Fogle, A. W., D. I. Carey, B. J. Barfield, R. I. Blevins, V. P. Evangelou, C. E. Madison, and S. P. Inamdar. 1994. Impact of riparian grass filter strips on surface water quality. *KGS Information Circular No. 46*, University of Kentucky, Lexington, KY.

Foster, G.R and L.J Lane. 1983. Erosion by concentrated flow in farm fields. Pp. 9.65-9.82. In *Proceedings of the D.B Simons Symposium on Erosion and Sedimentation*. Colorado State University, Fort Collins, CO.

Foster, G. R. 1982. Modeling the erosion process. PP.297-380. In C.T Haan (ed). *Hydrologic Modeling of Small Watersheds. Monograph no. 5*. ASAE St. Joseph. MI.

Foster, G. R and L. D Meyer. 1975. Mathematical Simulation of Upland Erosion by Fundamental Erosion Mechanics. In Present and Prospective Technology for Predicting Sediment Yields and Sources. ARS-S-40. USDA Agricultural Services. Pp. 190-207.

Foster, G. R and L. D Meyer. 1972. A closed for soil erosion equation for upland areas. In *Sedimentation* (Einstein). H.W Shen (ed). Colarado State University, Fort Collins, CO. Chapter 12.

Foster, G. R., L. J. Lane, M. A. Nearing, S. C. Finker, J. J. Stone, and L. T. West. 1989. USDA-Water Erosion Prediction Project: Hillslope Profile Version. Chapter 10. Erosin Component. NSERL Report no. 2, NSERL, USDA-ARS, W. Lafayette, IN.

Foster, G. R., R. A. Young, and W. H. Neibling. 1985. Sediment composition for nonpoint source pollution analyses. *Trans. ASAE.* Vol. 28(1):133-139.

Foster, G.T., L. D Meyer and C. A Onstad. 1977b. A runoff erositivity factor and variable slope length exponents for soil loss estimates. *Trans. ASAE* Vol.20(4):683-687.

Freeze, R. A. 1972. Role subsurface flow in generating surface runoff. 1:Base flow contributions to channel flow. *Water Resour. Res.* 8(3):609-623.

Gaiser, R. N. 1952. Root channels and roots in forest soils. *Soil Sci. Soc. Am. Proc.* Vol. 16(1):62-65.

Gash, J. H. C. 1979. An analytical model of rainfall interception by forests. *Q.J. Roy. Met. Soc.,* 105:43-55.

Germann, P. F. 1986. Rapid drainage response to precipitation. *Hydrological Processes,* 1:3-14.

Gillham, R. W. 1984. The effect of capilliary fringe on water table response. *J. Hydrol.* Vol. 67:307-324.

Gibbs, H. S. 1945. Tunnel-gully erosion on the Wither Hills, Marlborough, New Zealand. *New Zealand Journal of Science and Technology,* 27 section A(2): 135-146.

Gilman, K. and M. D. Newson. 1980. *Soil pipes and pipeflow - A hydrologic study in Upland Wales.* British Geomorphological Research Group Monograph No. 1, Geobooks, Norwich, UK. 114 pp.

Golden Software Inc. 1990. *SURFER for DOS. Version 4.15.* Golden Software Inc., 809, 14th St., Golden, CO.

Green, W.H., and G. Ampt, 1911. Studies of soil physics Part I - Flow of air and water through soils. *J. Agric. Sci.,* 4:1-24.

Green, R. D., and G. P. Askew. 1965. Observations on the biological development of macropores in soils of Romney Marsh. J. Soil Sci. Vol. 16(2):342.

Gregory, K. J. and D. E. walling. 1973. *Drainage basin form and process.* Arnold, London, 456 pp.

Groffman, P. M., A. J. Gold, R. C. Simmons. 1992. Nitrate dynamics in riparian forests: microbial studies. *J. Environ. Qual.* 21:666-671.

Hack, J. T. 1957. U.S. Geol. Surv. Prof. Paper 294B.

Haan, C. T., B. Allred, D. E. Storm, G. Sabbagh, and S. Prabhu. 1993. Evaluation of hydrologic/water quality models: A statistical procedure. *ASAE Paper No.* 932505. ASAE St. Joseph. MI.

Hammermeister, D. P., G. F. Kling, and J. A. Vomocil. 1982. Perched water tables on hillsides in Western Oregan: I. Some factors affecting their development and longevity. *Soil Sci Soc. Am J.* Vol. 46:811-818.

Harr, R. D. 1977. Water flux in soil and subsoil in a steep forested slope. *Journal of Hydrology,* 33: 37-58.

Hayes, J. C., B. J Barfield and R. I Barnhisel. 1984. Performance of grass filters under Laboratory and Field conditions. *Trans. ASAE.* Vol. 27(5):1321-1331.

Hayes, J. C and J. E Hairston. 1983. Modeling the long term effectiveness of vegetative filters as on-site sediment controls. *ASAE Paper no.* 83-2081. St. Joseph, MI.

Hayes, J. C., B. J Barfield and R. I Barnhisel. 1982. The use of grass filters for sediment control in

strip mine drainage. Vol. III. Empirical verification of the procedures using real vegetation. Report no. IMMR82/070, Institute for Mining and Minerals Research, University of Kentucky, Lexington, KY.

Hayes, J. C. 1979. Evaluation of design procedures for vegetal filtration of sediment flowing water strips. A thesis presented to the University of Kentucky in partial fulfillment of the requirements for the degree of Doctor of Philosophy. Lexington, KY.

Hayes, J. C., B. J Barfield and R. I Barnhisel. 1979. Filtration of the sediment by simulated vegetation II. Unsteady flow with non-homogenous sediment. *Trans. ASAE* 22(5):1063-1067.

Helvey, J. D, and J. H. Patric. 1965. Canopy and litter interception by hardwoods of Eastern United States. *Water Resour. Res.* Vol.1: 193-206.

Helvey, J. D. 1964. Rainfall interception by hardwood forest litter in the Southern Appalachains. *USDA-FS, Southeastern Forest Experiment Station*, SE-8.

Helvey, J. D. 1967. Interception by Eastern White Pine. *Water Resour. Res.*, Vol.3:723-729.

Hernandez, M., L. J. Lane, and J. J. Stone. 1989. Surface Runoff. In : WEPP - Hillslope Profile Version. L. J. Lane and M. A. Nearing (eds). USDA-ARS National Soil Erosion Laboratory, West Lafayette, IN. pp 5.1-5.18.

Hendrickson, O. Q., 1981. *Flux of nitrogen and carbon gases in bottomland soils of an agricultural watershed.* Ph.D. Dissertation, Univ. of Georgia, Athens, GA. 210pp.

Herrick, B. R. 1981. *Extractable soil pools of Calcium, Magnesium, Potassium, and Phosphorous in the riparian zone of an agricultural watershed.* M.S. Thesis, Univ. Of Georgia, Athens, · GA.

Hewlett, J. D. 1974. Comments on letters relating ti "Role of subsurface flow in generating runoff", by Freeze. *Water Resour. Res.*

Hewlett, J. D., and A. R. Hibbert. 1963. Moisture and energy conditions within a sloping soil mass during drainage. *J. Geophys. Res.*, Vol. 68(4):1081-1087.

Hewlett, J. D. and A. R. Hibbert. 1967. Factors affecting the response of small watersheds to precipitation in humid areas. In *International Sym. On Forest Hydrology*. Eds. W. E. Sopper and H.W. Lull, pp 275-290.

Hewlett, J. D. and W. L. Nutter. 1970. The varying source area of streamflow from upland basins. Paper presented at the Sym. on Interdisciplinary Aspects of Watershed management, Montana State University, Bozeman, ASCE, NY. pp65-83.

Higgins, C. G. 1984. Piping and sapping: Development of landforms by ground water flow outflow. In *Groundwater as a Geomorphic Agent*. Eds. R. G. LaFleur, Allen and Unwin, Winchester, MA.

Hirschi, M. C. and B. J Barfield. 1988a. KYERMO- A physically based research erosion model Part I. Model development. *Trans. ASAE* Vol. 31(3):804-813.

Hirschi, M. C. and B. J Barfield. 1988b. KYERMO- A physically based research erosion model Part II. Model Sensitivity analysis and testing. *Trans. ASAE* 31(3):814-820.

Hirschi, M. C. 1985. *Modeling soil erosion with emphasis on steep slopes and the rilling process.* A thesis presented to the University of Kentucky in partial fulfillment of the requirements for the degree of Doctor of Philosophy. Lexington, KY.

Holton, H. N. 1961. A concept for infiltration estimates in watershed engineering. *ARS 41-51, Agric. Res. Serv.*, USDA. Washington, D.C.

Horton, R.E. 1940. An approach towards physical interpretation of the infiltration-capacity. *Proc.*

Soil Sci. Soc. Am. Vol. 5:399-418.

Horton, R. E. 1939. Analysis of runoff-platt experiments with varying infiltration capacity. *Trans. Am. Geophys. Union*, Vol. 20:693-711.

Horton, R.E. 1937. Hydrologic interrealtions of water and soils. *Proc. Soil. Sci. Am.* 1:401-429.

Horton, R. E. 1935. Surface runoff phenomena - Part I. Analysis of the hydrograph. *Horton Hydrological Laboratory Publication* 101, Vorheesville, NY. 73 pp.

Horton, R. E. 1933. The role of infiltration in the hydrologic cycle. *Trans. Am. Geophys. Union.* 14:446-460.

Horton, R. E. 1919. Rainfall interception. *Monthly Weather Review*, 47:603-23.

Hoogmoed, W. D., and J. Bouma. 1980. A simulation model for predicting infiltration into cracked soil. *Soil Sci. Soc. Am J.* Vol. 44:458-461.

Hosking, P. L. 1967. Tunneling erosion in New Zealand. *J. Soil Water Conservation,* 22(4):149-151.

Howard, A. D. 1971. Simulation of stream networks by headward growth and branching. *Geogr. Anal.* Vol. 3:29-50.

Humphreys, B. 1978. *A study of some of the geomorphological and hydrological properties of natural soil piping.* Unpub. BSc. Dissertation, University of East Anglia, 35pp.

Huggins, L. F., and E. F. Monke. 1968. A mathematical model for simulating the hydrological response of a watershed. *Water Resour. Res.* Vol. 4(3):529-539.

Hursh, C. R. and E. F. Brater. 1941. Seperating storm hydrographs from small drainage area into surface and subsurafce flow. *Trans. Am. gephys. Union.* 863-870.

Inamdar, S. P. 1993. *Modeling sediment trapping in riparian vegetative filter strips.* MS. Thesis, University of Kentucky, Lexington, KY.

Jacobs, T. C., and J. W. Gilliam. 1985. Riparian losses of nitrate from agricultural drainage waters. J. Environ. Qual.. 14:472-478.

Jardine P. M., G. V. Wilson, and R. J. Luxmoore. 1990. Unsaturated solute transport through a forest soil during rain storm events. *Geoderma,* 46: 103-118.

Jenson, S. K and J. O Dominique. 1988. Extracting Topographic structure from digital elevation data for geographic information system analysis. *Photogrammetric Engineering and Remote Sensing* 54(11):1593-1600.

Johnson, D. W., and R. I. van Hook. 1989. *Analysis of biochemical cycling processes in Walker Branch Watershed.* 401 pp., Springer Verlag, NY.

Jones, J. A. A. 1971. Soil piping and stream channel initiation. *Water Resour. Res.,* 7:602-610.

Jones, J. A. A. 1975. *Soil piping and subsurface initiation of stream channel networks.* Unpub. Ph. D. Thesis, University of cambridge, 467 pp.

Jones, J. A. A. 1981. *The nature of soil piping: A review of research.* B. G. R. G. Research Monograph Series No. 3. Geo Books, Norwich, England.

Jones, J. A. A. 1986. Some limitations to the a/s index for predicting basin wide patterns of soil water drainage. *Zeistschrift fur Geomorphologie Supplementband,* 60: 7-20.

Jones, J. A. A. 1987. The effectes of soil piping on contributing areas and erosion patterns. *Earth Surface Processes and Landforms.* Vol. 12:229-248.

Jones, J. A. A. 1988. Modeling pipeflow contributions to stream runoff. *Hydrological Processes.* Vol. 2: 1-17.

Jones J. A. A. and F.G. Crane. 1984. Pipeflow and pipe erosion in the Maesnant experimental catchment. In Burt, T.P. and D. E. Walling (Eds), *Catchment Experiments in Fluvial*

Geomorphology, Geobooks, Norwich, UK. 55-72 pp.

Jordan, T. E., D. L. Correll, and D. E. Weller. 1993. Nutrient reception by a riparian forest receiving inputs from adjacent cropland. *J. Environ. Quality*. 22:467-473.

Kao, T. Y., and B. J. Barfield. 1978. Predictions of flow hydraulics of vegetated chaneels. *Trans. ASAE*. Vol. 21(3):489-494.

Karlinger, M. R and B. M Troutman. 1989. A random spatial network model based on elementary postulates. *Water Resour. Res.*, 25(5):793-798.

Kirkby, M. J. 1987. Modeling some influences of soil erosion, landslides and valley gradient on drainage density and hollow development. In *Geomorphological Models*. Eds. F. Ahnert. Catena Supplement No. 10. Cremlingen, FRG.

Kirkby, M. J. 1986. A runoff simulation based model based on hillslope topography. In *Scale Problems in Hydrology*. Eds. V.K. Gupta. D. Reidel Pub. Co., pp. 39-56.

Kitahara, H. 1989. Characteristics of pipe flow in a subsurface soil layer on a gentle slope (II) Hydraulic properties of pipes. *J. Jpn. For. Soc.* Vol. 71(8):317-322.

Kittredge, J. 1948. *Forest Influences* (first ed.), pp. 99-114. McGraw Hill Book Co. NY.

Kirkby, M. J. and R. J. Chorley. 1967. Throughfall, overlandflow and erosion. *Bull. Intern. Assoc. Sci. Hydro.* 12:5-21.

Klemes, V. 1983. Conceptualization and scale in hydrology. J. Hydrol. Vol. 65:1-23.

Knisel, W. G., R. A. Leonard and F. M. Davis. 1993. The GLEAMS model plant nutrient component. Part I: Model Documentation. USDA-ARS Grassland, Soil and Water Research Laboratory, Temple, TX.

Lane, L. J. and M. A. Nearing. 1989. USDA - Water Erosion Prediction Project: Hillslope Profile Model Documentation. NSERL Report No. 2. USDA-ARS National Soil Erosion Laboratory, West Lafayette, Ind.

Laursen, E. M. 1958. Total sediment load of streams. *J. Hydraulics Div.*, ASCE, 84(HY1):1530-1,1530-36.

Lee, D., T. A. Dillaha, and J. H. Sherrard. 1989. Modeling phosphorous transport in grass buffer strips. *J. Environ. Eng..* Vol. 115:409-427.

Leopold, L. B., and W. B. Langbein. 1962. The concept of entropy in landscape evolution. *U.S. Geol. Surv. Prof. Pap.* 500A.

Leopold, L. B., and J. P. Miller. 1956. U.S. Geol. Sur. Prof. Paper 282-A.

Leonard, R. A., W. G. Knisel, and D. A. Still. 1987. GLEAMS: Groundwater Loading Effects on Agricultural Management. *Trans. ASAE,* 30(5):1403-1418.

Leopold, L. B., M. G Wolman and J. P Miller. 1964. *Fluvial Processes in Geomorphology*. W.H Freeman and Co. 522 pp.

Lewis, S. M., D. E. Storm, B. J. Barfield, and L. E. Ormsbee. 1994. PRORIL- An erosion model using probability distributions for rill flow and density: I. Model development. *Trans. ASAE*. Vol. 37(1):115-123.

Logsdon, S. D., R. R. Allmaras, L.Wu, J. B. Swan, and G. W. Randall. 1990. Macroporosity and its realtion to saturated hydraulic conductivity under different tillage practices. *Soil Sci. Soc. Am. J.* Vol 54:1096-1101.

Lowrance, R.R. 1992. Groundwater nitrate and denitrification in a coastal plain riparian forest. *J. of Environ, Qual.* 21:401-405.

Lowrance, R. R., J. K. Sharpe, and J. M. Sheridian. 1986. Long-term sediment deposition in the riparian zone of a Coastal Plain Watershed. *J. Soil and Water Cons.* 41:266-271.

Lowrance, R., Ralph Leonard and J. Sheridian. 1985. Managing riparian ecosystems to control nonpoint pollution. *J. Soil and Water Conservation.* Vol 40.

Lowrance, R. R., R. L. Todd, and L. E. Asmusen. 1984. Nutrient cycling in an agricultural watershed. I. Phreatic movement. *J. Environ. Qual.,* 13:22-27.

Lowrance, R. R., R. L Todd and L. E. Asmussen. 1983. Waterborne nutrient budgets for the riparian zone on an agricultural watershed. *Agr. Ecosystems, and Environ.* 10:371-384.

Lowdermilk, W. C. 1930. Influence of forest litter on runoff percolation, and erosion. *J. Forestry,* 28: 474-91.

Lull, H. W., and J. H. Axley. 1958. Forest soils moisture relations in coastal plain sands of southern New Jersey. Forest Sci. 4:2-19.

Luxmoore, R. J. 1981. Micro-, meso, and macroporosity of soil. *Soil Sci. Soc. Am. J.* Vol 45:671.

Luxmoore, R. J., and C. H. Abner. 1987. Field facilities for subsurface transport research. OaK Ridge National Laboratory Report no. DOE/ER-0329, U.S. Department of Energy, Washington, D.C.

Mader, D. L. and H. W. Lull. 1968. Depth, weight and water storage on the forest floor. *North east Forest Experiment Station. Paper 109.*

Magette, W. L., R. B. Brinsfield, R. E. Palmer, and J. D. Wood. 1989. Nutrient and sediment removal by vegetative filter strips. *Trans. ASAE* 32:663-667.

Magette, W. L., R. B. Brinsfield, R. E. Palmer, J. D. Wood, T. A. Dillaha, and R. B. Reneau. 1987. Vegetative filter strips for agricultural runoff treatment. *USEPA Report No. CBP/TRS 2/87,* Washington, D.C.

Mantz, P. A. 1977. Incipient transport in fine grains and flakes buy fluids-extended Shield's Diagram. *J. Hydraulics. Div. ASCE,* 103 (HY6):601-615.

Marston, R. B. 1962. Influence of vegetative cover on soil moisture in eastern Ohio. *Soil. Sci Soc. Am. Proc.* 26:605-8.

McCaig, M. 1983. Contributions to storm quickflow in a small haedwater catchment - The role of natural pipes and soil macropores. *Earth Surface Processes and Landforms.* Vol 8: 239-252.

Mosley, M. P. 1979. Streamflow generation in a forested watershed, New Zealand. *Water Resouc. Res.* Vol. 15(4):795-806.

Mosley, M. P. 1982. Subsurface flow velocities through selected forest soils. *New Zealand Journal of Hydrology,* 555:65-92.

Morgan, R. P. C. 1977. Soil erosion in the United Kingdom: field studies in the Silsoe area, 1973-75. *National College Agricultural Engineering, Silsoe, Bedfordshire, Occasional Paper No. 5.*

Mein, R. G., and C. L. Larson. 1973. Modeling infiltration due to a steady rain. *Water Resour. Res.* Vol. 9(2): 384-394.

Mein, R.G., and Larson. 1971. Modeling infiltration component of the rainfall runoff process. *Water Resources Research Center Bull.* No. 43, University of Minnesota, Minneapolis, MN. 72pp.

Merriam, R. A. 1960. A note on the interception loss equation. *J. Geophys. Res.* 65(11):3850-3851.

Metz, L. J. and J. E. Douglass. 1959. Soil moisture depletion under several piedmont cover types. *US. Dept. Agr. Tech. Bull.* 1207, 23pp.

Meyer, L. D., G. R Foster, and S. Nikolov. 1975. Effect of flow rate and canopy on rill erosion.

Trans. ASAE 18(5):905-911.

Meyer, L. D., and E. J Monke. 1965. Mechanics of soil erosion by rainfall and overland flow. *Trans. ASAE.* 8(4):572-577, 580.

Meyer, L. D., and W.H Wischmeier. 1969. Mathematical simulation of the process of soil erosion by water. *Trans. ASAE.* Vol. 12(6):754-758, 762.

Moore, I. D., M. C Hirschi and B. J Barfield. 1983. Kentucky rainfall Simulator. *Trans. ASAE.* Vol. 26(4): 1085-1089.

Monteith, J. L. 1965. Evaporation and the environment. *Symp. Soc. Expl. Biol.* Vol. 19:205-234.

Montgomery, D. R., and W. E. Dietrich. 1988. Where do channels begin ? *Nature,* Vol. 336:232-234.

Montgomery, D. R., and W. E. Dietrich. 1992. Channel initiation and the problem of landscape scale. *Science,* Vol. 255:826-830.

Montgomery, D. R., and W. E. Dietrich. 1995. Hydrologic processes in a low-gradient source area. *Water Resources Res.* Vol.

Mossaad, M. E and T. H Wu. 1984. A stochastic model of soil erosion. *International Journal for Numerical and Analytical Methods in Geomechanics* 8:201-224.

Morisawa, M. 1985. *Rivers:Form and Processes.* Longman, New York.

Moyle, R. C. and R. Zahner. 1954. Soil moisture as affected by stand conditions. *US Forest Service South Forest Expt. Sta. Occas, Paper* 137, 44pp.

National Research Council (NRC). 1991. *Opportunities in the hydrologic sciences,* National Academy Press, Washington, D.C. 348 pp.

Neibling, W. H and E. E Alberts. 1979. Composition and yield of soil particles transported through sod strips. *ASAE paper* no. 79-2065. ASAE, St. Joseph, MI.

Newson, M. D. and J. G. Harrison. 1978. Channel studies in Plynlimon experimental ctachments. *Natural Environment Research Council Institute of Hydrology,* Report No. 7, Wallingford, UK. 61pp.

Nieber, J. L. 1979. *Hillslope runoff characteristics.* PhD. Thesis, Cornell Univ. Ithaca. NY.

Nieber, J. L. 1982. Hillslope soil moisture flow, approximation by a one-dimensional formulation. *ASAE paper* no. 82-2026, ASAE St. Joseph, MI.

Nieber, J. L., and M. F. Walter. 1981. Two dimensional soil moisture flow in a slopeing rectangular region: Experimental and numerical studies. *Water Resour.Res.* Vol. 17(6):1722-1730.

Nieber J. L. and G. S. Warner. 1991. Soil pipe contribution to steady subsurface flow. *Hydrological Processes,* Vol 5:329-344.

Nicks, A. D. 1985. Generation of climate data. *Proceeding of the Natural Resources Modeling Symposium.* USDA-ARS--30. pp. 297-300.

O'Louglin, E. M. 1986. Prediction of surface saturation zones in natural catchments by topographic analysis. *Water Resour. Res.* Vol. 22:794-804.

O'Louglin, E. M. 1981. Saturation regions in catchments and their relations to soil and topographic properties. *J. Hydrol.* Vol. 53:229-246.

Omoti, U., and A. Wild. 1979. Use of fluroscent dyes to mark the pathwways of solute movement through soils under leaching conditions, 2, Field experiments. *Soil Sci.* Vol. 128(2):98-104.

Overton, D. E. 1965. Mathematical refinement of an infiltration equation for watershed engineering. *ARS-41-99.* USDA-ARS, 11pp.

Parsons, J. E., R. B. Daniels, J. W. Gilliam, and T. A. Dillaha. 1991. The effect of vegetation filter strips on sediment and nutrient removal from agricultural runoff. *Proc. For the Environmentally Sound Agriculture Conference*. Vol. 1:324-332.

Patric, J. H. 1961. The San Dimas large lysimeters. *Jour. Soil. Water. Conserv.* 16:13-17.

Patric, J. H. 1962. Vegetative size and evapotranspiration from hardwood forest of the Southern Applalachians. *Forty Third Annual Meeting, Am. Geophys. Union.* 7pp.

Penman, H. L. 1956. Evaporation-an introductory survey. *Neth. J. Agric. Sci.* 4:9-29.

Penman, H. L. 1948. Natural evaporation from open water, bare soil, and grass. *Proc. Roy. Soc. London Ser. A.* Vol. 193:120-145.

Peters, D. L. 1994. *Subsurface flow processes in forested Canadian Shield hillslopes: Contributions to runoff production.* M. Sc. Thesis. 153 pp. Trent University, Ont. Canada.

Peters, D. L., J. M. Buttle, C. H. Taylor, and B. D. LaZerte. 1995. Runoff production in a forested shallow soil Canadian Shield basin. *Water Resour. Res.* Vol. 31(5):1291-1304.

Peterjohn, W. T. and D. L Corell. 1984. Nutrient dynamics in an agricultural watershed: Observations on the role of a riparian forest. *Ecology.* 65:1466-1475.

Pierce, R. S. 1967. Evidence of overland flow on forest watershed. In *Forest Hydrology,* eds. W.E. Sopper and H.W. Lull, pp 247-52, Pergamon Press, NY.

Pilgrim, D. H. 1966. Radioactive tracing of storm runoff on a small catchment. *J. Hydrol.* 4:289-326.

Pilgrim, D. H., D. D. Huff, and T. D. Steel. 1978. A field evaluation of subsurface and surface runoff, 2, Runoff processes, *J.Hydrol.* Vol. 38:319-341.

Pinay, G., and H. Decamps. 1988. The role of riparian woods in regulating nitrogen fluxes between the alluvial aquifer and surface water: A conceptual model. *Regulated Rivers: Research and Management* 2:507-516.

Plamadon, P. A., T. A. Black, and B. C. Goodell. 1972. The role of hydrologic propoerties of the forest floor in watershed hydrology. In National Symposium on Watershed in Transition, pp341-8. American Water Resources Association and Colorado State University, Fort Collins, Colorado.

Ragan, R. M. 1968. An experimental investigation of partial area contributions. Publ. 76, pp.241-249, *Int. Assoc. Sci. Hydrol.* Washington, D.C.

Rawls, W. J., P. Yates, and L. E. Asmussen. 1976. Calibration of selected infiltration equations for the Georgia Coastal Plain. USDA Agricultural Research Service, No. ARS-S-113, 110pp.

Rawls, W. J., and D. L. Brakensiek. 1985. Prediction of soil water properties for hydrologic modeling. *Watershed Management in the Eighties, ASCE,* pp. 293-299.

Reeves, M. J. 1980. Recharge of the English Chalk: A possible mechanism. *Eng. Geol.* Vol. 14(4):231-240.

Ritchie, J. T. 1972. Model for predicting evaporation from a row crop with incomplete cover. *Water Resour. Res.* Vol. 8:1204-1213.

Roessel, B. W. P. 1950. Hydrologic problem concerning the runoff in headwater regions. *Eos. Trans. AGU.* Vol. 31(3):431-442.

Rowe, P.B. 1963. Streamflow increases after removing woodland riparian vegetation from a southern California watershed. *J. Forestry* 61: 365-370.

Rowe, P. B. and L. F. Reimann. 1961. Water use by brush, grass, and grass-forb vegetation. *J. Forestry.* 59:175-81.

Rutter, A. J., K. A. Kershaw, P. C. Robbins, and A.J. Morton. 1971. A predictive model of rainfall

interception in forests. I. Derivation of the model from observations in a stand of Corsican pine. *Agric. Meteorol.* Vo. 9:367-384.

Rutter, A. J., A. J. Morton, and P. C. Robbins. 1975. A predictive model of rainfall interception in forests. II. Generalization of the model and comparison with observations in some coniferous and hardwood stands. *J. Appl. Ecol.* Vol. 12: 367-380.

Savabi, M. R., A. D. Nicks, J. R. Williams, and W. J. Rawls. 1989. Water balance and percolation. In WEPP - Hillslope ProfileVersion. L.J. Lane and M.A. Nearing (eds). USDA-ARS National Soil Erosion Research Laboratory, West Lafayette, IN. pp 7.1-7.13.

Saxton, K. E., and J. L. McGuinness. 1982. Evapotranspiration. In *Hydrologic Modeling of Small Watersheds*. Eds. C. T. Haan, H. J. Johnson, and D. L. Brakensiek. ASAE Monograph no. 5, pp.229-258.

Sharpley, A.N., and J.R Williams. 1990. EPIC-Erosion/Productivity Impact Calculator:1. Model documentation. U.S. Department of Agriculture Technical Bulletin, No. 1768. 235pp.

Sheridan, J. M., R. G. Williams, L. S. Altier, R. R. Lowrance, W. C. Mills, and D. L. Thomas. 1993. Hydrologic modeling for riparian management. *ASAE Paper No.* 932598. ASAE, St. Joseph, MI.

Sidle, R. C., H. Kitahara, T. Terajima, and Y. Nakai. 1995. Experimental studies on the effects of pipeflow on throughflow partitioning. *J. Hydrol.* Vol. 165:207-219.

Shields, A. 1936. Application of the theory of similarity and turbulence research to the bed load movement. *Mitt. Preuss. Vers. Wasser Schiff,* 26:5-24.

Simmons, R. C., A. J. Gold and P. M. Groffman. 1992. Nitrate dynamics in riparian forests: Groundwater studies. *J. Environ. Qual.* 21:659-665.

Simons, D.B., and F. Senturk. 1977. *Sediment transport technology.* Water Resources Publication, Ft. Collins, CO.

Sivapalan, M., and J.D. Kalma. 1995. Scale problems in hydrology: Contributions of the Robertson Workshop. *Hydrological Processes.* Vol. 9:243-250.

Sklash, M. G., and R. N. Farvolden. 1979. The role of groundwater in storm runoff. *J. Hydrol.* Vol. 43:45-65.

Sloan, P. G., I. D. Moore, G. B. Coltharp, and J. D. Eigel. 1983. Modeling surface and subsurface stormflow on steeply-slopeing forested watersheds. Rep. 142, 167 pp., *Water Resour. Res.* Inst. Univ. Of Kentucky, Lexington, KY.

Sloan, P. G., and I. D. Moore. 1984. Modeling subsurface stormflow on steeply sloping forested watersheds. *Water Resour. Res.,* Vol. 20(12):1815-1822.

Smetten, and Collis-George. 1985. Prediction of steady-state ponded infiltration distributions in a soil with vertical macropores. *J. Hydrol.* Vol. 79:115-122.

Smith, R. E., and R. H. B. Hebbert. 1983. Mathematical simulation of interdependent surface and subsurface hydrologic processes. *Water Resour. Res.* Vol. 19(4):987-1001.

Stone, J. J., R. H. Hawkins, and E. D. Shirley. 1994. An approximate form of the Green Ampt infiltration equation. *ASCE J. Irrigation and Drainage.* Vol. 120(1):128-137.

Storm, D. E. 1991. *Modeling dynamic rill networks from random surface on moderate slopes.* PhD. Thesis, Univ. Of Kentucky, Lexington, KY.

Sweeney, B. W. 1992. Streamside forests and the physical, chemical, and traophic characteristics of Piedmont streams in Eastern North America. *Wat. Sci. Tech.* Vol 26(12):2653-2673.

Tanaka, T., M. Yasuhara, H. Sakai, and A. Marui. 1988. The Hachioji Experimental Basin study - storm runoff processes and the mechanism of its generation. *J. Hydrol.* Vol. 102:139-164.

Thompson, D. B., T. L. London, and B. Garish. 1978. Winter and spring runoff from manure application plots. *ASAE Pap.* No. 78-2032. ASAE, St. Joseph, MI.

Thomas, D. L. and D. B. Beasley. 1986. A physically-based forest hydrology model I: Development and sensitivity of components. *Trans. ASAE* 29:962-972.

Tollner, E. W., B. J Barfield, and J. C hayes. 1982. Sedimentology of erect vegetal filters. *J. Hydraulics Division, ASCE.* 108(hy12):1518-1531.

Tollner, E. W., J. C Hayes, and B.J Barfield. 1978. The use of grass filters for sediment control in strip mine drainage. Vol I. Theoretical Studies on artificial media. *Report no. IMMR 35-RRR2-78. Institute for Mining and Minerals Research*, University of Kentucky, Lexington, KY.

Tollner, E. W., B. J Barfield., C. Vachirakornwatana and C. T Haan. 1977. Sediment Deposition patterns in simulated grass filters. *Trans. ASAE* 20(5):940-944.

Tollner, E. W., B. J Barfield., C. T Haan and T. Y Kao. 1976. Suspended sediment filtration capacity of simulated vegetation. *Trans. ASAE* 19(11):678-682.

Troendle, C. A. and J. W. Hoffmeyer. 1978. Storm flow related to measured physical parameters on small forested watersheds in West Virginia. *Eos. Trans. AGU*, 52, 204.

Tsukamoto, Y. 1961. An experiment on subsurface flow. *Jpn. Soc. Forest.* J. Vol. 43:61-68.

Tsukamoto, Y., and T. Ohta. 1988. Runoff processes on a steep forested hillslope. *J. Hydrol.* Vol. 102:165-178.

Tsuboyama, Y., R. C. Sidle, S. Noguchi, and I. Hosoda. 1994. Flow and solute transport through the soil matrix and macropores of a hillslope segment. *Water Resour. Res.* Vol. 30(4):879-. 890.

Turc, L. 1961. Evaluation des besoins en eau d'irrigation, evapotranspiration potentiallle. *Ann. Agron.* 12:13-49.

Van Bavel, C. H. M. 1966. Potential evaporation: the combination concept and its experimental verification. *Water Resour. Res.* Vol. 2:455-467.

Verma, R. D., and W. Brutsaert. 1971. Similitude criteria for flow from unconfined aquifers. *ASCE J. Hydraul. Div.* Vol. 97(HY9):1493-1509.

Watson, K. W., and R. J. Luxmoore. 1986. Estimating macroporosity in a forest watershed by uase of a tension infiltrometer.. *Soil Soc. Am. J.* Vol. 50:578-582.

Wilson, C. A. and P. Smart. 1984. Pipes and pipeflow processes in an upland catchment. *Catena*, Vol 11:145-158.

Welsch, D. J., 1991. Riparian forest buffers. *USDA Forest Service.* NA-PR-07-91.

Weyman, D. R. 1973. Measurement of the downslope flow of water in a soil. *J. Hydrol.* Vol. 20:267-288.

Weyman, D. R. 1970. Throughflow on hillslope and its relation to the stream hydrograph.. *Bull. Int. Assoc. Hydrol. Sci.* Vol. 15(2): 25-33.

Weyman, D. R. 1974. Runoff process, contributing area and streamflow in a small upland catchment. *Fluvial Process in Instrumented Watersheds.* Eds. K. J. Gregory and D. E. Walling, Spec. Publ. 6 pp. 33-43. Inst. Brit. Geogr. London.

Whipkey, R. J. 1965. Subsurface flow on forested hillslopes. *Bull. Int. Assoc. Sci. Hydrol.* Vol. 10(2): 74-85.

Whipkey, R. Z., and M. J. Kirkby. 1980. Flow within soil. In: *Hillslope hydrology,* M. J. Kirkby (editor), Wiley, Chichester. pp 121-144.

Wierda, A., A. W. L. Veen, and R. W. A. Hutjes. 1989. Infiltration at the Tai rain forest (Ivory

Coast): measurements and modeling. *Hydrol. Processes,* 3:371-382.

Wilson, G. V., and R. J. Luxmoore. 1988. Infiltration, macroporosity, and mesoporosity distributions on forested watersheds. *Soil Soc. Am. J.* Vol. 52:329-335.

Wilson, G. V., P. M. Jardine, R. J. Luxmoore, and J. R. Jones. 1990. Hydrology of a forested hillslope during storm events. *Geoderma.* Vol. 46:119-138.

Wilson, G. V., P. M. Jardine, J. D. O'Donell, and M. Collineau. 1993. Field scale transport from a buried line source in variably saturated soil. *J. Hydrol.* Vol. 145:83-109.

Wilson, B. N., B. J. Barfield, and I. D. Moore. 1983. A hydrology and sedimentology wateshed model. Part I: Modeling Techniques. Agricultural Engineering, University of Kentucky, Lexington, KY.

Williams, J. R., A. D. Nicks, and J. G. Arnold. 1985. Simulator for water resources in rural basins. *ASCE Hydraulics J.* 111(6):970-986.

Wood, E. F., M. Sivapalan, K. J. Beven, and L. Band. 1988. Effects of spatial variability and scale with implications to hydrological modeling. *J. Hydrol.* Vol. 102:29-47.

Wood, E. F., M. Sivapalan, and K. Beven. 1990. Similarity and scale in catchment storm response. *Rev. Geophys.* Vol.28:1-18.

Woodby, D. A. 1991. *An Ecosystem Model of Forest Tree Persistance.* Ph.D. Thesis, University of California, Santa Barbara, California.

Woolhiser, D. A., and J. A. Liggett. 1967. Unsteady one dimensional flow over a plane-The rising hydrograph. *Water Resour.Res.,* 3(3):753-771.

Yalin, M. S. 1963. An expression for bedload transportation. *Jour. of the HYdr. Div., ASCE,* 89(HY3):221-250.

Yates, P., and J.M. Sheridan. 1983. Estimating the effectiveness of vegetated floodplains/wetlands as nitrate-nitrite and orthophosphorous filters. *Agriculture-Ecosystems and Environment.* Vol. 9:303-314.

Yang, C. T. 1973. Incipient Motion and Sediment Transport. *Jour. of Hydr. Div., ASCE.* 99(HY10):1805-1826.

Young, R. A., T. Huntrods, and W. Anderson. 1980. Effectiveness of vegetated buffer strips in controlling pollution from feedlot runoff. *J. Environ. Qual.* Vol. 9:483-487.

Young, R. A., C. A. Onstad, and D. D. Bosch. 1986. Sediment transport capacity in rills and small channels. *In Proc. Fourth Federal Interagency Sediment Conf. Subcomm. On Sedimentation of the Interagency Advisory Comm. On Water Data,* Vol. 2. Washington, D.C. pp 6.225-6.33.

Zaslavsky, D., and G. Kasiff. 1965. Theoritical formation of piping mechanism in cohesive soils. *Geotechnique,* Vol. 15(3): 305-316.

Zaslavsky, D., and G. Sinai. 1981. Surface hydrology: I. Explanation of phenomena, II. Distribution of raindrops, III. Causes of lateral flow, IV. Flow in a slopeing layered soil, V. In-surface transient flow. *J. Hydraulics Div., ASCE.* Vol. 107(HY1):1-93.

Zaslavsky, D., and A. S. Rogoswski. 1969. Hydrologic and morphologic implications of anistropy and infiltration in soil profile development. *Soil Sci. Am. Proc.* Vol. 33:594-599.

Zinke, P. L., 1967. Forest interception studies in the United States. In *Forest Hydrology,* eds. W.E. Sopper and H.W. Lull, pp. 137-160, Pergamon Press, NY.

APPENDICES

APPENDIX I: FORTRAN PROGRAM FOR CATCHMENT SHAPE

PROGRAM LISTING:

```
      dimension nry(100), nrx(100), nbx(300),nby(300)
      dimension xlarat(300), nsubcel(300), nsubid(300)
      CHARACTER*5 runcde, idisk
      character*30 infile, outfile, infil2, infil3,outfil2
      write(*,*) 'input the runcode'
      read(5,50) runcde
50    format(a5)
      idisk = 'a1'
      infile = '/'// runcde //' chn '// idisk
      infil2 = '/'// runcde //' bnd '// idisk
      infil3 = '/'// runcde //' net '// idisk
      outfile= '/'// runcde //' wat '// idisk
      outfil2= '/'// runcde //' chk '// idisk
      write(*,*) infile
      write(*,*) infil2
      write(*,*) infil3
      OPEN(UNIT=12, FILE=infile)
      open(unit=14, file=infil2)
      open(unit=15, file=infil3)
      OPEN(UNIT=13, FILE=outfile)
      OPEN(UNIT=16, FILE=outfil2)
      write (6,*) 'input the number of rows'
      read(5,*) nrow
      write (6,*) 'input the number of columns'
      read(5,*) ncol
      read (12,*) nrill, nsub
      ncount = 0
      do 499 i = 1,nsub
      read(12,*) nrilno,nbr,nbrcel,nbrno,nboucel,nsubcel(i)
      if (nrilno.eq.0) then
      ncount=ncount+1
      endif
      if (nrilno.gt.0) then
      do 511 kl=1,nbrcel
      read(15,*) nrx(kl),nry(kl)
511   continue
      stmlen=0.0
      do 611 kl=2,nbrcel
      stminc = (float(nrx(kl-1)-nrx(kl))**2+float(nry(kl-1)-nry(kl))
     &      **2)**(1./2.)
      stmlen = stmlen+stminc
```

```
   611  continue
        nrilenx = nrx(nbrcel)
        nrileny = nry(nbrcel)
c       write(*,*) nrileny,nrilenx
        read(14,*) (nbx(l),nby(l),l=1,nboucel)
        axl =0.0
        do 521 jk = 1,nrow
        do 521 jm = 1,ncol
        if (nrilenx.lt. nrx(nbrcel-1)) then
        ncoorx = nrilenx-(jm-1)
        endif
        if (nrilenx.eq.nrx(nbrcel-1)) then
        ncoorx = nrilenx-(ncol/2)+(jm-1)
        endif
        if (nrilenx.gt.nrx(nbrcel-1)) then
        ncoorx = nrilenx+(jm-1)
        endif
        if(nrileny.lt.nry(nbrcel-1)) then
        ncoory = nrileny -(jk-1)
        endif
        if(nrileny.eq.nry(nbrcel-1)) then
        ncoory = nrileny+(nrow/2)+(jk-1)
        endif
        if(nrileny.gt.nry(nbrcel-1)) then
        ncoory = nrileny+(jk-1)
        endif
        if ((ncoorx.gt.ncol). or .(ncoory.gt.nrow)) go to 521
        if ((ncoorx.lt.0   ). or .(ncoory.lt.0   )) go to 521
        do 522 jn = 1,nboucel-1
        if ((ncoorx.eq.nbx(jn)). and .(ncoory.eq.nby(jn))) then
        axlen=(float(nbx(jn)-nrilenx)**2+float(nby(jn)-nrileny)**2)
     &      **(1./2.)
c       write (*,8) nrileny,nrilenx, nby(jn), nbx(jn), axlen
   8    format(3x,4(i3,2x),f7.3)
        if (axlen.gt.axl) then
        axl =axlen
        jmax = jn
        endif
        endif  -
   522  continue
   521  continue
        if (axl.eq.0) then
        nsubid(i)=0
        else
        nsubid(i)=1
        endif
        totlen = axl+stmlen
        if (nsubcel(i).eq.0)  then
        xlarat(i) = 0.0
```

```fortran
      else
      xlarat(i)= (totlen)/float(nsubcel(i))
      endif
      write(16,8) nrileny, nrilenx, nby(jmax),nbx(jmax), axl
      write(16,7) stmlen, totlen, nsubcel(i), xlarat(i)
7     format(5x,2(2x,f7.3),3x,i5,3x,f7.3)
      endif
499   continue
      do 225 i=1,nsub-ncount
      if (nsubcel(i).gt.1) then
      if (nsubid(i).eq.1) then
      write(13,*) i, nsubcel(i), xlarat(i)
      endif
      endif
225   continue
      STOP
      END
```

-

APPENDIX II: PROBABILITY DISTRIBUTION FUNCTIONS

1) LOGNORMAL DISTRIBUTION

If a population of values follows a Lognormal distribution it essentially means that the natural logarithms of those values follows a normal distribution. Thus, to compute the probability associated with values following a lognormal distribution, the normal distribution function ANORDF provided in IMSL was utilized.

The distribution function of a standard normal (Gaussian) random variable as computed in ANORDF is given by

$$\phi(x) = \frac{1}{\sqrt{2\pi}} \int_{-\infty}^{x} e^{-t^2/2} \, dt \qquad \text{II.1}$$

where $\phi(x)$ is the distribution function, and x is the argument for which the normal distribution function is to be evaluated. The standard normal distribution (for which ANORDF is the distribution function) has a mean of 0 and a variance of 1. The probability that a normal random variable with mean μ and variance σ^2 is less than y is given by ANORDF evaluated at $(y-\mu)/\sigma$.

2) GAMMA DISTRIBUTION

To compute the probability values associated with a population following a Gamma distribution, the IMSL Gamma distribution function GAMDF was utilized. The distribution function F of a gamma random variable with a shape parameter a, as computed in GAMDF is given by

$$F(x) = \frac{1}{\Gamma(a)} \int_{0}^{x} e^{-t} t^{a-1} \, dt \qquad \text{II.2}$$

where $\Gamma(\cdot)$ is the gamma function (that is, the integral from 0 to ∞ of the same integrand as above). Th above expression determines F(x) using only the shape parameter. Generally, the gamma distribution is defined with the three parameters - shape (a), scale (b), and location (c). For a random variable T which has all three parameters, the probability that $T \le t_o$ can be obtained by setting $X = (t_o - c)/b$.

3) WEIBULL DISTRIBUTION

Probability values for the Weibull distribution were not determined using IMSL. A separate FORTRAN program was written. The Weibull distribution function F(x) is given by

$$F(x) = \begin{array}{ll} 1 - e^{-[(x-c)/b]^a} & \textit{If } x > 0 \\ 0 & \textit{otherwise} \end{array} \qquad \text{II.3}$$

where the terms are as defined earlier.

Since all the three distributions mentioned above are continuous, probability for a discrete value x does not exist and is equal to zero. But, probability for x between an upper bound m and a lower bound n can be computed, and is equal to the area of the density function between these two bounds. This is expressed by

$$Prob(n < X \le m) = \int_n^m f(x) \, dx = F(m) - F(n) \qquad \text{II.4}$$

where f(x) is the density function for x. Thus, the probability associated with a discrete channel shape (w/d) value was given by $Prob[(w/d - \delta/2) < w/d \le (w/d + \delta/2)]$, where δ was the increment in w/d values.

APPENDIX III: CANADIAN SHIELD DATA
Source: (Peters, 1994)

Table III.1: Characteristics of orthic humo-ferric podzol (soil type of hillslope 1A)

Horizon	Thickness (m)	Textural Class
LFH	0.075	-
A_{he}	0.020	sandy loam
A_e	0.032	silty sand
B_{f1}	0.212	silty sand
B_{f2}	0.196	silty sand
BC	0.040	loamy sand
B	0.330	loamy sand

Table III.2: Characteristics of orthic ferro-humic podzol (soil type of hillslope 2A).

Horizon	Thickness (m)	Textural class
LFH	0.064	-
A_{He}	0.023	loam
A_e	0.029	loamy sand
Bh_{f1}	0.251	sandy loam
Bh_{f2}	0.215	sandy loam
B_{f1}	0.153	silty sand
BC	0.090	silty sand

Table III.3: Average soil properties at sites 1 and 2 (+/- standard deviation).

Site	Horizon	Porosity (%)
1	A_e	79.0 (12.5)
	B	58.8 (5.8)
2	A_e	79.6 (6.9)
	B	65.0 (7.3)

Table III.4: Vertical and lateral saturated conductivities at hillslope sites 1 and 2.

Site	Depth (cm)	Vertical x 10^{-4}(m/s)	Depth (cm)	Horizontal x 10^{-4}(m/s)
1	0-12	2.0	6	20
	12-24	0.7	18	2.0
	24-36	0.8	30	0.3
2	0-12	2.0	6	2.0
	12-24	2.0	18	2.0
	24-36	2.0	30	2.0
	36-48	0.2	42	2.0
	48-60	0.3	54	0.3

Table III.5: Trench physical characteristics

Site	Trough[c]	Trough depth below surface (m)	Trough distance above bedrock (m)[a]
1A	A_e	0.07[b]	0.41
	INT	0.37-0.45	0.09
	BR	0.40-0.52	0.0
2A	A_e	0.08[b]	0.41
	INT	0.24-0.57	0.12
	BR	0.32-0.65	0.0

Note: [a] average value
        [b] small range in horizon thickness
        [c] Ae: Organic/Ae horizon; INT: intermediate trough within B horizon; BR: trough at bedrock

Table III.6: Characteristics of micro-catchments drained by the hillslope trenches.

Site	Drainage area (m²)	Average soil depth micro-catchment (m)	Range of soil depth (m)	Bedrock gradient (%)
1A	397	0.43	0.0-1.00	17
2A	822	0.31	0.0-1.15	18
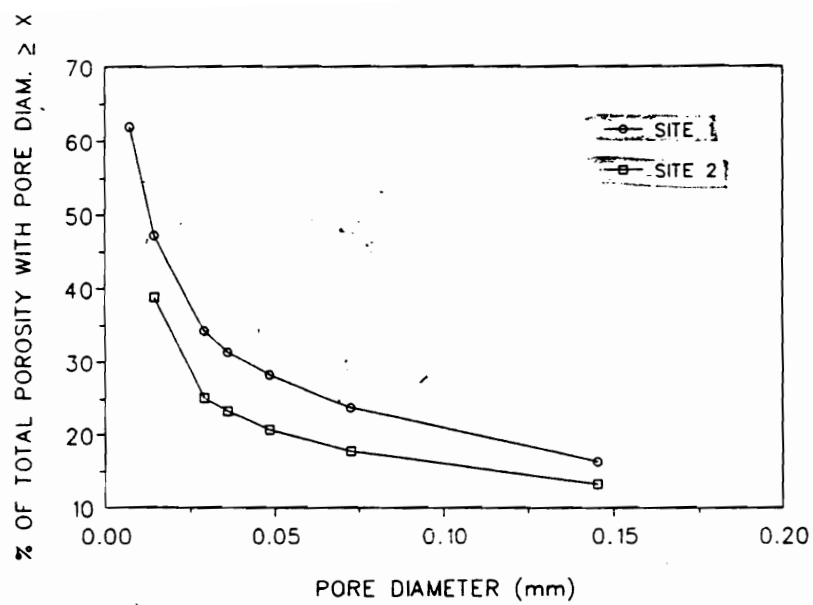
Figure III.1: Pore size distribution
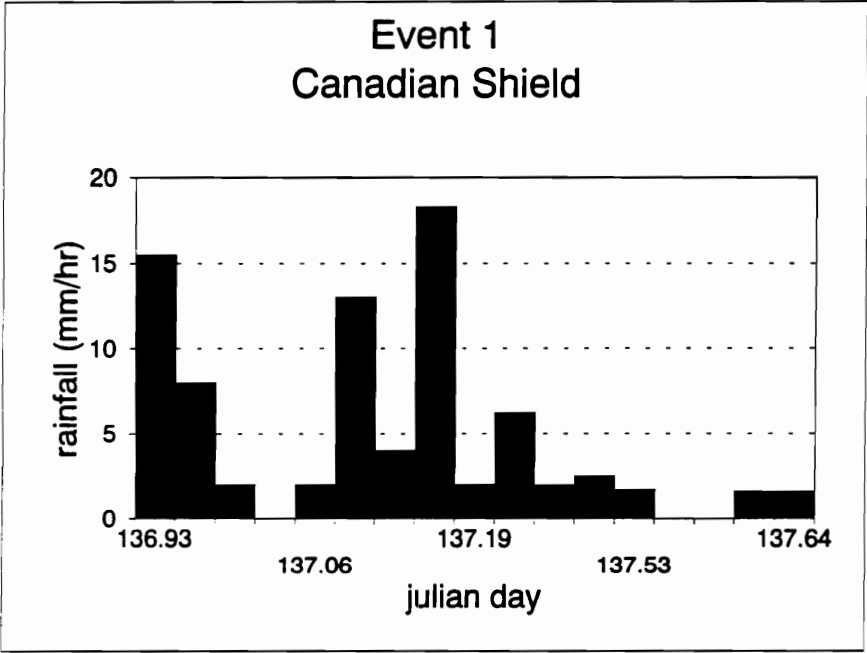
Figure III.2: Event C1 hyetograph.
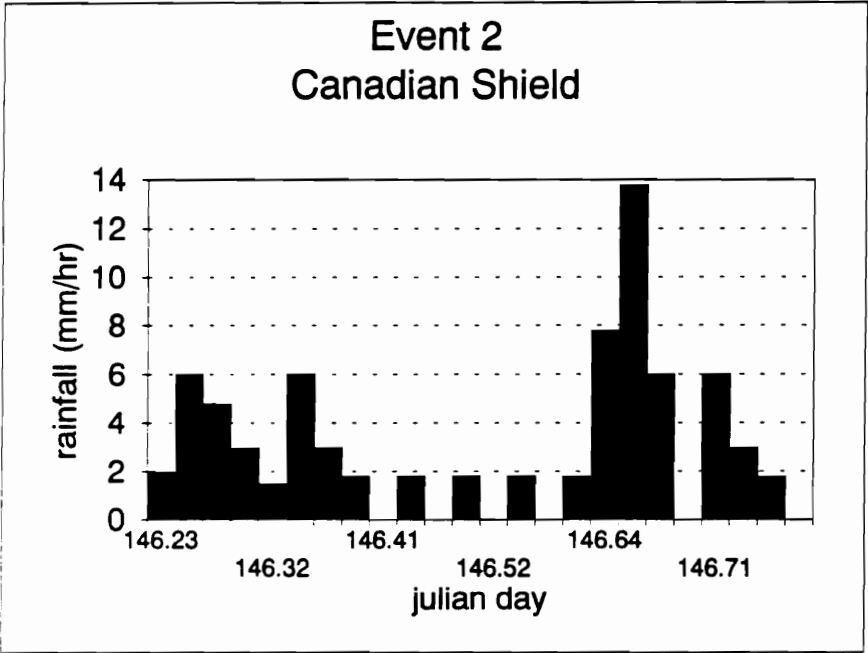
Figure III.3: Event C2 hyetograph.
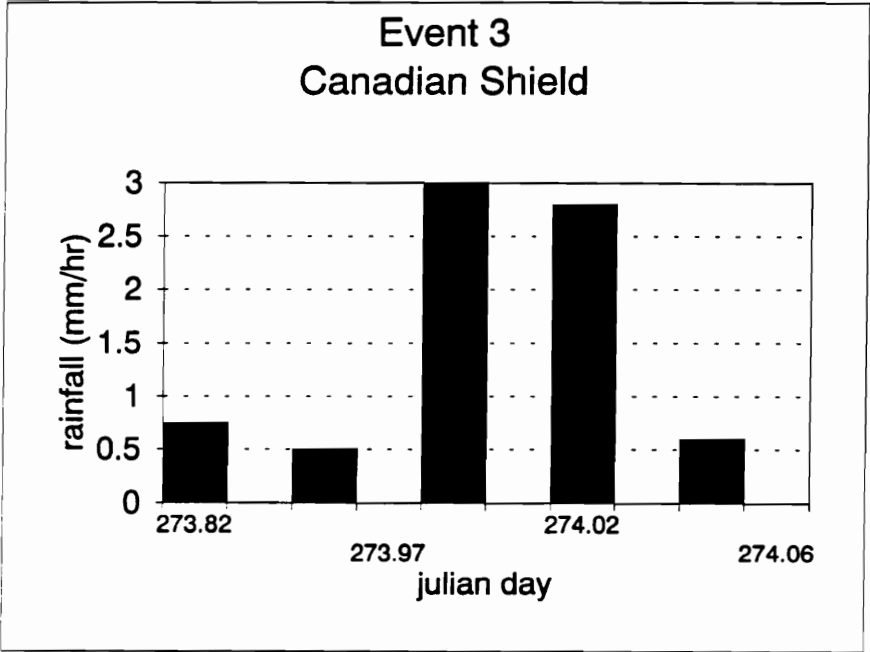
Event III.4: Event C3 hyetograph.

Event 4
Canadian Shield
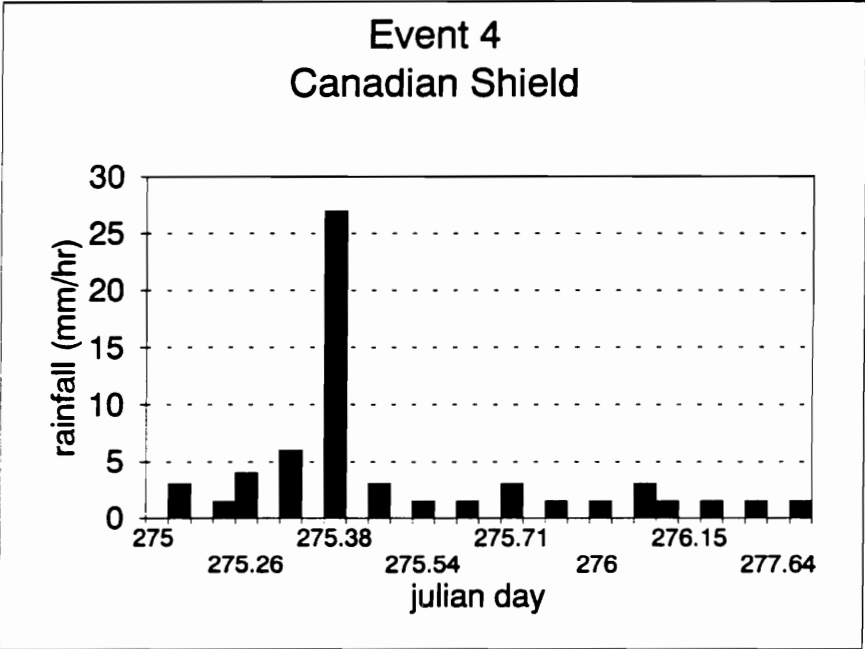
Event III.5: Event C4 hyetograph.
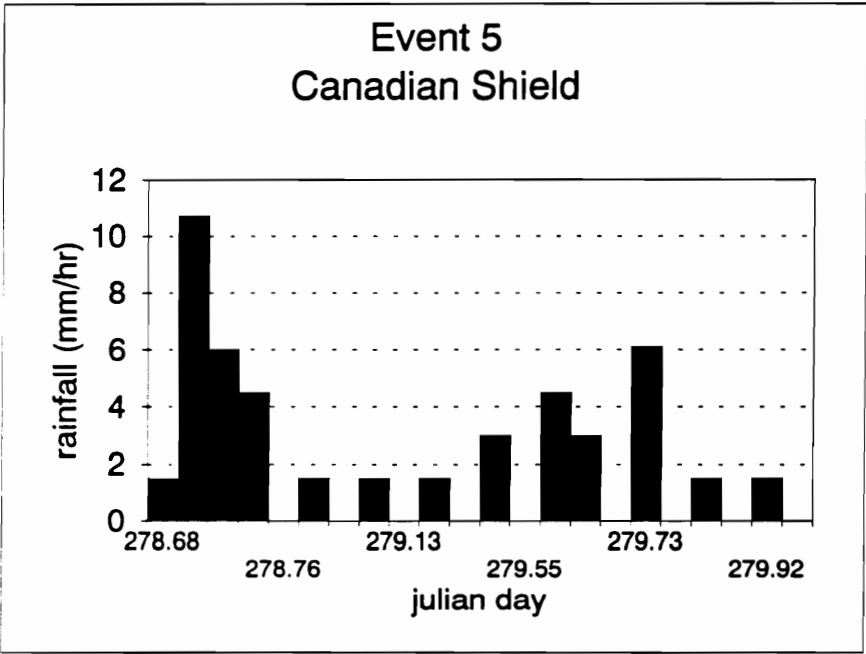
Event III.6: Event C5 hyetograph.
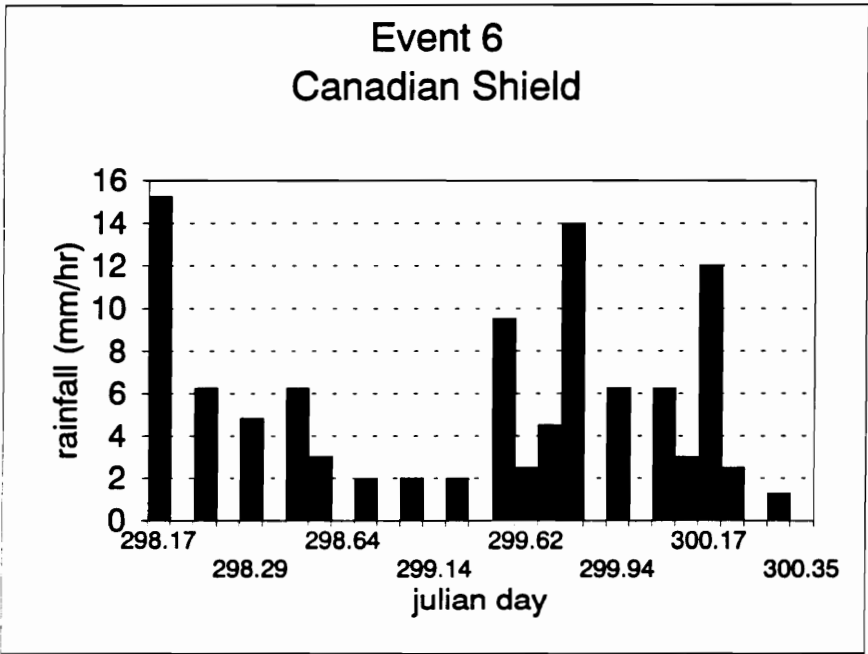
Figure III.7: Event C6 hyetograph.

APPENDIX IV: MELTON BRANCH, TENNESSEE
Source: (Wilson et al., 1993; Luxmoore and Abner, 1987)

Figure IV.1: Dimensions and depths of the subsurface pan collectors installed at the Melton Branch site (Luxmoore and Abner, 1987).
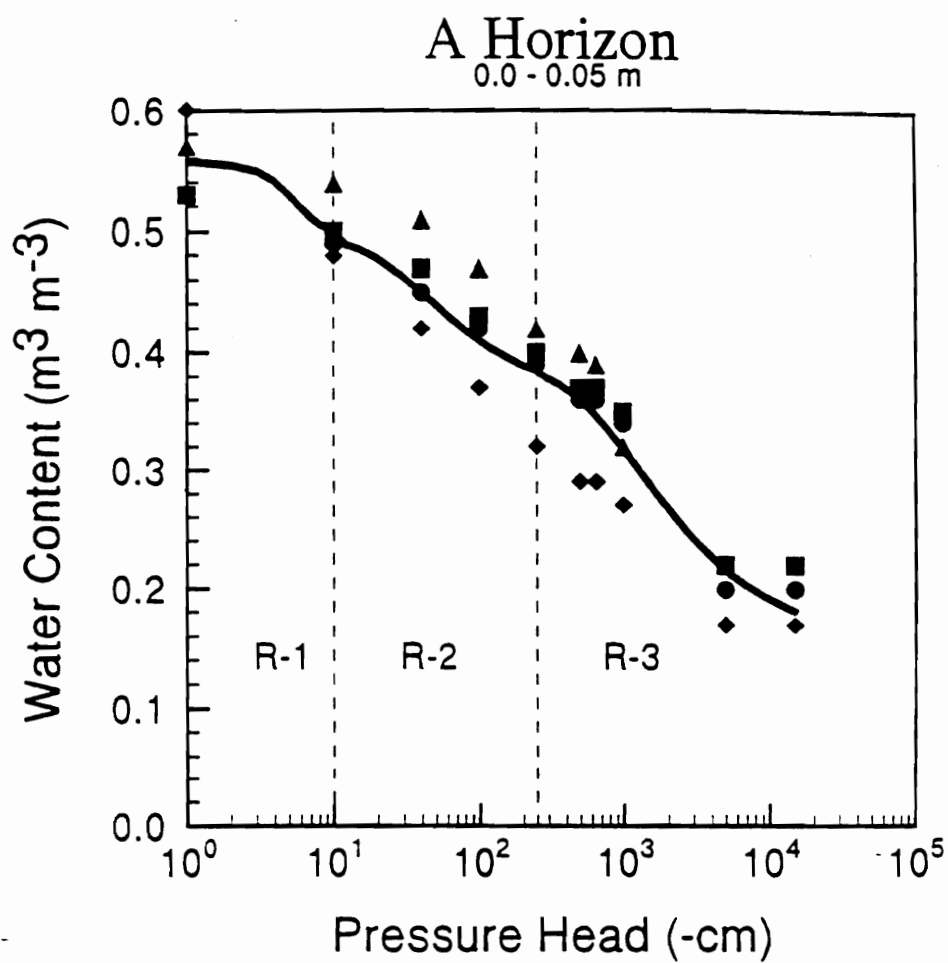
Figure IV.2: Pressure head versus water content A horizon.

B_W Horizon

0.05 - 0.30 m
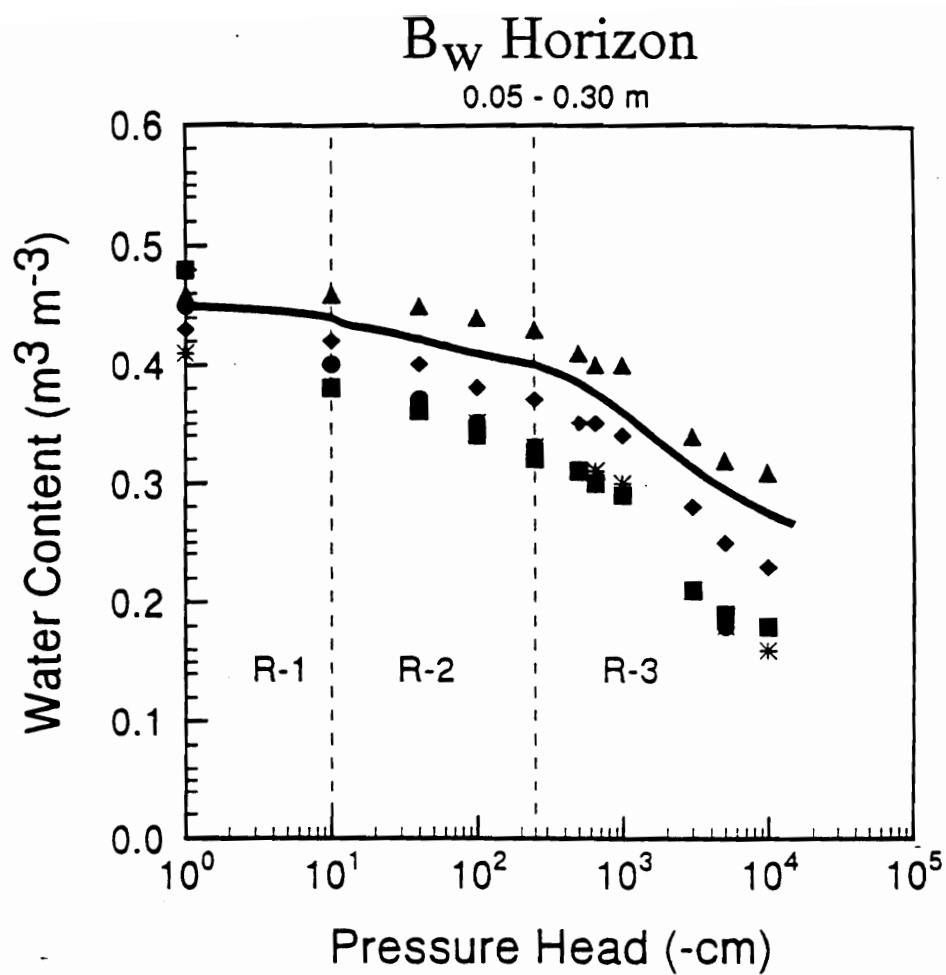
Figure IV.3: Pressure head versus water content for Bw horizon.
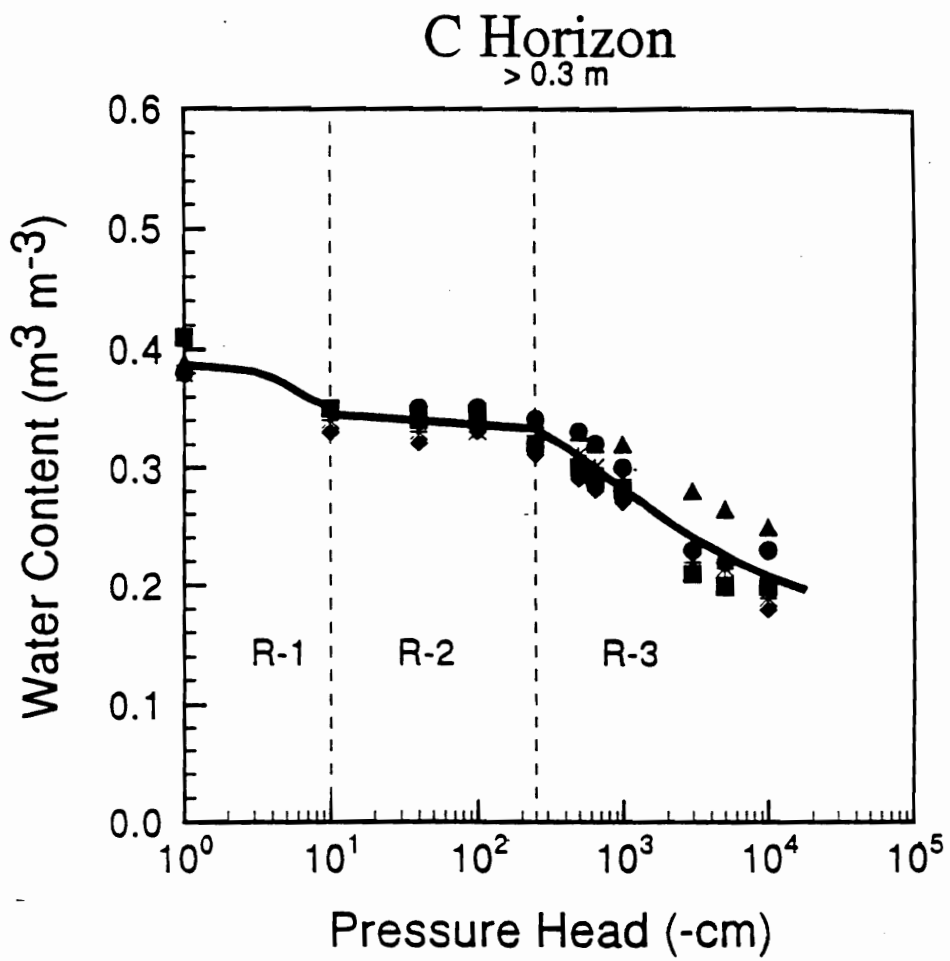
Figure IV.4: Pressure head versus water content for C horizon.
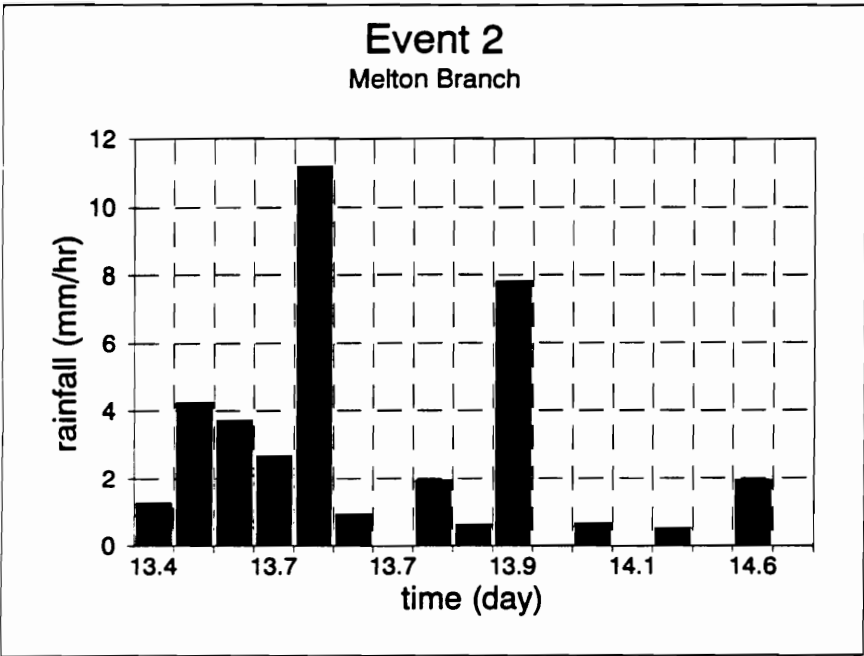
Figure IV.5: Rainfall hyetograph for Event 2 (Feb. 13).
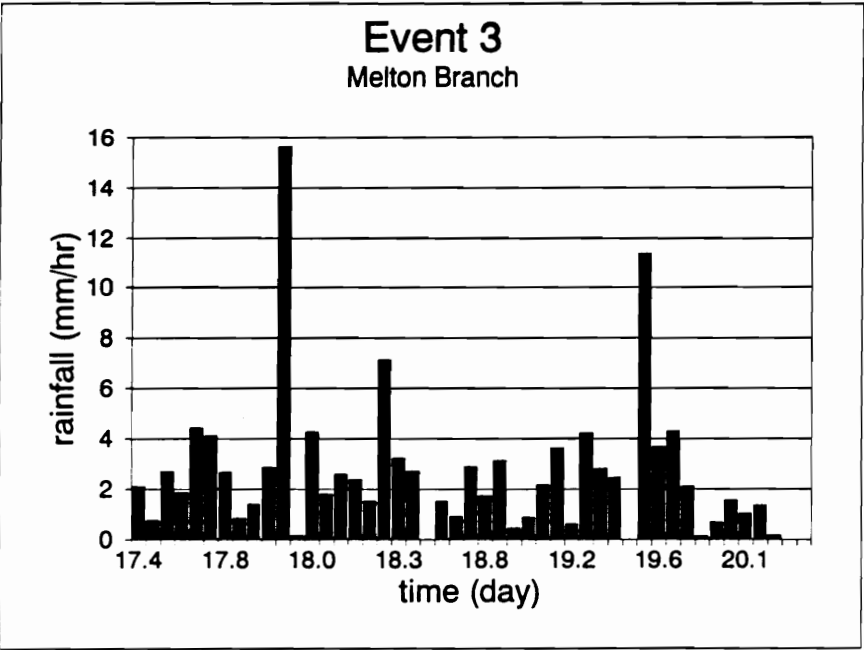
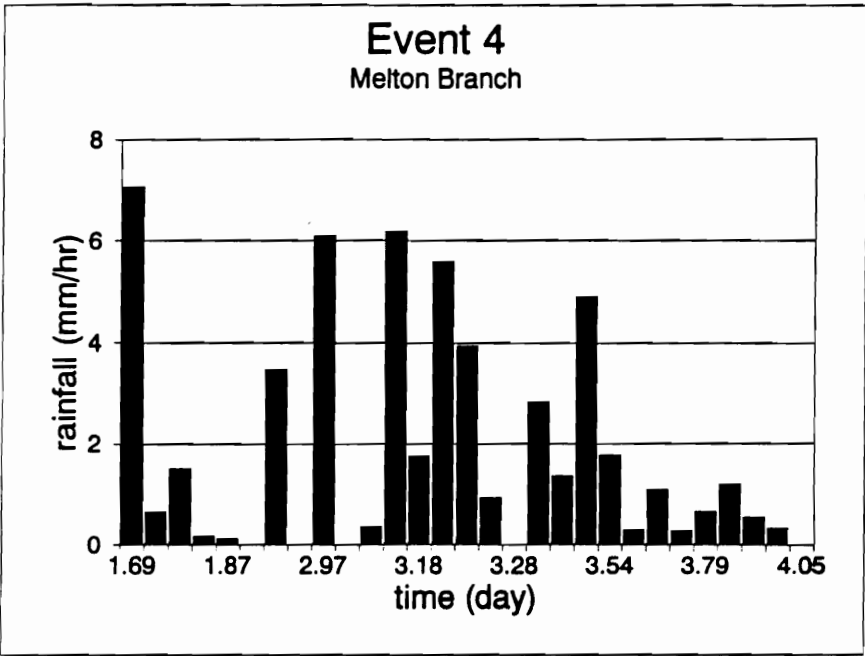Figure IV.6: Rainfall hyetograph for Event 3 (Feb 17).

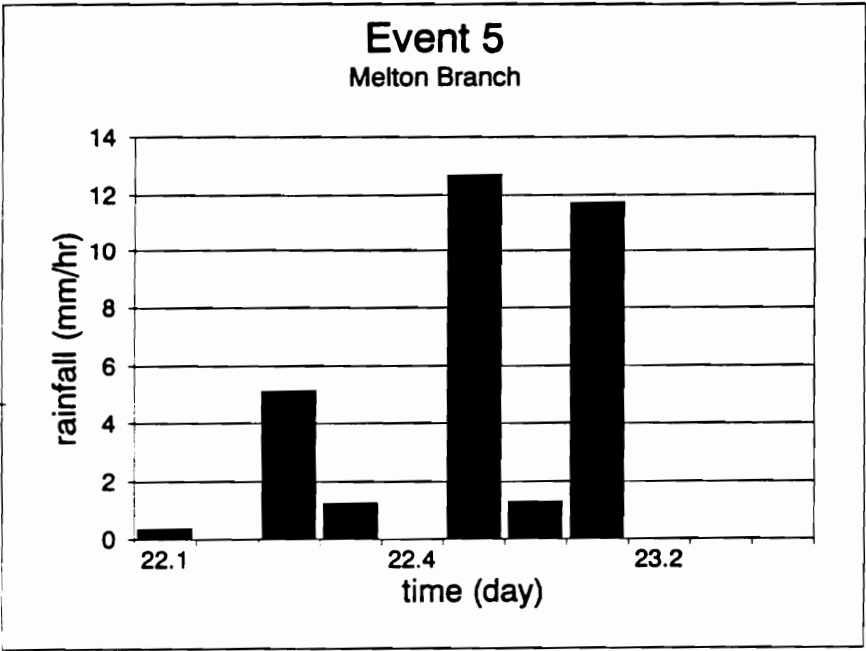Figure IV.7: Rainfall hyetograph for Event 4 (Mar. 01).

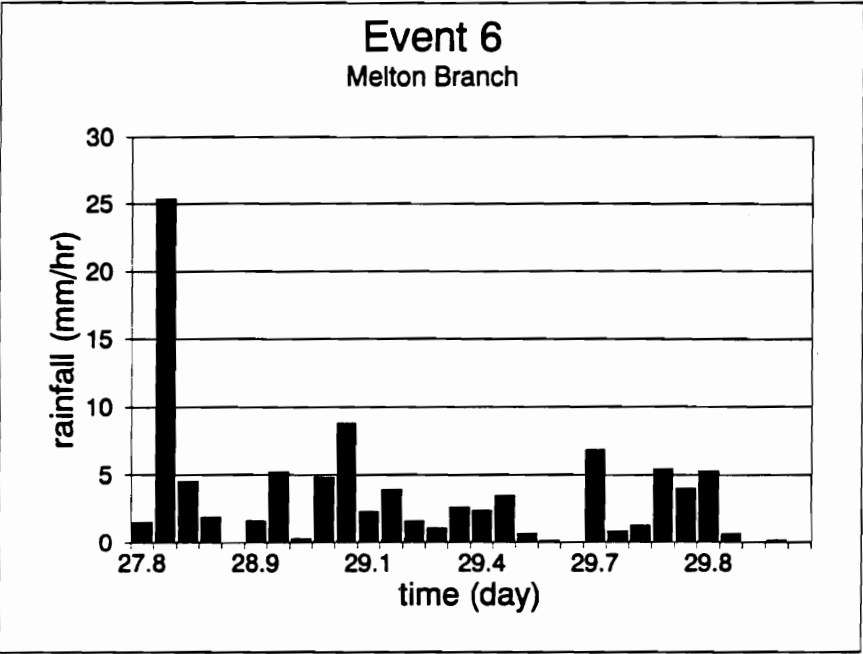Figure IV.8: Rainfall hyetograph for Event 5 (Mar. 22)

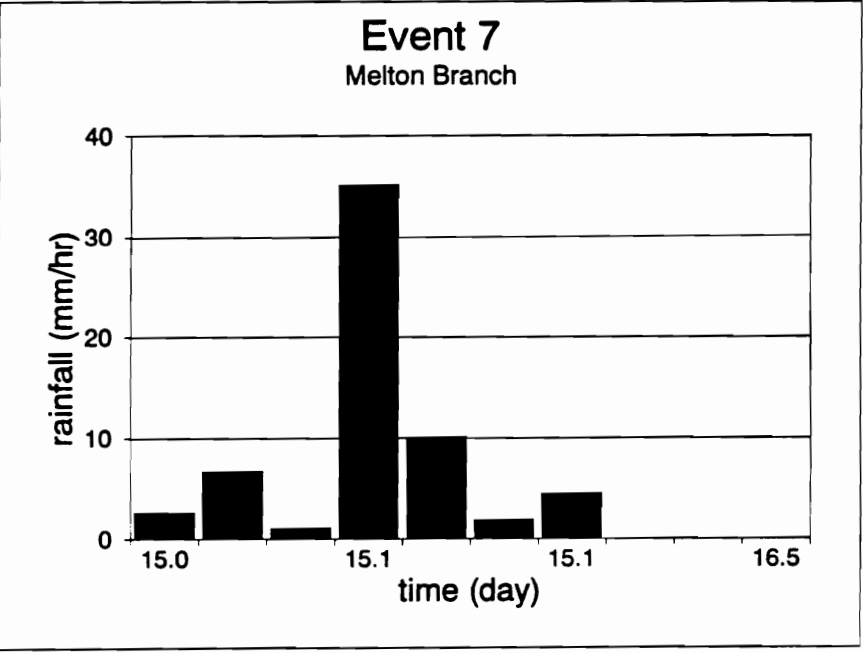Figure IV.9: Rainfall hyetograph for Event 6 (Mar. 27).

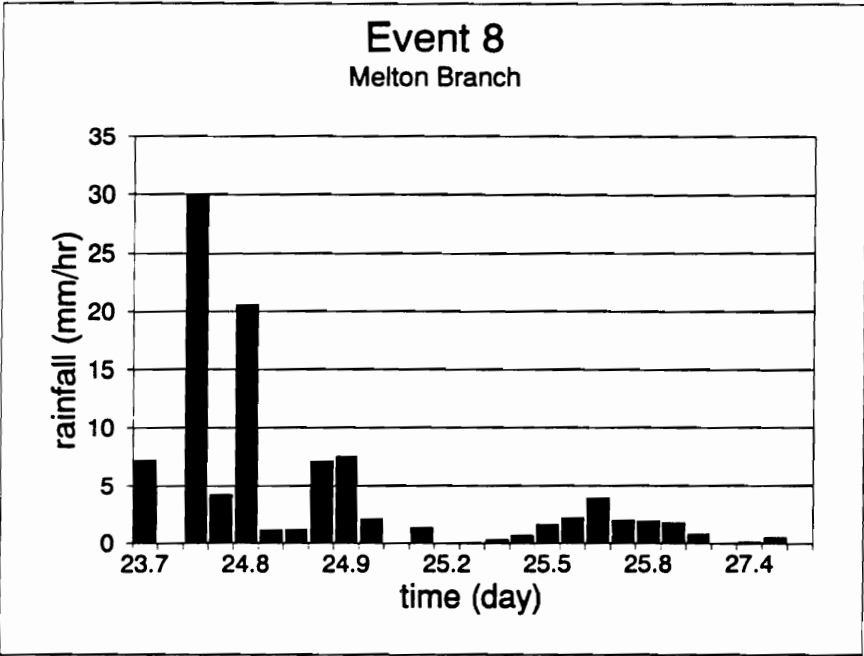Figure IV.10: Rainfall hyetograph for Event 7 (Apr. 15).

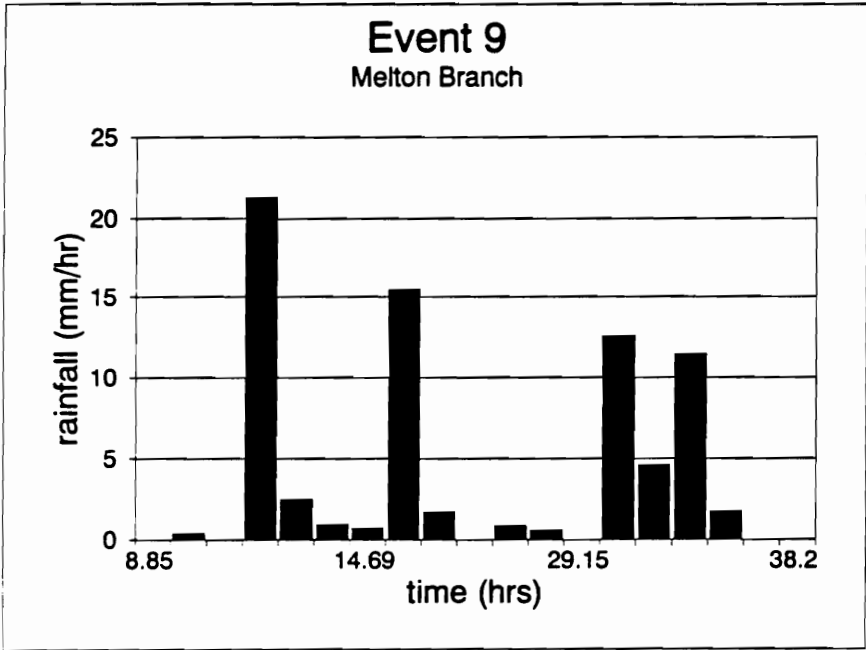Figure IV.11: Rainfall hyetograph for Event 8 (June 23).

Figure IV.12: Rainfall hyetograph for Event 9 (May 27).

APPENDIX V: HACHIOJI CATCHMENT, JAPAN
Source: (Tanaka et al., 1988)

Sample No.	K (cm/sec)	Sample No.	K (cm/sec)	Sample No.	K (cm/sec)
1	8.7×10^{-4}	8	2.1×10^{-6}	15	3.7×10^{-5}
2	2.8×10^{-4}	9	3.2×10^{-4}	16	1.1×10^{-5}
3	1.4×10^{-4}	10	1.5×10^{-5}	17	7.8×10^{-7}
4	2.2×10^{-6}	11	4.2×10^{-6}	18	3.0×10^{-4}
5	2.4×10^{-5}	12	2.0×10^{-6}	19	4.5×10^{-5}
6	3.0×10^{-7}	13	2.3×10^{-6}	20	5.6×10^{-4}
7	1.6×10^{-6}	14	6.5×10^{-7}	21	8.6×10^{-4}

Legend:
- ⊠ Surface soil
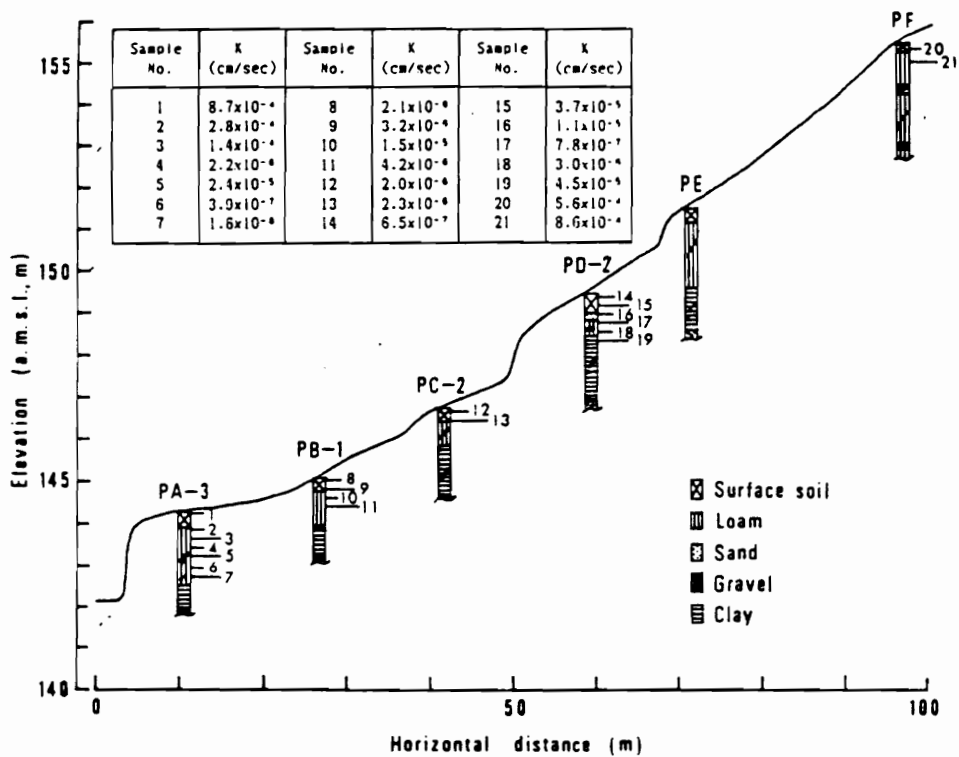- ▥ Loam
- ▨ Sand
- ▪ Gravel
- ▤ Clay

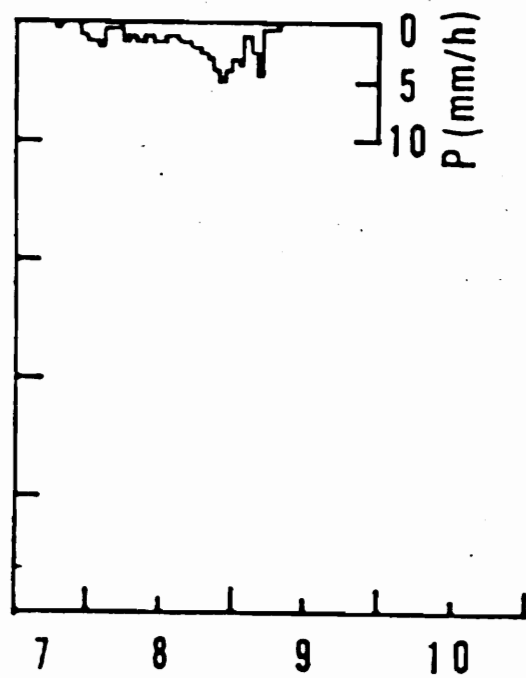Figure V.1: Soil horizon depth and hydraulic conductivities.

Figure V.2: Rainfall hyetograph for Event of Oct 7-9, 1982.

APPENDIX VI: FORTRAN PROGRAM LISTING AND INPUT FILES

Due to their large size, the program code and the input data files have not been included in this document. A listing of the fortran program and input data format can be obtained from this author by sending a request at the following e-mail address: **RIVERS@tifton.cpes.peachnet.edu**.

Date and place of birth:

May 06, 1967
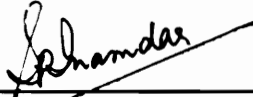Nagpur, India

Education:

- *Master of Science* in Agricultural Engineering, University of Kentucky, Lexington, KY: May 1993.
- *Bachelor of Engineering* in Civil Engineering, VRCE, Nagpur University, Nagpur, India: May 1988.

Professional positions:

- Feb. 19, 1996 to Present: *Post-Doctoral Research Associate*, University of Georgia, Biological and Agricultural Engineering Department, Coastal Plain Experiment Station, Tifton, GA.
- Jan. 1993 to Dec. 1995: *Research Assistant and Doctoral Candidate*, Biological Systems Engineering Department, Virginia Tech, Blacksburg, VA.
- Jan. 1991 to Dec. 1992: *Research Assistant and Masters Candidate*, Agricultural Engineering Department, University of Kentucky, Lexington, KY.
- Mar. 1990 to Oct. 1990: *Project Manager*, Shriprakash Consulting Engineers, Bombay, India
- Jul. 1988 to Feb. 1990: *Structural Engineer*, Structwel Designers and Consultants, Bombay, India.

Professional Honors:

Alpha Epsilon, Agricultural Engineering Honor Society.

Shreeram P. Inamdar

JUNE 03, 1996
Date